THE UNIVERSITY OF CHICAGO

HIDDEN TIME-REVERSAL SYMMETRY, QUANTUM DETAILED BALANCE, AND EXACT SOLUTIONS OF OPEN QUANTUM SYSTEMS

A DISSERTATION SUBMITTED TO
THE FACULTY OF THE DIVISION OF THE PHYSICAL SCIENCES
IN CANDIDACY FOR THE DEGREE OF
DOCTOR OF PHILOSOPHY

DEPARTMENT OF PHYSICS

BY
DAVID BENJAMIN ROBERTS

CHICAGO, ILLINOIS
AUGUST 2023

TABLE OF CONTENTS

LIST OF FIGURES

LIST OF TABLES

ACKNOWLEDGMENTS

I would like to acknowledge my PhD advisor, Aash, for supporting my career goals, and for placing me in a fascinating research area that had plenty of fertile ground to explore. At many times he had invaluable physical insights that helped enrich the thesis that I have presented here. Finally, I would like to acknowledge my girlfriend, Chloe, for helping me get through the toughest of times, and for helping out in designing some of the figures in the last chapter of this thesis.

ABSTRACT

Driven-dissipative quantum systems generically do not satisfy simple notions of detailed balance based on the time symmetry of correlation functions. We show that such systems can nonetheless exhibit a *hidden time-reversal symmetry* which most directly manifests itself in a doubled version of the original system prepared in an appropriate entangled thermofield double state. This hidden time-reversal symmetry has a direct operational utility: it provides a general method for finding exact solutions of non-trivial steady states. Special cases of this approach include the coherent quantum absorber and complex-P function methods from quantum optics. We also show that hidden-TRS has observable consequences even in single-system experiments, and can be broken by the non-trivial combination of nonlinearity, thermal fluctuations, and driving. To illustrate our ideas, we apply our methods to quantum many-body systems, and discover exact solutions to several new models, including a kind of many-body parametric oscillator model, as well as the infinite-range limit of the dissipative transverse-field Ising model.

CHAPTER 1

INTRODUCTION

Time-reversal is a basic symmetry that plays a crucial role in a vast variety of physical systems. For open classical systems subject to dissipation and driving, it manifests itself as detailed balance constraints on transition rates (or equivalently drift and diffusion functions). It also places a strong symmetry constraint on steady-state two-time correlation functions $\overline{A(t)B(0)}$: they must be invariant when each quantity is replaced by its time-reversed version and $t \to -t$. This symmetry is sometimes referred to as Onsager symmetry, as it plays a crucial role in the derivation of Onsager reciprocity relations. In classical systems, this symmetry has a direct operational utility: it provides a simple route for finding steady state probability distributions (i.e. potential conditions that can be used to solve Fokker-Planck equations Gardiner [2009]).

There is a long history of works that extend notions of Onsager symmetry and detailed balance to quantum open systems described by a Markovian master equation in Lindblad form Agarwal [1973], Carmichael and Walls [1976], Alicki [1976], Kossakowski et al. [1977], Majewski [1984], Majewski and Streater [1999], Denisov et al. [2002], Fagnola and Umanita [2007], Fagnola and Umanità [2010], Duvenhage and Snyman [2018], Carlen and Maas [2017], Ramezani et al. [2018]. The most natural definition requires that steady-state correlation functions in the quantum theory obey an Onsager symmetry analogous to the classical case Agarwal [1973], Carmichael and Walls [1976], Denisov et al. [2002]; this condition necessarily holds if the microscopic system-bath dynamics obey time-reversal symmetry Carmichael and Walls [1976]. Later more formal works considered generalized definitions of quantum detailed balance Fagnola and Umanita [2007], Fagnola and Umanità [2010], framed in terms of quantities that are not directly measurable and whose physical interpretation is somewhat opaque. The ultimate operational utility of all these quantum definitions of detailed balance are unclear. Unlike classical detailed balance, these quantum symmetries are not known to

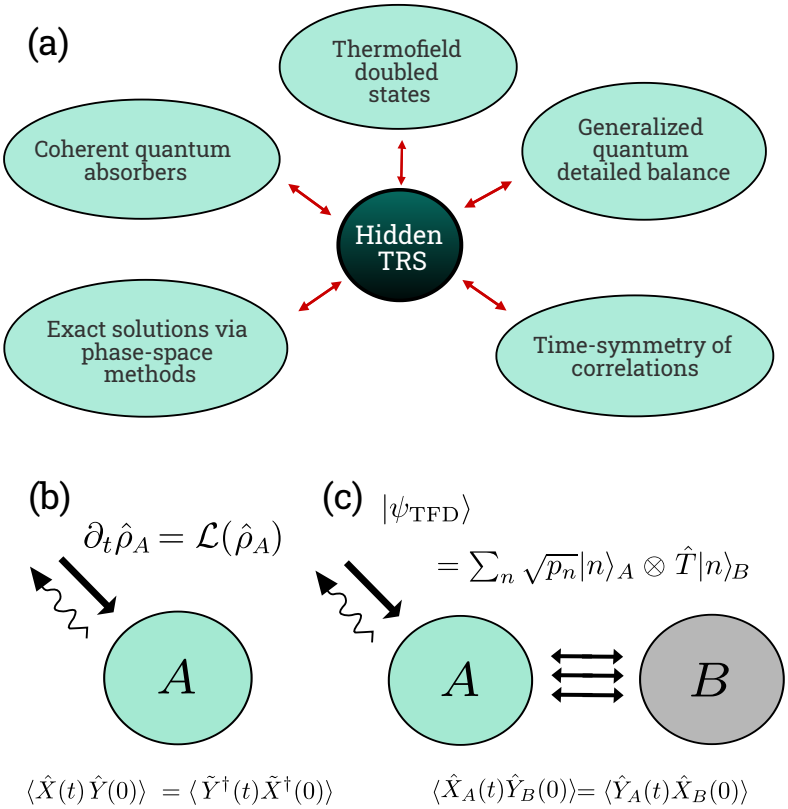

Figure 1.1: (a) The concept of hidden time-reversal symmetry helps unify disparate-seeming topics in the study of driven-dissipative quantum systems. (b) A driven dissipative system described by a Lindblad master equation. The conventional definition of quantum detailed balance is formulated as a time symmetry of steady-state correlation functions. (c) Hidden TRS is a symmetry ensuring that correlation functions of a doubled version of the original system, prepared in a thermofield double state, are time symmetric. It is defined by an anti-unitary operator $\hat{T}$. Hidden TRS can hold even when the correlation function symmetry in (b) fails; it also enables a powerful method for finding exact solutions.

enable a simple method for finding a non-trivial system's steady state density matrix[1].

In this thesis, we introduce a powerful, symmetry-based formulation of quantum detailed balance (QDB) that goes beyond the simple definition in Ref. Agarwal [1973], and that *directly* enables an efficient way for finding non-trivial steady states. Our work builds on Ref. Duvenhage and Snyman [2018], which showed that a particular generalized definition

1. The only attempt at such connections in the past were limited to systems that were easily solvable by other means (e.g. linear bosonic systems, or systems that could be reduced to a classical master equation) Agarwal [1973].

of QDB introduced in Ref. Goldstein and Lindsay [1995] can be formulated using an entangled, thermofield double state Takahashi and Umezawa [1996]. We use this to introduce the notion of "hidden" time reversal symmetry (TRS) in an open quantum system. This anti-unitary symmetry need not reveal itself through some simple invariance of the original master equation, nor through a standard Onsager symmetry of two-time correlation functions. Instead, this symmetry is directly tied to a time symmetry of correlation functions of a *doubled* version of the original system prepared in an thermofield double state whose form is directly tied to the symmetry operator (see Fig. 1.1(c)). Crucially, we show that a system can possess hidden TRS even if it fails to have the conventional quantum detailed balance (CQDB) defined in Ref. Agarwal [1973] (though in the limit of infinitely weak dissipation, these notions coincide).

Hidden TRS is not just a formal curiosity: it provides a powerful tool for understanding complex non-thermal and non-classical steady states. We show that *the existence of hidden TRS directly yields a simple and direct method for analytically finding the steady state density matrix of a Lindblad driven-dissipative quantum system.* This method is not limited to situations of weak driving, interactions or dissipation. It represents a generalization of the coherent quantum absorber (CQA) method introduced in Ref. Stannigel et al. [2012b], and extended in Ref. Roberts and Clerk [2020]. Hidden-TRS is also connected to well-known exact solution methods from quantum optics based on the complex-P phase space quasiprobability Drummond and Gardiner [1980], Drummond and Walls [1980b], Bartolo et al. [2016], Elliott and Ginossar [2016]: these methods can be viewed as special cases of our more general approach.

In the final two chapters of this thesis, we show how such quantum detailed balance methods can be used to solve nontrivial driven-dissipative many-body systems, systems whose steady states are non-thermal, and for which no conventional notion of time-reversal symmetry is possible. These systems include a many-body generalization of the Kerr para-

metric oscillator (KPO), as well as the infinite-range limit of the dissipative transverse-field Ising model, depicted in Figure 1.3. The many-body systems that we solve in this thesis in many respects are inspired by the original exact solution of Drummond of a linearly-driven and damped nonlinear quantum oscillator Drummond and Walls [1980b]. They also share many characteristic features in common. One unifying theme is that the thermofield double states for each system can be written in the parametric form

$$|\Psi_{\hat{T}}\rangle = \frac{{}_1F_0(r;\hat{X})}{\mathcal{N}}|\Omega\rangle \tag{1.1}$$

where r is a suitably defined dimensionless detuning, $|\Omega\rangle$ is a suitably-defined vacuum state, and $\hat{X}$ is some operator that creates excitations in that vacuum state. Here, ${}_0F_1$ is the limiting confluent hypergeometric series. In a linearly driven-damped nonlinear oscillator, the operator $\hat{X}$ is a bosonic raising operator, and as such $\hat{X}, \hat{X}^\dagger$ generate the Heisenberg algebra. In the many-body parametric oscillator model that we introduce in Ch. 4, $\hat{X}$ is a quadratic form in bosonic raising operators, and hence generates an $SU(1,1)$ algebra. In the dissipative transverse-field Ising model that we discuss in the last chapter of the thesis, $\hat{X}$ generates an $SU(2)$ algebra, albeit with a somewhat unusual presentation.

However, despite these similarities, the process of extracting information from the exact solution (1.1) is slightly more difficult in the many-body case. For example, in our multimode bosonic model, in the case that the corresponding $SU(1,1)$ lowering operator (call it $\hat{X}'$) satisfies $\hat{X}' \propto \hat{X}^\dagger$, the problem of evaluating equal-time correlation functions is a somewhat nontrivial exercise in the multimode representation theory of the group $SU(1,1)$, something that is solved explicitly in Ch. 4. In general, with a nonunitary representation, one cannot find closed-form expressions and instead must resort to a recursive solution for such correlations. A similar story plays out in the driven-dissipative Ising model that we solve in Ch. 5 - the problem of calculating correlation functions there also bifurcates into the general problem in a situation with $\hat{X}$ generating nonunitary representation of $SU(2)$, and

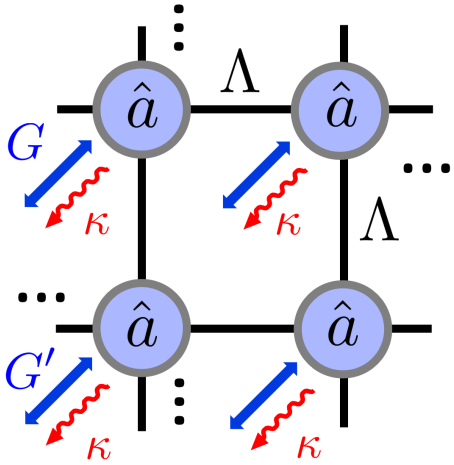

Figure 1.2: Schematic of the many-body parametric oscillator model. Schematic of the model: a lattice of bosonic modes, with two-photon drives on each site (G) and on each nearest-neighbor (nn) bond (Λ). There is also single-photon loss κ on each site, and a global Hubbard (Kerr) interaction U.

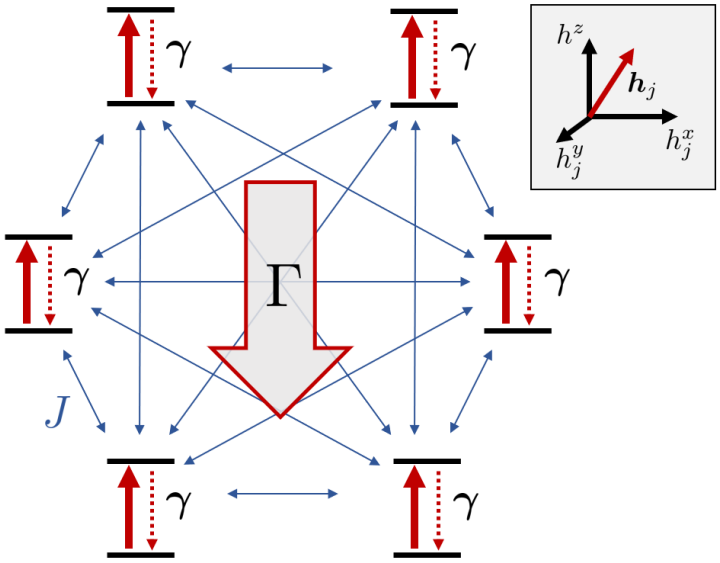

Figure 1.3: Schematic of the (infinite-range) dissipative transverse-field Ising model. A collection of N spin-1/2 particles is subject to local T_1 decay at a rate γ, as well as collective decay at a rate Γ. The spins interact via an all-to-all Ising interaction with strength J. Inset: each spin is subject to a separate external magnetic field with both axial and transverse components. The axial component of the external field is the same for each spin.

a more symmetric problem where $\hat{X}$ generates a unitary representation of $SU(2)$. In both models, whenever $\hat{X}$ generates a unitary representation of (Lie algebra of) the relevant Lie group G, closed-form solutions take a somewhat simple form as a ratio of hypergeometric functions, just as in Drummond and Walls [1980b].

To summarize, this thesis presents a new symmetry that can exist in driven-dissipative systems described by a Lindblad master equation: hidden time-reversal symmetry. We have shown explicitly how this goes beyond the conventional definition of quantum detailed balance (CQDB) introduced by Agarwal Agarwal [1973]; crucially, hidden-TRS can exist in systems whose steady states have non-zero energy-eigenstate coherences, something that makes it impossible to have CQDB. While hidden-TRS is most naturally formulated in terms of a doubled system prepared in a thermofield double state, we demonstrated that it has a direct observable consequence: a certain class of single-system correlation functions are guaranteed to be time-symmetric. This is in contrast to CQDB, which requires all correlation functions to obey a time-symmetry. To illustrate our ideas, we have analyzed how several ubiquitous driven quantum systems (qubit and nonlinear cavity models) can have hidden-TRS despite not having CQDB.

We hope that our results will lay the groundwork for further studies exploiting hidden-TRS as a means to understand even more complex systems. This symmetry could provide an interesting means for finding non-trivial, exactly-solvable fermionic driven dissipative systems, not just qubit and bosonic systems. It could also lead to novel perturbative techniques for studying systems that weakly break hidden-TRS. Another interesting direction would be to see whether these ideas could be extended to systems with a Floquet structure, i.e. Lindblad master equations where the Hamiltonian and/or jump operators have a periodic time dependence (see e.g. Kamleitner and Shnirman [2011], Ferron et al. [2012], Blattmann et al. [2015], Reimer et al. [2018]). Finally, the prospect of using hidden TRS to explore many-body models is exciting and provides a fruitful direction for future work. For example,

there is work soon to come out, solving a driven-dissipative spin chain model. This work demonstrates that our ideas have applicability well beyond the global interaction models explored in this thesis. Thinking even more generally, it would also be extremely interesting to rephrase this symmetry fully in terms of a dissipative field theory describing the system of interest (i.e. in terms of a Keldysh action Kamenev [2011], Sieberer et al. [2015, 2016]). This could yield further insights, and also perhaps enable an extension of these ideas into non-Markovian regimes.

CHAPTER 2

DRIVEN-DISSIPATIVE KERR OSCILLATORS

2.1 Introduction

Exact solutions of interacting, driven-dissipative quantum problems are rare, and thus occupy a special place in the study of open quantum systems. A canonical example is the solution of the driven-dissipative Kerr resonator. Here, a bosonic mode with a Kerr nonlinearity (i.e. a Hubbard U interaction) is subject to a coherent linear drive and Markovian single photon loss. As shown by Drummond and Walls [1980b], one can exactly solve for the steady state of this system using a positive-P phase space representation. Later work showed that models including two-photon driving and loss are also solvable using this technique Drummond and Walls [1980b], Bartolo et al. [2016], Elliott and Ginossar [2016]. These driven nonlinear cavity systems have renewed relevance, as they can be directly implemented in superconducting circuit QED setups (see, e.g., Kirchmair et al. [2013], Leghtas et al. [2015b], Touzard et al. [2018], Lescanne et al. [2019], Grimm et al. [2019]). Their ability to exhibit multiple steady states has utility in quantum information processing Mirrahimi et al. [2014b], Goto [2016], Puri et al. [2017].

While the existence of exact solutions here are remarkable, they are somewhat physically opaque and unwieldy (e.g. they are typically expressed as infinite sums of special functions). Their derivation is also somewhat intricate, requiring a non-trivial integration to relate the solution of an effective classical problem to the underlying quantum system. More direct methods for obtaining and possibly extending these solutions are thus highly desirable. For the simplest version of the Kerr-cavity problem (single-photon drive and loss only), Stannigel et al. [2012b] were able to reproduce the exact solution of Ref. Drummond and Walls [1980b] using a simple, purely algebraic approach. While extremely elegant, it was unclear whether this approach could be extended to more complex problems.

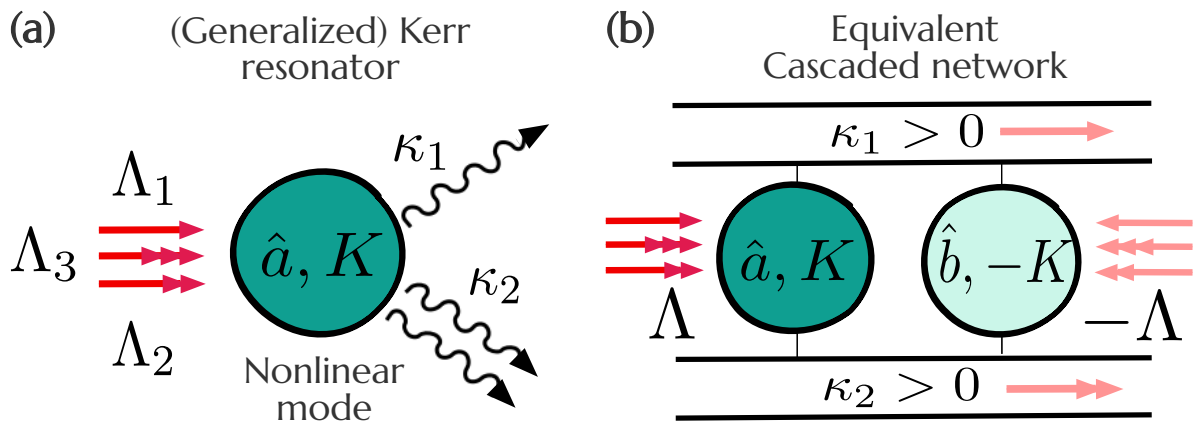

Figure 2.1: (a) Generalized driven Kerr cavity problem, where a single interacting bosonic mode is subject to linear and nonlinear coherent drives Λ_j, as well as independent one and two photon loss (rates κ_1, κ_2). (b) The coherent quantum absorber (CQA) method represents each dissipative bath as a chiral waveguide, and couples a second auxiliary b cavity downstream. By picking its Hamiltonian judiciously, the entire composite system can relax to a pure state, providing an efficient means for finding the steady state of cavity-a.

In this chapter, we show that such an extension is indeed possible: the "coherent quantum absorber" (CQA) method of Ref. Stannigel et al. [2012b] can be extended to a wide class of systems which include nonlinear coherent driving as well as multiple dissipators (see Fig. 2.1). Our extension employs a new ingredient: the Segal-Bargmann representation of a single-mode pure state wavefunction Bargmann [1961], Segal [1962, 1963], Bargmann [1967]. This enables non-trivial transformations that are crucial for finding exact solutions. Our approach yields several new insights. We find and describe new parameter regimes where the steady-state exhibits a surprising generalized photon-blockade phenomenon. We also find an infinite number of points in parameter space where our generalized driven Kerr system exhibits quantum bistability, despite the lack of photon-number parity conservation; these parameters can be achieved asymptotically in the limit of weak single-photon loss. Our solution also provides a simple intuitive picture when there is a unique steady state (see Fig. 2.2): the steady state is formed by mixing a pure state with vacuum at a 50-50 beamsplitter, and then discarding one of the outputs. At a technical level, our work also provides new, simple closed-form expressions for the steady-state Wigner function and

normally-ordered moments.

The remainder of this chapter is organized as follows. In Sec. 2.2 we introduce the basic system. In Sec. 2.3, we review the CQA method, and in Sec. 2.4 present our extension to nonlinear driving and multiple dissipators. Sec. 2.5 summarizes the new physical phenomena uncovered by our exact solution, while Sec. 2.6 and Sec. 2.7 discuss regimes of classical and quantum bistability. We conclude in Sec. 2.15.

2.2 System

We consider a driven Kerr resonator whose coherent dynamics is described by the Hamiltonian

$$\begin{aligned}\hat{H}_a = &\frac{K}{2}\hat{a}^\dagger\hat{a}^\dagger\hat{a}\hat{a} - \Delta\hat{a}^\dagger\hat{a} \\ &+ \left[\left(\Lambda_1\hat{a}^\dagger + \frac{\Lambda_2}{2}\hat{a}^\dagger\hat{a}^\dagger + \Lambda_3\hat{a}^\dagger\hat{a}^\dagger\hat{a}\right) + h.c.\right].\end{aligned} \tag{2.1}$$

We work in a rotating frame in which the drives are stationary. Here Δ is the drive detuning, K is the Kerr nonlinearity, and $\Lambda_1, \Lambda_2, \Lambda_3$ are the complex amplitudes of standard coherent one and two photon driving terms. Λ_3 represents an unusual kind of nonlinear single-photon driving term; as we will see, it enables a striking new kind of photon blockade effect that does not require strong nonlienarity. We show in 2.9 how this Λ_3 drive can be implemented using the superconducting circuit architecture of Ref. Sivak et al. [2019].

The full dissipative dynamics includes one and two photon loss processes, and is described by the Lindblad master equation

$$\frac{d}{dt}\hat{\rho} = -i[\hat{H}_a, \hat{\rho}] + \kappa_1\mathcal{D}[\hat{a}]\hat{\rho} + \kappa_2\mathcal{D}[\hat{a}^2]\hat{\rho} \equiv \mathcal{L}_0\hat{\rho}, \tag{2.2}$$

where $\mathcal{D}[\hat{X}]\hat{\rho} \equiv \hat{X}\hat{\rho}\hat{X}^\dagger - (1/2)\left\{\hat{X}^\dagger\hat{X}, \hat{\rho}\right\}$ is the usual Lindblad dissipative superoperator,

and κ_1 (κ_2) are the one (two) photon decay rates. Note that the dissipative evolution corresponds to coupling the system to two distinct zero-temperature baths.

We will focus exclusively on finding the steady states of this kind of system, i.e. density matrices $\hat{\rho}_{\rm ss}$ satisfying

$$\mathcal{L}_0 \hat{\rho}_{\rm ss} = 0. \tag{2.3}$$

We briefly summarize prior work on this model. For $\Lambda_3 \equiv 0$, exact solutions for $\hat{\rho}_{\rm ss}$ have been found using the positive-P approach Drummond and Walls [1980b], Drummond et al. [1981], Elliott and Ginossar [2016], Bartolo et al. [2016]. The solutions express matrix elements of $\hat{\rho}_{\rm ss}$ in the Fock basis as sums of special functions. In the semiclassical limit, solutions for the steady state can be found using an alternate approach developed by Dykman and co-workers Marthaler and Dykman [2006], Dykman [2012]; unlike the positive-P approach, these can also be used to describe dissipation at a non-zero temperature. Systems with a non-zero three-photon drive $\Lambda_3 \neq 0$ have not to our knowledge been studied before, nor were they previously known to be solvable.

While the prior work on driven Kerr resonators is a remarkable achievement, it leaves several mysteries unanswered. First, in the presence of single photon loss, the unique steady state that one finds *always* yields a positive-definite Wigner function. Given the nonlinearity in the system, it is not *a priori* obvious that this should necessarily be the case. Second, in the absence of single photon processes (i.e. $\Lambda_1 = \kappa_1 = 0$), this system exhibits multiple steady states Krippner et al. [1994], Wolinsky and Carmichael [1988a], Hach III and Gerry [1994], Gilles et al. [1994], Mirrahimi et al. [2014b]. We are not aware of any discussion of this using the positive-P approach. For $\Delta = 0$, the system is simple enough that the multiple steady states can be found via elementary means, in terms of superpositions of coherent states Goto [2016], Puri et al. [2017]. Conditions needed for Wigner function negativity were recently discussed in Ref. Braasch et al. [2019], though these are not directly applicable to our system. In the sections that follow, we discuss an alternate, physically-transparent

method for solving this class of problems that addresses the open issues mentioned above.

2.3 Exact solutions using the quantum absorber method

Our approach to solving driven-dissipative Kerr problems is to adapt and extend the so-called "coherent quantum absorber" (CQA) approach first introduced by Stannigel et al. [2012b] to solve the simplest driven Kerr problem where there are no two photon drive or loss processes. We quickly recap the philosophy of this approach, and then show how it can be extended to deal with more complex problems involving two and even three photon processes.

2.3.1 Recap of the basic approach

Consider first the case where our system in Eq. (2.2) has no two photon loss ($\kappa_2 = 0$). The starting point of the CQA method is to represent the one photon loss as arising from a coupling to a chiral (i.e. unidirectional) waveguide. Further, one imagines coupling a second auxiliary bosonic mode (annihilation operator $\hat{b}$, system Hamiltonian $\hat{H}_b$) to the waveguide, downstream from the physical a cavity (see Fig. 2.1). Given the chirality of the waveguide, the dynamics of this auxiliary cavity can have no impact on the physical cavity a. The entire composite system can be described using standard cascaded quantum systems theory Carmichael [1993], Gardiner [1993], Gardiner and Zoller [2000]. The dynamics of the reduced density matrix $\hat{\rho}_{ab}$ describing both cavities is described by a Lindblad master equation of the form:

$$\frac{d}{dt}\hat{\rho}_{ab} = -i[\hat{H}_{ab}, \hat{\rho}_{ab}] + \kappa_1 \mathcal{D}[\hat{a} - \hat{b}]\hat{\rho}_{ab}, \tag{2.4}$$

$$\hat{H}_{ab} = \hat{H}_a + \hat{H}_b - \frac{i\kappa_1}{2}(\hat{a}^\dagger \hat{b} - h.c.). \tag{2.5}$$

Note that one can rigorously trace out cavity b from this equation, recovering Eq. (2.2) for cavity a alone.

While the introduction of the auxiliary cavity b has no impact on cavity a, it provides a useful tool for finding its steady state. As shown in Ref. Stannigel et al. [2012b], for a general cavity a Lindblad master equation having only single-photon loss (i.e. Eq. (2.2) with $\kappa_2 = 0$ and arbitrary $\hat{H}_a$), one can *always* construct a Hamiltonian $\hat{H}_b$ for the auxiliary cavity b such that the composite system has a pure steady state. This steady state state necessarily has vanishing emission to the waveguide– it is a "dark" state. Letting $\hat{\rho}_{ab,ss}$ denote the steady-state density matrix of the two-cavity problem, this means:

$$\hat{\rho}_{ab,ss} = |\psi\rangle \langle\psi| , \qquad \left(\hat{a} - \hat{b}\right) |\psi\rangle = 0. \tag{2.6}$$

Note that the dark state condition implies that $|\psi\rangle$ is essentially a single mode state. Introducing new composite mode operators

$$\hat{c}_{\pm} \equiv \frac{\hat{a} \pm \hat{b}}{\sqrt{2}}, \tag{2.7}$$

one notes that the dark state condition forces the composite mode $\hat{c}_-$ to be in vacuum. Hence, one just needs to solve for the (pure) state of the composite $\hat{c}_+$ mode.

In physical terms, the CQA approach seeks to construct $\hat{H}_b$ such that the auxiliary cavity b acts as a "perfect absorber" for all photons emitted into the waveguide by cavity a. By tracing out cavity b, one obtains the desired steady state for the physical cavity-a problem. One generically obtains an impure state, as the two cavities will be entangled in the state $|\psi\rangle$.

While such a construction is always possible, in practice it would seem to be of no utility, as one can only construct the required $\hat{H}_b$ by first *independently* solving for the cavity-a steady $\hat{\rho}_{a,ss}$, Despite this seeming obstacle, Ref. Stannigel et al. [2012b] demonstrated that

for a range of problems, one could essentially guess the form of $\hat{H}_b$ without first knowing $\hat{\rho}_{a,ss}$. This educated guess is extremely simple: $\hat{H}_b$ is taken to be identical to $\hat{H}_a$ up to an overall minus sign. Ref. Stannigel et al. [2012b] applied this to the simplest driven Kerr problem ($\Lambda_2 = \Lambda_3 = \kappa_2 = 0$ in Eq. (2.1)), in which case

$$\hat{H}_b = -\frac{K}{2}\hat{b}^\dagger\hat{b}^\dagger\hat{b}\hat{b} + \Delta\hat{b}^\dagger\hat{b} - \left[\Lambda_1\hat{b}^\dagger + h.c.\right]. \tag{2.8}$$

With this choice, Stannigel et al. were able to find a pure-state solution of the cascaded master equation in Eq. (2.4) by solving a simple one-term recursion relation. By then tracing out cavity b, they recovered (in a much simpler manner) the classic solution of Drummond and Walls [1980b] for the linear-drive Kerr problem.

2.3.2 Extension to nonlinear driving and two-photon loss

It is natural to ask whether the the absorber method approach can be extended to solve problems with nonlinear driving and two-photon loss. An immediate issue is the presence of two independent dissipators in the master equation Eq. (2.2). We find that the CQA approach is easily modified to deal with this situation. As shown in Fig. 2.1(b), one can represent the two-photon loss process as a nonlinear coupling to a second chiral waveguide.

One again needs to add something downstream along this waveguide to absorb the emitted exctitations. While there are many possible options, we find the simplest approach is sufficient: we assume that there is still a single auxiliary cavity b that now couples to *both* these independent chiral waveguides. The cascaded master equation now takes the form:

$$\frac{d}{dt}\hat{\rho}_{ab} = -i[\hat{H}_{ab}, \hat{\rho}_{ab}] + \kappa_1\mathcal{D}[\hat{a} - \hat{b}]\hat{\rho}_{ab} + \kappa_2\mathcal{D}[\hat{a}^2 - \hat{b}^2]\hat{\rho}_{ab}, \tag{2.9}$$

with

$$\hat{H}_{ab} \equiv \hat{H}_a - \hat{H}_b - \frac{i\kappa_1}{2}(\hat{a}^\dagger \hat{b} - h.c.) - \frac{i\kappa_2}{2}(\hat{a}^\dagger \hat{a}^\dagger \hat{b}^2 - h.c.). \tag{2.10}$$

Again, tracing out cavity b from the above equation recovers the cavity a master equation given in Eq. (2.2), independent of the choice of $\hat{H}_b$.

The next step is the same as before: we want to pick $\hat{H}_b$ so that cavity b absorbs all photons emitted by cavity a into *either* of the two chiral waveguides. We thus want a pure steady state $|\psi\rangle$ of the two cavity system that is a dark state of both collective loss operators appearing in Eq. (2.9). Fortunately, these dark state conditions are not independent: having $(\hat{a} - \hat{b})\,|\psi\rangle = 0$ as before ensures that the state is dark with respect to emission to either waveguide.

Finally, there remains the question of how exactly to find the desired $\hat{H}_b$. As we show in Sec. 2.4, the simple educated guess of taking $\hat{H}_b$ to be the negative of $\hat{H}_a$ still works in the presence of two photon driving and loss, and even for a wider class of problems.

2.3.3 Connection to Segal-Bargmann representations

A second crucial element in our extension of the CQA method is to combine it with the Segal-Bargmann (SB) representation of single-mode pure-state wavefunctions in terms of holomorphic functions Bargmann [1961], Segal [1962, 1963], Bargmann [1967]. This provides an extremely efficient way of solving the complex recursion relations that determine the desired dark state wavefunction $|\psi\rangle$. More importantly, it is an extremely useful tool for developing physical intuition. It renders the operation of tracing out the auxiliary cavity b trivial, and allows one to directly obtain the Wigner function of the cavity-a steady state.

Basics of the representation

Consider a single bosonic mode in a pure state $|\psi\rangle$ that in is written in terms of Fock states $|m\rangle$ as:

$$|\psi\rangle = \sum_{m=0}^{\infty} \alpha_m |m\rangle. \tag{2.11}$$

In the SB representation, this state is associated with a holomorphic function $\psi_{\mathrm{SB}}(z)$ defined on the complex plane:

$$\psi_{\mathrm{SB}}(z) = \sum_{m=0}^{\infty} \frac{\alpha_m}{\sqrt{m!}} z^m. \tag{2.12}$$

The space of these functions forms a Hilbert space that is unitarily equivalent to the original Fock space, with an induced inner product:

$$\langle \psi_{\mathrm{SB}}, \phi_{\mathrm{SB}} \rangle_{\mathrm{SB}} \equiv \frac{1}{\pi} \int_{\mathbb{C}} d^2 z \, \psi^*_{\mathrm{SB}}(z) \phi_{\mathrm{SB}}(z) e^{-|z|^2}. \tag{2.13}$$

The SB wavefunction has a direct physical interpretation: its modulus determines the Husimi Q-function of the state $|\psi\rangle$. Letting $|z\rangle$ denote a coherent state with amplitude z, we have

$$Q(z) \equiv \frac{1}{\pi} \left| \langle z | \, \psi \rangle \right|^2 = \frac{1}{\pi} \left| \psi_{\mathrm{SB}}(z^*) \right|^2 e^{-|z|^2}. \tag{2.14}$$

Finally, the canonical $\hat{c}$ and creation $\hat{c}^\dagger$ operators become linear differential operators in the Bargmann space: $\hat{c} \mapsto \partial/\partial z$, $\hat{c}^\dagger \mapsto z$.

Tracing out the auxiliary cavity

As we will see, the CQA method reduces to finding a single-mode, pure-state wavefunction $|\psi_+\rangle$ for the collective mode $\hat{c}_+ = (\hat{a} + \hat{b})/\sqrt{2}$; the orthogonal mode $\hat{c}_-$ must be in vacuum to have a dark state. To find the corresponding state of the physical cavity a, one transforms from the $\hat{c}_\pm$ basis to the $\hat{a}/\hat{b}$ basis, and then traces out the state of the auxiliary cavity b.

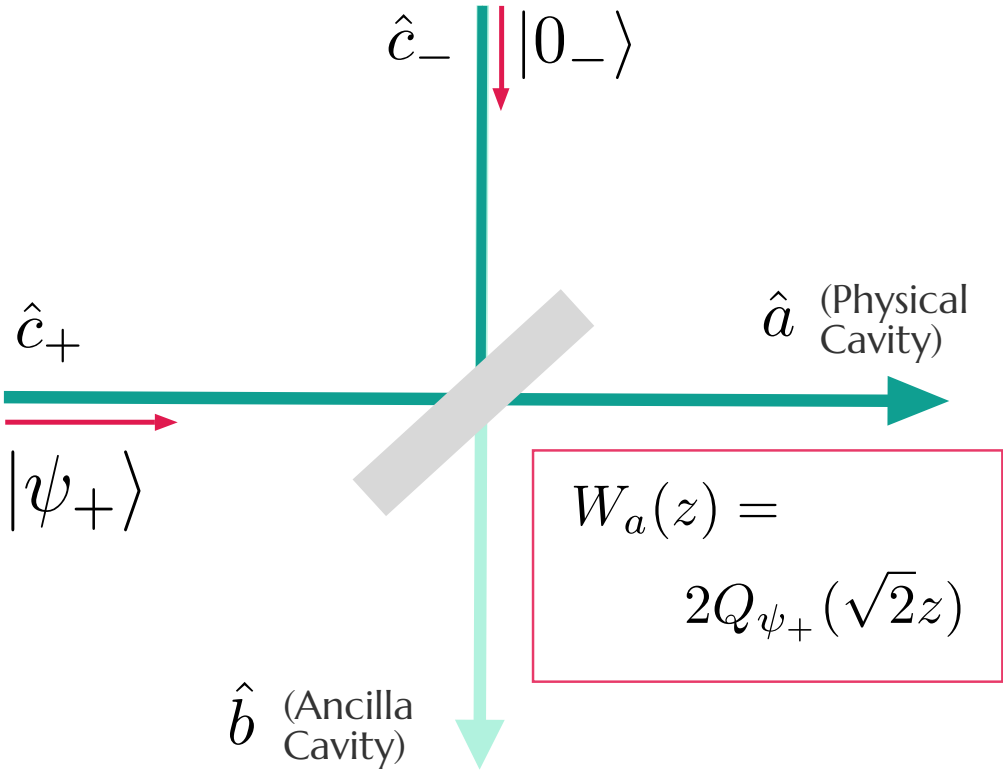

Figure 2.2: Simple picture of the unique steady state of the generalized driven Kerr resonator with non-zero single-photon loss. One starts with a pure state, single-mode wavefunction $|\psi_+\rangle$. This is mixed with vacuum noise at a 50-50 beamsplitter; the output ports represent the final steady state of the physical a cavity and the auxiliary b cavity. This operation implies that the cavity-a steady state is $|\psi_+\rangle$ convolved with vacuum noise. As a result, cavity-a's steady-state Wigner function $W_a(z)$ is equal (up to scaling) to the Q function $Q_{\psi_+}(z)$ of the pure state $|\psi_+\rangle$.

This operation has a very simple physical interpretation (see Fig. 2.2): it corresponds to mixing the state $|\psi_+\rangle$ with vacuum noise at a 50-50 beamsplitter, and then discarding one of the output modes.

At a heuristic level, this operation implies that in phase space, the cavity-a steady state will be equivalent to that of the state $|\psi_+\rangle$ convolved with an extra half-quantum of vacuum noise. Recall that this is the same transformation that converts a Wigner function into a Q-function. As a result, we find a very simple expression for the cavity-a steady state Wigner function. Letting $\psi_{+,\mathrm{SB}}(z)$ denote the SB representation of the pure state $|\psi_+\rangle$, we have:

$$W_a(z) = 2Q_+(\sqrt{2}z) = \frac{2}{\pi}\left|\psi_{+,\mathrm{SB}}\left(\sqrt{2}z^*\right)\right|^2 e^{-2|z|^2} \tag{2.15}$$

We see that the SB "wavefunction" $\psi_{+,\mathrm{SB}}(z)$ has a direct physical interpretation: its modulus determines the cavity-a steady-state Wigner function. We also see that this Wigner function must necessarily be positive (as it is equivalent to the Q-function of the state $|\psi_+\rangle$, and the Q function is always positive). The above relation follows from the fact that Wigner functions transform in the expected way (i.e. like classical probability distributions) under a beamsplitter transformation.

As a simple corollary, one can also obtain strong constraints on the steady-state P-function. Applying the same smoothing and rescaling procedure to the Wigner function of the state $|\psi_+\rangle$ yields an expression for the cavity-a steady-state P-function:

$$P_a(z) = 2W_+(\sqrt{2}z). \tag{2.16}$$

Therefore, the P-function is nonsingular. Furthermore, as a consequence of Hudson's theorem, the P-function is non-positive whenever the pure state $|\psi_+\rangle$ is non-Gaussian. Thus, the cavity-a steady state cannot be interpreted as a statistical mixture of coherent states. Therefore, in the negativity of the P-function, we have a tell-tale signature of nonclassicality.

2.4 CQA solution of the general driven Kerr cavity

We now use the results of Sec. 2.3 to solve Eq. (2.2) for a driven Kerr resonator subject to both one and two photon driving, and one and two-photon loss. This will allow us to reproduce results previously derived using positive-P methods Drummond et al. [1981], Bartolo et al. [2016], Minganti et al. [2016b], Elliott and Ginossar [2016], but in a manner that allows greater physical intuition. We are also able to solve an extended model which includes a three-photon driving term; this model has not been previously solved. Our approach yields several new physical insights: the possibility of photon blockade and "anti-blockade" phenomena, and the possibility of near quantum-bistability without parity conservation. We focus in this section on the case where there is non-zero single-photon loss ($\kappa_1 \neq 0$), implying the existence of a unique steady state. In Sec. 2.7, we turn to the case where there is no single photon driving or loss; we are able to use the CQA method to provide insights into the bistability in this system, and how this changes from quantum to classical bistability with the addition of a drive detuning.

2.4.1 Solution without nonlinear single-photon driving

We are interested in the driven-Kerr system described by Eqs. (2.1) and (2.2) with $\Lambda_3 = 0$ and $\kappa_1 > 0$. The CQA approach represents this system using the equivalent two-cavity cascaded system in Eqs. (2.9) and (2.10). We seek a pure-state steady-state $|\psi\rangle$ that is necessarily dark with respect to dissipation, meaning that Eq. (2.6) is satisfied: $\sqrt{2}\hat{c}_- |\psi\rangle \equiv (\hat{a} - \hat{b}) |\psi\rangle = 0$. Our steady state can thus be written as a tensor product of a non-trivial state of the $\hat{c}_+$ collective mode, and a vacuum state for the $\hat{c}_-$ mode:

$$|\psi\rangle = |\psi_+\rangle |0_-\rangle . \tag{2.17}$$

In order for $|\psi\rangle$ to be a steady state, it also needs to be an eigenstate of the cascaded

Hamiltonian $\hat{H}_{ab}$ with energy E. Writing $\hat{H}_{ab}$ in terms of $\hat{c}_{\pm}$, and using the fact that $\hat{c}_{-}\left|\psi\right\rangle$ vanishes, the eigenvalue equation becomes

$$\frac{1}{2}\hat{c}_{-}^{\dagger}\,\hat{\mathcal{H}}_{+}\left|\psi\right\rangle = E\left|\psi\right\rangle, \tag{2.18}$$

with

$$\hat{\mathcal{H}}_{+} \equiv (K - i\kappa_2)\hat{c}_{+}^{\dagger}\hat{c}_{+}^{2} - (2\Delta + i\kappa_1)\hat{c}_{+} + 2\Lambda_2\hat{c}_{+}^{\dagger} + 2\sqrt{2}\Lambda_1. \tag{2.19}$$

Our choice of the auxiliary-cavity Hamiltonian $\hat{H}_b$ thus leads to a cascaded Hamiltonian that *necessarily* creates an excitation in the $\hat{c}_{-}$ mode. It follows that we must have $E = 0$. Having $\left|\psi\right\rangle$ be a stationary state then reduces to a single mode problem:

$$\hat{\mathcal{H}}_{+}\left|\psi_{+}\right\rangle = 0, \tag{2.20}$$

i.e. we need to find a pure state $\left|\psi_{+}\right\rangle$ that is annihilated by the non-Hermitian operator $\hat{\mathcal{H}}_{+}$.

The seemingly obvious next step is to follow the approach used in Ref. Stannigel et al. [2012b]: express $\left|\psi_{+}\right\rangle$ in the Fock state basis, and turn Eq. (2.20) into a recursion relation for the expansion coefficients α_j:

$$\begin{aligned}\Big[(K - i\kappa_2)m - (2\Delta + i\kappa_1)\Big]\sqrt{m+1}\alpha_{m+1} \\ +2\Lambda_2\sqrt{m}\alpha_{m-1} + 2\sqrt{2}\Lambda_1\alpha_m = 0.\end{aligned} \tag{2.21}$$

In special cases, this reduces to an easily solvable single-term recursion relation: either the case of no two-photon driving $\Lambda_2 = 0$ Stannigel et al. [2012b], or the case of no one-photon driving $\Lambda_1 = 0$ Mamaev [2018]. In the more general case, the resulting two-term recursion relation is more unwieldy.

A more direct way of getting the desired solution is to use the SB representation $\psi_{+,\mathrm{SB}}(z)$

of the state $|\psi_+\rangle$. Eq. (2.20) is then transformed into a second-order ordinary differential equation:

$$\Big[z\frac{\partial^2}{\partial z^2} - D\frac{\partial}{\partial z} + (\lambda_2 z + \lambda_1)\Big]\psi_{+,\mathrm{SB}}(z) = 0, \tag{2.22}$$

where

$$D = \frac{2\widetilde{\Delta}}{\widetilde{K}}, \quad \lambda_2 = \frac{2\Lambda_2}{\widetilde{K}}, \quad \lambda_1 = \frac{2\sqrt{2}\Lambda_1}{\widetilde{K}}. \tag{2.23}$$

Here, $\widetilde{\Delta} \equiv \Delta + i\kappa_1/2$ and $\widetilde{K} \equiv K - i\kappa_2$ are, respectively, effective complex detuning and Kerr nonlinearity parameters.

Without two-photon driving (i.e. $\lambda_2 = 0$), Eq. (2.22) is a standard hypergeometric equation. It has a unique analytic solution:

$$\psi_{+,\mathrm{SB}}(z) = N z^{(D+1)/2} J_{-(D+1)}\left(2\sqrt{\lambda_1 z}\right), \tag{2.24}$$

where $J_n(x)$ is a Bessel function and N is a normalization constant. Using the correspondence between the SB wavefunction and Fock state amplitudes (c.f. Eq. (2.12)), we recover the infinite series result given in Ref. Stannigel et al. [2012b], which in turn corresponds to the classic solution of Ref. Drummond and Walls [1980b]. The closed form we have here has additional virtues. Via Eq. (2.15), it directly yields a closed form expression for the steady-state Wigner function of the physical cavity a; this is in contrast to expressions involving infinite sums that are the usual result of positive-P solutions. Our expression for this case agrees with that derived earlier (via an alternate method) Kheruntsyan [1999].

We turn now to the more interesting case where $\lambda_2 \neq 0$. Eq. (2.21) is now a more nontrivial second-order recursion relation. The SB representation allows us, however, to simplify the system via non-standard transformations. An example is a "non-unitary gauge

transformation"

$$\psi_{+,\mathrm{SB}}(z) \equiv e^{-\theta(z)}\phi(z), \tag{2.25}$$

where $\theta(z)$ is the "gauge potential". This transformation shifts the differentiation operator by the gradient of $\theta(z)$, $\partial_z \mapsto \partial_z - \partial_z\theta(z)$. Here, we try the simplest potential $\theta(z) \equiv \epsilon z$, with ϵ some constant. Note that as θ is not purely imaginary, the resulting transformation on the Hilbert space is non-unitary. In the Fock representation, it is equivalent to acting on the state by the exponential of a raising operator:

$$|\psi_+\rangle \propto e^{-\epsilon\hat{c}_+^\dagger}\,|\phi\rangle\,. \tag{2.26}$$

After our transformation, the problematic two-photon driving term is effectively shifted by an amount ϵ^2:

$$\Big[z\frac{\partial^2}{\partial z^2} - (2\epsilon z + D)\frac{\partial}{\partial z} \\ (\lambda_2 + \epsilon^2)z + (\lambda_1 + \epsilon D)\Big]\phi(z) = 0. \tag{2.27}$$

It can thus be eliminated by choosing ϵ such that

$$\epsilon_\pm = \pm i\sqrt{\lambda_2}. \tag{2.28}$$

We will call these non-unitary gauges *plus*-gauge and *minus*-gauge. Choosing, e.g. the plus gauge $\epsilon \equiv \epsilon_+$, we see that the gauge-transformed state $\phi(z)$ satisfies Kummer's differential equation (see Brychkov), so that:

$$\phi(z) = N_0\Big[{}_1F_1\Big(-\frac{\lambda_1 + \epsilon D}{2\epsilon}; -D; 2\epsilon z\Big)\Big], \tag{2.29}$$

where N_0 is a normalization factor, and ${}_1F_1(r_1; r_2; z)$ is Kummer's hypergeometric function, the same special function which appears in the hydrogen atom problem (see, e.g. Sakurai and Napolitano [2017]). We stress that that the special case where D is a positive integer must be treated specially; this is discussed in Sec. 2.5. Note also that in the $\epsilon \to 0$ limit, the solution above tends smoothly to the Bessel-function solution in Eq. (2.24).

The above result combined with Eq. (2.15) immediately yields a closed-form expression for the steady-state Wigner function of the physical a cavity of interest:

$$W_{a,ss}(z) = N|\phi(\sqrt{2}z^*)|^2\, e^{-2|z+\epsilon/\sqrt{2}|^2}, \tag{2.30}$$

where N is a normalization constant. Note that if $\phi(z) = 1$, then $W_{a,ss}(z)$ corresponds to a coherent state with amplitude $\alpha = \sqrt{-\lambda_2/2}$. Thus, a non-unity $\phi(z)$ describes corrections to the dark state being just a simple coherent state. Note also that if one had chosen the minus gauge in Eq. (2.25), one obtains an identical solution (see Section 2.11).

2.4.2 Including nonlinear single-photon driving

We now allow $\Lambda_3 \neq 0$ in Eq. (2.1). We are still able to exactly solve for the steady state in this case; unless $\kappa_2 = 0$, it has a qualitatively different form from the $\Lambda_3 = 0$ case. The CQA method proceeds as in Sec. 2.4.1. We again write the two-mode dark state as $|\psi\rangle = |\psi_+\rangle|0_-\rangle$, and the eigenvalue equation again reduces to finding the kernel of a non-Hermitian operator $\hat{\mathcal{H}}_+$:

$$\begin{aligned}\hat{\mathcal{H}}_+ = \left(\widetilde{K}\hat{c}_+^\dagger + \sqrt{2}\Lambda_3^*\right)\hat{c}_+^2 + \left(2\sqrt{2}\Lambda_3\hat{c}_+^\dagger - 2\widetilde{\Delta}\right)\hat{c}_+ \\ + \left(2\Lambda_2\hat{c}_+^\dagger + 2\sqrt{2}\Lambda_1\right).\end{aligned} \tag{2.31}$$

Comparing against Eq. (2.19), we see that the presence of Λ_3 creates a term proportional to $\hat{c}_+^2$. Attempting to solve directly for $|\psi_+\rangle$ in the Fock basis leads a complicated recursion

relation, as now we have terms that add a photon ($\propto \hat{c}_+^\dagger$), as well as those that subtract two photons ($\propto \hat{c}_+^2$). One obtains a third-order recursion, in place of the second-order recursion that we had before.

One can nonetheless still solve for the dark state in closed-form. We first perform a displacement,

$$|\xi_+\rangle = \hat{D}(\alpha_+)|\psi_+\rangle, \tag{2.32}$$

where $\alpha_+ = \sqrt{2}\Lambda_3/\widetilde{K}^*$, and $\hat{D}(\alpha) \equiv e^{\alpha\hat{c}_+^\dagger - h.c.}$ is the standard displacement operator. We can then remove the two-photon drive by applying a non-unitary gauge transformation (as before), yielding a differential equation which again has a simple solution in terms of Kummer's confluent hypergeometric function:

$$\phi(z) = N_0\left[{}_1F_1\left(-\frac{\lambda_1 + \epsilon_+ D}{\epsilon_+ - \epsilon_-}; -D; (\epsilon_+ - \epsilon_-)z\right)\right]. \tag{2.33}$$

Here, $\epsilon_\pm$ correspond to the non-unitary gauge choices in which the displaced two-photon drive vanishes (c.f. Eq. (2.28)):

$$\lambda_2 - \lambda_3\epsilon + \epsilon^2 = 0 \tag{2.34}$$

To be manifestly consistent with the solution of the driven Kerr cavity without three-photon terms, we have again written the solution in the *plus* gauge. Finally, $\lambda_3, \lambda_2, \lambda_1, D$ are the

following general complex constants:

$$D = \frac{2}{\widetilde{K}}\left(\widetilde{\Delta} + \frac{2|\Lambda_3|^2}{\widetilde{K}}\right), \tag{2.35}$$

$$\lambda_1 = \frac{\sqrt{2}\Lambda_3}{|\widetilde{K}|^2}\left(\frac{4|\Lambda_3|^2}{\widetilde{K}} + 2\widetilde{\Delta}\right) + \frac{2\sqrt{2}}{\widetilde{K}}\left(\Lambda_1 - \frac{\Lambda_2\Lambda_3^*}{\widetilde{K}}\right), \tag{2.36}$$

$$\lambda_3 = \frac{2\sqrt{2}\Lambda_3}{\widetilde{K}}\left(1 - \frac{\widetilde{K}}{\widetilde{K}^*}\right), \quad \lambda_2 = \frac{2\Lambda_3^2}{|\widetilde{K}|^2}\left(\frac{\widetilde{K}}{\widetilde{K}^*} - 2\right) + \frac{2\Lambda_2}{\widetilde{K}}. \tag{2.37}$$

We have again defined $\tilde{\Delta} = \Delta + i\kappa_1/2$, $\tilde{K} = K - i\kappa_2$. For the case where $\Lambda_3 \to 0$, these parameters revert to those given before Eq. (2.23). Note that for vanishing two-photon loss, $\widetilde{K}$ is real, and hence Eq. (2.37) implies that $\lambda_3 = 0$. In this case, the three photon drive does not give us anything qualitatively new, as it can be completely eliminated by our displacement transformation. In contrast, for non-zero κ_2, three photon driving gives rise to genuinely new phenomena.

As before, the solution above directly determines the steady-state Wigner function of the physical cavity:

$$W_{a,ss}(z - \alpha) = N|\phi(\sqrt{2}z^*)|^2\, e^{-2|z+\epsilon_+/\sqrt{2}|^2}, \tag{2.38}$$

where $\alpha \equiv \alpha_+/\sqrt{2}$, and N is a normalization constant. Note that, if $\lambda_3 \equiv 0$, then the non-unitary gauge choices in Eq. (2.34) satisfy $\epsilon_+ = -\epsilon_-$, and so $\epsilon_+ - \epsilon_- \to 2\epsilon_+$, and we recover the standard solution Eq. (2.30).

2.5 Steady-state phase diagram of the generalized driven Kerr resonator

We now use our exact solutions in Eqs. (2.29) and (2.33) to explore the parameter dependence of the steady state of our generalized driven-dissipative Kerr resonator. The steady-state is

largely controlled by just two dimensionless parameters r_1, r_2. For the usual case $\Lambda_3 = 0$ (no three photon drive), these are:

$$r_1 \equiv \frac{\lambda_1 + \epsilon D}{2\epsilon} = \frac{\Delta + i\frac{\kappa_1}{2}}{K - i\kappa_2} - \frac{i\Lambda_1}{\sqrt{\Lambda_2(K - i\kappa_2)}} \tag{2.39}$$

$$r_2 \equiv D = \frac{2\Delta + i\kappa_1}{K - i\kappa_2}. \tag{2.40}$$

The various drive amplitudes Λ_j enter only through r_1; in contrast, r_2 is a generalized detuning parameter which is independent of drive amplitudes. With a non-zero Λ_3, one has $r_1 = (\lambda_1 + \epsilon_+ D)/(\epsilon_+ - \epsilon_-)$, $r_2 = D$, where $\lambda_1, D, \epsilon_\pm$ are defined in Eqs. (2.34)-(2.37).

As we now show, the steady state exhibits remarkable properties whenever system parameters are tuned to make one or both of r_1, r_2 be non-negative integers (see Fig. 2.3). At these points in parameter space, the solution can exhibit generalized forms of photon blockade and anti-blockade, as well as new kinds of bistability. This latter result generalizes the previously studied cat-state bistability that occurs when $\Lambda_1 = \Delta = \kappa_1 = 0$ (i.e. $r_1 = r_2 = 0$) Mirrahimi et al. [2014b]. We stress that all of these features have clear observable signatures, and are quantum in nature. In what follows, we focus primarily on the standard case $\Lambda_3 = 0$. We also highlight the fact that with a non-zero three-photon drive, the observable consequences of the photon blockade and anti-blockade phenomena can be made even more dramatic.

2.5.1 Basic intuition

Recall that the steady state is determined by a single-mode pure-state $|\psi_+\rangle$ (c.f. Fig. (2.2)), and that further, this state is related to a simpler state $|\phi\rangle$ via a "non-unitary gauge transformation" (c.f. Eq. (2.26)). We could always expand the transformed state $|\phi\rangle$ in the Fock basis as:

$$|\phi\rangle = \sum_{m=0}^{\infty} \beta_m |m\rangle_+ . \tag{2.41}$$

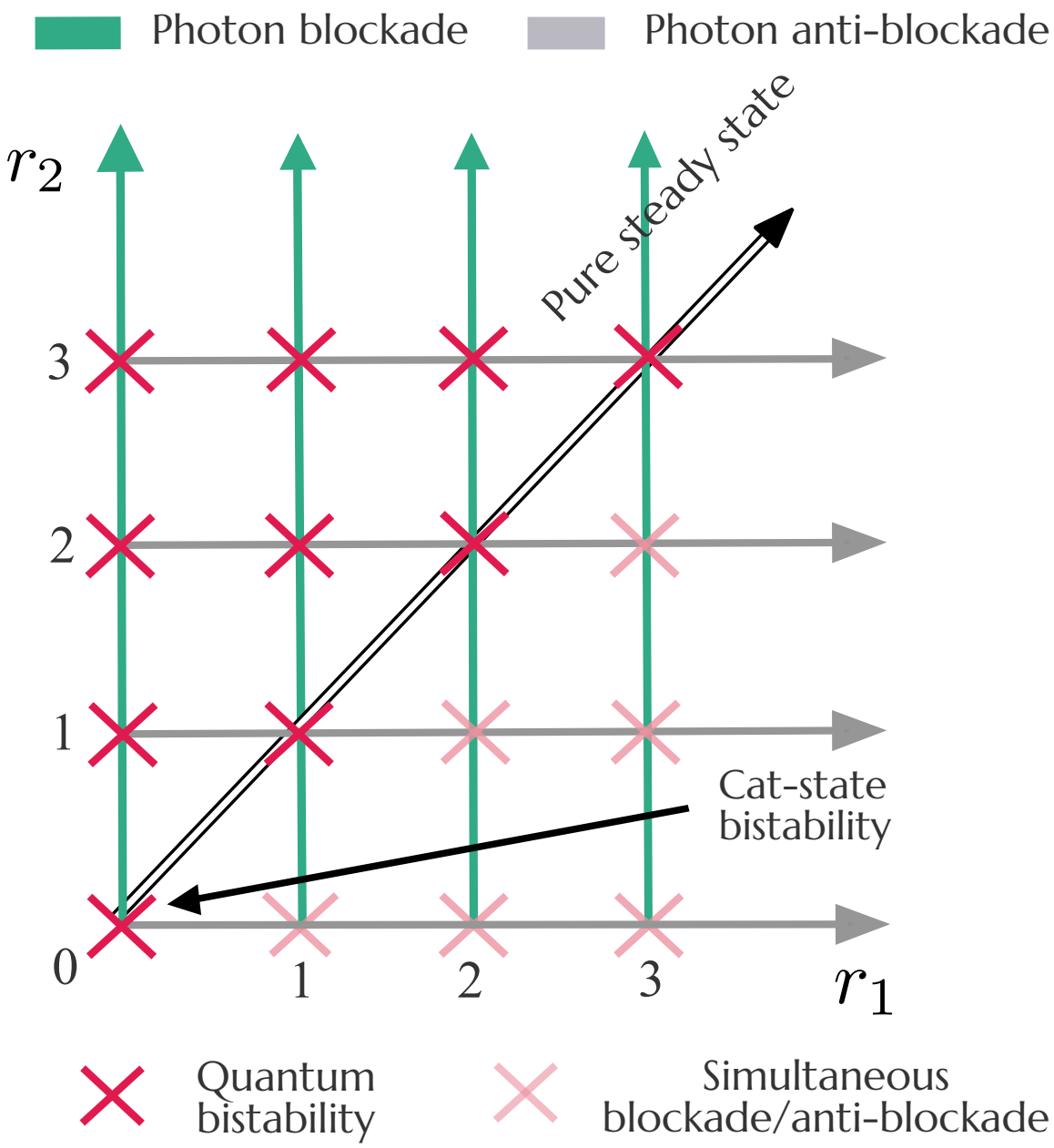

Figure 2.3: Steady-state phase diagram for the generalized, driven-dissipative Kerr resonator. r_2 is a dimensionless detuning parameter, whereas r_1 is a drive-dependent dimensionless parameter; both are defined in Eqs. (2.39)-(2.40). The phase diagram indicates parameter choices that lead to unusual steady states.

Defining the scaled Fock state amplitudes (c.f. Eq. (2.41))

$$c_m = \beta_m \frac{\sqrt{m!}}{(2\epsilon)^m} \tag{2.42}$$

the ODE defining the gauge-transformed state $|\phi\rangle$ in Eq. (2.29) is equivalent to the simple recursion relation ($m \geq 0$)

$$(m - r_2)c_{m+1} = (m - r_1)c_m \tag{2.43}$$

with r_1, r_2 defined in Eqs. (2.39),(2.40). The significance of r_1, r_2 being positive integers is now clear: in this case, there is the possibility of the recursion relation terminating (i.e. vanishing for certain values of m). This termination corresponds to a kind of quantum interference effect, and will be at the heart of the new blockade, anti-blockade and bistability phenomena we describe.

Note that we can directly go from the Fock state structure of $|\phi\rangle$ to the SB wavefunction of the desired, untransformed state $|\psi_+\rangle$. For $\Lambda_3 = 0$ the SB wavefunction of $|\psi_+\rangle$ is

$$\psi_{+,\mathrm{SB}}(z) \propto e^{-\epsilon z} \sum_{m=0}^{\infty} c_m \frac{(2\epsilon z)^m}{m!}, \tag{2.44}$$

with $\epsilon = i\sqrt{\lambda_2}$. For the more general case with non-zero Λ_3, up to a displacement, we have:

$$\psi_{+,\mathrm{SB}}(z) \propto e^{-\epsilon_+ z} \sum_{m=0}^{\infty} c_m \frac{\{(\epsilon_+ - \epsilon_-)z\}^m}{m!} \tag{2.45}$$

where $\epsilon_\pm$ are defined in Eq. (2.34). Recall that these SB wavefunctions directly determine the steady-state Wigner function of the physical cavity via Eq. (2.15).

2.5.2 *Pure unique steady states:* $r_1 = r_2$

The first surprising phenomena we describe is the emergence of unique pure steady states even with nonlinearity. In general, the combination of dissipation and nonlinearity leads us to anticipate impure cavity-a steady states. Surprisingly, there are a range of parameters where the unique steady state of cavity a is a pure coherent state (as would be expected from a damped, linearly-driven, linear cavity). This occurs when parameters are chosen such that $r_1 = r_2$ (without either being a positive integer). In terms of physical parameters, and for $\Lambda_3 = 0$, this requires tuning the one and two photon drives Λ_1, Λ_2 so that:

$$-\frac{\Lambda_1}{\sqrt{-\Lambda_2(K - i\kappa_2)}} = \frac{\Delta + i\frac{\kappa_1}{2}}{K - i\kappa_2} \tag{2.46}$$

For this parameter tuning, Eq. (2.43) implies that all the scaled Fock state amplitudes c_m are identical. This in turn implies from Eq. (2.44) and (2.12) that the the state $|\psi_+\rangle$ is a coherent state with amplitude $\gamma = i\sqrt{2\Lambda_2/(K - i\kappa_2)} = i\sqrt{\lambda_2}$. As sending coherent states through a beamsplitter also generates coherent states at the output, this also implies that the cavity-a steady state is a simple, pure coherent state of amplitude $\gamma/\sqrt{2}$. This follows directly from Eq. (2.44) and the general expression in Eq. (2.15) for the steady-state cavity-a Wigner function. Note that this steady-state coherent state amplitude is consistent with the semiclassical cavity-a equations of motion.

2.5.3 *Higher-order photon blockade:* $r_1 = n_0$

Surprising effects also occur when drives and detuning are chosen so that $r_1 = n_0$, where n_0 is a non-negative integer. The recursion relation in Eq. (2.43) now terminates at $m = n_0$: Fock state amplitudes c_m vanish for all $m \geq n_0 + 1$. This is an example of a generalized strong photon-blockade phenomena: the gauge-transformed steady-state $|\phi\rangle$ has strictly zero probability to have more than n_0 photons. Unlike standard photon blockade Imamoglu et al.

[1997], the mechanism here does not require infinitely strong nonlinearity. Also, unlike the so-called "unconventional" photon blockade Liew and Savona [2010], Bamba et al. [2011], Lemonde et al. [2014], the blockade here is complete: there is strictly no probability to have more than n_0 photons in the state.

While the "gauge-transformed" state $|\phi\rangle$ exhibits blockade, physical phenomena is controlled by the untransformed state $|\psi_+\rangle$. Eq. (2.26) shows that this state is a "smeared" version of the blockaded state. Despite this, the physical cavity a steady state still shows a pronounced suppressed photon population whenever the parameter r_1 is tuned to an integer. This blockade-induced suppression can be observed by considering how the steady state changes as a function of the single photon drive amplitude Λ_1 (as this tunes r_1 but not r_2). From Eq. (2.39), one sees that blockade occurs periodically as a function of Λ_1, with the nth-order blockade occuring when

$$\Lambda_1 \equiv \Lambda_1^{(0)} - in\sqrt{[K - i\kappa_2]\Lambda_2}, \tag{2.47}$$

where $\Lambda_1^{(0)} = -i(\Delta + i\kappa_1/2)(K - i\kappa_2)^{-1}(\Lambda_2/\widetilde{K})^{1/2}$ is a constant offset. Fig. 2.4 shows representative results for $\kappa_2 = \Lambda_3 = 0$: the average cavity photon number shows a sharp suppression whenever Λ_1 is tuned to make r_1 a positive integer. We stress that this is a purely quantum phenomena: the semiclassical solution does not exhibit any such oscillations. We also stress that the width of these blockade suppressions (as a function of Λ_1) are much smaller than κ_1.

The results shown in Fig. 2.4 are for the usual case of no three-photon drive, i.e. $\Lambda_3 = 0$. The situation becomes even more interesting with $\Lambda_2 = 0$. By tuning this drive, the generalized photon blockades associated with $r_1 = n_0$ can be made sharp. The localized nature of the steady state along the classical minima suggests that a simple explanation of these effects is obtained by considering the normally-ordered (Husimi) classical symbol of

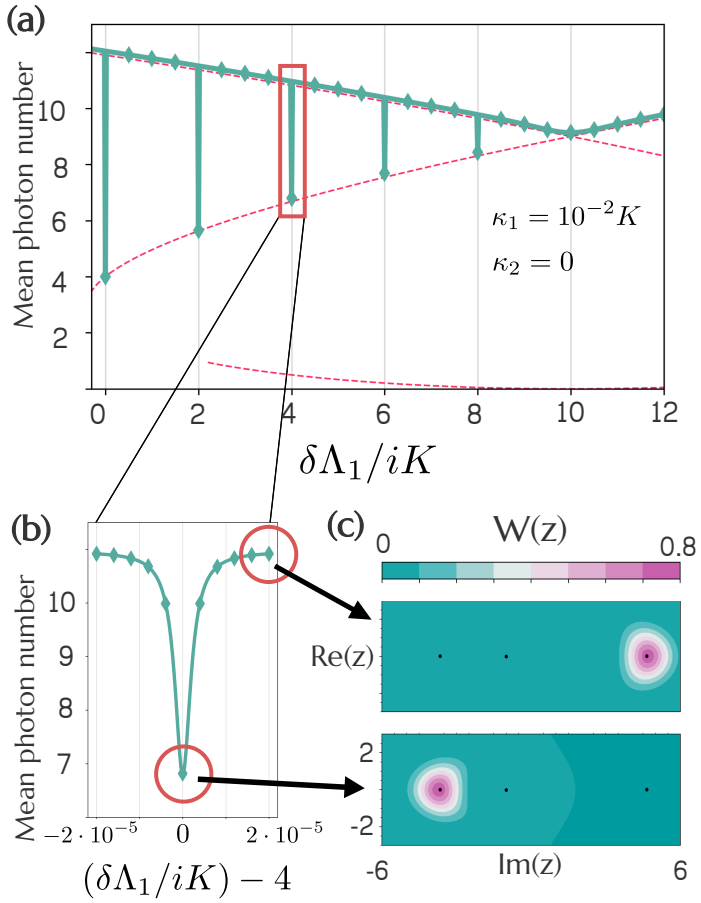

Figure 2.4: Generalized Photon Blockade. (a) Mean steady-state cavity-a photon number as a function of single photon drive Eq. (2.47). The periodic, sharp drop in photon number corresponds to a generalized photon blockade phenomena, which occurs whenever the parameter r_1 (c.f. Eq. (2.39))is a non-negative integer. Solid lines: analytic exact solution, diamonds: master equation numerics. Photon numbers associated with the semiclassical stable amplitudes are also plotted (dashed red lines). (b) Zoom-in of one of the blockade anti-resonances. (c) Steady-state Wigner function, for two choices of $\delta\Lambda_1$ corresponding to being either at (off) a blockaded parameter value; black dots indicate semiclassical amplitudes. For all results, $\Delta = 5K$, $\Lambda_2 = 4K$, $\kappa_1 = 10^{-2}K$, and $\Lambda_3 = \kappa_2 = 0$. By using a non-zero three-photon drive Λ_3, this blockade phenomena can be made sharp (i.e. there is a sharp cutoff in the photon number distribution).

the Hamiltonian, called the *metapotential*:

$$M(z) \equiv \langle z|\hat{H}|z\rangle. \tag{2.48}$$

However, the effects we witness here have nothing to do with the metapotential, as the addition of Λ_1 driving tilts the metapotential in the orthogonal direction to the one containing the two classical minima. Indeed, under a perturbation by Λ_1, the metapotential transforms as

$$M(z) \to M(z) + \delta\Lambda_1 \,\mathrm{Re}\, z. \tag{2.49}$$

Since the minima of the metapotential differ only by the imaginary part of z, this tilt cannot explain this sudden switching behavior. Instead, our effect relies on subtle physics for how the quantum system switches between and populates the different classical steady states Marthaler and Dykman [2006].

Finally, we note that when $r_1 = n_0$, the SB wavefunction for the dark state $|\psi_+\rangle$ (which directly determines the cavity-a Wigner function) reduces to an associated Laguerre polynomial $L_m^{(\alpha)}(z)$:

$$\psi_{+,\mathrm{SB}}(z) \underset{r_1 \to n_0}{\propto} e^{-\epsilon z} L_{n_0}^{(1-D)}\left(2\epsilon z\right), \tag{2.50}$$

where for $\Lambda_3 = 0$, we have $\epsilon = i\sqrt{\lambda_2}$.

2.5.4 Photon blockade: physical intuition

We now describe the generalized photon blockade at a more basic and intuitive level. In terms of the displacement parameter $\alpha_+ = \sqrt{2}\Lambda_3/\widetilde{K}^*$, recall that we must displace the dark

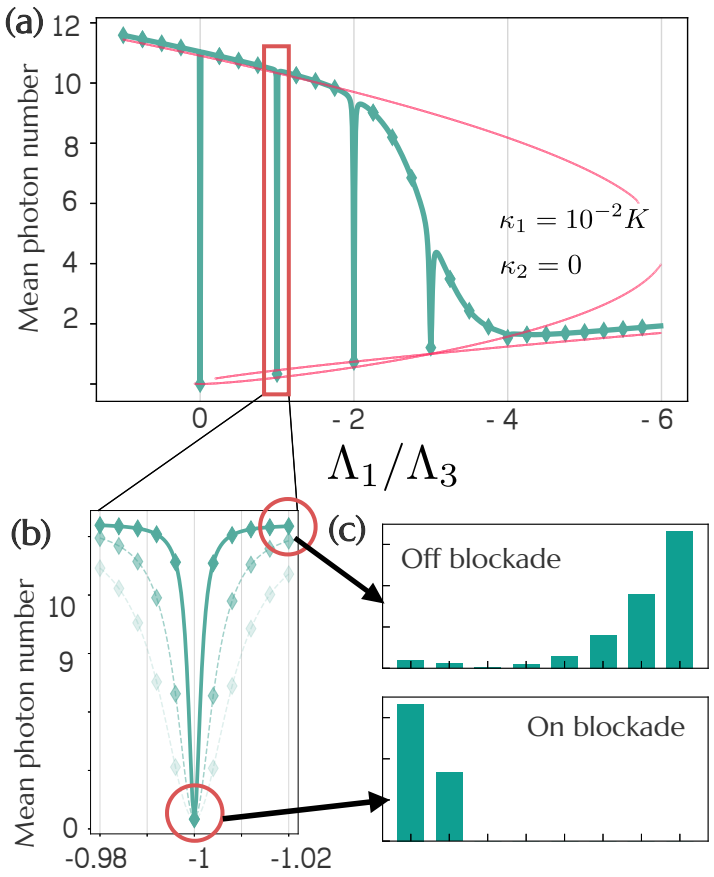

Figure 2.5: Generalized Photon Blockade. (a) Mean steady-state cavity-a photon number as a function of single photon drive $\delta\Lambda_1 \equiv \Lambda_1 - \Lambda_1^{(0)}$, where the offset $\Lambda_1^{(0)} = (0.01 - 10i) \cdot K$ is defined in Eq. (2.47). The periodic, sharp drop in photon number corresponds to a generalized photon blockade phenomena, which occurs whenever the parameter r_1 (c.f. Eq. (2.39))is a non-negative integer. Solid lines: analytic exact solution, diamonds: master equation numerics. Photon numbers associated with the semiclassical stable amplitudes are also plotted (dashed red lines). (b) Zoom-in of one of the blockade anti-resonances. (c) Steady-state Wigner function, for two choices of $\delta\Lambda_1$ corresponding to being either at (off) a blockaded parameter value; black dots indicate semiclassical amplitudes. For all results, $\Delta = 5K$, $\Lambda_2 = 4K$, $\kappa_1 = 10^{-2}K$, and $\Lambda_3 = \kappa_2 = 0$. By using a non-zero three-photon drive Λ_3, this blockade phenomena can be made sharp (i.e. there is a sharp cutoff in the photon number distribution).

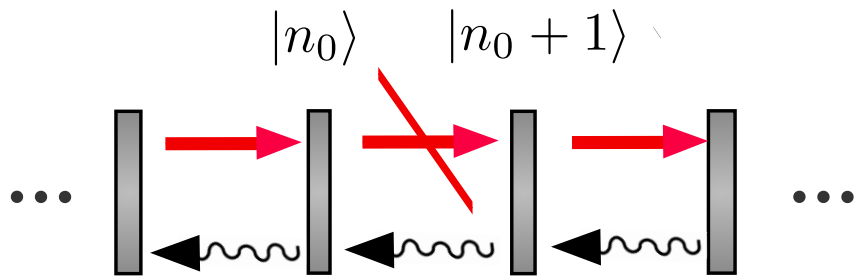

Figure 2.6: Drive-interference causes generalized photon blockade. By adding a nonlinear one-photon drive with the right strength, one can trap the steady-state in a low-photon-number subspace. This blockade phenomenon persists for arbitrarily weak nonlinearity $\Lambda_3 \to 0$.

state to obtain a closed-form solution:

$$|\psi_+\rangle = \hat{D}(\alpha_+)e^{-\epsilon_+\hat{c}_+^\dagger}|\phi\rangle \tag{2.51}$$

where $|\phi\rangle$ is the core state defined in Eq. (2.41). The photon blockade phenomenon is best intuitively understood when there is nonlinear one-photon driving, but no two-photon driving. In the limit that Λ_2 vanishes, $\alpha_+ \to -\epsilon_+$, meaning that, after direct application of the Baker-Campbell Hausdorff identity, the displacement transformation partially cancels the exponential factor:

$$\psi_{+,\mathrm{SB}}(z) \underset{\Lambda_2\to 0}{\sim} \phi_{\mathrm{SB}}(z+\alpha_+) \tag{2.52}$$

where ϕ_{SB} is the Segal-Bargmann representation of the core state defined in Eq. (2.41). Therefore, we see that the $\Lambda_2 \to 0$ is physically important because it removes the smearing factors that spoil the bare physics contained in the state $|\phi\rangle$. Furthermore, in this limit,

$$r_1 \underset{\Lambda_2\to 0}{\sim} -\Lambda_1/\Lambda_3, \tag{2.53}$$

and so a photon blockade occurs each time the ratio of nonlinear to linear one-photon driving

is a negative integer. Indeed, we see that, in this limit, photon blockade results from the destructive interference between linear and nonlinear one-photon driving. In this limit, we can express the Hamiltonian as

$$\begin{aligned}\hat{H} = &\frac{K}{2}\hat{a}^\dagger\hat{a}^\dagger\hat{a}\hat{a} - \Delta\hat{a}^\dagger\hat{a} \\ &+ \Lambda_3(\hat{n} - r_1)\hat{a}^\dagger + \Lambda_3^*\hat{a}(\hat{n} - r_1^*)\end{aligned} \tag{2.54}$$

Therefore, at a blockade $r_1 = n_0$, we can define a *blockaded subspace*, which is the linear span of all Fock states up to $|n_0\rangle$, e.g. consisting of states of the form

$$|\psi\rangle = \sum_{n=0}^{n_0} c_n|n\rangle. \tag{2.55}$$

In particular, when r_1 is tuned to a non-negative integer n_0, the matrix elements of the Hamiltonian Eq. (2.54) connecting states of photon number n_0 or less with those of photon number equal to $n_0 + 1$ or greater vanish, "trapping" the quantum dissipative dynamics in this subspace, as there is no process (dissipative or coherent) in this case that can add photons to the resonator beyond the cutoff (see Figure 2.6). As a consequence, the steady state $\hat{\rho}_{ss}$ of the resonator is constrained to lie in the blockaded subspace.

Exact blockade with weak nonlinearity

As it turns out, contrary to many other schemes involving nonlinear elements (such as qubits), it is possible to realize this generalized photon blockade without strong nonlinearity. We examine the case $n_0 = 1$. In the simplest case $\Delta = 0$, in the absence of any nonlinearity (except for the driving), the steady state depends only on a single dimenionless parameter $\Lambda \equiv \Lambda_3/\kappa_1$, and is the following impure state in the subspace spanned by the Fock states

$|0\rangle$ and $|1\rangle$:

$$\hat{\rho}_{\rm ss} = \frac{1}{8\Lambda^2+1}\begin{pmatrix} 4\Lambda^2+1 & -2i\Lambda \\ 2i\Lambda & 4\Lambda^2 \end{pmatrix} \tag{2.56}$$

For extremely weak nonlinearity/interactions $\Lambda \to 0$, the cutoff is still exact. From a basic Taylor expansion of the resonator steady state Eq. (2.56) in powers of the nonlinearity Λ, we see that a nontrivial one-photon population appears at second order. In Section 2.9, we show how the state Eq. (2.56) is easily dissipatively stabilized using the SNAIL circuit QED architecture. Generalized photon blockade may have applications in quantum information settings where nonlinearity is a limited resource.

2.5.5 Photon anti-blockade: $r_2 = m_0$

Tuning the parameter r_2 to be an integer m_0 in the recurrence relation Eq. (2.43) also results in unusual behaviour of our dark states. For zero-dissipation, $r_2 = m_0$ is simply the condition for the Fock states $n = 0$ and $n = m_0$ of our physical a cavity to be degenerate in the absence of any driving (i.e. the detuning and Kerr terms cancel out) Bartolo et al. [2016]. Our exact solution shows that this resonance condition has strong consequences even with dissipation and drive. When $r_2 = m_0$, the only solution to the recurrence relation has the coefficients c_1 through c_{m_0} be exactly zero. This implies that the gauge-transformed dark state in Eq. (2.41) will have strictly zero probability to have a photon number equal to m_0 or smaller (while higher Fock states will be occupied). We call this phenomenon a photon "anti-blockade". As with the photon-blockade phenomena, this will also have implications for our physical cavity, via Eq. (2.26).

For any non-zero amount of dissipation, it is clear from Eq. (2.40) that we can never have r_2 exactly be a positive integer (as $\kappa_1, \kappa_2 \geq 0$). This remains true even in the presence of a three-photon drive, where $r_2 = D$, with D given by Eq. (2.35). Nonetheless, for weak

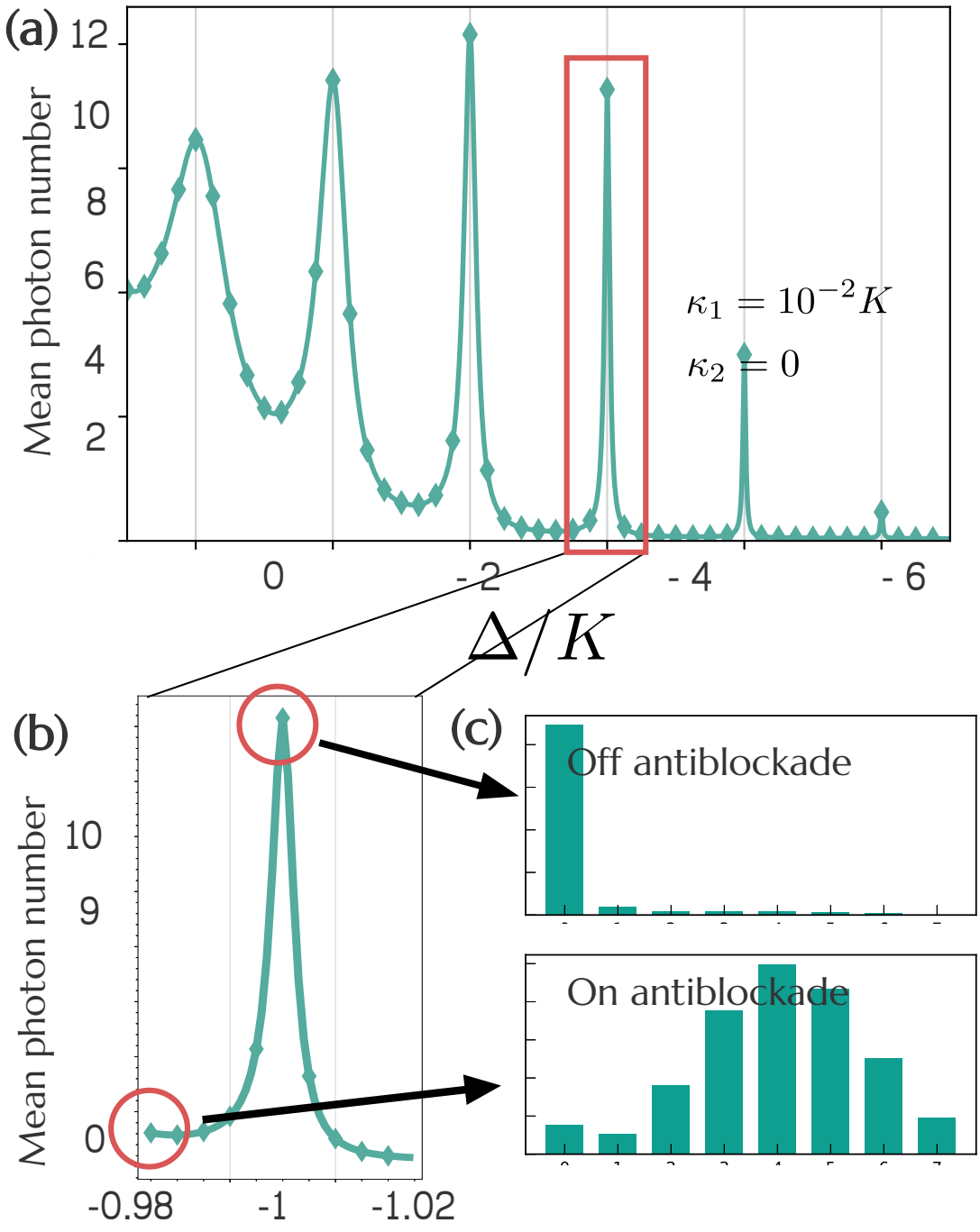

Figure 2.7: Photon anti-blockade. Average cavity-a steady-state photon number as a function of drive detuning Δ, with drive amplitudes fixed at $\Lambda_1 = \Lambda_2 = K/2$, $\Lambda_3 = 0$. Resonances here correspond to having tuned the parameter r_2 (c.f. Eq. (2.40)) to be near a non-negative integer. Other parameters are $\kappa_1 = 0.01K$, $\kappa_2 = 0$.

dissipation (namely $\kappa_1 \ll \Delta$, $\kappa_2 \ll K$), one can still tune r_2 to be extremely close to an integer. In this regime, one still has strong signatures of the anti-blockade behaviour. For the physical cavity a, this translates into a kind of resonant enhancement of photon number and skewed photon number statistics. Representative behaviour is shown in Fig. 2.7. Note that this resonance phenomena was observed in Ref. Bartolo et al. [2016], though connections to photon statistics and the properties of the analytic steady-state solution were not discussed.

2.5.6 Simultaneous/coexisting blockade and anti-blockade

What if r_1, r_2 are both non-negative integers, and $r_2 < r_1$? In this case, neither the photon-blockaded *nor* the photon-resonant solution is permitted. Instead, a *medium*-photon number solution exists, and serves as the unique dark state. For $\Lambda_3 = 0$, we have

$$\psi_{+,\mathrm{SB}}(z) = \frac{e^{-\epsilon z}}{N^{1/2}} \sum_{r_2+1}^{r_1} c_m \frac{(2\epsilon z)^m}{m!} \tag{2.57}$$

with $\epsilon \equiv i\sqrt{\lambda_2}$. Without the exponential prefactor, this state would exhibit both photon blockade and anti-blockade (i.e. the its photon number distribution is cut-off at small and large photon numbers).

2.5.7 Generalized bistability: $(r_1, r_2) = (n_1, n_2)$

Having understood photon blockade and anti-blockade phenomena, the natural remaining case is when both these phenomena coexist. This occurs when parameters are chosen so that $(r_1, r_2) = (n_1, n_2)$, where $n_2 \geq n_1$ are both non-negative integers. Eq. (2.43) then yields *both* a photon-blockaded solution, and a distinct anti-blockaded solution. These correspond

to two distinct dark states of the + mode, described respectively by SB wavefunctions:

$$\psi_{1,\mathrm{SB}}(z) = \frac{e^{-\epsilon z}}{N_1^{1/2}} \sum_{m=0}^{r_1} \frac{c_m (2\epsilon z)^m}{m!}, \tag{2.58}$$

$$\psi_{2,\mathrm{SB}}(z) = \frac{e^{-\epsilon z}}{N_2^{1/2}} \sum_{m=r_2+1}^{\infty} \frac{c_m (2\epsilon z)^m}{m!}. \tag{2.59}$$

Any linear combination of these solutions is also a dark steady-state. We refer to this situation as "quantum bistability": the extended, two-cavity cascaded system in Fig. 2.1(b) has an infinite number of steady states, corresponding to any superposition state of the form:

$$\left|\tilde{\psi}[a_1, a_2]\right\rangle = a_1 \left|\psi_1\right\rangle_+ \left|0\right\rangle_- + a_2 \left|\psi_2\right\rangle_+ \left|0\right\rangle_- \tag{2.60}$$

This also implies multi-stability for the physical a cavity, which exhibits a two-parameter continuous family of steady states,

$$\hat{\rho}_{a,\mathrm{ss}} = \mathrm{tr}_b \left[\left|\tilde{\psi}[a_1, a_2]\right\rangle \left\langle\tilde{\psi}[a_1, a_2]\right|\right]. \tag{2.61}$$

The upshot is that the generalized driven-dissipative Kerr cavity has a multitude of distinct parameter points that yield multi-stability, despite any obvious symmetry.

Unfortunately, we have the same issue as with the anti-blockade phenomena: non-zero dissipation makes it impossible to exactly tune to bistable parameter values *except* for the case $n_1 = n_2 = 0$. This is because the constraint of having one or both of κ_1, κ_2 be positive implies r_2 cannot be exactly equal to a positive integer (c.f. Eq. (2.40)). The only exactly-achievable bistable point is the case $n_1 = n_2 = 0$, which can be reached if $\kappa_1 = 0, \kappa_2 > 0$. This parameter point corresponds to the well-studied cat-state bistability in a two-photon driven Kerr resonator Wolinsky and Carmichael [1988a].

Despite these caveats, the new bistable points are physically relevant: for weak dissipation, one can come arbitrarily close to them in parameter space, with striking observable

consequences for the steady state. We explore this further in the next section. We also discuss in Section 2.8 how one can *exactly* achieve the physics of these new bistable points using a non-cascaded version of the two cavity setup depicted in Fig. 2.1(b).

2.6 Consequences of new quantum bistable points

As discussed in the previous section, there are an infinite number of points in parameter space where our generalized driven-dissipative Kerr resonator is *almost* quantum bistable (c.f. Fig. 2.3). With non-zero one-photon loss, one cannot exactly achieve the required parameter tuning for bistability, but one can come arbitrarily close to a given bistable parameter point. In this section, we explore the physical consequences of this near-bistability. We show that there is an extremely strong sensitivity to small parameter changes when one is in this near-bistable regime, and that the unique steady state can be understood as "picking-out" a unique state from the bistable manifold in Eq. (2.61).

Suppose we chose parameters that result in (r_1, r_2) being close to integers (n_1, n_2):

$$r_1 = n_1 + \delta r_1, \qquad r_2 = n_2 + \delta r_2, \tag{2.62}$$

These small deviations kill the bistability. However, for small δr_j the resulting pure steady state of the + mode is a particular linear combination of the states $\phi_j(z)$ that span the bistable manifold at $\delta r_j = 0$. Moreover, the precise form of this combination is *extremely* sensitive to parameter variations.

For example, consider the simple case where the unperturbed recursion parameters are $(r_1, r_2) = (n, n)$. In this case, the recursion relation Eq. (2.43) simplifies to

$$c_{m+1} = \frac{(m-n) - \delta r_1}{(m-n) - \delta r_2} c_m. \tag{2.63}$$

In the regime that $\delta r_1, \delta r_2 \ll 1$, we can see that the ratio c_{m+1}/c_m is essentially 1, except

for the ratio $c_{n+1}/c_n = \delta r_1/\delta r_2$. Therefore, as $\delta r_1, \delta r_2 \to 0$, the unique steady state solution (i.e. solution to the recursion relation) has the limiting form

$$\psi_{+,\mathrm{SB}}(z) \underset{\delta r_1,\delta r_2\to 0}{\sim} \psi_{1,\mathrm{SB}}(z) + \frac{\delta r_1}{\delta r_2}\psi_{2,\mathrm{SB}}(z) \tag{2.64}$$

as a superposition of the bistable solutions given in Eqs. (2.58),(2.59). Note that in writing this equation, we must pick the overall phase of $\psi_{2,\mathrm{SB}}$ such that the ratio between c_{n+1} (appearing in $\psi_{2,\mathrm{SB}}$) and c_n (appearing in $\psi_{1,\mathrm{SB}}$) is precisely $\delta r_1/\delta r_2$.

As a result, the unique steady state Wigner function of the physical a cavity will be:

$$W_{a,ss}(z) \simeq \frac{e^{-2|z|^2}}{N}\left|\psi_{1,\mathrm{SB}}(\sqrt{2}z^*) + \frac{\delta r_1}{\delta r_2}\cdot\psi_{2,\mathrm{SB}}(\sqrt{2}z^*)\right|^2. \tag{2.65}$$

This equation is the crucial result of this subsection: for parameters that bring us close to a quantum bistable point, it provides a simple way to understand the system's steady state and its extreme sensitivity to small parameter changes.

2.6.1 Cat-state bistability: $(r_1, r_2) = (0, 0)$

The simplest bistable point is where $r_1 = r_2 = 0$. From Eqs. (2.39),(2.40), we see that this requires there to be no single photon drive or loss, nor any detuning: $\Lambda_1 = \Delta = \kappa_1 = 0$. This corresponds to the well-known quantum bistability that occurs in a two-photon driven Kerr resonator Goto [2016], Puri et al. [2017], Grimm et al. [2019], a system where photon number parity is conserved. The two distinct solutions to the recurrence relation in Eq. (2.43) are $c_j = \delta_{j,0}$ and $c_j = 1 - \delta_{j,0}$ (c.f. Eqs. (2.58)-(2.59)). This corresponds to two distinct dark

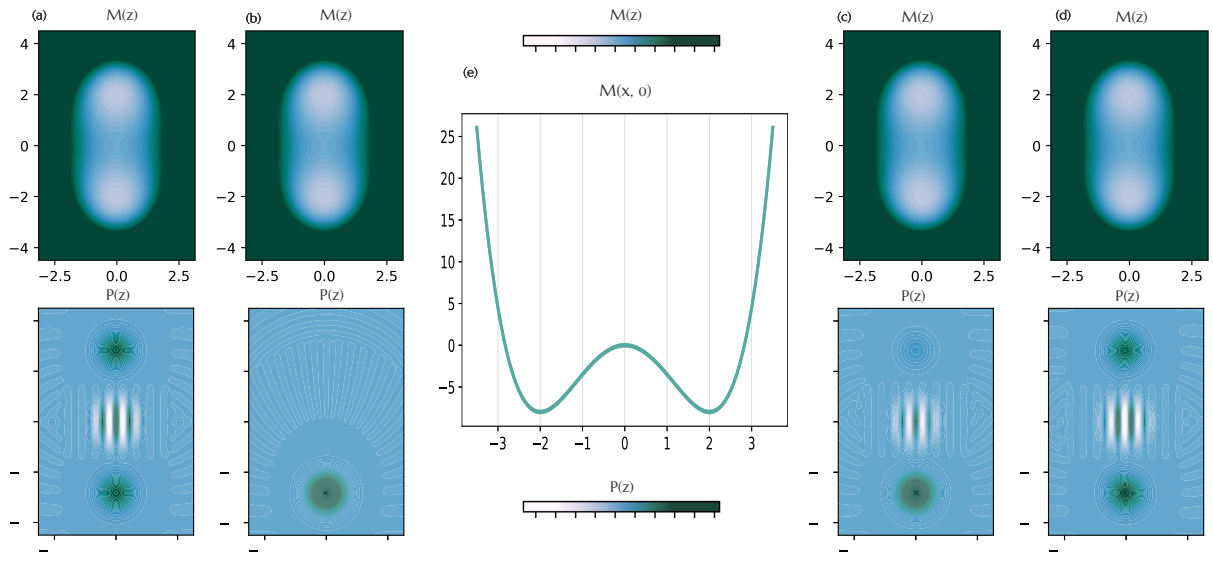

Figure 2.8: Quasi-bistability without engineered dissipation: $(r_1, r_2) = (0, 0)$ bistable point. Steady-state P-function for increasing single-photon drive amplitude Λ_1: (a) $\Lambda_1 = 0$, (b), $\Lambda_1 = 0.01K$, (c) $\Lambda_1 = 0.02K$, and (d) $\Lambda_1 = 0.1K$. For all plots, $\Lambda_3 = \Delta = \kappa_2 = 0$, $\kappa_1 = 10^{-2}K$, and $\Lambda_2 = 4K$. By tuning the single-photon drive amplitude Λ_1, one can pick out a particular state in the "bistable" manifold by tuning the parameter Q, c.f. Eq. (2.71)). Note the strong non-classicality exhibited by the steady-state P-function near these bistable points.

states for the + mode, with SB wavefunctions

$$\psi_{1,\mathrm{SB}}(z) = e^{-\epsilon z} \tag{2.66}$$

$$\psi_{2,\mathrm{SB}}(z) = e^{\epsilon z} - e^{-\epsilon z} \tag{2.67}$$

$\psi_{1,\mathrm{SB}}(z)$ corresponds to a coherent state with amplitude $\epsilon \equiv i\sqrt{\lambda_2}$, whereas $\psi_{2,\mathrm{SB}}(z)$ corresponds to an odd cat state (odd superposition of coherent states with amplitude ϵ). Note that we have picked the global phase of $\psi_{2,\mathrm{SB}}$ to be compatible with Eq. (2.65).

We thus have a direct connection between this parity-based bistability and the photon blockade and anti-blockade discussed above: bistability corresponds to both these phenomena occurring simultaneously. As always, any amount of single-photon loss will kill the bistability and yield a unique steady state (though relaxation to this state could be extremely slow). Our approach gives a simple way to understand the unique steady state when there is weak single photon loss, and possibly other weak perturbations (such as single photon driving and/or a detuning). These imperfections cause a shift in the recursion parameters away from $\delta r_1 = \delta r_2 = 0$:

$$\delta r_2 = \frac{2\Delta + i\kappa_1}{K - i\kappa_2} \tag{2.68}$$

$$\delta r_1 = \frac{\delta r_2}{2} - \frac{i\Lambda_1}{\sqrt{\Lambda_2(K - i\kappa_2)}} \tag{2.69}$$

For small imperfections, we can then use Eq. (2.65) to give us the steady-state SB wavefunction:

$$\psi_{+,\mathrm{SB}}(z) = N\left[(1+Q)e^{-\epsilon z} + (1-Q)e^{\epsilon z})\right], \tag{2.70}$$

where N is a normalization constant, and

$$Q = \sqrt{\frac{K - i\kappa_2}{\Lambda_2/4}} \frac{i\Lambda_1}{2\Delta + i\kappa_1}. \tag{2.71}$$

Eq. (2.70) directly gives us the Wigner function of the unique steady state via Eq. (2.15). Each term in Eq. (2.70) on its own corresponds to a simple coherent state (amplitudes $\pm\epsilon \equiv \pm i\sqrt{\lambda_2}$); thus, in general we have a steady state that is an incoherent mixture of two coherent states. This equation also reveals something surprising: the localization of the steady state in phase space is a non-monotonic function of Λ_1. The state is delocalized both for $\Lambda_1 = 0$, and for Λ_1 large enough to make $Q \gg 1$. Representative results are shown in Figure 2.8. Again, we stress that in Fig. 2.8, the single photon drive is orthogonal to the axes separating the two potential wells, hence it does not simply tilt the potential to favour one well versus the other. Hence, there is no simple metapotential picture.

2.6.2 Quantum bistability with a single photon drive: $(r_1, r_2) = (n, n)$

A more surprising regime of near bistability is when the recursion parameters are both tuned to be close to the same positive integer, i.e. $(r_1, r_2) \simeq (n, n)$. As discussed, for an exact tuning to this point, the expanded system exhibits quantum bistability. There are two orthogonal solutions to the recurrence relations, given by $c_j = \sum_{k=1}^{n} \delta_{j,k}$ and $c_j = \sum_{k=1}^{n}(1 - \delta_{j,k})$ (c.f. Eq. (2.58-2.59)). These in turn correspond to two distinct +-mode states

$$\psi_{1,\mathrm{SB}}(z) = N_1 e^{-\epsilon z}\, \Gamma(n+1, 2\epsilon z) \tag{2.72}$$

$$\psi_{2,\mathrm{SB}}(z) = N_2 e^{-\epsilon z} \left(1 - \frac{\Gamma(n+1, 2\epsilon z)}{\Gamma(n+1)}\right) \tag{2.73}$$

where $\Gamma(r, z) \equiv \int_z^\infty t^{r-1} e^{-t} dt$ is the incomplete Gamma function.

In the absence of any loss, tuning $r_1 = r_2 = n$ requires a detuning $\Delta = n/2K$ and a single photon drive $\Lambda_1 = -i(n/2)\sqrt{\Lambda_2 K}$. If we now include single photon loss (but keep $\kappa_2 = 0$), and also shift Λ_1 slightly from the above value, the recurrence parameters are slightly shifted as well:

$$r_1 = n + \frac{i\kappa_1}{2K} \equiv n + \delta r_1 \tag{2.74}$$

$$r_2 = n + \frac{i\kappa_1}{4K} - i\frac{\delta\Lambda_1}{\sqrt{K\Lambda_2}} \equiv n + \delta r_2 \tag{2.75}$$

Hence, via Eq. (2.65), by slightly varying the one photon drive amplitude, one can pick out completely different linear combinations of the two different bistable states as the single unique steady state. This leads to an extreme sensitivity of the final state to small changes in Λ_1. Note that by picking parameters so that $\delta r_1 = \delta r_2$, the steady state becomes a coherent state with amplitude $\gamma = \sqrt{-\Lambda_2/K}$, whereas if $\delta r_1 = 0$, it has a bimodal form. Should we make a figure for this? I was thinking of maybe replacing Fig. 7 with the same exact data, except gathered from the $(r_1, r_2) = (4, 4)$ bistable point, instead of the already well-known $(r_1, r_2) = (0, 0)$ bistable point.

2.6.3 Metastability due to proximal quantum bistability

Tuning parameters to be close to a quantum bistable point also has consequences for dynamics. The characteristic decay rates of the system correspond to the non-zero eigenvalues of the Liouvillian $\mathcal{L}_0$ (c.f. Eq. (2.2)). We find that tuning to a regime of near-bistability gives rise to an extremely slow population-decay mode, and also a clear dissipative gap separating the rate of this slow-mode from other decay modes. Formally, if we let γ_j denote the decay modes of the Liouvillian (i.e. negative real parts of the eigenvalues of $\mathcal{L}_0$), and order rates

such that $\gamma_1 \leq \gamma_2 \leq ....$, then in near-bistable regimes:

$$\gamma_1 \ll \kappa_1, \quad \gamma_2 \gg \gamma_1 \tag{2.76}$$

Note that this hierarchy of dissipative rates has already been described for the more familiar $(r_1, r_2) = (0, 0)$ "cat-state" bistable point Puri et al. [2017]; we show that this is also true for our new bistable points. An exact description of this dynamical behaviour is outside the scope of the CQA method. It can however be studied numerically. Representative behavior of a driven Kerr cavity whose parameters are close to either the $(r_1, r_2) = (2, 2)$ or $(4, 4)$ bistable points are shown in Fig. 2.9(a).

For near-bistable parameters, the CQA approach provides insight into the nature of the slow decay mode of $\mathcal{L}_0$. As one might expect, this mode corresponds to slow relaxation within the bistable manifold of states. To make this precise, recall that if one tuned exactly to a bistable parameter point, cavity-a has a continuous three-parameter family of possible steady states corresponding to Eq. (2.61) (and incoherent mixtures of these states). Density matrices in this bistable manifold lie in the span of the four operators $(i, j = 1, 2)$:

$$\hat{M}_{ij} = \mathrm{tr}_b \left[\left(|\psi_i\rangle \langle \psi_j| \right)_+ (|0\rangle \langle 0|)_- \right] \tag{2.77}$$

By Section 2.10, these operators have Wigner transforms

$$W_{ij}(z) = N \psi_{i,\mathrm{SB}}(\sqrt{2}z^*) \psi^*_{j,\mathrm{SB}}(\sqrt{2}z^*) e^{-2|z|^2} \tag{2.78}$$

with N a normalization constant.

The slow mode (rate γ_1) has an associated right eigenvector $\hat{M}_{\mathrm{slow}}$, i.e. $\mathcal{L}_0 \hat{M}_{\mathrm{slow}} = -\gamma_1 \hat{M}_{\mathrm{slow}}$. If the slow dynamics is entirely in the bistable manifold, then $\hat{M}_{\mathrm{slow}}$ should lie completely within the span of the $\hat{M}_{ij}$. To see whether this is the case, we pick parameters

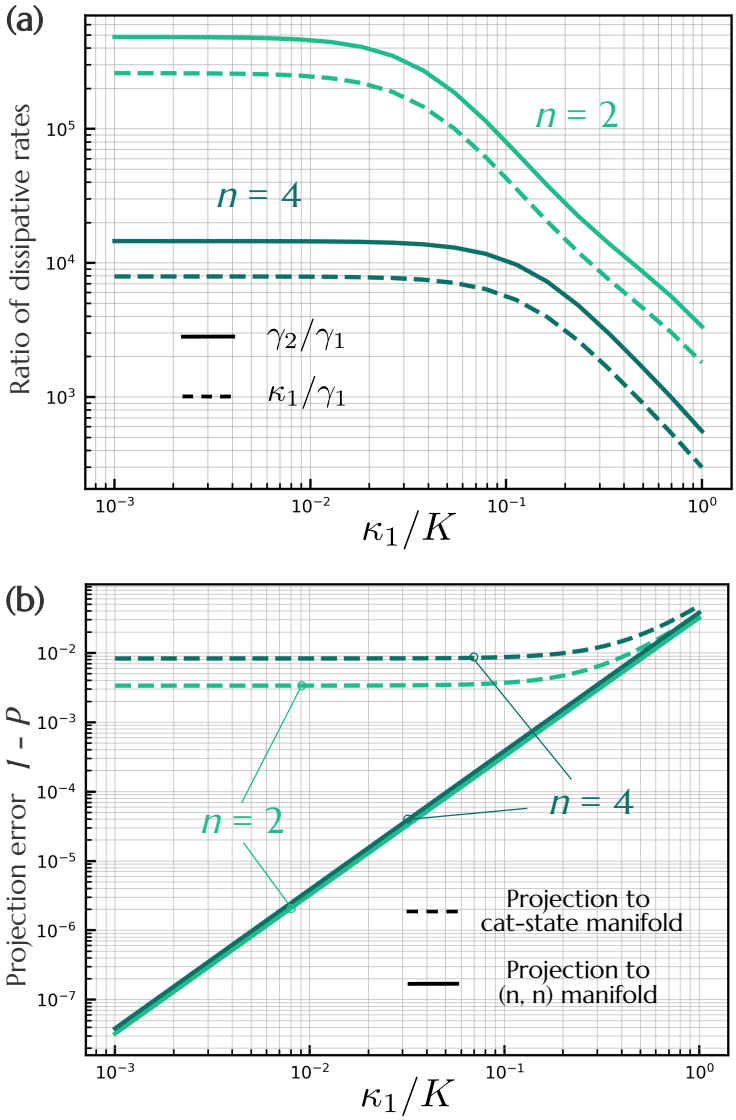

Figure 2.9: Slow dynamics near generalized bistable regimes. (a) Solid line: ratio of the two smallest relaxation rates (i.e. dissipative rates of the system Liouvillian $\mathcal{L}_0$), as a function of κ_1. Dashed line: κ_1/γ_1. $\kappa_1 \to 0$ corresponds to being at a bistable parameter point $(r_1, r_2) = (n, n)$, either $n = 2$ (light green) or $n = 4$ (dark green). Parameters are $\Lambda_2 = 6K$, $\Lambda_3 = \kappa_2 = 0$, $\Delta = nK/2$, and $\Lambda_1 = -in\sqrt{\Lambda_2}/2$. One sees that the slow rate γ_1 is much slower than κ_1, and that there is a pronounced dissipative gap. (b) Solid line: The measure $1 - P$ (c.f. Eq. (2.79)) of how closely the slowest system decay mode (with rate γ_1) corresponds to dynamics in the bistable manifold. Dashed lines: same, but measuring how closely this mode is described by coherent states centered at the semiclassical stable amplitudes. One clearly sees that the bistable manifold gives a far better description. Same parameters as in (a).

for near-bistability, and numerically calculate the Hilbert-Schmidt norm P of the projection of the slow mode onto the bistable subspace:

$$P \equiv \sum_{i,j=1,2} |\mathrm{Tr}[\widetilde{M}_{ij}^{\dagger} \hat{M}_{\mathrm{slow}}]|^2 \tag{2.79}$$

Here $\widetilde{M}_{ij}$ is an orthonormal basis for the span of $\hat{M}_{ij}$ (obtained via the standard Gram-Schmidt process). As $0 \leq P \leq 1$, the quantity $1 - P$ measures how much of the slow mode's dynamics lies outside the bistable manifold.

Representative results for $1 - P$ are shown in Fig. 2.9(b). One sees that for small κ_1 (i.e. when one is close to the bistable point), the slow mode is almost entirely described by the bistable state manifold. For comparison, we have also tried to describe the slow mode in terms of simple coherent states centered at the expected classical bistable steady-state amplitudes. This involves taking

$$\hat{M}_{\mathrm{cat}}^{ij} = |\alpha_i\rangle\langle\alpha_j| \tag{2.80}$$

with α_j the classical amplitudes, determined by (with $K \equiv 1$):

$$\Delta(\alpha_j - i\sqrt{\Lambda_2}) - \Lambda_2 \alpha_j^* - \alpha_j |\alpha_j|^2 \equiv 0, \quad j = 1, 2 \tag{2.81}$$

One sees from Fig. 2.9(b) that this coherent-state description does a far poorer job of describing the dynamical slow mode, compared to the states from the bistable manifold.

2.7 Parity-conserving dynamics: true quantum bistability

We now focus on a special case that has received considerable recent attention Mirrahimi et al. [2014b], Goto [2016], Puri et al. [2017], Grimm et al. [2019]: a system where $\kappa_1 = \Lambda_1 = 0$ in Eq. (2.2), implying that the full dynamics conserves photon number parity. This in turn

implies that there are at least two distinct steady states, and opens the possibility of true quantum bistability Albert and Jiang [2014]. Our exact-solution CQA method provides several insights into this regime. Among other things, it allows one to understand why adding a drive-detuning destroys quantum bistability despite parity still being conserved. More generally, the CQA method provides a transparent understanding of this quantum bistability that is difficult to achieve using the positive-P solution method.

We start by revisiting the CQA method of Sec. 2.3 for systems described by Eq. (2.2) with $\kappa_1 = \Lambda_1 = 0$. The corresponding cascaded two-cavity system is described by Eqs. (2.9) and (2.10). The first step as always is to insist that we have a state that is dark with respect to the cascaded dissipators. For $\kappa_1 = 0$, we only have the a two-photon loss dissipator, given by

$$\mathcal{D}[\hat{a}^2 - \hat{b}^2] = \mathcal{D}[2\hat{c}_+\hat{c}_-] \tag{2.82}$$

where again the collective $\hat{c}_\pm$ modes are defined in Eq. (2.7). There are now two distinct possibilities for a non-trivial dark state: either the $\hat{c}_-$ mode is forced to be in vacuum (with the $+$ mode occupied), or the $\hat{c}_+$ mode is forced to be in vacuum (with the $-$ mode occupied). The first option is the same as what we did for $\kappa_1 = 0$; the second option is a new possibility enabled by the lack of one photon loss.

It follows that the most general 2-cavity dark state has the form:

$$|\psi_{\rm dk}\rangle = \alpha_+ |\psi\rangle_+ |0\rangle_- + \alpha_- |0\rangle_+ |\theta\rangle_- \tag{2.83}$$

This structure is a direct consequence of parity conservation, which guarantees the existence of at least two orthogonal steady states (one even parity, one odd parity). This structure also implies that the general argument in Sec. 2.3 ensuring a positive cavity-a steady-state Wigner function no longer holds, as $|\psi_{\rm dk}\rangle$ can have both $+$ and $-$ modes occupied.

2.7.1 Zero detuning: quantum bistability

Consider first the case $\Delta = 0$, meaning that we have a resonantly-driven Kerr parametric oscillator subject to two photon loss. Without dissipation, this system has degenerate coherent state eigenstates Goto [2016], Puri et al. [2017]. Including two-photon loss, the dissipative system exhibits true quantum bistability: it admits multiple steady states. We show how this structure emerges via the CQA method.

The first step of the CQA method is to identify possible pure dark states of the collective cascaded-systems dissipators; in our case, this is Eq. (2.83). To have this state be a steady state, it must also be an eigenstate of the cascaded Hamiltonian (c.f. Eq. (2.10)). For $\Delta = 0$, this leads to the equation:

$$\hat{c}_-^\dagger \hat{c}_+^\dagger \Bigg(\alpha_+ \left[\hat{c}_+^2 + \lambda_2\right] |\psi\rangle_+ |0\rangle_- + \alpha_- \left[\hat{c}_-^2 + \lambda_2\right] |0\rangle_+ |\theta\rangle_- \Bigg) = E\, |\psi_{\mathrm{dk}}\rangle \tag{2.84}$$

with $\lambda_2 = 2\Lambda_2/(K - i\kappa_2)$. Since $\hat{H}_{\mathrm{casc}}$ always adds an excitation to *both* modes $\hat{c}_-$ and $\hat{c}_+$, the only possible energy eigenvalue is $E = 0$. The equation then decouples into separate equations for $|\psi\rangle_+, |\theta\rangle_-$ which are easily solved. Crucially, each of these equations admits two possible solutions.

As a result, one finds that the most general dark state solution can be written in terms of coherent states as:

$$|\psi_{\mathrm{dk}}\rangle = \sum_{\pm} \left(\mu_\pm |\pm\epsilon\rangle_+ |0\rangle_- + \nu_\pm |0\rangle_+ |\pm\epsilon\rangle_-\right) \tag{2.85}$$

where the coherent state amplitude $\epsilon = i\sqrt{\lambda_2}$, as in the previous section. We see that the cascaded two-cavity system has a four dimensional subspace of possible steady-state, dark states.

The last step is to determine the corresponding steady state structure of the physical a cavity. As discussed in Sec. 2.3, this effectively corresponds to taking a given two-cavity state, sending it through a 50-50 beamsplitter, and then discarding one of the outputs. This procedure is easy to carry out on the general state in Eq. (2.85), as coherent states transform in a simple manner under a beamsplitter operation. In the basis of the physical a cavity and auxiliary b cavity, our general dark state has the form:

$$\begin{aligned} |\psi_{\rm dk}\rangle &= \sum_{\pm} \Big(\mu_{\pm} \left|\pm\tilde{\epsilon}\right\rangle_a \left|\pm\tilde{\epsilon}\right\rangle_b \\ &\qquad\qquad + \nu_{\pm} \left|\pm\tilde{\epsilon}\right\rangle_a \left|\mp\tilde{\epsilon}\right\rangle_b \Big) \qquad (2.86) \\ &= \Big(\mu_{+} \left|\tilde{\epsilon}\right\rangle_a + \nu_{-} \left|\tilde{\epsilon}\right\rangle_a \Big) \left|\tilde{\epsilon}\right\rangle_b \\ &\quad + \Big(\mu_{-} \left|-\tilde{\epsilon}\right\rangle_a + \nu_{+} \left|+\tilde{\epsilon}\right\rangle_a \Big) \left|-\tilde{\epsilon}\right\rangle_b , \qquad (2.87) \end{aligned}$$

with $\tilde{\epsilon} \equiv \epsilon/\sqrt{2}$. As there is in general entanglement between the physical a cavity and the auxiliary b cavity, one in general is left with an impure state for cavity a. However, pure cavity-a steady states are indeed possible; consider for example the case where $\mu_{-} = \nu_{+} = 0$.

The upshot is that we have a steady state manifold for cavity a that is two dimensional, and spanned by the states $\left|\pm\tilde{\epsilon}\right\rangle_a$ (in agreement with previous work Mirrahimi et al. [2014b]). In simple terms, the steady-state manifold corresponds to a quantum bit, i.e. a full single-qubit Bloch sphere Albert and Jiang [2014]. This is what we mean by the system exhibiting quantum bistability.

2.7.2 Non-zero detuning: classical bistability

Loss of quantum bistability

We next consider the case of a non-zero detuning Δ. While parity continues to be conserved, this addition has a dramatic consequence for the nature of the bistability. Solving the system

again using the CQA method, the requirement of having our general dark state in Eq. (2.83) be a energy eigenstate of the cascaded Hamiltonian leads to the equations

$$\hat{c}_-^\dagger \left(\hat{c}_+^\dagger \hat{c}_+^2 - D\hat{c}_+ + \lambda_2 \hat{c}_+^\dagger\right) |\psi\rangle_+ = 0, \tag{2.88}$$

$$\hat{c}_+^\dagger \left(\hat{c}_-^\dagger \hat{c}_-^2 - D\hat{c}_- + \lambda_2 \hat{c}_-^\dagger\right) |\theta\rangle_- = 0. \tag{2.89}$$

where $D = 2\Delta/(K - i\kappa_2)$. As before, the equations determining $|\psi\rangle_+$ and $|\theta\rangle_-$ are identical (reflecting parity conservation). The equation in each case can be solved by using a SB representation for the state, and turning the operator equations into differential equations. We get the same ODE in each case:

$$\left(z\frac{\partial^2}{\partial z^2} - D\frac{\partial}{\partial z} + \lambda_2 z\right)\psi_{\mathrm{SB}}(z) = 0 \tag{2.90}$$

With the same equation for θ_{SB}, and with λ_2, D having the same definitions as earlier.

At the qualitative level, one can see how true quantum bistability is lost in the presence of detuning: for zero detuning $D \equiv 0$, the ODE above has no singular points, and thus the standard existence theorem (§12.22 in Ince [1956]) guarantees two independent, analytic solutions. As discussed earlier, this leads to quantum bistability for the physical mode a. However, the term $\propto D\partial_z$ introduces a singular point into the ODE at $z = 0$, and the existence of two dark steady states is no longer guaranteed. Indeed, the singular point at $z = 0$ produces a branch-cut discontinuity in one of the solutions. Generically, only one analytic solution survives:

$$\psi_{\mathrm{SB}}(z) = \frac{1}{N^{1/2}}\, {}_0F_1(1/2 - D/2; -\lambda_2 z^2/4), \tag{2.91}$$

where N is a normalization constant.

As we will see, this two-fold reduction in the number of dark steady-states has dramatic

consequences for the bistability of the physical mode a. As there is a unique choice for both $|\psi\rangle_+$ and $|\theta\rangle_-$, the most general dark state has the form of Eq. (2.83), and corresponds to a two-dimensional subspace. In what follows, it will be useful to write this general dark state as

$$|\psi_{\rm dk}\rangle = \mu_{\rm e}\,|\Phi_{\rm e}\rangle + \mu_{\rm o}\,|\Phi_{\rm o}\rangle \tag{2.92}$$

with

$$\left|\Phi_{\rm e/o}\right\rangle = \frac{1}{\sqrt{2 \pm 2N^{-1}}}\left(|\psi\rangle_+\,|0\rangle_- \pm |0\rangle_+\,|\psi\rangle_-\right). \tag{2.93}$$

We now trace-out the auxiliary b cavity. Note that the pure dark states above span a subspace of dimension 2. Incoherent mixtures in this subspace are also stationary states; hence the cascaded 2 cavity problem has a steady-state manifold corresponding to a Bloch sphere. We imagine starting with an abitrary mixed state in this subspace (described by a 2 cavity density matrix), and then tracing out cavity a to determine the corresponding cavity a state. Understanding the full range of cavity a states produced here determines the steady-state manifold of cavity a.

This procedure leads us to consider four linearly-independent cavity-a operators (that determine the cavity a density matrix after tracing out cavity b):

$$\begin{aligned}
\hat{M}^{++}_{a,ss} &\equiv {\rm tr}_b[|\psi\rangle_+|0\rangle_-\langle\psi|_+\langle 0|_-] \\
\hat{M}^{--}_{a,ss} &\equiv {\rm tr}_b[|0\rangle_+|\psi\rangle_-\langle 0|_+\langle\psi|_-] \\
\hat{M}^{+-}_{a,ss} &\equiv {\rm tr}_b[|\psi\rangle_+|0\rangle_-\langle 0|_+\langle\psi|_-] \\
\hat{M}^{-+}_{a,ss} &\equiv (\hat{M}^{+-}_{a,ss})^\dagger
\end{aligned} \tag{2.94}$$

To understand the structure of these operators, we consider their corresponding Q-functions

(easily obtainable using the SB representation):

$$Q^{\pm\pm}_{a,ss}(z) = \int d^2u\, \psi^*_{\rm SB}\Big(\frac{z\pm u}{\sqrt{2}}\Big)\psi_{\rm SB}\Big(\frac{z\pm u}{\sqrt{2}}\Big) \tag{2.95}$$

$$Q^{\pm\mp}_{a,ss}(z) = \int d^2u\, \psi^*_{\rm SB}\Big(\frac{z\pm u}{\sqrt{2}}\Big)\psi_{\rm SB}\Big(\frac{z\mp u}{\sqrt{2}}\Big) \tag{2.96}$$

We obtain an important result: these four operators are not all independent. Because of the symmetry of each integral under the mapping $u \to -u$, we have

$$\hat{M}^{++}_{a,ss} = \hat{M}^{--}_{a,ss}, \qquad \hat{M}^{+-}_{a,ss} = \hat{M}^{-+}_{a,ss} = (\hat{M}^{+-}_{a,ss})^\dagger \tag{2.97}$$

These equalities imply a loss of information in tracing out cavity-b, and result in the cavity-a steady state manifold being simply two-dimensional. It is spanned by the quantities

$$\begin{aligned}\hat{\rho}^{+}_{a,ss} &\equiv \hat{M}^{++}_{a,ss} \\ \hat{\rho}^{-}_{a,ss} &\equiv \hat{M}^{+-}_{a,ss}.\end{aligned} \tag{2.98}$$

with $\hat{\rho}^{\pm}_{a,ss}$ both Hermitian. We now have enough information to calculate each steady state exactly: since the steady-state manifold is two-dimensional, and since parity is a conserved quantity, every density matrix in the manifold must then be an impure mixture of the form

$$\hat{\rho}_{a,ss} = p\hat{\rho}_e + (1-p)\hat{\rho}_o \tag{2.99}$$

where the extremal states $\hat{\rho}_{e/o}$ are uniquely characterized by the property of having definite photon number parity (even and odd respectively).

Thus, in summary, in this case there is a distinct steady state in both the even and odd photon number sectors; any mixture of these is also a possible steady state. The steady state manifold is indexed by just a single number $0 \le p \le 1$, which simply corresponds to

the dynamically-conserved probability of having an even photon number parity. In simpler terms, the cavity-a steady-state manifold corresponds to a classical bit Albert and Jiang [2014].

Full characterization of the steady state manifold

To conclude our discussion of $\Delta \neq 0$, we use the CQA method to compute exactly each steady state in the bistable manifold. We begin by noting that the states $|\Phi_{e/o}\rangle$ in Eq. (2.93) have definite photon-number parity, and thus so do the corresponding states of the physical cavity-a (obtained by tracing over cavity-b). Therefore, by uniqueness of the extremal states, these states must be precisely $\hat{\rho}_{e/o}$:

$$\begin{aligned} \hat{\rho}_e &= \mathrm{tr}_b[|\Phi_e\rangle\langle\Phi_e|] \\ \hat{\rho}_o &= \mathrm{tr}_b[|\Phi_o\rangle\langle\Phi_o|]. \end{aligned} \tag{2.100}$$

To compute these steady-states, we note that by substituting Eq. (2.93) into Eq. (2.100) we can expand, e.g.

$$\hat{\rho}_{e/o} = \frac{N}{N \pm 1}(\hat{\rho}^{+}_{a,ss} \pm \hat{\rho}^{-}_{a,ss}) \tag{2.101}$$

where N is just the normalization constant N for the dark state $|\psi\rangle_+$, which has the exact expression

$$N = {}_1F_2(1/2; 1/2 - D/2, (1/2 - D/2)^*; |\lambda_2/2|^2). \tag{2.102}$$

Inverting the above linear relation, we get

$$\hat{\rho}^{+}_{a,ss} = \frac{1}{2}\left[\frac{N+1}{N}\hat{\rho}_e + \frac{N-1}{N}\hat{\rho}_o\right] \tag{2.103}$$

This equation immediately leads to exact expressions for $\hat{\rho}_{e/o}$, which are given in Section 2.14.

Incidentally, Eq. (2.103) tells us which state is selected from the bistable manifold in the presence of an infinitessimal amount of single-photon loss (or any other symmetry-breaking perturbation, e.g. one- or three-photon driving). Indeed, we can rewrite it as

$$\hat{\rho}_{a,ss} \underset{\kappa_1,\Lambda_1,\Lambda_3\to 0}{\sim} \frac{1}{2}\left[\left(1+\frac{1}{N}\right)\hat{\rho}_e + \left(1+\frac{1}{N}\right)\hat{\rho}_o\right]. \tag{2.104}$$

We will briefly discuss physical intuition from this formula, as well as the closed form of N. In the weak-driving limit $\lambda_2 \to 0$, the hypergeometric series defining N collapses to just the first term, and we get $N^{-1} \to 1$, so

$$\hat{\rho}_{a,ss} \underset{\Lambda_2\to 0}{\sim} \hat{\rho}_e.$$

In contrast, in the strong-driving limit N diverges, and thus

$$\hat{\rho}_{a,ss} \underset{\Lambda_2\to \infty}{\sim} \frac{\hat{\rho}_e + \hat{\rho}_o}{2} \tag{2.105}$$

A final piece of physical intuition: since N is a function only of the modulus $|\lambda_2|$, the relative bias (towards either $\hat{\rho}_{o/e}$) is independent of the phase ϕ of the drive $\lambda_2 \equiv e^{i\phi}|\lambda_2|$.

2.8 Exact realization of new quantum bistable regimes using a two-cavity non-cascaded setup

In Sec. 2.5.7, we discussed how the generalized driven-dissipative Kerr problem could be tuned to be arbitrarily close to points in parameter space where we have true quantum bistability. Exact tuning to a bistable point was not possible due to the constraint that

neither κ_1 nor κ_2 could be made negative.

An exact realization of these quantum bistable points is nonetheless possible if one works with the two cavity system in Fig. 2.1. Making one of κ_1 or κ_2 negative now has a simple physical interpretation: we simply *reverse* the chirality of one of the waveguides in the absorber setup (see Fig. 2.10). Reversing the chirality of the (e.g. linearly-coupled) waveguide leads to the dynamics of the master equation Eq. (2.4) with the same dissipators but with the Hamiltonian (c.f. Eq. (2.5)) changed to

$$\hat{H}_{ab} \to \hat{H}_a - \hat{H}_b + \frac{i\kappa_1}{2}(\hat{a}^\dagger \hat{b} - h.c.) - \frac{i\kappa_2}{2}(\hat{a}^\dagger \hat{a}^\dagger \hat{b}^2 - h.c.). \tag{2.106}$$

Again, using the absorber method, we can solve this master equation in a manner identical to before, i.e. with $|\psi\rangle = |\psi_+\rangle|0_-\rangle$, except now we have $\kappa_1 \to -\kappa_1$. So the master equation specified by Eq. (2.106) constitutes an analytic extension of the steady state to negative values of $\kappa_{1,2}$ (and thus arbitrary values of D), and thus can exhibit quantum bistability. For a depiction of the setup, see Fig. (2.10).

In this case Eq. (2.64) actually becomes a relation for selecting a pure state in the bistable manifold:

$$|\psi_+\rangle = \delta r_2 |\psi_{+,1}\rangle + \delta r_1 |\psi_{+,2}\rangle. \tag{2.107}$$

In this case, $|\psi_{+,j}\rangle$ are the photon-added coherent states of the symmetric mode defined in Sec. 2.3. The states are perhaps best understood in the Fock basis. For $\Lambda_3 = 0$,

$$|\psi_{+,1}\rangle = \sum_{m=0}^{n} \frac{(2\epsilon \hat{c}_+^\dagger)^m}{m!} |-\epsilon\rangle \tag{2.108}$$

$$|\psi_{+,2}\rangle = \sum_{m=n+1}^{\infty} \frac{(2\epsilon \hat{c}_+^\dagger)^m}{m!} |-\epsilon\rangle \tag{2.109}$$

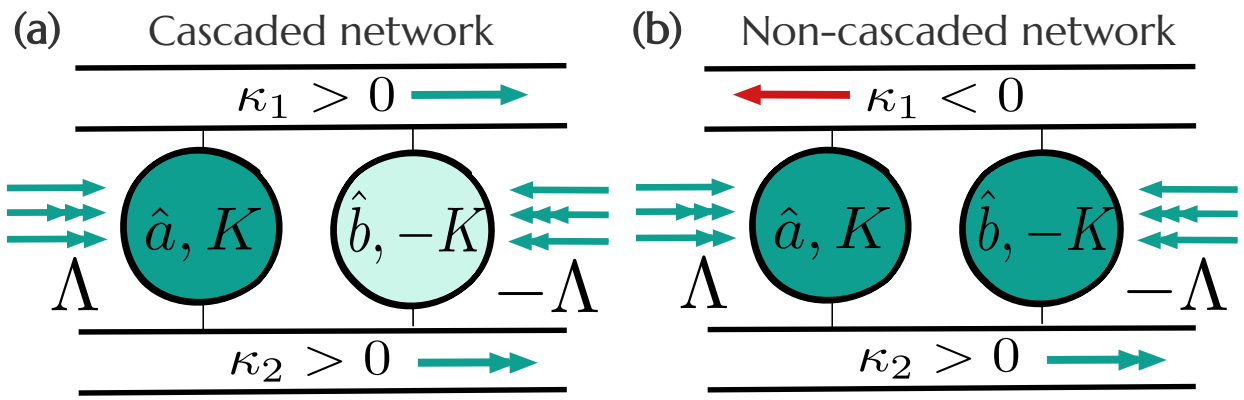

Figure 2.10: Realizing quantum bistability by breaking chirality. The generalized bistable points in our phase diagram (c.f. Fig. 2.3) are *exactly* realizable by using a two-cavity setup (b) which is not cascaded, i.e. where the chirality of one of the waveguides is reversed.

where $|z\rangle$ as usual denotes a coherent state with amplitude z. Note that their sum *is* Gaussian, i.e. a coherent state, as is expected from properties of Kummer's hypergeometric function. In the more general case of the "off-diagonal" bistable points (i.e. the (n, m) points with $n \neq m$), one stabilizes even more exotic states, whose sum may no longer be Gaussian.

2.9 A circuit-QED implementation of the three-photon driving effect

We now show that it is possible to realize the generalized driven-Kerr oscillator using circuit QED devices that already exist, in particular, a SNAIL device Sivak et al. [2019]. The Hamiltonian for a SNAIL, as a function of applied magnetic flux, can be written as (following the notation of Sivak et al. [2019])

$$\hat{H} = \omega \hat{a}^\dagger \hat{a} + g_3(\Phi)(\hat{a} + \hat{a}^\dagger)^3 + g_4(\Phi)(\hat{a} + \hat{a}^\dagger)^4. \tag{2.110}$$

We now introduce time dependence into the flux parameter Φ in such a way that $g_3(t) \equiv g_3[\Phi(t)]$ is oscillating at the cavity frequency with amplitude $g_3^{(0)}$, whereas $g_4(t) \equiv g_4^{(0)}$ is essentially constant (cf. Fig. 1 in Ref. Sivak et al. [2019]). In the frame rotating at the

cavity frequency, the time-dependent Hamiltonian then has the form

$$\hat{U}\hat{H}\hat{U}^\dagger = 3g_3^{(0)}\{\hat{a}^\dagger\hat{a}^\dagger\hat{a} + \hat{a}^\dagger\hat{a}\hat{a}\} \tag{2.111}$$

$$+ 3g_4^{(0)}\{2\hat{a}^\dagger\hat{a}^\dagger\hat{a}\hat{a} + 4\hat{a}^\dagger\hat{a} + 1\} \tag{2.112}$$

$$+ \text{counter-rotating terms.} \tag{2.113}$$

Under the rotating-wave approximation, if the drives are weak we can neglect all counter-rotating terms, which yields the effective Kerr Hamiltonian

$$\hat{H}_{\text{RWA}} = \frac{K}{2}\hat{a}^\dagger\hat{a}^\dagger\hat{a}\hat{a} - \Delta\hat{a}^\dagger\hat{a} + (\Lambda_1\hat{a}^\dagger + \Lambda_3\hat{a}^\dagger\hat{a}^\dagger\hat{a} + h.c.) \tag{2.114}$$

where $\Lambda_1 = \Lambda_3 = 3g_3^{(0)}$, and $K = 12g_4^{(0)} = -\Delta$. In conclusion, realization of the nonlinear coherent driving effect, for weak driving strengths, is possible using a superconducting nonlinear asymmetric inductive element, by modulating its flux parameter at the cavity frequency. We can also see from this analysis how it would be even harder to realize the three-photon additional or removal terms $(\hat{a}^\dagger)^3, \hat{a}^3$ within this scheme, as this would require modulating the external flux Φ 3 times more rapidly (specifically, 18 GHz, for the device considered in Ref. Sivak et al. [2019]).

2.10 Steady-state Wigner function

We will now rigorously prove the connection between the Wigner function of the steady-state $\hat{\rho}_{a,ss}$ of the driven Kerr cavity, and the modulus squared of the SB representation of its purification $|\psi_+\rangle$. We will also show how the calculation generalizes to the case where there are multiple dark states.

The result here relies on a deep fact relating operator ordering conventions for a quantum-mechanical mode, and the heat semigroup on the corresponding classical phase space. This

was originally pointed out by Glauber and Cahill in Cahill and Glauber [1969], and we will review the salient results here. Specifically, given a (possibly non-Hermitian operator) $\hat{A}$ of a quantum-mechanical mode, define its *normally-ordered symbol* σ_N to be

$$\sigma_A^N(z) :=: \hat{A} : \big|_{\hat{a}^\dagger, \hat{a} \mapsto z, z^*}, \tag{2.115}$$

where $: \hat{A} :$ is the operator $\hat{A}$ but re-expressed in normal order, i.e. with all of the creation operators to the left of the annihilation operators. Analogously, we can define the *symmetrically-ordered symbol*:

$$\sigma_A(z) :=: \hat{A} :_S \big|_{\hat{a}^\dagger, \hat{a} \mapsto z, z^*}, \tag{2.116}$$

where $: \hat{A} :_S$ is the operator $\hat{A}$ but re-expressed according to the symmetric ordering convention (as defined in Cahill and Glauber [1969]). The symmetrically-ordered symbol is proportional to the standard *Wigner transform*, which can be formally computed via an integral:

$$\sigma_A(z) \propto \int d^2\xi \, \mathrm{Tr}[e^{\xi^* \hat{a} - \xi \hat{a}^\dagger} \hat{A}] e^{\xi z^* - \xi^* z} \tag{2.117}$$

For positive semi-definite operators, e.g. a density matrix $\hat{\rho} \equiv \hat{\rho}^\dagger$, the symmetrically-ordered and normally-ordered symbols coincide with the Wigner- and Q-functions respectively:

$$Q(z) = \frac{1}{\pi} \sigma_\rho^N(z), \qquad W(z) = \frac{1}{\pi} \sigma_\rho(z). \tag{2.118}$$

What Glauber and Cahill showed in Cahill and Glauber [1969] is that operator symbols corresponding to different ordering conventions are related by the heat semigroup. In particular, we have the following theorem:

Theorem. (Cahill and Glauber [1969]). *Let $\hat{A}$ be a Hilbert-Schmidt operator (i.e. $Tr[\hat{A}^\dagger \hat{A}] <$*

∞). *Then its normally-ordered symbol can be obtained by "cooling" (i.e. running the heat equation on) the symmetrically-ordered symbol for a time* $t = 1/4$, *i.e.*

$$\sigma_A^N(z) = \int_{\mathbb{C}} d^2z' \mathcal{K}(t, z, z')\sigma_A(z')\Big|_{t=1/4} \tag{2.119}$$

where $K(t, z, z')$ *is the heat kernel on* $\mathbb{C}$, *which can be exactly computed and comes out to*

$$\mathcal{K}(t, z, z') = \frac{e^{\frac{-|z-z'|^2}{4t}}}{4\pi t}. \tag{2.120}$$

We can use the theorem above to directly trace-out the ancilla cavity used in the absorber method. Following the notation earlier, suppose we have an orthonormal basis $|\psi_1\rangle, \cdots, |\psi_k\rangle$ of the space of dark states, i.e.

$$\hat{c}_-|\psi_j\rangle = 0. \tag{2.121}$$

Clearly, these states form a k-dimensional Bloch sphere, spanned by their outer-products:

$$|\psi_i\rangle\langle\psi_j|. \tag{2.122}$$

According to CQA, to obtain the corresponding stationary modes $\hat{M}_{ij}$ of the physical cavity-a Lindbladian, we must trace-out the ancilla mode:

$$\hat{M}_{ij} = \mathrm{Tr}_b[|\psi_i\rangle\langle\psi_j|]. \tag{2.123}$$

We now compute the Wigner transform of the above stationary modes. First, we take advantage of the fact that a dark state factorizes across the two-modes $\hat{c}_\pm$ as $|\psi_j\rangle = |\psi_{j,+}\rangle|0_-\rangle$:

$$\hat{M}_{ij} = \mathrm{Tr}_b[(|\psi_{i,+}\rangle\langle\psi_{j,+}|)\,(|0_-\rangle\langle 0_-|)]. \tag{2.124}$$

Letting $\sigma_{+,ij}(z)$ denote the symmetrically-ordered symbol (i.e. Wigner transform) of the outer-product $|\psi_{i,+}\rangle\langle\psi_{j,+}|$, and $\sigma_-(z)$ denote the symmetrically-ordered symbol of the vacuum state $|0_-\rangle\langle 0_-|$, let $\sigma_{ij}(z)$ denote the symmetrically-ordered symbol (i.e. the Wigner transform) of the stationary mode $\hat{M}_{ij}$. We can then rewrite the expression for the partial trace completely in terms of symmetrically-ordered symbols: in this case, the partial trace becomes an integral, and the symmetrized-antisymmetrized nature of the input states means that the integral convolves the operator symbols. The symbol $\sigma_-(z)$ then acts as a Gaussian filter for the symbol $\sigma_{+,ij}(z)$:

$$\sigma_{ij}(z) = \int_{\mathbb{C}} d^2z' \; \sigma_-\left(\frac{z-z'}{\sqrt{2}}\right)\sigma_{+,ij}\left(\frac{z+z'}{\sqrt{2}}\right) \tag{2.125}$$

$$= \int_{\mathbb{C}} d^2z_+ \; \frac{2e^{-2|z_+-\sqrt{2}z|^2}}{\pi}\sigma_{+,ij}(z_+), \tag{2.126}$$

where we have defined symmetrized and anti-symmetrized phase-space variables $z_\pm \equiv (z \pm z')/\sqrt{2}$. The above filtering operation is the same exact operation which "reorders" a normally-ordered symbol into a symmetrically-ordered symbol, up to a rescaling of the phase space $z \mapsto \sqrt{2}z$. Indeed, we can rewrite it in terms of the heat kernel:

$$\sigma_{ij}(z) = 2\int_{\mathbb{C}} d^2u \, \mathcal{K}(t, \sqrt{2}z, u)\sigma_{+,ij}(u)\Big|_{t=1/4} \tag{2.127}$$

$$= 2\sigma^N_{+,ij}(\sqrt{2}z), \tag{2.128}$$

where $\sigma^N_{+,ij}$ is the normally-ordered symbol of the mode $|\psi_{i,+}\rangle\langle\psi_{j,+}|$. This form highly constrains the Wigner function of the steady state of any single-mode system with single-photon loss that is solvable via CQA.

In particular, now we can compute the symbol exactly in terms of the Segal-Bargmann representation. It is easy to show that the normally-ordered symbol of an operator has the

simple form:

$$\sigma_A^N(z) = \langle z|\hat{A}|z\rangle \tag{2.129}$$

where $|z\rangle$ denotes a coherent state with amplitude z. By expanding $\hat{A}$ in terms of outer-products as

$$\hat{A} = \sum_{ij} \alpha_{ij}|\psi_i\rangle\langle\psi_j|, \tag{2.130}$$

and utilizing the property $\psi_{\rm SB}(z) = \langle z^*|\psi\rangle e^{-|z|^2/2}$, Bargmann in Bargmann [1967] was able to show that this implies

$$\sigma_A^N(z) = \sum_{ij} \alpha_{ij}\psi_{i,\rm SB}(z^*)\psi_{j,\rm SB}(z^*)e^{-|z|^2}. \tag{2.131}$$

By substituting the exact expression for the normally-ordered symbol into Eq. (2.128), we can finally state the main result:

$$\sigma_{ij}(z) = 2\psi_{i,\rm SB}(\sqrt{2}z^*)\psi_{j,\rm SB}(\sqrt{2}z^*)e^{-2|z|^2}. \tag{2.132}$$

By taking linear combinations of the above stationary modes, the Wigner function of any stationary *density matrix* of the physical cavity a has the closed-form

$$W_{a,ss}(z) = \frac{2}{\pi}\sum_{ij} \alpha_{ij}\psi_{i,\rm SB}(\sqrt{2}z^*)\psi^*_{j,\rm SB}(\sqrt{2}z^*)e^{-2|z|^2}, \tag{2.133}$$

where $\alpha_{ij} = \alpha^*_{ji}$ is a positive semi-definite matrix with unit trace.

We can also write the CQA ansatz in a manifestly positive-form. Letting $\{p_j\}$ denote the eigenvalues of the positive semi-definite matrix $\{\alpha_{ij}\}$, and letting $\{\phi_j(z)\}$ denote the

Segal-Bargmann representations of the corresponding eigenvectors, the Wigner function can be equivalently written as

$$W_{a,ss}(z) = \frac{2}{\pi} \sum_j p_j |\phi_j(\sqrt{2}z^*)|^2 e^{-2|z|^2} \geq 0, \tag{2.134}$$

where normalization forces $\sum_j p_j = 1$.

As a simple example, when the dark-state subspace is one-dimensional, the Wigner function is the squared-modulus of the SB representation of the unique, normalized dark state in that subspace:

$$W_{a,ss}(z) = \frac{2}{\pi} |\phi(\sqrt{2}z^*)|^2 e^{-2|z|^2}. \tag{2.135}$$

In summary, we have derived an exact, closed-form expression for the steady-state Wigner function of a cavity that is solvable via CQA. What is most striking from this analysis is the absence of any consideration of the Hamiltonian of the cavity: the CQA method, if it works, will predict that the Wigner function will be positive-definite, simply as a consequence of the presence of single-photon loss in the system.

2.11 "Gauge-invariance" of the dark state

Eq. (2.34) makes it manifest that there exist two distinct (non-unitary) gauge choices in which the troublesome two-photon term vanishes in the dark state equation Eq. (2.18). We solved the dark state equations in the plus-gauge. This leads to the question of what would happen if we solved the dark state conditions in the minus-gauge. If we had solved for the dark state in the minus gauge, we would have ended up with the solution

$$\widetilde{\psi}_{+,\mathrm{SB}}(z) \equiv e^{-\epsilon_- z}\, {}_1F_1\bigg(-\frac{\lambda_1 + \epsilon_- D}{\epsilon_- - \epsilon_+}; -D; (\epsilon_- - \epsilon_+)z \bigg). \tag{2.136}$$

However, the results are gauge-invariant, as we can write

$$\begin{aligned}
\widetilde{\psi}_{+,\mathrm{SB}}(z) &= e^{-\epsilon_- z+(\epsilon_- -\epsilon_+)z} \\
&\quad {}_1F_1\bigg(-D - \frac{\lambda_1+\epsilon_- D}{\epsilon_+-\epsilon_-}; -D; (\epsilon_+-\epsilon_-)z\bigg) \qquad (2.137)\\
&= e^{-\epsilon_+ z} \\
&\quad {}_1F_1\bigg(-\frac{(\epsilon_+-\epsilon_-)D}{\epsilon_+-\epsilon_-} - \frac{\lambda_1+\epsilon_- D}{\epsilon_+-\epsilon_-}; -D; (\epsilon_+-\epsilon_-)z\bigg) \\
&= e^{-\epsilon_+ z}\, {}_1F_1\bigg(-\frac{\lambda_1+\epsilon_+ D}{\epsilon_+-\epsilon_-}; -D; (\epsilon_+-\epsilon_-)z\bigg) = \psi_{+,\mathrm{SB}}, \qquad (2.138)
\end{aligned}$$

where $\psi_{+,\mathrm{SB}}$ is the dark state Eq. (2.33), and in the first line (Eq. (2.137)) we utilized *Kummer's transformation* (see e.g. Ref. Brychkov), which is a fundamental symmetry of the confluent hypergeometric differential equation:

$$ {}_1F_1(r_1; r_2; z) = e^z\, {}_1F_1(r_2 - r_1; r_2; -z). \qquad (2.139)$$

2.12 Stationary density matrix and moments of a driven Kerr cavity

We show here how to compute exact analytic expressions from our steady-state solution for density matrix elements in the Fock basis, as well as normal-ordered cavity moments. Although the expressions obtained here are considerably more complex/physically opaque, this will allow us to make contact with older results obtained via P-function methods Bartolo et al. [2016], Elliott and Ginossar [2016]. Expanding the purification of the density matrix

$|\psi\rangle = |\psi_+\rangle \otimes |0_-\rangle$, and writing the symmetric component in the SB representation yields

$$\psi_{+,\mathrm{SB}}(z) \equiv \sum_{l=0}^{\infty} \psi_l \frac{z^l}{l!}, \tag{2.140}$$

which implicitly defines coefficients $\psi_l \equiv \psi^{(l)}_{+,\mathrm{SB}}(0)$ which are the derivatives of the Bargmann state evaluated at the origin $z = 0$ in phase space. In the special cases $\lambda_1 \equiv \lambda_3 \equiv 0$, reproducing results in Bartolo et al. [2016]), or the more generic regime $\lambda_2 \equiv 0$, which represents new results, we can actually evaluate the sums, resulting in compact, closed-form expressions.

Steady-state density matrix

In terms of these Taylor coefficients, the steady state density matrix can be computed in the Fock basis:

$$\begin{aligned}
&\langle m|\hat{\rho}_{a,ss}|n\rangle \qquad (2.141)\\
&= \sum_{l=0}^{\infty} \langle m,l| \Bigg(\sum_{j,k=0}^{\infty} \frac{\psi_j \psi_k^*}{j!k!} (\hat{c}_+^\dagger)^j |0\rangle\langle 0|\hat{c}_+^k \Bigg) |n,l\rangle \\
&= \frac{1}{(2^{m+n} n! m!)^{1/2}} \\
&\sum_{l,j,k=0}^{\infty} \frac{\psi_j \psi_k^*}{j!k!} \langle 0| \frac{(\hat{c}_+ - \hat{c}_-)^l}{\sqrt{2^l l!}} (\hat{c}_+ + \hat{c}_-)^m (\hat{c}_+^\dagger)^j |0\rangle \\
&\qquad\qquad \cdot \langle 0|\hat{c}_+^k (\hat{c}_+^\dagger + \hat{c}_-^\dagger)^n \frac{(\hat{c}_+^\dagger - \hat{c}_-^\dagger)^l}{\sqrt{2^l l!}} |0\rangle \\
&= \frac{1}{(2^{m+n} n! m!)^{1/2}} \\
&\sum_{j,k,l=0}^{\infty} \frac{\psi_j \psi_k^*}{j!k!} \frac{1}{2^l l!} \langle 0|\hat{c}_+^{m+l} (\hat{c}_+^\dagger)^j |0\rangle\langle 0|\hat{c}_+^k (\hat{c}_+^\dagger)^{n+l} |0\rangle. \qquad (2.142)
\end{aligned}$$

Using identities of the form $\langle 0|\hat{c}_+^{m+l}(\hat{c}_+^\dagger)^j|0\rangle = \delta_{m+l,j}j!$, etc., we get the remarkably simple result:

$$\langle m|\hat{\rho}_{a,ss}|n\rangle = \frac{1}{\sqrt{2^{m+n}n!m!}}\sum_{l=0}^{\infty}\frac{\psi_{m+l}\psi_{n+l}^*}{2^l l!}. \tag{2.143}$$

This expression matches similar expressions obtained using positive-P solutions, as we will see later in this section.

Cavity moments

We can also express the normally-ordered moments of a driven Kerr cavity exactly in terms of the scaled Fock-state amplitudes ψ_l. The calculation is slightly more straightforward:

$$\begin{aligned}\mathrm{Tr}[\hat{\rho}_{a,ss}(a^\dagger)^n a^m] &= \langle\psi|(a^\dagger)^n a^m|\psi\rangle \\ &= \frac{1}{\sqrt{2^{m+n}}}\langle\psi|(\hat{c}_+^\dagger + \hat{c}_-^\dagger)^n(\hat{c}_+ + \hat{c}_-)^m|\psi\rangle,\end{aligned} \tag{2.144}$$

where $|\psi\rangle$, as before, is the purification of the density matrix obtained from the absorber method. Expanding the dark state yields

$$\begin{aligned}&\mathrm{Tr}[\hat{\rho}_{a,ss}(a^\dagger)^n a^m] \\ &= \frac{1}{\sqrt{2^{m+n}}}\sum_{j,k=0}^{\infty}\frac{\psi_j^*\psi_k}{j!k!}\langle 0|\hat{c}_+^j(\hat{c}_+^\dagger)^n\hat{c}_+^m(\hat{c}_+^\dagger)^k|0\rangle \\ &= \frac{1}{\sqrt{2^{m+n}}}\sum_{j,k=0}^{\infty}\frac{\psi_j^*\psi_k}{\sqrt{j!k!}}\langle j_+|(\hat{c}_+^\dagger)^n\hat{c}_+^m|k_+\rangle.\end{aligned} \tag{2.145}$$

Defining a new variable l such that $j \equiv n + l$, we find that $k = m + l$, and that furthermore $l \geq 0$. So our sum simplifies to

$$\begin{aligned}&\mathrm{Tr}[\hat{\rho}_{a,ss}(a^\dagger)^n a^m] \\ &\frac{1}{\sqrt{2^{m+n}}} \sum_{l=0}^{\infty} \frac{\psi^*_{n+l}\psi_{m+l}}{\sqrt{(m+l)!(n+l)!}} \frac{\sqrt{(m+l)!}}{\sqrt{l!}} \frac{\sqrt{(n+l)!}}{\sqrt{l!}}.\end{aligned} \tag{2.146}$$

We thus obtain the simple result

$$\mathrm{Tr}[\hat{\rho}_{a,ss}(a^\dagger)^n a^m] = \frac{1}{\sqrt{2^{m+n}}} \sum_{l=0}^{\infty} \frac{\psi_{m+l}\psi^*_{n+l}}{l!}. \tag{2.147}$$

This is the formula used to produce exact-solution plots of average photon number in Fig. 2.4; a similar-looking expression was derived independently in Bartolo et al. [2016], using P-function methods.

Normalization

Throughout this section, we have assumed that the normalization of $|\psi_+\rangle$ is known. Supposing that this is *not* the case, and $|\psi_+\rangle$ is written instead in the form

$$\psi_{+,\mathrm{SB}}(z) = \frac{1}{\sqrt{N}} \sum_{l=0}^{\infty} \widetilde{\psi}_l \frac{z^l}{l!}, \tag{2.148}$$

we can write an exact expression for N:

$$N = \sum_{l=0}^{\infty} \frac{\widetilde{\psi}_l}{\sqrt{l!}} \frac{\widetilde{\psi}_l^*}{\sqrt{l!}} = \sum_{l=0}^{\infty} \frac{|\widetilde{\psi}_l|^2}{l!}. \tag{2.149}$$

Expression for ψ_l in general regime

The scaled Fock-state amplitudes ψ_l can be computed in closed-form in terms of the Gauss hypergeometric function. We can then utilize this closed form to show that our exact expressions derived here agree with earlier solutions Bartolo et al. [2016], Elliott and Ginossar [2016] in the limit of $\Lambda_3 \to 0$:

$$\psi_l \equiv \partial^l \psi_{+,\mathrm{SB}}(0). \tag{2.150}$$

The above quantity is particularly difficult to evaluate in the general case, so we evaluate instead

$$\xi_l \equiv \partial^l \xi_{+,\mathrm{SB}}(0). \tag{2.151}$$

where $|\xi\rangle$ is the displaced dark state used earlier. Eq. (2.151) then represents the Fock-state amplitudes of the purification of the *displaced* steady-state $\hat{\rho}' \equiv \hat{D}_\alpha \hat{\rho}_{a,ss} \hat{D}_\alpha^\dagger$, where α is defined earlier and vanishes when $\Lambda_3 \to 0$.

Expanding $\xi_{+,\mathrm{SB}}(z) \equiv \Theta(z)\phi(z)$, where $\Theta(z) \equiv \exp(-\theta(z))$ is the non-unitary gauge transformation defined earlier. Expanding via the Leibniz rule, we get

$$\xi_l = \sum_{n=0}^{l} \binom{l}{n} \partial^{l-n}\Theta(0)\partial^n\phi(0). \tag{2.152}$$

Plugging in $\Theta(z) \equiv e^{-\epsilon_+ z}$ and $\phi(z) = {}_1F_1(-r_1; -r_2; (\epsilon_+ - \epsilon_-)z)$, we get

$$\partial^k \Theta(0) = (-\epsilon_+)^k \tag{2.153}$$

$$\partial^k \phi(0) = \frac{(-r_1)_k}{(-r_2)_k} (\epsilon_+ - \epsilon_-)^k \tag{2.154}$$

So, in total, we get

$$\begin{aligned}
\xi_l &= \sum_{n=0}^{l} \binom{l}{n} \frac{(-r_1)_n}{(-r_2)_n} (-\epsilon_+)^{l-n} (\epsilon_+ - \epsilon_-)^n \\
&= (-\epsilon_+)^l \sum_{n=0}^{l} (-1)^n \binom{l}{n} \frac{(-r_1)_n}{(-r_2)_n} \left(1 - \frac{\epsilon_-}{\epsilon_+}\right)^n \\
&= (-\epsilon_+)^l \sum_{n=0}^{l} \frac{(-l)_n (-r_1)_n}{(-r_2)_n} \frac{(1 - \frac{\epsilon_-}{\epsilon_+})^n}{n!}. \\
&= (-\epsilon_+)^l \sum_{n=0}^{\infty} \frac{(-l)_n (-r_1)_n}{(-r_2)_n} \frac{(1 - \frac{\epsilon_-}{\epsilon_+})^n}{n!}.
\end{aligned} \tag{2.155}$$

Therefore, we have a closed-form expression for the scaled Fock-state amplitudes of the displaced dark state:

$$\xi_l = (-\epsilon_+)^l \, {}_2F_1(-l, -r_1; -r_2; 1 - \tfrac{\epsilon_-}{\epsilon_+}). \tag{2.156}$$

In the limit $\Lambda_3 \to 0$, $\epsilon_+ \to -\epsilon_-$, and so, as before, defining $\epsilon \equiv \epsilon_+$, we get

$$\psi_l \underset{\Lambda_3 \to 0}{\sim} (-\epsilon)^l \, {}_2F_1(-l, -r_1; -r_2; 2). \tag{2.157}$$

where we are implicitly utilizing the fact that $\xi_l \to \psi_l$ in this limit, as the displacement parameter α vanishes in the limit $\Lambda_3 \to 0$. From Eq. (2.157), it is straightforward to recover the previous solutions Bartolo et al. [2016], Elliott and Ginossar [2016] of the Kerr resonator in the limit $\Lambda_3 \equiv 0$.

2.13 Exact results when the non-unitary gauge transformation is trivial

The series expressions derived in Section 2.12 have simple closed forms when we have $\lambda_2 \equiv 0$, which, for $\Lambda_2 \neq 0$, represents previously unexplored physics. We emphasize the generic nature of this regime, in that there are 8 real parameters to play with: Λ_1, Λ_3, and $K, \Delta, \kappa_1, \kappa_2$. In this limit, the displaced SB wavefunction Eq. (2.32) is purely hypergeometric:

$$\xi_{+,\mathrm{SB}}(z) = \frac{1}{N^{1/2}}\, {}_1F_1(-r_1; -r_2; -\lambda_3 z), \tag{2.158}$$

where $r_1 \equiv -\lambda_1/\lambda_3$, and $r_2 \equiv D$. In this case, the coefficients ξ_l of the displaced steady state simplify to ratios of Pochhammer symbols:

$$\xi_l = \frac{1}{N^{1/2}} \frac{(-r_1)_l}{(-r_2)_l} (-\lambda_3)^l, \tag{2.159}$$

where the Pochhammer symbol is defined as $(z)_l \equiv \Gamma(z+l)/\Gamma(z)$. Therefore, the normalization is computable in closed form:

$$\begin{aligned} N &= \sum_{l=0}^{\infty} \frac{(-r_1)_l (-r_1^*)_l}{(-r_2)_l (-r_2^*)_l} \frac{|\lambda_3|^{2l}}{l!} \\ &= {}_2F_2(-r_1, -r_1^*; -r_2, -r_2^*; |\lambda_3|^2). \end{aligned} \tag{2.160}$$

Here, ${}_pF_q(a_1 \cdots a_p; b_1, \cdots b_q; z)$ denotes the generalized hypergeometric function (see, e.g. Brychkov). The normalization of the steady-state Wigner function is thus exactly computable:

$$W_{a,ss}(z-\alpha) = \frac{2|{}_1F_1(-r_1; -r_2; -\sqrt{2}\lambda_3 z^*)|^2 e^{-2|z|^2}}{\pi\, {}_2F_2(-r_1, -r_1^*; -r_2, -r_2^*; |\lambda_3|^2)^{1/2}}, \tag{2.161}$$

where here $\alpha \equiv \alpha_+/\sqrt{2}$ is the appropriately normalized displacement factor given in Eq. (2.32) defined earlier. We now move on to compute the matrix elements of the density matrix in the displaced frame (here, $\hat{D}_\alpha \equiv e^{-\alpha\hat{a}^\dagger - h.c.}$ is the standard displacement operator of the physical cavity).

$$\langle m|\hat{D}_\alpha\hat{\rho}_{a,ss}\hat{D}_\alpha^\dagger|n\rangle = \frac{(-\lambda_3)^m(-\lambda_3^*)^n}{N\sqrt{2^{m+n}n!m!}} \cdot \sum_{l=0}^{\infty}\frac{(-r_1)_{m+l}(-r_1^*)_{n+l}}{(-r_2)_{m+l}(-r_2^*)_{n+l}}\frac{(|\lambda_3|^2/2)^l}{l!}.$$

Utilizing the identity $(z)_{m+l} = (z)_m(z+m)_l$, the sum closes, and we get

$$\langle m|\hat{D}_\alpha\hat{\rho}_{a,ss}\hat{D}_\alpha^\dagger|n\rangle = \frac{\xi_m\xi_n^*}{\sqrt{2^{m+n}n!m!}} \cdot {}_2F_2(n-r_1, m-r_1^*; m-r_2; n-r_2^*; |\lambda_3|^2/2) \tag{2.162}$$

As for the normally-ordered cavity moments in the displaced frame, in a similar fashion, we get an analogous closed-form in terms of a generalized hypergeometric function:

$$\mathrm{Tr}[\hat{D}_\alpha\hat{\rho}_{a,ss}\hat{D}_\alpha^\dagger(\hat{a}^\dagger)^n\hat{a}^m] = \frac{\xi_m\xi_n^*}{\sqrt{2^{m+n}}} \cdot {}_2F_2(m-r_1, n-r_1^*; m-r_2; n-r_2^*; |\lambda_3|^2) \tag{2.163}$$

2.14 Exact results in the parity-conserving regime

We now will complete the process started in Section 2.7, namely that of tracing-out the ancilla resonator for each of the dark steady states obtained by the CQA method. We begin

with the formula in Section 2.12 on unique steady states:

$$\langle m|\hat{\rho}_{a,ss}|n\rangle = \frac{1}{\sqrt{2^{m+n}m!n!}}\sum_{l=0}^{\infty}\frac{\psi_{m+l}\psi_{n+l}^{*}}{2^{l}l!} \tag{2.164}$$

note that, as a direct consequence of $\psi_{2l-1} \equiv 0$, we have

$$\langle 2j+1|\hat{\rho}_{a,ss}|2k\rangle = \langle 2j|\hat{\rho}_{a,ss}|2k+1\rangle = 0, \tag{2.165}$$

as each term in the sum over l would identically vanish in these cases. In summary,

$$\hat{\Pi}_{e}\hat{\rho}_{a,ss}\hat{\Pi}_{o} = \hat{\Pi}_{o}\hat{\rho}_{a,ss}\hat{\Pi}_{e} = 0, \tag{2.166}$$

where $\hat{\Pi}_{e/o}$ are the the projections onto the subspaces of the resonator Hilbert space spanned by even/odd photon number states.

Therefore, by taking matrix elements on both sides of Eq. (2.104), one obtains

$$\langle m|\hat{\rho}_{e}|n\rangle = \frac{2N}{N+1}\langle m|\hat{\rho}_{a,ss}|n\rangle, \quad m,n \ \text{ even} \tag{2.167}$$

$$\langle m|\hat{\rho}_{o}|n\rangle = \frac{2N}{N-1}\langle m|\hat{\rho}_{a,ss}|n\rangle, \quad m,n \ \text{ odd}. \tag{2.168}$$

Therefore, to compute the steady states $\hat{\rho}_{e/o}$, it suffices to compute matrix elements of $\hat{\rho}_{a,ss}$. We note that this was done in Bartolo et al. [2016] (as this represents the unique steady-state regime $\kappa_1 \neq 0$), and so we're technically done, as we could simply cite the result here.

For completeness, however, we show that the calculation of the expressions on the RHS's of Eqs. (2.167-2.168) can be reproduced in a straightforward manner within the quantum

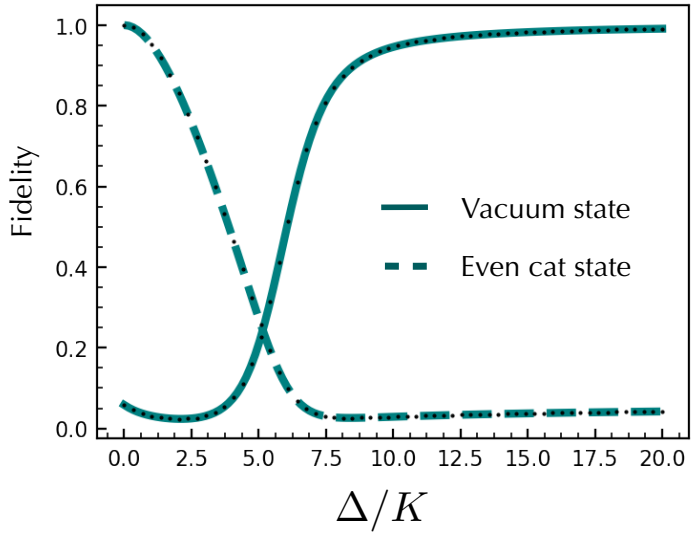

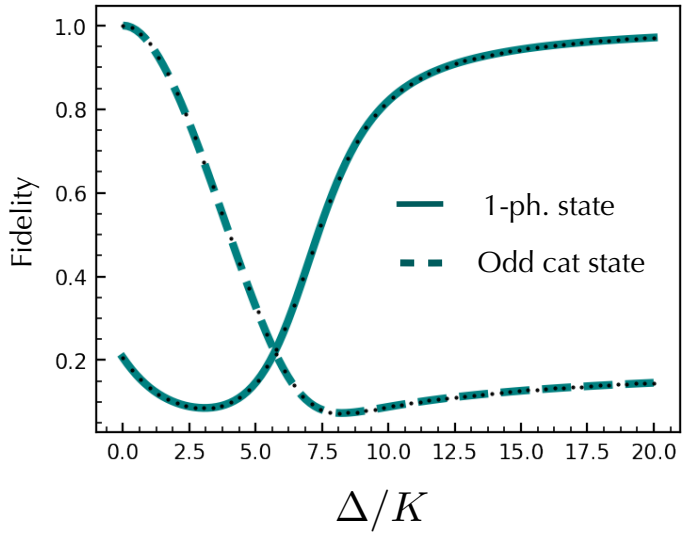

Figure 2.11: Limiting behavior of bistable states. (a). We plot the fidelity of $\hat{\rho}_e$ (c.f. Eq. (2.167)) with an even cat state with amplitude $\alpha = i\sqrt{\lambda_2/2}$ (solid line) and the vacuum state (dashed line). Corresponding results from exact diagonalization are also given (black dots) (b) We plot the fidelity of $\hat{\rho}_o$ (c.f. Eq. (2.168)) with an amplitude-α odd cat state (solid line) and a 1-photon Fock state (dashed line). Corresponding results from exact diagonalization are also given (black dots). *Parameter choices*: In both plots, $\Lambda_2 = 5K$, $\kappa_2 = K$, and $\Lambda_1, \kappa_1 \equiv 0$.

absorber formalism. Assuming $m \equiv 2j$, $n \equiv 2k$ are both even, we have

$$\begin{aligned}
\sum_{l=0}^{\infty} \frac{\psi_{m+l}\psi^*_{n+l}}{2^l l!} &= \sum_{l=0}^{\infty} \frac{\psi_{2(j+l)}\psi^*_{2(k+l)}}{2^{2l}(2l)!} \\
&= \psi_{2j}\psi^*_{2k} \sum_{l=0}^{\infty} \frac{(j+\frac{1}{2})_l (k+\frac{1}{2})_l}{(j-r_2)_l (k-r_2^*)_l} \frac{|\lambda_2|^{2l}}{2^{2l}(2l)!} \\
&= \psi_{2j}\psi^*_{2k} \sum_{l=0}^{\infty} \frac{(j+\frac{1}{2})_l (k+\frac{1}{2})_l}{(j-r_2)_l (k-r_2^*)_l (\frac{1}{2})_l} \frac{|\lambda_2/4|^{2l}}{l!}
\end{aligned} \tag{2.169}$$

Therefore, in total we have

$$\sum_{l=0}^{\infty} \frac{\psi_{m+l}\psi^*_{n+l}}{2^l l!} \tag{2.170}$$

$$= \psi_{2j}\psi^*_{2k} \cdot {}_2F_3(j+\frac{1}{2},\ k+\frac{1}{2}; j-r_2, k-r_2^*, \frac{1}{2}; |\lambda_2/4|^2). \tag{2.171}$$

Assuming $m \equiv 2j+1$, $n \equiv 2k+1$ are both odd, we have

$$\begin{aligned}
\sum_{l=0}^{\infty} \frac{\psi_{m+l}\psi^*_{n+l}}{2^l l!} &= \sum_{l=0}^{\infty} \frac{\psi_{2(j+l+1)}\psi^*_{2(k+l+1)}}{2^{2l+1}(2l+1)!} \\
&= 4\sum_{l=1}^{\infty} \frac{l\psi_{2(j+l)}\psi^*_{2(k+l)}}{2^{2l}(2l)!} \\
&= 4\psi_{2j}\psi^*_{2k} \sum_{l=1}^{\infty} \frac{l(\frac{1}{2}+j)_l (\frac{1}{2}+k)_l}{(j-r_2)_l (k-r_2^*)_l (\frac{1}{2})_l} \frac{|\lambda_2/4|^{2l}}{l!} \\
&= 4\psi_{2j}\psi^*_{2k} \frac{(j+\frac{1}{2})(k+\frac{1}{2})|\lambda_2/4|^2}{(j-r_2)(k-r_2^*)(\frac{1}{2})} \\
&\quad \cdot \sum_{l=1}^{\infty} \frac{(\frac{3}{2}+j)_l (\frac{3}{2}+k)_l}{(j+1-r_2)_l (k+1-r_2^*)_l (\frac{3}{2})_l} \frac{|\lambda_2/4|^{2l}}{l!}
\end{aligned} \tag{2.172}$$

Therefore, in total we have

$$\sum_{l=0}^{\infty} \frac{\psi_{m+l}\psi_{n+l}^*}{2^l l!} = \frac{\psi_{2j}\psi_{2k}^*}{2} \frac{(j+\frac{1}{2})(k+\frac{1}{2})|\lambda_2|^2}{(j-r_2)(k-r_2^*)} \cdot {}_2F_3(j+\frac{3}{2},\ k+\frac{3}{2}; j+1-r_2, k+1-r_2^*, \frac{3}{2}; |\lambda_2/4|^2). \tag{2.173}$$

In summary, we have the following closed-form for $\hat{\rho}_{a,ss}$ in the Fock basis:

$$\langle m|\hat{\rho}_{a,ss}|n\rangle \underset{m,n\in 2\mathbb{Z}}{=} \frac{\psi_m\psi_n^*}{\sqrt{2^{m+n}m!n!}} {}_2F_3(\frac{m+1}{2}, \frac{n+1}{2}; \frac{m-D+1}{2}, \frac{n-D^*+1}{2}, \frac{1}{2}; \left|\frac{\lambda_2}{4}\right|^2), \tag{2.174}$$

$$\langle m|\hat{\rho}_{a,ss}|n\rangle \underset{m,n\in 1+2\mathbb{Z}}{=} \frac{\psi_{m-1}\psi_{n-1}^*}{\sqrt{2^{m+n}m!n!}} \frac{|\lambda_2|^2 mn}{2(m-D)(n-D^*)} \cdot {}_2F_3(\frac{m+2}{2}, \frac{n+2}{2}; \frac{m-D+2}{2}, \frac{n-D^*+2}{2}, \frac{3}{2}; \left|\frac{\lambda_2}{4}\right|^2). \tag{2.175}$$

Substituting Eq.'s (2.174-2.175) into Eq.'s (2.167-2.168) , we get that the bistable manifold of the Kerr cavity in this regime is spanned by the following density matrices:

$$\langle m|\hat{\rho}_e|n\rangle \underset{m,n\in 2\mathbb{Z}}{=} \frac{2N}{N+1} \frac{\psi_m\psi_n^*}{\sqrt{2^{m+n}m!n!}} \cdot {}_2F_3(\frac{m+1}{2}, \frac{n+1}{2}; \frac{m-D+1}{2}, \frac{n-D^*+1}{2}, \frac{1}{2}; \left|\frac{\lambda_2}{4}\right|^2), \tag{2.176}$$

$$\langle m|\hat{\rho}_o|n\rangle \underset{m,n\in 1+2\mathbb{Z}}{=} \frac{2N}{N-1} \frac{\psi_{m-1}\psi_{n-1}^*}{\sqrt{2^{m+n}m!n!}} \frac{|\lambda_2|^2 mn}{2(m-D)(n-D^*)} {}_2F_3(\frac{m+2}{2}, \frac{n+2}{2}; \frac{m-D+2}{2}, \frac{n-D^*+2}{2}, \frac{3}{2}; \left|\frac{\lambda_2}{4}\right|^2), \tag{2.177}$$

and with all other matrix elements vanishing. Here, N has the closed-form expression (also given in Eq. (2.102)):

$$N = {}_1F_2(1/2; 1/2-D/2, (1/2-D/2)^*; |\lambda_2/2|^2). \tag{2.178}$$

For small detuning $|D| \ll 1$, the CQA solutions above approach even/odd cat states, both of which exhibit Wigner function negativity. In the large detuning limit $|D| \gg 1$, $\hat{\rho}_{e/o}$ also approach pure states: the vacuum state and one-photon state respectively, one of which exhibits Wigner function negativity. The exact CQA solutions are validated against master equation numerics in Figure 2.11.

For completeness, we include here the calculation of N in Eq. (2.178) (this expression also shows up in Eq. (2.104), where it controls the average parity of the unique steady state selected when parity-symmetry is spontaneously broken). The derivatives of the dark state, evaluated at the origin in phase space, are

$$\psi_{2l} = \frac{1}{N^{1/2}} \frac{(2l)!}{l!(\frac{1}{2} - \frac{D}{2})_l} (-\lambda_2/4)^l \tag{2.179}$$

whereas the odd derivatives vanish at the origin ($\psi_{2l-1} = 0$). However, note the following identity $\frac{(2l)!}{l!} = 2^{2l}(\frac{1}{2})_l$. With this identity, the Fock state amplitudes take the simpler form:

$$\psi_{2l} = \frac{1}{N^{1/2}} \frac{(-r_1)_l}{(-r_2)_l} (-\lambda_2)^l \tag{2.180}$$

with $r_1 \equiv -1/2$, and $r_2 \equiv r_1 + D/2$. Having computed the Taylor coefficients ψ_l, Eq. (2.149) gives us the normalization:

$$\begin{aligned} N &= \sum_{l=0}^{\infty} \frac{(\frac{1}{2})_l (\frac{1}{2})_l}{(-r_2)_l (-r_2^*)_l} \frac{|\lambda_2|^{2l}}{(2l)!} \\ &= \sum_{l=0}^{\infty} \frac{(\frac{1}{2})_l}{(-r_2)_l (-r_2^*)_l} \frac{|\lambda_2/2|^{2l}}{l!} \\ &= {}_1F_2(\tfrac{1}{2}; -r_2, -r_2^*; |\lambda_2|^2). \end{aligned} \tag{2.181}$$

This concludes the calculation of the normalization constants in the expressions Eqs. (2.167-2.168).

2.15 Conclusions

In this, work, we have presented a generalization of the coherent quantum absorber method developed by Stannigel et al. [2012b] for solving the simplest driven Kerr resonator problem. Our generalization exploited the Segal-Bargmann representation, and allows one to analytically solve for the steady state of driven-dissipative Kerr cavity models with nonlinear driving and nonlinear loss. We used these analytic solutions to describe a host of new physical phenomena, including generalized photon-blockade phenomena, and new regimes of near quantum bistability. These phenomena should be experimentally accessible in a number of different platforms, including superconducting circuit experiments.

Our work naturally suggests many new open questions and directions for future study. For example, can the new bistable parameter points we have identified be utilized for quantum-information applications? Are there other forms of nonlinear dissipation and driving that could also be included in our system that still leave it amenable to solution via the CQA method? Can this approach be extended to nonlinear driven-dissipative systems with more than one cavity?

At a fundamental level, there is also the basic question of *why* the CQA method is able to yield exact solutions to systems that are on the surface highly non-trivial (because of strong nonlinearities and driving). Is there some general physical principle here, or perhaps a dissipative version of integrability that underlies this method? These are all questions we hope to explore in future works.

CHAPTER 3

HIDDEN TIME-REVERSAL SYMMETRY

3.1 Introduction

In this chapter, we introduce the foundational theory of hidden time-reversal symmetry, which includes how it relates to classical detailed balance, quantum absorber approaches to solving quantum master equations in quantum optics, as well as connections to prior work in mathematical physics, dating back to the mid 1990's.

In particular, we explore in detail two classes of ubiquitous, experimentally-accessible systems (see Table 3.1): Rabi-driven qubits subject to dissipation, and driven-dissipative nonlinear quantum cavities. These systems exhibit in general no correlation function time-symmetry, and hence do not possess CQDB as defined in Agarwal [1973]. They however do possess hidden-TRS in the low temperature or small nonlinearity limit. This explains the surprising exact solvability of a variety of driven nonlinear cavity models Drummond and Gardiner [1980], Drummond and Walls [1980b], Bartolo et al. [2016], Elliott and Ginossar [2016], Roberts and Clerk [2020]. We explore how hidden TRS is broken in these models by the combination of non-zero temperature, driving and nonlinearity. For nonlinear cavities, breaking of detailed balance was extensively studied in the semiclassical limit Dykman and Krivoglaz [1979], Dykman and Smelyanskii [1988], Marthaler and Dykman [2006], Dykman [2012], Guo et al. [2013], Guo [2013], Zhang and Dykman [2019].

For clarity, the specific example systems we have chosen to illustrate our ideas are either single qubit or nonlinear cavity systems. We wish to stress though that the basic notion of hidden-TRS and connection to exact solutions we present is extremely general, going far beyond these simple examples. We thus anticipate these ideas will also have utility in the study of driven-dissipative many-body systems. This is an increasingly active area of research, both experimentally (see e.g. Baumann et al. [2010b], Landig et al. [2016], Dogra

System	CQDB	Hidden TRS	Hidden TRS: unique?
Thermal qubit	Yes	Yes	$\hat{T}_\theta,\ e^{i\theta} \equiv 1$
Thermal linear cavity	Yes	Yes	$\hat{T}_\theta,\ e^{i\theta} \equiv 1$
Kerr cavity, 1-ph. drive	*No*	*Yes*	*Yes*
Kerr cavity, 2-ph. drive	*No*	*Yes*	No; $\hat{T}_+, \hat{T}_-$
with nonzero temp.	No	No	N/A
Driven qubit	*No*	*Yes*	*Yes*
with non-zero temp.	No	No	N/A

Table 3.1: Common driven-dissipative quantum systems and their status both with respect to conventional quantum detailed balance (CQDB) (c.f. Sec. 3.2.4), and our new notion of hidden-TRS. Italics indicate systems with hidden-TRS that do not have CQDB. Some of these systems possess multiple distinct hidden TRS (right-most column).

et al. [2019], Muniz et al. [2020]) and theoretically (see e.g. Nagy et al. [2010b], Buca and Jaksch [2019], Ivanov et al. [2020], Jager et al. [2019], Mivehvar et al. [2019], Caballero-Benitez and Mekhov [2015]).

While experiments on doubled quantum systems prepared in thermofield double states have recently been performed Zhu and Monroe [2020], hidden TRS also has experimental consequences in experiments on just a single system. Unlike CQDB, systems with hidden TRS will not exhibit Onsager time-symmetry of all correlators. However, we show that there are always a class of special correlation functions that are guaranteed to have this time symmetry. This provides a direct means for probing hidden TRS (and its possible breaking) in a variety of experimental platforms.

3.2 Classical detailed balance and conventional quantum detailed balance

3.2.1 Classical detailed balance

Consider a classical stochastic system with a discrete set of microstates indexed by integers n, whose Markovian dynamics is fully described by a set of transition rates $\Gamma_{n\to m}$. The

time-dependent probability $p(n,t)$ for the system to be in a given state n then obeys:

$$\frac{d}{dt}p(n,t) = \sum_m p(m,t)\Gamma_{m\to n} - \sum_m p(n,t)\Gamma_{n\to m}. \tag{3.1}$$

We assume that this equation admits a time-independent steady-state probability distribution $\bar{p}(n)$. This steady state is said to have detailed balance if there is a balancing of probability fluxes between any given pair of states and their time-reversed partners. Letting $\tilde{n}$ denote the time-reversed version of the microstate n, the condition is (see e.g. Gardiner [2009]):

$$\bar{p}(n)\Gamma_{n\to m} = \bar{p}(\tilde{m})\Gamma_{\tilde{m}\to\tilde{n}}. \tag{3.2}$$

This definition generalizes directly to systems with a continuous state space: Eq. (3.1) then becomes a Fokker-Planck equation, and Eq. (3.2) becomes a constraint on drift and diffusion matrices (so-called potential conditions). As is well known, these "zero probability flux" conditions give a direct way to find the steady state distribution. In the discrete case, one uses the zero-flux condition to iteratively find the probability of each microstate in terms of the rates. The continuous version of this yields the steady state in terms of a potential function that is determined by drift and diffusion matrices (see e.g. Gardiner [2009]).

One can equivalently define detailed balance by a time symmetry of correlation functions, what we term here an Onsager symmetry. Suppose X and Y are arbitrary functions of the microstate n of our system. Steady state correlation functions can be defined in the usual manner in terms of conditional probabilities $p(m,t|n,0)$, which can be computed from Eq. (3.1). For example:

$$\overline{X(t)Y(0)} \equiv \sum_{m,n} X(m)p(m,t|n,0)Y(n)\bar{p}(n) \tag{3.3}$$

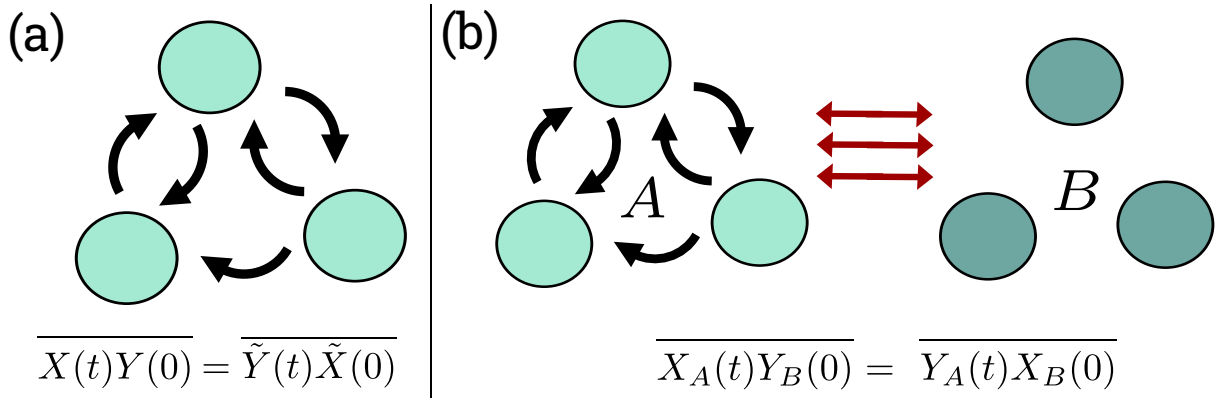

Figure 3.1: (a) System with discrete microstates, described by a classical master equation. Detailed balance (Eq. (3.2)) is equivalent to a time-symmetry of stationary correlation functions. (b) Equivalent formulation of classical detailed balance, involving a doubled system prepared in an initial correlated state given in Eq. (3.6); the auxiliary system B has no dynamics. The detailed balance condition in (a) is equivalent to requiring a time-symmetry of doubled-system correlators.

The detailed balance condition of Eq. (3.2) is then equivalent to requiring that the following symmetry hold for all steady state correlation functions:

$$\overline{X(t)Y(0)} = \overline{\tilde{Y}(t)\tilde{X}(0)}. \tag{3.4}$$

Here, the time-reversed function $\tilde{X}$ is defined as $\tilde{X}(n) \equiv X(\tilde{n})$.

3.2.2 Doubled-system formulation of classical detailed balance

Consider now an alternate but equivalent formulation of classical detailed balance Duvenhage and Snyman [2018]. We imagine making a copy of our original system that has exactly the same set of microstates as the original. This auxiliary system (system B) is completely static, whereas the original system (system A) retains its transition rates and dynamics, see Fig. 3.1. To be explicit, the doubled-system is described by a probability distribution

$p_{AB}(n_A, n_B; t)$ which satisfies the master equation:

$$\frac{d}{dt}p_{AB}(n, n'; t) = \sum_m p_{AB}(m, n'; t)\Gamma_{m\to n} - \sum_m p_{AB}(n, n'; t)\Gamma_{n\to m}. \tag{3.5}$$

We further assume that the doubled system is initially prepared in a correlated state described by the probability distribution:

$$p_{AB}(n, m; 0) = \bar{p}(n)\delta_{m,\tilde{n}}, \tag{3.6}$$

where $\bar{p}(n)$ is the single-system steady state of interest. Note that the correlations in this state partner each microstate n in system A with its time-reversed partner $\tilde{n}$ in system B. It is easy to confirm that the marginal probability distribution describing each subsystem alone (A or B) is time independent and equal to $\bar{p}(n)$ for system A, and $\bar{p}(\tilde{n})$ for system B. In contrast, the total state of the two systems will evolve non-trivially. The result is that while quantities involving only each subsystem are completely static, correlations between the two subsystems will evolve in time.

Given this dynamics and initial state, we now ask whether inter-system correlations at time $t > 0$ are invariant if we "exchange" the two subsystems. To be concrete, we consider two observable quantities X and Y that we could measure on either system A or B; these are functions of microstates, i.e. $X_A(n, m) = X(n)$, $X_B(n, m) = X(m)$. We now define a doubled-system Onsager time-symmetry by the requirement:

$$\overline{X_A(t)Y_B(0)} = \overline{Y_A(t)X_B(0)}, \tag{3.7}$$

for all possible observables X, Y. We stress that system B is not dynamical.

Superficially, this looks very different from the standard Onsager time-symmetry con-

straint in Eq. (3.4). We are not exchanging observation times, but rather the subsystem in which each quantity is measured. There is also no explicit time-reversal operation in this equation (it is instead hardwired into the initial correlated state). Despite these differences, one can easily show (see Ref. Duvenhage and Snyman [2018] and Sec. 3.9) that the above symmetry relation is *completely* equivalent to standard Onsager time symmetry. While this formulation thus provides nothing new in the classical context, we will see that it motivates an extremely powerful generalized notion for quantum systems, namely the notion of a hidden time-reversal symmetry.

3.2.3 Markovian quantum open system: general setting

Onsager-like correlation function time-symmetries can also be considered in the context of open quantum systems Agarwal [1973], Carmichael and Walls [1976], Denisov et al. [2002]. For systems well-described by a Lindblad master equation, the dynamics is completely specified by the Hermitian system Hamiltonian $\hat{H}$ and a set of jump operators $\hat{c}_l$ that describe the influence of external dissipative reservoirs. Defining $\hat{H}_{\text{eff}} = \hat{H} - \frac{i}{2}\sum_l \hat{c}_l^\dagger \hat{c}_l$, our general Lindblad equation of motion for the system density matrix $\hat{\rho}(t)$ is:

$$\frac{d}{dt}\hat{\rho} = -i(\hat{H}_{\text{eff}}\hat{\rho} - \hat{\rho}\hat{H}_{\text{eff}}^\dagger) + \sum_{l=1}^{M} \hat{c}_l \hat{\rho} \hat{c}_l^\dagger \equiv \mathcal{L}[\hat{\rho}], \tag{3.8}$$

where we have introduced the Liouvillian superoperator $\mathcal{L}$. Given a particular steady state of this equation (i.e. a time-independent solution $\hat{\rho}_{\text{ss}}$), steady-state correlators between two system operators $\hat{X}$ and $\hat{Y}$ obey time-translation symmetry and can be calculated from the master equation (see, e.g., Breuer and Petruccione [2002]). To state this compactly, we first introduce the adjoint Liouvillian superoperator $\bar{\mathcal{L}}$, determined by (see e.g. Ref. Gardiner and

Zoller [2000])

$$\bar{\mathcal{L}}[\hat{A}] \equiv i(\hat{H}_{\text{eff}}^{\dagger}\hat{A} - \hat{A}\hat{H}_{\text{eff}}) + \sum_{l=1}^{M} \hat{c}_l^{\dagger}\hat{A}\hat{c}_l. \tag{3.9}$$

Following the quantum regression theorem Gardiner and Collett [1985], correlation functions are then computed as

$$\langle \hat{X}(t)\hat{Y}(0)\rangle \equiv \text{Tr}\left(\mathcal{E}_t[\hat{X}]\hat{Y}\hat{\rho}_{\text{ss}}\right), \quad \mathcal{E}_t \equiv \exp\left(\bar{\mathcal{L}}t\right). \tag{3.10}$$

Stated explicitly, $\mathcal{E}_t$ is a superoperator generated by exponentiating the superoperator $\bar{\mathcal{L}}$ times t. $\mathcal{E}_t[\hat{X}]$ is then a standard operator generated by having $\mathcal{E}_t$ act on the operator $\hat{X}$, i.e. $\mathcal{E}_t[\hat{X}] = \sum_{n=0}^{\infty} \frac{t^n \bar{\mathcal{L}}^n[\hat{X}]}{n!}$.

We briefly note that while time-independent Lindblad master equations provide an excellent description of many physical systems and are ubiquitous in many areas of physics, there are of course more general kinds of open-systems descriptions. For example, if one is interested in describing driving effects beyond the rotating-wave approximation, one is often lead to master equations that are explicitly time-dependent (see e.g. Kamleitner and Shnirman [2011], Ferron et al. [2012], Blattmann et al. [2015], Reimer et al. [2018]). Similar to previous studies of quantum detailed balance, we will not consider this situation here. We note that even in a strictly classical context, there is no universally accepted definition of detailed balance for systems described by explicitly time-dependent master equations. Standard textbook discussions only discuss detailed balance in the time-independent case Gardiner [2009].

3.2.4 Conventional quantum detailed balance (CQDB)

As mentioned in the introduction, a variety of definitions of quantum detailed balance have been formulated for Lindblad Markovian master equations Duvenhage and Snyman [2018],

Agarwal [1973], Cipriani [1997], Kossakowski et al. [1977]. The simplest and best-known definition of quantum detailed balance involves the same constraint on correlation functions that exists in the classical setting Agarwal [1973], Carmichael and Walls [1976]. With this definition (which we call conventional quantum detailed balance (CQDB)), detailed balance requires:

$$\langle \hat{X}(t)\hat{Y}(0)\rangle = \langle \tilde{Y}^\dagger(t)\tilde{X}^\dagger(0)\rangle. \tag{3.11}$$

Here $\hat{X}$ and $\hat{Y}$ are arbitrary system operators, and tilde is used to denote the time-reversed version of an operator, i.e. $\tilde{B} \equiv \hat{T}\hat{B}\hat{T}^{-1}$, where $\hat{T}$ is the anti-unitary time-reversal operator. Note that on the RHS of Eq. (3.11), we have $\tilde{Y}^\dagger(t) \equiv \mathcal{E}_t\left[\tilde{Y}^\dagger\right]$.

Besides being simple to state, the CQDB correlation function symmetry also has a direct connection to a microscopic symmetry: this correlation function time symmetry *necessarily* holds if the microscopic system-bath dynamics has time-reversal symmetry Carmichael and Walls [1976]. This requires both that the entire system-plus-bath Hamiltonian has time-reversal, and that the bath state also relaxes to a time-independent state (not just the system state). This connection to microscopics (and the fact that it involves measurable correlation functions) has led many to consider CQDB the most natural generalization of classical detailed balance to quantum systems Denisov et al. [2002]. Note that CQDB is also referred to as "GNS detailed balance" Carlen and Maas [2017].

3.2.5 CQDB implies a trivial steady state

As has been noted previously Alicki [1976], Fagnola and Umanita [2007], Fagnola and Umanità [2010], the CQDB condition is extremely restrictive: it *only* holds for systems with steady states that are diagonal in the energy eigenstate basis (i.e. $[\hat{H}, \hat{\rho}_{\text{ss}}] = 0$)[1]. Such states are

1. The Hamiltonian in a Lindblad master equation is in general not unique. Our condition holds for the case where jump operators are chosen to be traceless.

in some sense trivial, as they can be found by solving a classical (Pauli) master equation, obtained by setting all energy-eigenstate coherences in Eq. (3.8) to zero. The resulting steady state can thus be interpreted classically: the Hamiltonian plays no role, and steady-state probabilities are determined by balancing incoherent transition rates between different eigenstates. A simple proof of this result is presented in Sec. 3.10.

The upshot is that CQDB is found in an extremely limited class of systems, and is not a useful tool for finding non-trivial quantum steady states; in fact, the presence of CQDB makes it impossible to have such a state. In Sec. 3.11, we show explicitly that an extremely simple model of a Rabi-driven dissipative qubit fails to have CQDB (though it will possess the hidden time-reversal symmetry we introduce in the next section).

3.3 Hidden time-reversal symmetry and generalized detailed balance

3.3.1 Basic formulation

As we have discussed, the simple CQDB condition of Eq. (3.11) corresponds directly to microscopic time-reversal symmetry Carmichael and Walls [1976]. We now consider something more general, the notion of *hidden* time-reversal symmetry, which we will formulate in a doubled version of our original system (in rough analogy to the classical construction in Sec. 3.2.2). This unusual symmetry will connect directly to an abstract variant of quantum detailed balance (so called "SQDB-θ") studied in the mathematical physics literature Fagnola and Umanita [2007], Fagnola and Umanità [2010], and which was recently linked to entanglement Duvenhage and Snyman [2018]. Our work complements these studies by providing a direct physical motivation for this definition and connects it explicitly to symmetry. More importantly, we show that this formulation has great practical utility: it allows us to solve for non-trivial steady states. This connection was not previously known.

Our starting point is again the Lindblad master equation of Eq. (3.8) and particular steady state $\hat{\rho}_{\rm ss}$, which we write in diagonal form as

$$\hat{\rho}_{\rm ss} = \sum_n p_n |n\rangle\langle n|. \tag{3.12}$$

Throughout this chapter, we will assume that $\hat{\rho}_{\rm ss}$ is full rank, and further, that the p_n have no degeneracies.

We next construct a purification of this state: an entangled pure state $|\psi_T\rangle$ of a doubled version of our system that yields $\hat{\rho}_{\rm ss}$ if we trace out the auxiliary system B. We take system B to have the same Hilbert space as the original system A. To construct $|\psi_T\rangle$, we first chose an anti-unitary operator $\hat{T}$ which will define our hidden time-reversal symmetry. We then use this choice to construct $|\psi_T\rangle$ in a manner that mimics the classical doubled-system state in Eq. (3.6): we pair each pointer state $|n\rangle$ in the original system with its time-reversed partner in the auxiliary system. We thus have

$$|\psi_T\rangle \equiv \sum_n \sqrt{p_n}\, |n\rangle_A \left(\hat{T}\, |n\rangle_B\right) \equiv \sum_n \sqrt{p_n}\, |n\rangle_A\, |\tilde{n}\rangle_B \tag{3.13}$$

With this definition, $|\psi_T\rangle$ is invariant under a gauge change of the $\hat{\rho}_{\rm ss}$ eigenkets $|n\rangle \to e^{i\alpha_n}|n\rangle$. The state $|\psi_T\rangle$ has the form of a so-called "thermofield double state"; such states have been studied in many different contexts Takahashi and Umezawa [1996], though usually without including a time-reversal operation in its definition. We stress that the form of $|\psi_T\rangle$ is contingent on the choice of $\hat{T}$.

We next specify the dynamics of the doubled system: as we did in the classical case, we take subsystem A to evolve as per the master equation in Eq. (3.8), but take the auxiliary subsystem B to have no dynamics at all. The dynamics of the joint system thus follows the

Lindblad master equation:

$$\frac{d}{dt}\hat{\rho}_{AB}(t) = [\mathcal{L} \otimes \mathbb{1}_B]\, \hat{\rho}_{AB}(t) \tag{3.14}$$

where $\mathcal{L}$ is our original single-system Liouvillian, and $\mathbb{1}_B$ denotes the unit superoperator acting on subsystem B. Starting the doubled system at $t = 0$ in the pure state $\hat{\rho}_{AB}(0) = |\psi_T\rangle\langle\psi_T|$, this dynamics leaves the reduced density matrices of each subsystem invariant. It does not however leave the full joint state $\hat{\rho}_{AB}$ time invariant. The result is that single-system expectation values are time-independent, but correlations between them can evolve.

We will now use these evolving inter-system correlations to define the notion of a hidden time reversal symmetry. We define single-subsystem operators in the natural way, i.e. $\hat{X}_A \equiv \hat{X} \otimes \hat{1}$, $\hat{X}_B \equiv \hat{1} \otimes \hat{X}$. Starting in the state $|\psi_T\rangle$ and evolving as per Eq. (3.14), hidden TRS holds if all inter-system correlations obey the following symmetry:

$$\mathrm{Tr}\left[\hat{X}_A \hat{Y}_B\, \hat{\rho}_{AB}(t)\right] = \mathrm{Tr}\left[\hat{Y}_A \hat{X}_B\, \hat{\rho}_{AB}(t)\right] \tag{3.15}$$

Stated explicitly, the symmetry requires that inter-system correlations at any time $t \geq 0$ are invariant if we exchange which subsystem each quantity is measured in. Note that as system B has no dynamics, we can equivalently write this condition in the Heisenberg picture. Defining

$$C_{XY}^{\mathrm{TFD}}(t) \equiv \begin{cases} \langle\psi_T|\hat{X}_A(t)\hat{Y}_B|\psi_T\rangle & t \geq 0 \\ \langle\psi_T|\hat{Y}_A(-t)\hat{X}_B|\psi_T\rangle & t < 0 \end{cases} \tag{3.16}$$

the condition for having hidden TRS condition then becomes

$$C_{XY}^{\mathrm{TFD}}(t) = C_{XY}^{\mathrm{TFD}}(-t) \tag{3.17}$$

Note that for a general system that does not have hidden TRS, the definition in Eq. (3.16)

implies that not only can $C_{XY}^{\mathrm{TFD}}(t)$ be asymmetric, it can even fail to be continuous at $t = 0$. We also stress again that the hidden-TRS condition above is contingent on the choice of anti-unitary $\hat{T}$. As we will see, there exist physical systems where hidden-TRS is in some sense degenerate: there are a whole family of distinct operators $\hat{T}$ for which Eq. (3.17) holds.

Despite mirroring the classical doubled-system construction, in the quantum case Eq. (3.17) gives us something truly new: there are systems that fail to satisfy the Onsager symmetry condition of Eq. (3.11), but nonetheless satisfy the generalized condition in Eq. (3.17). In these cases, we describe the particular anti-unitary operator $\hat{T}$ used to define $|\psi_T\rangle$ as a *hidden time-reversal symmetry*. Note that *if* a system has hidden TRS, the steady state is invariant under the corresponding time-reversal operation:

$$\hat{T}\hat{\rho}_{\mathrm{ss}}\hat{T}^{-1} = \hat{\rho}_{\mathrm{ss}} \tag{3.18}$$

This follows directly by assuming hidden TRS (i.e. Eq. (3.15)), and taking the choice $\hat{Y} = 1$. The only way the remaining condition can hold for all $\hat{X}$ is if Eq. (3.18) holds.

To gain intuition for the role of entanglement in our formulation of hidden TRS, it is useful to express the doubled correlation function in terms of the eigenstates of $\hat{\rho}_{\mathrm{ss}}$, c.f. Eq. (3.12). Using Eq. (3.16), we have

$$\begin{aligned} C_{XY}^{\mathrm{TFD}}(t > 0) &= \sum_{nm} \sqrt{p_n p_m}\langle n|\hat{X}(t)|m\rangle\langle\tilde{n}|\hat{Y}|\tilde{m}\rangle \\ &= C_{XY}^{\mathrm{cl}}(t) + C_{XY}^{\mathrm{en}}(t), \end{aligned} \tag{3.19}$$

where

$$C_{XY}^{\mathrm{cl}}(t) \equiv \sum_n p_n \langle n|\hat{X}(t)|n\rangle\langle\tilde{n}|\hat{Y}|\tilde{n}\rangle \tag{3.20}$$

$$C_{XY}^{\mathrm{en}}(t) \equiv \sum_{n\neq m} \sqrt{p_n p_m}\langle n|\hat{X}(t)|m\rangle\langle\tilde{n}|\hat{Y}|\tilde{m}\rangle. \tag{3.21}$$

For times $t < 0$, Eqs. (3.19)-(3.21) are defined analogously to $C_{XY}^{\mathrm{TFD}}(t)$ itself.

The above separation has a direct physical significance, as it is the second contribution in Eq. (3.21) that encodes the contribution from quantum entanglement. To see this explicitly, suppose that we initially had prepared our doubled system in a state that only had classical correlations (but not entanglement) between systems A and B, i.e.

$$\hat{\rho}_{AB}(0) = \sum_n p_n |n,\tilde{n}\rangle\langle n,\tilde{n}|. \tag{3.22}$$

In this case, our *entire* inter-system correlation functions would be given by Eq. (3.20):

$$\begin{aligned}\mathrm{Tr}\left[\hat{X}_A(t)\hat{Y}_B\,\hat{\rho}_{AB}\right] &= \sum_n p_n \langle n|\hat{X}(t)|n\rangle\langle\tilde{n}|\hat{Y}|\tilde{n}\rangle \\ &= C_{XY}^{\mathrm{cl}}(t).\end{aligned} \tag{3.23}$$

We can thus view $C_{XY}^{\mathrm{en}}(t)$ in Eq. (3.21) as the extra contribution to the TFD correlator that stems from having quantum entanglement (as opposed to purely classical correlations).

3.3.2 CQDB as a special case of hidden TRS

At this point, it is natural to ask whether there is any simple relation between our notion of hidden TRS and conventional CQDB (which we stress is directly connected to microscopic time-reversal of the complete system-plus-environment Carmichael and Walls [1976]). The first key result here is that *CQDB is a special case of hidden-TRS*: any system satisfying

CQDB automatically has a hidden-TRS, but *the converse is not true*. Recall from Sec. 3.2.5 that systems satisfying CQDB necessarily have somewhat trivial steady states (in that they are diagonal in the energy eigenstate basis). In contrast, there are many systems with have hidden TRS but not CQDB, and have steady states with non-zero coherences between energy eigenstates. This is a crucial result: hidden TRS does not preclude having a non-trivial steady state.

To understand the origin of the above result, it is useful to introduce an effective dimensionless Hermitian Hamiltonian defined by the steady-state density matrix $\hat{\rho}_{\rm ss}$, the so-called modular Hamiltonian:

$$\hat{H}_\rho \equiv -\log \hat{\rho}_{\rm ss}. \tag{3.24}$$

Any system possessing CQDB has an extremely tight constraint on its dynamics Bratteli and Haagerup [1978]: dynamical evolution generated by the full Liouvillian $\mathcal{L}$ must commute with evolution generated by $\hat{H}_\rho$ (i.e. by the unitary $e^{-i\hat{H}_\rho t}$). This symmetry allows one to demonstrate that CQDB is a special case of hidden TRS, using the same methods introduced to study a class of generalized QDB conditions in Refs. Fagnola and Umanita [2007], Fagnola and Umanità [2010]. In Section 3.13, we give a non-technical proof of this result: for any system with modular symmetry, CQDB and hidden TRS are equivalent Fagnola and Umanita [2007], and thus CQDB implies hidden TRS.

The second key result connecting hidden TRS and CQDB involves the limit of vanishing incoherent dynamics. Consider a system that possesses hidden-TRS even as the strength of the incoherent dynamics is tuned to zero (i.e. replace the jump operators $\hat{c}_l \to \lambda \hat{c}_l$ in the master equation, and let $\lambda \to 0$). In such systems, hidden TRS reduces to CQDB in the limit of vanishing dissipation. Hence, while in many cases finite dissipation destroys CQDB, hidden TRS can continue to be a symmetry.

This result can also be understood using the modular Hamiltonian. In the limit of van-

ishing dissipation, the full dynamics is completely generated by the Hermitian Hamiltonian $\hat{H}$, i.e.

$$\mathcal{L}[\hat{\rho}] \sim -i[\hat{H}, \hat{\rho}]. \tag{3.25}$$

Further, in this limit the steady state $\hat{\rho}_{\text{ss}}$ must commute with $\hat{H}$ in order to be stationary. These two facts then necessarily imply that in this asymptotic zero dissipation limit, the full Liouvillian commutes with the modular Hamiltonian. As discussed above, this then implies that our system has CQDB in the zero-dissipation limit. This proves the desired result: systems with hidden TRS always recover CQDB in the weak dissipation limit. At a more physical level, systems with hidden TRS do not necessarily have (single system) correlation functions that are time-symmetric. However, the lack of time-symmetry vanishes in the zero-dissipation limit.

3.3.3 Hidden TRS has observable consequences for a single system

Hidden TRS might initially seem to be experimentally irrelevant in most settings, as it is defined in terms of TFD correlators (c.f. Eq. (3.16)) that require one to prepare two copies of the system of interest in an initial entangled state. This is usually extremely challenging (though see the recent trapped ion experiment in Ref. Zhu and Monroe [2020]). Formally, one could define this correlator as a single-system quantity involving a *state-dependent* observable. We first introduce a superoperator $\mathcal{J}$ which acts on single-system operators:

$$\mathcal{J}[\hat{X}]_A|\psi_T\rangle \equiv \hat{X}_B|\psi_T\rangle \tag{3.26}$$

$\mathcal{J}$ is well-defined and unique when $\hat{\rho}_{ss}$ is full-rank, and is given by the explicit formula (see Sec. 3.12)

$$\mathcal{J}[\hat{X}] = \hat{\rho}_{\rm ss}^{1/2} \tilde{X}^\dagger \hat{\rho}_{\rm ss}^{-1/2}. \tag{3.27}$$

The TFD correlator in Eq. (3.16) can then be written as a single system correlator, e.g. for $t > 0$:

$$C_{XY}^{\rm TFD}(t) = \langle \hat{X}(t) \mathcal{J}[\hat{Y}] \rangle = {\rm tr}\left(\hat{X}(t) \mathcal{J}[\hat{Y}] \hat{\rho}_{\rm ss} \right) \tag{3.28}$$

Using this correspondence, the defining symmetry condition of hidden TRS in Eq. (3.17) can be written in a manner that only involves a single system:

$${\rm tr}\left(\hat{X}(t) \mathcal{J}[\hat{Y}] \hat{\rho}_{\rm ss} \right) = {\rm tr}\left(\hat{Y}(t) \mathcal{J}[\hat{X}] \hat{\rho}_{\rm ss} \right) \tag{3.29}$$

The above condition is formally equivalent to one of the many generalized quantum detailed balance conditions discussed in Ref. Fagnola and Umanita [2007], Fagnola and Umanità [2010] (so-called SQDB-θ). It is also referred to as "KMS detailed balance" Carlen and Maas [2017].

In general, the symmetry condition in Eq. (3.29) is not helpful as an experimental tool, as it involves an operator whose very form depends on the system state $\hat{\rho}_{\rm ss}$, i.e. it is nonlinear in $\hat{\rho}_{\rm ss}$. This is reminiscent of the problem of measuring Renyi entropies Ekert et al. [2002], Islam et al. [2015], Kaufman et al. [2016]. Remarkably, all hope is not lost. As we will show in Sec. 3.5, systems with hidden TRS are guaranteed to have their effective Hamiltonian $\hat{H}_{\rm eff}$ and jump operators $\hat{c}_k$ transform very simply under the action of $\mathcal{J}$. For correlation functions involving these operators, Eq. (3.29) becomes a standard (and often simple) single-system correlator.

We thus have a key result that makes it possible to directly and simply test for hidden TRS in experiment: hidden TRS implies that only a certain restricted class of correlation functions (directly identifiable from the master equation) are guaranteed to have Onsager time-symmetry.

3.3.4 Example: Hidden TRS in dissipative Rabi-driven qubit

We show in Sec. 3.11 that a simple Rabi-driven qubit with loss fails to respect CQDB: its correlation functions do not exhibit Onsager time-symmetry, regardless of how one tries to define time-reversal. Here we show that this system nonetheless possesses a hidden TRS. Working in the rotating frame set by the drive, and making a rotating wave approximation, the master equation has the form of Eq. (3.8) with $M = 1$ and

$$\hat{H} = \Delta\hat{\sigma}_z + \frac{\Omega}{2}\hat{\sigma}_x, \;\; \hat{c}_1 = \sqrt{\kappa}\hat{\sigma}_-. \tag{3.30}$$

For simplicity, we consider the resonant-driving case $\Delta = 0$ in what follows.

This system has a unique steady state, and corresponding thermofield doubled states can be constructed according to Eq. (3.13). This construction depends on the choice of the hidden TRS operator $\hat{T}$; as discussed in Sec. 3.11, the requirement that the steady state be TRS invariant (c.f. Eq. (3.18)) constrains $\hat{T}$ to the form:

$$\hat{T} = \left[\frac{\sin(\psi/2)}{\sqrt{4b^2+1}}\left(\hat{1} - 2ib\hat{\sigma}_x\right) + i\cos(\psi/2)\hat{\sigma}_z\right]\hat{K}_z, \tag{3.31}$$

where $b = \Omega/\kappa$, $\hat{K}_z$ is the complex conjugation operator acting in the $\hat{\sigma}_z$ basis, and ψ is at this stage an arbitrary real parameter.

To determine whether our system has hidden-TRS, we must find a $\hat{T}$ such that Eq. (3.17) holds (i.e. intra-system TFD correlators have a time symmetry). We thus compute TFD correlators between different pairs of Pauli operators. Here we will consider only the correlation

function $C_{yz}^{\mathrm{TFD}}(t)$, and we leave the other two correlation functions to Sec. 3.15.

Using Eq. (3.19) we can decompose this into the classical correlation $C_{yz}^{\mathrm{cl}}(t)$ and the entanglement correction $C_{yz}^{\mathrm{en}}(t)$ as: $C_{yz}^{\mathrm{TFD}}(t) = C_{yz}^{\mathrm{cl}}(t) + C_{yz}^{\mathrm{en}}(t)$. The classical correlation is independent of ψ, and its time asymmetry is nonzero irrespective of how $\hat{T}$ is chosen:

$$C_{yz}^{\mathrm{cl}}(t) - C_{yz}^{\mathrm{cl}}(-t) = -\frac{32b^5 \sin\left(\frac{\alpha}{4}\kappa t\right) e^{-\frac{3}{4}\kappa t}}{\alpha(2b^2+1)(4b^2+1)}. \tag{3.32}$$

Here, $\alpha = \sqrt{16b^2 - 1}$. We thus see that were we to neglect the entanglement correction, the system could never have hidden TRS.

Now, we look at the time asymmetry of the entanglement correction, which is dependent on ψ:

$$C_{yz}^{\mathrm{en}}(t) - C_{yz}^{\mathrm{en}}(-t) = -\frac{32b^5 \sin\left(\frac{\alpha}{4}\kappa t\right) e^{-\frac{3}{4}\kappa t}}{\alpha(2b^2+1)(4b^2+1)} \cos\psi. \tag{3.33}$$

Comparing Eqs. (3.32) and (3.33), we see that for the TRS with $\psi = \pi$, the entanglement correction to $C_{yz}^{\mathrm{TFD}}(t)$ modifies the classical correlation in just the right way to cancel the net time asymmetry. We see just how stark the effect is in Fig. 3.2 which compares the full TFD correlation function with the classical correlation terms for $b = 1$ at the TRS $\psi = \pi$. For reference, the single qubit correlation function $C_{yz}(t)$ for $b = 1$ at $\psi = \pi$ is also included. This result shows the importance of the entanglement correction to restoring a notion of detailed balance to the Rabi-driven qubit and highlights the fact that the notion of hidden TRS has a distinctly quantum nature.

From the above, we conclude that our model does have a unique hidden TRS, described by the anti-unitary operator $\hat{T}_h$

$$\hat{T}_{\mathrm{h}} = \frac{1}{\sqrt{4b^2+1}}(\hat{1} - 2ib\hat{\sigma}_x)\hat{K}_z. \tag{3.34}$$

In Sec. 3.15 we confirm that the remaining two correlation functions are time symmetric for

this TRS.

It is interesting to consider the form of $\hat{T}_h$ in various limits. For weak Rabi driving (i.e. $b \to 0$), Eq. (3.34) reduces to $\hat{T}_h = \hat{K}_z$. In this limit the qubit system in fact satisfies SDQB with $\hat{T} = \hat{K}_z$ (i.e. all correlation functions have standard Onsager time-symmetry). In the strong drive limit $b \gg 1$, $\hat{T}_h \to -i\hat{\sigma}_x \hat{K}_z$. Up to a phase, this just complex conjugation in the $\hat{\sigma}_y$ basis. To make sense of this, consider the steady state Eq. (3.117) in this limit. To first order in small $b^{-1} \ll 1$, the steady state reduces to $\hat{\rho}_{\rm ss} = \frac{\hat{1}}{2} + \frac{b^{-1}}{2}\hat{\sigma}_y$. The form of the hidden-TRS operator in this limit thus directly reflects the eigenvectors of $\hat{\rho}_{\rm ss}$. Furthermore, one can show that for any b, the hidden TRS $\hat{T}_{\rm h}$ corresponds to complex conjugation in the steady state eigenbasis.

3.4 Hidden time reversal symmetry and dynamical constraints

We have now introduced our notion of hidden TRS (c.f. Eqs. (3.15), (3.17)), and demonstrated that this symmetry can hold even when the more standard CQDB symmetry is broken. It still however may seem that hidden-TRS is nothing more than a formal curiosity. We show here that this is not the case: hidden-TRS is a symmetry that has direct operational utility in helping us understand complex phenomena, as it enables the exact solution of steady-states of non-trivial systems. In particular, it is the symmetry condition that enables the surprising but powerful coherent quantum absorber method introduced in Ref. Stannigel et al. [2012b] and extended in Ref. Roberts and Clerk [2020].

3.4.1 Equivalent subsystem dynamics and hidden TRS as a self-dual condition

We start by demonstrating that the hidden TRS condition can also expressed as a kind of *dynamical* equivalence between the two subsystems in our TFD state. Consider a general

system and a TFD state which does not necessarily satisfy the hidden TRS condition of Eq. (3.17). We stress that the TFD state is defined completely by the steady state of interest $\hat{\rho}_{\text{ss}}$ and choice of anti-unitary $\hat{T}$. We will take $\hat{\rho}_{\text{ss}}$ to be full rank in what follows, and will consider intra-system correlations in this TFD state as defining a bilinear form:

$$\langle\langle \hat{X}, \hat{Y} \rangle\rangle_{\mathcal{T}} \equiv \langle \psi_T | \hat{X}_A \hat{Y}_B | \psi_T \rangle. \tag{3.35}$$

where $\hat{X}$, $\hat{Y}$ denote arbitrary single-system operators. This bilinear form can then be used to define the dual $\mathcal{E}^*$ of any given single-system superoperator $\mathcal{E}$ via

$$\langle\langle \mathcal{E}[\hat{X}], \hat{Y} \rangle\rangle_{\mathcal{T}} \equiv \langle\langle \hat{X}, \mathcal{E}^*[\hat{Y}] \rangle\rangle_{\mathcal{T}}. \tag{3.36}$$

Of particular interest is the case where $\mathcal{E}$ is the adjoint evolution operator $\mathcal{E}_t = \exp[\bar{\mathcal{L}}t]$ defined in Eq. (3.10) in terms of the adjoint Liouvillian $\bar{\mathcal{L}}$ (c.f. Eq. (3.9)). The LHS of Eq. (3.36) then describes the correlation of a subsystem-A operator at time t and a subsystem B operator at time zero. In this case, the dual $(\mathcal{E}_t)^*$ has a direct physical interpretation: it represents an alternate and equivalent time evolution of subsystem B that would result in the same inter-system correlation. This dual time evolution can be written as $(\mathcal{E}_t)^* = \exp\left[\bar{\mathcal{L}}^* t\right]$. Thus, for a given subsystem-A dynamics $\bar{\mathcal{L}}$, we have a corresponding "mirrored" dynamics $\bar{\mathcal{L}}^*$ for subsystem-B, defined by the constraint that it yield identical inter-system correlations, i.e.

$$\left\langle \left(\exp\left[\bar{\mathcal{L}}t\right] \hat{X} \right)_A \hat{Y}_B \right\rangle_T = \left\langle \hat{X}_A \left(\exp\left[\bar{\mathcal{L}}^* t\right] \hat{Y} \right)_B \right\rangle_T \tag{3.37}$$

These notions now give an extremely transparent way to rephrase the hidden-time reversal condition of Eq. (3.17): *the original system-A dynamics and its mirrored version must be*

identical, that is $\bar{\mathcal{L}}$ is self-dual,

$$\bar{\mathcal{L}}^* = \bar{\mathcal{L}}. \tag{3.38}$$

To see this, note first that if a system satisfies the hidden TRS condition of Eq. (3.17), then the bilnear form in Eq. (3.35) must be symmetric, i.e. $\langle\langle \hat{X}, \hat{Y}\rangle\rangle_{\mathcal{T}} = \langle\langle \hat{Y}, \hat{X}\rangle\rangle_{\mathcal{T}}$; this follows from the $t = 0$ limit of Eq. (3.17). This in turn implies that the steady state $\hat{\rho}_{\rm ss}$ of the original master equation must be invariant under our hidden time-reversal operator $\hat{T}$ (i.e. consider the case $\hat{Y} = \hat{1}$). Combining these two conditions lets us express the hidden-TRS condition of Eq. (3.17) as:

$$\langle\psi_T|\hat{X}_A(t)\hat{Y}_B(0)|\psi_T\rangle = \langle\psi_T|\hat{X}_A(0)\hat{Y}_B(t)|\psi_T\rangle. \tag{3.39}$$

where for either subsystem, $\hat{O}(t) = \mathcal{E}_t[\hat{O}]$. This now looks more like a standard Onsager-type correlation function symmetry, except that the two operators are measured on different subsystems. Finally, comparing this equation against Eq. (3.36) directly yields the self-duality condition in Eq. (3.38) [2].

3.4.2 Hidden TRS as a symmetry of the Liouvillian

We now show that the hidden TRS condition can be viewed as a dynamical symmetry that directly constrains the system's adjoint Liouvillian $\bar{\mathcal{L}}$. To do this, we step back and consider a general system and $\hat{T}$, such that hidden TRS is not necessarily satisfied. We then explicitly construct the dual Liouvillian $\bar{\mathcal{L}}^*$ that generates the mirrored-system dynamics, by considering each term in Eq. (3.9). Our construction will explicitly make use of the exchange superoperator $\mathcal{J}$ introduced in Eqs. (3.26) and (3.27); recall that this superoperator lets us convert subsystem-A into corresponding subsystem-B operators (and vice-versa) such that

2. Note that we are implicitly using the fact that our bilinear form is non-degenerate (as $\hat{\rho}_{\rm ss}$ is full rank), something which guarantees the uniqueness of the dual.

TFD expectation values are preserved.

The exchange superoperator allows us to efficiently express the desired dual of the adjoint Liouvillian $\bar{\mathcal{L}}$. This is done using the following relations, that follow directly from the definition of $\mathcal{J}$ in Eq. (3.26):

$$\langle\langle \hat{X}\hat{O}, \hat{Y}\rangle\rangle_{\mathcal{T}} = \langle\langle \hat{X}, \hat{Y}\mathcal{J}[\hat{O}]\rangle\rangle_{\mathcal{T}}, \tag{3.40}$$

$$\langle\langle \hat{O}^\dagger\hat{X}, \hat{Y}\rangle\rangle_{\mathcal{T}} = \langle\langle \hat{X}, \mathcal{J}[\hat{O}]^\dagger\hat{Y}\rangle\rangle_{\mathcal{T}}. \tag{3.41}$$

We can thus obtain an explicit expression for the desired dual $\bar{\mathcal{L}}^*$ as

$$\begin{aligned}\bar{\mathcal{L}}^*[\hat{A}] \equiv i(\mathcal{J}[\hat{H}_{\text{eff}}]^\dagger\hat{A} - \hat{A}\mathcal{J}[\hat{H}_{\text{eff}}]) \\ + \sum_l \mathcal{J}[\hat{c}_l]^\dagger\hat{A}\mathcal{J}[\hat{c}_l].\end{aligned} \tag{3.42}$$

Recall $\hat{H}_{\text{eff}}$ is the effective non-Hermitian Hamiltonian, and $\hat{c}_l$ the jump operators in our original Lindblad master equation Eq. (3.8). We thus see that the properties of the system-B "mirrored dynamics" are encoded in the exchange superoperator $\mathcal{J}$.

We now ask what constraints ensue when we insist that the hidden TRS condition holds, and hence $\bar{\mathcal{L}}^* = \bar{\mathcal{L}}$. For two Liouvillians (each defined with traceless jump operators) to be equivalent, the effective Hamiltonians for each must be identical (up to an additive real constant), and the jump operators related by a unitary mixing matrix (see e.g. Ref. Parthasarathy [1992]).

Hence, insisting that our system has hidden TRS leads to the following constraint equations:

$$\mathcal{J}[\hat{H}_{\text{eff}}] = \hat{H}_{\text{eff}} + E, \quad \mathcal{J}[\hat{c}_l] = \sum_{k=1}^{M} U_{lk}\hat{c}_k, \quad U^2 = 1. \tag{3.43}$$

E is a real number, and U_{lk} is a $M \times M$ unitary matrix. The last constraint on U (i.e. that

it is involutory) follows from the fact that if hidden TRS holds, then the steady state is itself invariant under $\hat{T}$ (c.f. Eq. (3.18)). This resulting additional symmetry of the TFD state then implies (via Eq. (3.26)) that two exchanges yield the identify superoperator: $\mathcal{J}^2 = \mathbb{1}$. This immediately constrains the unitary matrix U_{lk} to have purely real eigenvalues [3].

Eqs. (3.43) represent necessary and sufficient conditions for our system to have a hidden TRS. They are however somewhat unwieldy, as they directly involve the exchange superoperator, which is itself a function of $\hat{T}$ and the steady state $\hat{\rho}_{\text{ss}}$. We can eliminate the explicit appearance of $\mathcal{J}$ by using the fact that since $\hat{\rho}_{\text{ss}}$ is full rank, the TFD state is *separating* (see e.g. Bratteli and Robinson [1997]): if two subsystem-A operators have the same action on the TFD state, then they *must* be identical operators. Stated explicitly:

$$\left(\hat{X}_A|\psi\rangle = \hat{Y}_A|\psi\rangle\right) \Leftrightarrow \left(\hat{X} = \hat{Y}\right). \tag{3.44}$$

Using this, we can eliminate $\mathcal{J}$ from each equation in Eqs. (3.43) by taking each side of each equation to be a system-A operator, and applying it to the TFD state $|\psi_T\rangle$. Using the definition of the exchange operator on the resulting state, this gives us an equivalent but more useful set of constraint equations:

$$\hat{H}_{\text{eff},B}\,|\psi_T\rangle = (\hat{H}_{\text{eff},A} + E)\,|\psi_T\rangle \tag{3.45}$$

$$\hat{c}_{l,B}\,|\psi_T\rangle = \left(\sum_{k=1}^{M} U_{lk}\hat{c}_{k,A}\right)|\psi_T\rangle \tag{3.46}$$

$$U^2 = UU^\dagger = 1 \tag{3.47}$$

Eqs. (3.45)-(3.47) are the main result of this subsection: *they express the existence of a*

3. Note that the condition in Eq. (3.43) on the jump operators implies the exchange superoperator acts as a unitary on the subspace spanned by the Lindblad operators c_l. Since $\mathcal{J}$ squares to one, the unitary operation in Eq. (3.43), which is the restriction of $\mathcal{J}$ to the subspace spanned by the Lindblad operators c_l, *also* squares to one. It follows that its eigenvalues can only be 1 or -1.

hidden TRS symmetry directly as a constraint on the Hamiltonian and jump operators that define our open system dynamics. Heuristically, these conditions imply that the action of $\hat{H}_{\text{eff}}$ and the jump operators are "almost" the same whether they act on subsystem A or B. Hidden TRS requires that these equations must hold for some pure state $|\psi_T\rangle$ of the doubled system, some constant E and some involutory $M \times M$ unitary matrix U. One can view this as a generalization of the classical detailed balance condition in Eq. (3.2). While the classical condition only involves transition rates, our quantum conditions above constrain both the incoherent dynamics generated by the $\hat{c}_l$ operators, as well as the coherent system Hamiltonian $\hat{H}$.

We stress that the above equations are equivalent to those derived in Ref. Fagnola and Umanita [2007] when considering the abstract "SQDB-θ" version of quantum detailed balance. By phrasing these conditions directly in terms of the thermofield double state, we will be able to directly exploit them as a means for efficiently *finding* unknown steady states (something that was not considered previously).

Finally, we note that Eq. (3.45) - Eq. (3.46) tells us that if hidden-TRS holds, the action of the exchange superoperator is extremely simple when acting on $\hat{H}_{\text{eff}}$ or the jump operators $\hat{c}_l$. This means that doubled-system TFD correlation functions involving these operators can be directly converted to single-system correlation functions. As discussed extensively in Sec. 3.3.3, this gives a direct means for experimentally testing for hidden-TRS in a single system: hidden-TRS ensures that a certain reduced class of correlation functions will obey Onsager-like time symmetry (c.f. Eq. (3.29)).

3.5 Hidden TRS as a route to exact solutions

3.5.1 Basic idea

Classical detailed balance has a profound operational utility: it provides an extremely efficient method for finding the steady state of a given dynamical model (i.e. so called potential solutions of Fokker-Planck equations Gardiner [2009]). It is thus natural to ask whether something similar is possible using our notion of hidden TRS. If a system satisfies this symmetry, does this directly provide a method for solving for the steady state? As we now show, the answer is a resounding yes. The existence of hidden TRS places a strong constraint on the form of our dynamics via Eqs. (3.45) - (3.47). *These equations also provide an efficient method for finding an unknown steady state.* To see this, we change perspective, and view $|\psi_T\rangle$ in these equations as an unknown pure state of a doubled version of the original system. The goal is then to *find* a pure state $|\psi_T\rangle$, constant E, and unitary matrix U such that Eqs. (3.45) - (3.47) are satisfied. If we are able to do this, then as we will show, our system has hidden TRS, and the desired system-A steady state $\hat{\rho}_{\rm ss}$ is obtained by tracing out system-B from $|\psi_T\rangle$. Conversely, if we cannot do this, then our system does not have hidden TRS, and there is no generic simple route to finding the steady state.

We stress that the above procedure for finding the steady state is simpler than a direct brute-force approach. Suppose our original system has a Hilbert space dimension d. Without assuming hidden TRS, solving for the steady state of Eq. (3.8) reduces to the problem of solving for the null space of a matrix with dimensions $d^2 \times d^2$. Without additional assumptions, this matrix does not have any obvious sparseness properties. In contrast, with the assumption of hidden TRS, we need to solve Eqs. (3.45) and (3.46). Each of these $M+1$ equations also involves a $d^2 \times d^2$ matrix. However, each of these matrices has a simplified structure as there are no terms corresponding to an interaction between the two subsystems. As a result, there can be at most $\mathcal{O}[d^3]$ non-zero matrix elements. In addition,

our constraint equations decouple the effective Hamiltonian physics (Eq. (3.45)) from the incoherent "jump" physics (Eq. (3.46)). This effective non-interacting property provides a considerable simplification, as we will exploit more fully in the next section.

3.5.2 Connection to perfect quantum absorbers

As we show below, the presence of hidden TRS guarantees that we can construct a simple mirrored system that *perfectly absorbs* everything emitted by the main system into its environment. Such absorbing systems have been studied previously as a method for deriving exact solutions of certain Lindblad master equations Stannigel et al. [2012b], Roberts and Clerk [2020]. Our discussion here will provide a generalization of this "coherent quantum absorber" method to systems with multiple jump operators, and also show that its success is indeed intimately connected to hidden time-reversal symmetry.

To establish this connection, we again consider a general system described by the master equation Eq. (3.8) with a steady state $\hat{\rho}_{\rm ss}$. We also construct a doubled system as in Sec. 3.3.1 with a TFD state given by Eq. (3.13). To start, we do not assume that the system has hidden TRS. As discussed in Sec. 3.4, for a given subsystem A dynamics (generated by $\bar{\mathcal{L}}$), we can always construct a corresponding "mirrored" dynamics on subsystem B (generated by $\bar{\mathcal{L}}^*$), such that *either* evolution generates the same time-dependent inter-system correlations, c.f. Eq. (3.37).

Somewhat remarkably, this mirrored dynamics is also *exactly* what is needed make subsystem-B a "perfect absorber" of energy and information emitted by subsystem-A into its environment (Fig. 3.3). This can be established by using the exchange superoperator $\mathcal{J}$ introduced in Eq. (3.26), which converts the action of a subsystem-A operator acting on the

TFD state to a subsystem-B operator (and vice-versa). From the definition of $\mathcal{J}$ we have:

$$\hat{H}_{\text{eff},A}\,|\psi_T\rangle = \mathcal{J}[\hat{H}_{\text{eff}}]_B\,|\psi_T\rangle \tag{3.48}$$

$$\hat{c}_{l,A}\,|\psi_T\rangle = \mathcal{J}[\hat{c}_l]_B\,|\psi_T\rangle \tag{3.49}$$

where $\hat{H}_{\text{eff}}$ is the effective Hamiltonian in our master equation, and $\hat{c}_l$ are the jump operators.

As shown in Sec. 3.16, these equations can be re-written as:

$$\hat{H}_{AB}\,|\psi_T\rangle = 0, \qquad (\mathcal{J}[\hat{c}_l]_B - \hat{c}_{l,A})|\psi_T\rangle = 0. \tag{3.50}$$

Here, the Hermitian Hamiltonian $\hat{H}_{AB}$ describes an *interaction* between the two subsystems in our doubled system:

$$\hat{H}_{AB} = \hat{H}_A - \hat{H}'_B - \frac{i}{2}\sum_{l=1}^{M}(\hat{c}^\dagger_{l,A}\mathcal{J}[\hat{c}_l]_B - h.c.) \tag{3.51}$$

with

$$\hat{H}' \equiv \text{Re}\left[\mathcal{J}[\hat{H}_{\text{eff}}]\right], \quad \hat{H} \equiv \text{Re}\left[\hat{H}_{\text{eff}}\right] \tag{3.52}$$

We denote the Hermitian part of an operator $\hat{A}$ as $\text{Re}[\hat{A}]$. Note that $\hat{H}$ is nothing but the Hermitian Hamiltonian in our original master equation.

Eq. (3.50) has an extremely suggestive form: it tells us that $|\psi_T\rangle$ is necessarily a zero-energy eigenstate of a Hermitian Hamiltonian describing a doubled system with an inter-system coupling, and that it is also annihilated by particular combinations of jump operators. Together, these conditions imply that $|\psi_T\rangle$ is a zero energy pure-state, steady-state of the *cascaded* doubled system sketched in Fig. 3.3c. In this cascaded system Gardiner [1993], Carmichael [1993], there is an independent chiral (directional) waveguide associated with

each jump operator $\hat{c}_l$ in our original master equation. These channels mediate a directional coupling between systems A and B, with B downstream from A. Using the standard theory of cascaded quantum systems Gardiner [1993], Gardiner and Zoller [2000], the full master equation for this system is:

$$\partial_t \hat{\rho}_{AB} = -i[\hat{H}_{AB}, \hat{\rho}_{AB}] + \sum_{l=1}^{M} \mathcal{D}\Big[\hat{c}_{l,A} - \mathcal{J}[\hat{c}_l]_B\Big]\hat{\rho}_{AB}. \tag{3.53}$$

Here $\hat{\rho}_{AB}$ is the density matrix of the doubled system, and $\mathcal{D}[\hat{z}]\hat{\rho} = \hat{z}\hat{\rho}\hat{z}^\dagger - \{\hat{z}^\dagger\hat{z}, \hat{\rho}\}/2$ is the standard Lindblad dissipation operator. One can easily verify that if $|\psi_T\rangle$ satisfies Eq. (3.50), then it is a steady state of Eq. (3.53).

We thus have established the desired connection: the same formal construction that gives us a correlation-conserving mirrored dynamics on subsystem-B also tells us the precise dynamics that is needed for subsystem-B to be a perfect absorber for subsystem-A. We stress that for each possible choice of candidate time-reversal operator $\hat{T}$, we have a different TFD state, a different mirrored-dynamics (i.e. Hamiltonian $\hat{H}'$, jump operators $\mathcal{J}[\hat{c}_l]$), and hence a different possible coherent quantum absorber.

3.5.3 Hidden TRS and simple absorbing dynamics

The cascaded master equation in Eq. (3.53) in principle provides a route for finding the steady state of the physical system A. If one could find the steady state of this master equation, then tracing out system B necessarily yields a steady state of the original single-system master equation. One could simplify this procedure by trying to find a pure state solution to Eq. (3.53). Of course, there is an obvious problem to this approach: the construction of Eq. (3.53) is contingent on *already* knowing the steady state $\hat{\rho}_{\rm ss}$, as this is needed to construct the exchange superoperator $\mathcal{J}$.

Things simplify considerably though in the case where our system possesses a hidden

TRS. In this case, we can use Eqs. (3.45)-(3.47) to dramatically simplify the cascaded master equation for our system. The system-B jump operators and Hamiltonian are then given by

$$\mathcal{J}[\hat{c}_l] \to \left(\hat{d}_l = \sum_{m=1}^{M} U_{lm} \hat{c}_m \right), \ \mathrm{Re}\left[\mathcal{J}[\hat{H}_{\mathrm{eff}}]\right] \to \hat{H} + E \tag{3.54}$$

for some involutory unitary $M \times M$ matrix U and real constant E, and the Hamiltonian of the coupled system becomes

$$\hat{H}_{AB} = \hat{H}_A - \hat{H}_B - \frac{i}{2} \sum_{l=1}^{M} \left(\hat{c}_{l,A}^{\dagger} \hat{d}_{l,B} - h.c. \right), \tag{3.55}$$

where E is now implicitly absorbed into an energy-shift of the dark state.

We can now view this as a *method* for finding an unknown steady state of our original system-A master equation in Eq. (3.8). If we assume the existence of hidden TRS, finding this steady state is equivalent to finding a involutory $M \times M$ unitary matrix U and energy E, such that the cascaded master equation in Eq. (3.53) (with the simplifications of Eqs. (3.54) and (3.55)) yields a pure-state, steady state. This pure state then gives us the desired system-A steady state by just tracing over system B.

The technique detailed above is a generalized version of the CQA exact solution method introduced in Ref. Stannigel et al. [2012b] for solving master equations with a single jump operator. Our extension to systems with multiple jump operators involves a new object, the involutory unitary matrix U. We have shown that this solution technique is thus intimately connected to the notion of a hidden TRS, and thus to the generalized SQDB-θ quantum detailed balance conditions introduced earlier on purely formal grounds Fagnola and Umanita [2007], Fagnola and Umanità [2010]. As far as we know, this is the first example of this notion of quantum detailed balance having an operational utility.

3.6 Hidden-TRS in nonlinear driven-dissipative quantum cavities

At this stage, we have established the basic notion of hidden TRS. This symmetry can hold even if the more conventional CQDB condition (Sec. 3.2.4) is broken. Moreover, it directly enables a simple but powerful method for finding non-trivial steady states (Sec. 3.5). We have illustrated these ideas by explicitly considering hidden TRS in a model of a dissipative Rabi-driven qubit (see Sec. 3.11 and 3.3.4). In this section, we turn to a more complex class of models. These describe a bosonic mode (canonical annihilation operator $\hat{a}$) with a Kerr or Hubbard-U type interaction, subject to both one and two particle coherent driving, as well as one and two-particle losses. The system is described by a Lindblad master equation Eq. (3.8) with a coherent Hamiltonian:

$$\hat{H} = \frac{K}{2}\hat{a}^\dagger\hat{a}^\dagger\hat{a}\hat{a} + \Delta\hat{a}^\dagger\hat{a} + \left(\Lambda_1\hat{a}^\dagger + \frac{\Lambda_2}{2}\hat{a}^\dagger\hat{a}^\dagger + h.c.\right) \tag{3.56}$$

and with jump operators

$$\hat{c}_1 = \sqrt{\kappa_1}\hat{a}, \quad \hat{c}_2 = \sqrt{\kappa_2}\hat{a}^2 \tag{3.57}$$

This model describes a dissipative cavity mode driven both with linear and parametric drives that have commensurate frequencies (working within rotating-wave approximations, and in a rotating frame that eliminates the time dependence of the drives). It is a ubiquitous system, having both been studied extensively in quantum optics, and more recently in the field of superconducting quantum circuits as a route to error-corrected quantum memories Mirrahimi et al. [2014b], Leghtas et al. [2015b], Wang et al. [2016], Puri et al. [2017], Grimm et al. [2020].

It is well known that the steady state of this class of systems can be found analytically

using quantum-optical phase space methods Drummond and Gardiner [1980], Wolinsky and Carmichael [1988a], Bartolo et al. [2016]; more recent work has shown that these exact solutions can be derived more directly (and even extended) using the coherent quantum absorber method (CQA) Stannigel et al. [2012b], Roberts and Clerk [2020]. An underlying explanation however for *why* these models are solvable has been lacking. We now have such an explanation: this class of models possess hidden-TRS, which directly leads to their solvability.

In what follows, we discuss the nature of hidden-TRS in these systems, showing that hidden-TRS is present even though (generically) CQDB does not hold. Crucially, we show that the presence of hidden-TRS has observable consequences even in experiments on a single system: while generic correlation functions do not exhibit a time-symmetry, there is a special class of correlators that do. In Sec. 3.8, we will show how hidden-TRS directly enables the required symmetry exploited in the complex-P function phase space methods that were first used to solve these systems Drummond and Gardiner [1980], Wolinsky and Carmichael [1988a].

3.6.1 Multiple non-trivial hidden-TRS symmetries

We start by noting that our general driven-dissipative resonator problem does not satisfy CQDB, and thus its correlation functions do not all exhibit a simple time-symmetry. An example of such a lack of correlation function symmetry is shown in Fig. 3.5. More generally, as discussed in Sec. 3.2.5, CQDB can only hold if the system's steady state commutes with $\hat{H}$. This condition is violated except in the vanishing dissipation limit $\kappa_1, \kappa_2 \to 0^+$.

Despite the lack of CQDB, these systems *always* possess hidden-TRS, which explains their solvability. The specific nature however of the symmetry operator (or operators) depends on the particular version of the model. Consider first the most common case, where there is no two-photon loss, $\kappa_2 = 0$. To determine whether our system has hidden-TRS, we consider a

doubled two-cavity system and a two-cavity state $|\psi_T\rangle$. The question is whether this state could represent a TFD state constructed using an anti-unitary operator $\hat{T}$ which describes a hidden-TRS (c.f. Eq. (3.13)). From Eqs. (3.45)-(3.47), such a state must satisfy:

$$\hat{a}|\psi_T\rangle = u\hat{b}|\psi_T\rangle \tag{3.58}$$

$$\hat{H}_{\text{eff},A}|\psi_T\rangle = (\hat{H}_{\text{eff},B} + E)|\psi_T\rangle \tag{3.59}$$

for some real energy E and constant $u = \pm 1$. Here (as always) $\hat{H}_{\text{eff}} = \hat{H} - i\kappa_1\hat{a}^\dagger\hat{a}/2$ is the effective non-Hermitian Hamiltonian in our master equation. If we can find a two-cavity state $|\psi_T\rangle$ satisfying the above equations, then we are *guaranteed* both to have hidden TRS, and to be able to solve for our system using the CQA method of Sec. 3.5.

If we have a non-zero single-photon drive Λ_1, one can only solve Eqs. (3.58)-(3.59) if $u = 1$ and $E = 0$. With these choices, there is a unique solution for the two-cavity state $|\psi_T\rangle$. This was explicitly found and expressed as a confluent hypergeometric function in Ref. Roberts and Clerk [2020], which demonstrated that this model can be solved using CQA. Hence, the system has a unique hidden-TRS operator $\hat{T}$ in this case. As we will see in the next section, this gives us more than just a way to understand the solvability of the model: it also directly lets us predict a surprising correlation function symmetry.

It is also interesting to consider the special case where there is no single-photon drive, $\Lambda_1 \to 0$. Because of the single photon loss, the system still has a unique steady state. However, there are now *two distinct* hidden-TRS symmetries $\hat{T}_\pm$, each corresponding to distinct TFD states $|\psi_T^\pm\rangle$:

$$|\psi_T^\pm\rangle = \sum_n \sqrt{p_n}|n\rangle_A \hat{T}_\pm |n\rangle_B. \tag{3.60}$$

We stress that both these states each yield the same $\hat{\rho}_{\text{ss}}$ when the auxiliary second cavity is traced out. Formally, the two TFD states (and corresponding $\hat{T}_\pm$) are found by solving

Eqs. (3.58)-(3.59) for $E = 0, u = 1$ and $E = 0, u = -1$. The explicit states can be found analytically in terms of Bessel functions Roberts and Clerk [2020].

We thus have our first example of a physical system with multiple, distinct hidden TRS symmetries; other examples are listed in Table 3.1. Using the explicit forms of the TFD states, we can explicitly compute the action of the hidden TRS symmetry operators $\hat{T}_+$ and $\hat{T}_-$. In general, their action is highly non-trivial (as can be seen in Fig. 3.4, where we show their action in phase space on an initial coherent state).

In the limit of vanishing nonlinearity $K \to 0$, the hidden-TRS operators $\hat{T}_\sigma$ take a simple form. In this case, the two TFD states limit to simple two-mode squeezed states:

$$|\psi_T^\pm\rangle \underset{K\to 0}{\sim} e^{\frac{\Lambda_2}{2\Delta_{\text{eff}}}(\hat{a}^\dagger \pm \hat{b}^\dagger)^2}|0,0\rangle, \tag{3.61}$$

where $\Delta_{\text{eff}} \equiv \Delta + i\kappa_1/2$ and $|0,0\rangle$ is the two-cavity vacuum state. Expanding out the exponential allows us to pick out the corresponding hidden time-reversal operators, which correspond to simple phase-space reflections about the axes $\theta = \pm \arg(\Lambda_2/\Delta_{\text{eff}})$ in phase space:

$$\hat{T}_\pm \underset{K\to 0}{\sim} e^{\arg(\pm\Lambda_2/\Delta_{\text{eff}})\hat{a}^\dagger \hat{a}}\hat{K}, \tag{3.62}$$

where here, $\hat{K}$ denotes complex-conjugation in the Fock basis. For non-zero Kerr, the corresponding time-reversal operations become highly nontrivial and non-Gaussian, and must be extracted via a numerical Schmidt decomposition. In Fig. 3.4, we show the action of $\hat{T}_\pm$ for both $K = 5 \times 10^{-4}\kappa_1$ (weak nonlinearity) and $K = \kappa_1$ (strong nonlinearity).

3.6.2 Experimental consequences of hidden-TRS

Our finding that driven-dissipative nonlinear cavities possess a hidden-TRS does more than simply explain why these systems are exactly solvable: it also lets us predict observable phe-

nomena that are accessible in a standard single-system experiment. Recall our discussion in Sec. 3.3.3: while hidden-TRS (by definition) guarantees a symmetry of doubled-system TFD correlation functions, for certain operators, this directly implies time-symmetry of standard, single-system correlators. In particular, these special operators are ones that transform simply under the exchange operator $\mathcal{J}$. By virtue of Eqs. (3.45)-(3.47), the effective Hamiltonian $\hat{H}_{\text{eff}}$ and jump operators $\hat{c}_k$ are guaranteed to be such special operators.

As a specific example, consider the following steady-state, single-system correlation function:

$$C_{a^3,a}(t) \equiv \begin{cases} \langle \hat{a}^3(t)\hat{a}(0)\rangle & t \geq 0 \\ \langle \hat{a}(-t)\hat{a}^3(0)\rangle & t < 0. \end{cases} \tag{3.63}$$

If we set $\kappa_2 = 0$, Eqs. (3.45)-(3.47) ensure that $\mathcal{J}[\hat{a}] = \pm\hat{a}$. From the definition of the exchange operator, it follows that $\mathcal{J}[\hat{a}^m] = (-1)^m\hat{a}^m$. As a result, hidden-TRS guarantees (via Eq. (3.29)) the above correlator has an Onsager-like time symmetry: $C_{a^3,a}(t) = C_{a^3,a}(-t)$. We stress that this correlation function symmetry is special: unlike the case with CQDB, most correlation functions *will not* exhibit any time-symmetry. This behavior is shown explicitly in Fig. 3.5, where we contrast the correlator $C_{a^3,a}(t)$ (time-symmetric) with a more generic correlator involving quadrature operators $\hat{X} = (\hat{a} + \hat{a}^\dagger)/\sqrt{2}$, $\hat{P} = -i(\hat{a} - \hat{a}^\dagger)/\sqrt{2}$. Hidden-TRS does not enforce any special symmetry of this latter correlator; hence, as expected, it is manifestly not symmetric in time. We stress that even though $\mathcal{J}[\hat{a}^2]$ is simple, this does not imply that $\mathcal{J}[\hat{a}^\dagger\hat{a}]$ is simple.

We thus have a clear experimental test for confirming the existence of hidden-TRS in this class of systems.

3.7 Breaking of hidden-TRS by thermal fluctuations and interactions

We have now demonstrated that hidden-TRS holds in two very different zero-temperature dissipative models: a Rabi-driven qubit with loss (Sec. 3.3.4), and a driven nonlinear cavity with one and possibly two photon loss processes (Sec. 3.6). Within the setting of our Lindblad master equations, zero temperature corresponds to only having dissipators that remove (and not add) excitations.

The natural next question is to ask what happens to hidden-TRS if we introduce a non-zero temperature to the above systems. This corresponds to adding dissipative processes that can add excitations. We show that in a generic setting where there is both coherent (Hamiltonian) driving as well as nonlinearity, introducing such thermal dissipators can break hidden-TRS. The only exceptions to this are the case of no driving (where the system is effectively classical), or the case of no nonlinearity (where the steady state is Gaussian). Our results here suggest that for a generic nonlinear driven-dissipative system, hidden-TRS is a symmetry associated with vacuum fluctuations, and hence only emerges as one approaches the zero-temperature limit.

Our work here is inspired by and complements seminal studies from Dykman and co-workers of related phenomena in driven nonlinear oscillators Dykman and Krivoglaz [1979], Dykman and Smelyanskii [1988], Marthaler and Dykman [2006], Dykman [2012], Guo et al. [2013], Guo [2013], Zhang and Dykman [2019]. These works studied the basic nonlinear resonator model of Eqs. (3.56)-(3.57) in the limit of weak dissipation, where the quantum master equation can be reduced to a simpler Pauli master equation (i.e. one can drop off-diagonal elements of the density matrix in the energy eigenstate basis). The resulting classical master equation was found to satisfy the classical detailed balance condition of Eq. (3.2) at zero-temperature; in a semiclassical limit, this could be shown analytically. Further, it was shown that this classical detailed balance failed to hold at non-zero temperatures, and that in

the semiclassical limit, the corresponding transition temperature became exponentially small. Our work extends these results: by formulating detailed balance in completely quantum manner using hidden TRS, we are not limited to weak-damping or semiclassical regimes. We also discuss how the breaking of hidden-TRS by thermal fluctuations is contingent on having driving and nonlinearity; without both these ingredients, there is no symmetry breaking. Finally, we discuss how this symmetry breaking could be directly probed in experiment by measuring the time-symmetry of correlation functions.

3.7.1 Rabi-driven qubit subject to thermal dissipation

A driven-dissipative qubit is a simple example to illustrate the breaking of hidden TRS due to thermal fluctuations. While this model has hidden-TRS at zero temperature (c.f. Sec. 3.3.4), this symmetry is broken in the presence of *both* coherent driving and thermal fluctuations. We consider a Rabi driven qubit in the standard weak-coupling, rotating-wave limit. The master equation is of the form Eq. (3.8) but now with $M = 2$ and

$$\begin{aligned} \hat{H} &= \Delta\hat{\sigma}_z + \frac{\Omega}{2}\hat{\sigma}_x, \\ \hat{c}_1 &= \sqrt{\kappa(1+\bar{n}_{\rm th})}\hat{\sigma}_-, \;\; \hat{c}_2 = \sqrt{\kappa\bar{n}_{\rm th}}\hat{\sigma}_+. \end{aligned} \tag{3.64}$$

Here Ω is the amplitude of the Rabi drive, and $\Delta = \omega_{\rm qb} - \omega_{\rm dr}$ is the drive detuning, i.e. the difference between the qubit splitting frequency $\omega_{\rm qb}$ and the drive frequency $\omega_{\rm dr}$. The dissipation here describes T_1 relaxation of the qubit due to a transverse coupling to a thermal bath. The coupling rate to this bath is κ, and $\bar{n}_{\rm th}$ represents the bath thermal occupancy at the qubit frequency: $\bar{n}_{\rm th} = (\exp(\omega_{\rm qb}/T) - 1)^{-1}$ where T is the temperature of the bath. This master equation is widely used to describe driven two-level systems both in a variety of atomic, quantum optical and quantum information settings.

Thermal dissipation with no drive

In the absence of a Rabi drive (i.e. $\Omega = 0$), the unique steady state of our master equation has the thermal equilibrium form:

$$\hat{\rho} = \frac{1 + \bar{n}_{\text{th}}}{1 + 2\bar{n}_{\text{th}}} |g\rangle \langle g| + \frac{\bar{n}_{\text{th}}}{1 + 2\bar{n}_{\text{th}}} |e\rangle \langle e| . \tag{3.65}$$

where $|g\rangle, |e\rangle$ denote $\hat{\sigma}_z$ eigenstates. This steady state commutes with $\hat{H}$, and it is easy to confirm that the system has CQDB. Due to the lack of coherences, the problem is analogous to a classical two-state system; hence, the presence of detailed balance is not surprising.

Formally, the system still possesses a set of hidden-TRS symmetries; this symmetry is however not unique. There is a one parameter family of hidden TRS operators

$$\hat{T} = (e^{i\psi}|e\rangle\langle e| + |g\rangle\langle g|)\hat{K}_z. \tag{3.66}$$

For each ψ there is a corresponding U matrix (c.f. Eq. (3.43))

$$U_\psi = \begin{pmatrix} 0 & e^{-i\psi} \\ e^{i\psi} & 0 \end{pmatrix} \tag{3.67}$$

for which the dynamical constraints Eqs. (3.45)-(3.47) are satisfied.

The presence of hidden TRS in the finite-temperature, undriven qubit system implies that it can be solved using the coherent absorber method of Sec. 3.5.2. The qubit-plus-absorber system has the cascaded Hamiltonian Eq. (3.55) where $\hat{H}_A$ is the qubit Hamiltonian $\hat{H} = \frac{1}{2}\omega_0\hat{\sigma}_z$ acting on the physical qubit A and $\hat{H}_B$ is the Hamiltonian acting on the auxiliary

qubit B (the absorber). The cascaded system also has the collective jump operators

$$\hat{C}_1 = \hat{c}_{1,A} - e^{-i\psi}\hat{c}_{2,B}, \tag{3.68}$$

$$\hat{C}_2 = \hat{c}_{2,A} - e^{i\psi}\hat{c}_{1,B}. \tag{3.69}$$

The pure state which is simultaneously dark with respect to $\hat{H}_{AB}$, $\hat{C}_1$, and $\hat{C}_2$ is

$$|\psi_0\rangle = \frac{1}{\sqrt{1+2\bar{n}_{\rm th}}}\left(\sqrt{1+\bar{n}_{\rm th}}|gg\rangle + e^{i\psi}\sqrt{\bar{n}_{\rm th}}|ee\rangle\right). \tag{3.70}$$

After tracing out the absorber system, the single site steady state density matrix is precisely Eq. (3.65).

Thermal dissipation with a non-zero drive

We now ask what happens to our thermal qubit when a non-zero drive is added ($\Omega \neq 0$). For simplicity we take $\Delta = 0$ (resonant driving), and define the dimensionless driving $b' \equiv \Omega/\kappa(1+2\bar{n}_{\rm th})$. With this definition, the steady state $\hat{\rho}_{ss,T}$ of the driven qubit with thermal dissipation is given by the zero temperature result in Eq. (3.117) with the simple substitution $b \to b'$.

Furthermore the eigensystem of the Liouvillian at finite temperature is obtained from the zero temperature results in Eqs. (3.120)-(3.123) by replacements $\hat{\rho}_{\rm ss} \to \hat{\rho}_{ss,T}$, $b \to b'$, and $\kappa \to \kappa(1+2\bar{n}_{\rm th})$. Finally, the permissible TRS of the finite temperature system are given by Eq. (3.31) with $b \to b'$.

We consider the TFD correlation function $C_{yz}^{\rm TFD}(t)$ defined in Eq. (3.16) for Pauli operators $\hat{\sigma}_y, \hat{\sigma}_z$. As in the zero-temperature case, we decompose this into classical correlation and the entanglement correction using Eq. (3.19), and we look at the time asymmetry of each. At finite temperature, the classical correlation asymmetry picks up new temperature

dependent terms:

$$C_{yz}^{\mathrm{cl}}(t) - C_{yz}^{\mathrm{cl}}(-t) = \\ -\frac{8b' \sin\left(\frac{\alpha}{4}\kappa t\right) e^{-\frac{3}{4}\kappa t}}{\alpha(2b'^2+1)(4b'^2+1)}\left[4b'^4 + (4b'^2+1)\eta_{\mathrm{th}}\right] \tag{3.71}$$

where we have defined

$$\eta_{\mathrm{th}} = 1 - \frac{1}{(1+2\bar{n}_{\mathrm{th}})^2}. \tag{3.72}$$

In contrast, the ψ-dependent entanglement correction is

$$C_{yz}^{\mathrm{en}}(t) - C_{yz}^{\mathrm{en}}(-t) = \\ -\frac{8b' \sin\left(\frac{\alpha}{4}\kappa t\right) e^{-\frac{3}{4}\kappa t}}{\alpha(2b'^2+1)(4b'^2+1)}\left[2b'^2\sqrt{4b'^4 + (4b'^2+1)\eta_{\mathrm{th}}}\right]\cos\psi, \tag{3.73}$$

which also gains temperature-dependent terms.

At zero temperature the above expressions reduce to Eqs. (3.32)-(3.33) so for $\psi = \pi$, $C_{yz}^{\mathrm{TFD}}(t)$ has time symmetry, and our system has a hidden-TRS. However, as soon as $\bar{n}_{\mathrm{th}}$ is non-zero, hidden-TRS is broken. For non-zero temperature, there is choice of ψ for which the time-asymmetry of the correlation function. To see this explicitly, suppose we set the time asymmetry of $C_{yz}^{\mathrm{TFD}}(t)$ to zero and attempt to solve for $\cos\psi$. We obtain

$$\cos\psi \stackrel{?}{=} -\sqrt{1 + \eta\frac{4b'^2+1}{4b'^4}} \tag{3.74}$$

For any finite temperature $\eta > 0$ so the right-hand side has a magnitude greater than 1, thus there is no solution for ψ. This shows explicitly that for finite temperature and non-zero driving, the driven-dissipative qubit problem has no hidden-TRS. This breaking of correlation function time symmetry is shown explicitly in Fig. 3.6. At a heuristic level, this symmetry breaking is a result of the classical contribution growing faster with $\bar{n}_{\mathrm{th}}$ than the

entanglement contribution, breaking the cancellation that occurs at $\bar{n}_{\rm th} = 0$.

3.7.2 Parametrically-driven nonlinear cavity at finite temperature

The qubit example above corresponds to a system where the strength of the nonlinearity is essentially infinite. We now consider a driven-dissipative system where the strength of the nonlinearity is tuneable: the parametrically-driven damped nonlinear cavity of Sec. 3.6, but now with thermal dissipation. For simplicity, we consider where there is only a parametric (two-photon) drive, and there are only single-photon dissipation processes. We then have a Lindblad master equation with a Hamiltonian given by Eq. (3.56) (with $\Lambda_1 = \Delta = 0$), and dissipators

$$\hat{c}_1 = \sqrt{\kappa(1+\bar{n}_{\rm th})}\hat{a}, \;\; \hat{c}_2 = \sqrt{\kappa\bar{n}_{\rm th}}\hat{a}^\dagger. \tag{3.75}$$

As is standard in the derivation of quantum optics master equations, the thermal occupancy $\bar{n}_{\rm th}$ corresponds to a Bose-Einstein factor evaluated at the bath temperature T and cavity resonance frequency $\omega_{\rm cav}$: $\bar{n}_{\rm th} = 1/\left(\exp[\hbar\omega_{\rm cav}/k_B T] - 1\right)$. For simplicity, we ignore two-photon dissipative processes (i.e. $\kappa_2 = 0$).

At non-zero temperature, hidden TRS is broken unless one or both of the nonlinearity K or drive Λ_2 are zero. To see this, note that for hidden-TRS to hold, Eq. (3.46) requires that for some two-mode state $|\psi_T\rangle$ and 2×2 involutory unitary matrix U the jump operators must satisfy

$$\left[\hat{c}_{1,A} - (U_{11}\hat{c}_{1,B} + U_{12}\hat{c}_{2,B})\right]|\psi_T\rangle = 0, \tag{3.76}$$

$$\left[\hat{c}_{2,A} - (U_{21}\hat{c}_{1,B} + U_{22}\hat{c}_{2,B})\right]|\psi_T\rangle = 0. \tag{3.77}$$

The equations imply that $|\psi_T\rangle$ is annihilated by two independent canonical annihilation

operators. As such, this state must be Gaussian, which in turn implies that $\hat{\rho}_{\rm ss}$ must be Gaussian. However, this steady state is Gaussian *only* if one or both of Λ_2 and K are zero. We thus have an important conclusion: *the combination of thermal fluctuations, driving and nonlinearity together can break hidden-TRS.* Note that for a more explicit proof that hidden-TRS does not hold, one can explicitly try to solve both Eqs. (3.45) and (3.46); for both Λ_2 and K non-zero, one can confirm that it is impossible to solve these equations.

It is interesting to consider the simple case of an undriven, linear thermal cavity (i.e. $K = 0$, $\Lambda_2 = 0$, $\bar{n}_{\rm th} > 0$). In this case, the steady state is essentially classical (no Fock-state coherences), and it is well known that CQDB holds Agarwal [1973]. Formally, our system also has hidden-TRS, implying that this system can be solved using the CQA method. This can be explicitly shown by solving Eqs. (3.45)-(3.47). We find that solutions are possible when $E = 0$ and when U is chosen to have the form

$$U = \begin{pmatrix} 0 & e^{i\theta} \\ e^{-i\theta} & 0 \end{pmatrix}. \tag{3.78}$$

Here, θ is a real parameter. We thus have a continuous family of distinct hidden-TRS operators $\hat{T}_\theta$ (see Tab. 3.1), in contrast to the pair of hidden time-reversal operators $\hat{T}_\sigma$ seen for nonzero parametric driving and zero temperature (i.e. $K = 0, \Lambda_1 = 0, \bar{n}_{\rm th} = 0$).

For each possible hidden-TRS operator $\hat{T}_\theta$, we have a corresponding thermofield double state. These always have the form of Gaussian, two-mode squeezed states:

$$|\psi_T(\theta)\rangle \equiv \sum_{n=0}^{\infty} e^{-n(\beta/2+i\theta)}|n,n\rangle. \tag{3.79}$$

Returning now to the more interesting case where we add both parametric driving and nonlinearity, we can study how thermal fluctuations break the hidden-TRS that is present at zero temperature. We focus on an experimentally-accessible quantity that shows this

symmetry breaking: the time-asymmetry of the steady-state correlation function

$$C_{a^2,H_{\text{eff}}}(t) \equiv \begin{cases} \langle \hat{a}^2(t)\hat{H}_{\text{eff}}(0)\rangle & t \geq 0 \\ \langle \hat{H}_{\text{eff}}(-t)\hat{a}^2(0)\rangle & t < 0 \end{cases}, \tag{3.80}$$

where as always, $\hat{H}_{\text{eff}}$ is the non-Hermitian effective Hamiltonian associated with our master equation. As discussed above, at zero temperature hidden-TRS guarantees that this special correlator has time-symmetry. This time-symmetry is lost as $\bar{n}_{\text{th}}$ is increased.

To see this explicitly, we plot the total time-*asymmetry* vs. temperature, which we define as:

$$m(T) \equiv \int_0^\infty |C_{a^2,H_{\text{eff}}}(t) - C_{a^2,H_{\text{eff}}}(-t)|dt. \tag{3.81}$$

As shown in Fig. 3.7, the total asymmetry remains zero as long as the temperature T is small, but then suddenly jumps at a critical "transition" temperature, consistent with a sudden breaking of detailed balance. This temperature can be understood from the size of the system's dissipative gap Γ at $\bar{n}_{\text{th}} = 0$. At a heuristic level, the transition occurs when the new thermal excitation rate $\kappa\bar{n}_{\text{th}}$ is comparable to Γ. Γ corresponds to the slow switching rate between two coherent states $|\pm\alpha\rangle$ ($|\alpha| = \sqrt{\Lambda_2/K}$) that are eigenstates of the coherent Hamiltonian Mirrahimi et al. [2014b], Puri et al. [2017]. Using Lindblad perturbation theory, one finds that for large $|\alpha|$ this rate is exponentially small Mamaev et al. [2018], Mamaev [2018]:

$$\Gamma = 2\kappa|\alpha|^2 e^{-4|\alpha|^2} \tag{3.82}$$

Defining a cross-over temperature via $\bar{n}_{\text{th,cross}} = \Gamma/\kappa$ provides a good qualitative estimate for the symmetry-breaking temperature in Fig. 3.7.

We stress that even at zero temperature, most system correlation functions do not exhibit any time-symmetry. Such correlation functions do not show any dramatic behavior as a

Hidden TRS	**Classical TRS**
$\|\tilde{\psi}\rangle \equiv \hat{T}\|\psi\rangle$	$(\tilde{\alpha}, \tilde{\beta}) \equiv (U\alpha, U\beta)$
$C^{\mathrm{TFD}}_{X,Y}(t) \equiv \langle \hat{X}_A(t)\hat{Y}_B(0)\rangle$	$C^{\mathcal{P}}_{X,Y}(t) \equiv \overline{X(t)\tilde{Y}(0)}$
$\mathcal{J}[\hat{a}] \equiv U\hat{a}$, $\mathcal{J}[\hat{H}_{\mathrm{eff}}] \equiv \hat{H}_{\mathrm{eff}} + E$.	Potential conditions (U must be unity)

Table 3.2: Dictionary connecting hidden TRS and an effective classical notion of TRS in the effective phase space used in the complex-P function method. We list objects/conditions commonly appearing in the solution of quantum master equations via quantum detailed balance (i.e. hidden TRS), and their counterparts in the language of classical detailed balance in the complex-P representation. This correspondence only exists for multimode bosonic systems coupled to local zero-temperature dissipation.

function of temperature. As an example, we plot the asymmetry of the correlation function $C_{X^2,P^2}(t)$, defined as

$$m_{X^2P^2}(T) \equiv \int_0^\infty |C_{X^2,P^2}(t) - C_{X^2,P^2}(-t)|dt, \tag{3.83}$$

in Fig. 3.7; here, $\hat{X}$, $\hat{P}$ are standard quadrature operators.

3.8 Hidden TRS and phase-space methods: a quantum-classical correspondence

In this final section, we turn to driven-dissipative systems comprised of one or more bosonic modes, and connect our notion of hidden TRS to phase space methods that are well known in quantum optics, and have been used to solve non-trivial problems using an effective Fokker-Planck equation in an expanded phase space. The focus is on Lindblad master equations of the form

$$\partial_t \hat{\rho} = -i[\hat{H}, \hat{\rho}] + \sum_j \kappa_j \mathcal{D}[\hat{a}_j] \tag{3.84}$$

Here, $[\hat{a}_j, \hat{a}_k^\dagger] = \delta_{jk}$ is a standard set of independent bosonic modes, κ_j represents a decay rate for each mode, and $\hat{H}$ is an arbitrary bosonic quantum many-body Hamiltonian. We will establish that for this restricted class of models, the fully quantum notion of hidden-TRS (described by an anti-unitary operator $\hat{T}$) coincides with a classical notion of time-reversal in an expanded phase space, i.e. an involution of the form $(x, p) \to (\tilde{x}, \tilde{p})$ (where x, p are classical phase space coordinates). Hence, the effective detailed balance properties (and potential conditions) of a complex-P Fokker-Planck equation is directly tied to hidden-TRS. This allows us to directly understand the success of the complex-P method in solving several non-trivial driven cavity problems Drummond and Gardiner [1980]. Interestingly, we show that for extended models, this correspondence no longer necessarily holds. For example, by simply adding two-photon loss processes, there exist hidden-TRS operators that have no correspondence to a simple operation in an extended phase space.

The context of our discussion will be the complex-P phase-space representation of the general bosonic master equation in Eq. (3.84). This is a particular non-diagonal expansion of the system's density matrix in terms of coherent states that can be used to convert the master equation into a well-behaved, Fokker-Planck-like equation (see Walls and Milburn [2008] for a pedagogical introduction). Consider the single-mode case first for simplicity. We consider a doubled phase space described by complex coordinates (α, β), and chose appropriate integration contours $\mathcal{C}, \mathcal{C}'$ for each of these variables. This lets us express the density matrix as

$$\hat{\rho} = \int_{\mathcal{C}} d\alpha \int_{\mathcal{C}'} d\beta \frac{|\alpha\rangle\langle\beta^*|}{\langle\alpha|\beta^*\rangle} P(\alpha, \beta). \tag{3.85}$$

where $P(\alpha, \beta)$ is the complex-P quasi-distribution function. Using standard techniques Drummond and Gardiner [1980], one can often convert the Lindblad master equation for $\hat{\rho}$ into a Fokker-Planck equation for this function, which is required to be nonsingular on the integration surface $\mathcal{C} \times \mathcal{C}'$ defined by the contours. The resulting equation has the standard

form:

$$\partial_t P(\alpha,\beta) = \partial_\mu \Big[C^\mu(\alpha,\beta) P(\alpha,\beta) \Big] + \partial_\mu \partial_\nu \Big[D^{\mu\nu}(\alpha,\beta) P(\alpha,\beta) \Big] \tag{3.86}$$

Here, $C^\mu(\alpha,\beta)$ represents a generalized drift vector, and $D^{\mu\nu}(\alpha,\beta)$ a generalized diffusion tensor. The above derivatives are holomorphic derivatives Drummond and Gardiner [1980], and Einstein summation notation is implied.

We can now state our quantum-classical correspondence principle: *if the quantum master equation Eq.* (3.84) *has a hidden quantum time-reversal symmetry* $\hat{T}$ *and corresponds to a well-defined Fokker-Planck equation in the complex-P representation, then this associated Fokker-Planck equation has a well-defined classical TRS corresponding to* $\hat{T}$. In the case where this classical TRS operation is trivial (i.e. the identity operation), this symmetry then correspond to a standard detailed balance condition, meaning that the drift and diffusion matrices satisfy potential conditions Gardiner [2009]. This directly enables an efficient solution for the steady-state distribution function $P(\alpha,\beta)$, and hence the steady-state density matrix.

The fact that the complex-P Fokker-Planck equations satisfy potential conditions is precisely the property that enabled exact solutions of a variety of nonlinear driven cavity models Drummond and Walls [1980b]. Our result shows that this surprising property is directly tied to a more general, and fully quantum symmetry: hidden-TRS. In what follows, we will describe precisely how to construct the classical time-reversal operator corresponding to a hidden TRS $\hat{T}$, and then show how this correspondence can be broken by considering higher-order Markovian loss channels.

3.8.1 Detailed balance in generalized P-representations

We start by defining a notion of time-reversal symmetry that is meaningful for the complex-P distribution function $P(\alpha, \beta)$. We stress the well-known fact that this distribution function is in general complex valued, and thus does not represent a meaningful probability distribution. Nonetheless, we can formally use it to define quantities analogous to expectation values and correlation functions.

Note first that the expectation value of a holomorphic function $X(\alpha, \beta)$ defined on our complex phase space is defined as:

$$\overline{X} \equiv \int_{\mathcal{C}} d\alpha \int_{\mathcal{C}'} d\beta P_{ss}(\alpha, \beta) X(\alpha, \beta). \tag{3.87}$$

We can also define a time-evolved function $X(\alpha, \beta; t)$ defined by the solution of the dual Fokker-Planck equation

$$\begin{aligned} \partial_t X(\alpha, \beta) = -\partial_\mu \Big[C^\mu(\alpha, \beta) X(\alpha, \beta) \Big] \\ + \partial_\mu \partial_\nu \Big[D^{\mu\nu}(\alpha, \beta) X(\alpha, \beta) \Big]. \end{aligned} \tag{3.88}$$

With these definitions in hand, we define time-reversal symmetry in our doubled, complex classical phase space as the existence of a phase-space involution

$$(\alpha, \beta) \to \widetilde{(\alpha, \beta)}, \tag{3.89}$$

such that all two-time correlation functions (calculated as defined above) are time-symmetric:

$$C^{\mathcal{P}}_{X,Y}(t) \equiv \begin{cases} \overline{X(t) Y(0)} & t \geq 0 \\ \overline{\tilde{Y}(-t) \tilde{X}(0)} & t < 0 \end{cases}, \tag{3.90}$$

Here X, Y are any two holomorphic functions, and the time-reversed functions are given as

$$\tilde{X}(\alpha, \beta) \equiv X(\widetilde{\alpha, \beta}) \tag{3.91}$$

where $\widetilde{(\alpha, \beta)}$ is the time-reversed counterpart to (α, β), i.e. another point in the integration surface on which the complex Fokker-Planck evolution is taking place. All we require is that this time-reversal operation squares to the identity, namely, time-reversing a point twice recovers the original point on $\mathcal{C} \times \mathcal{C}'$.

For complex-P distributions, one can establish a generalization of a standard result in classical probability theory, which we rigorously establish in Section 3.18: in the limit where the time-reversal operation is just the identity, the classical detailed balance condition Eq. (3.90) is equivalent to the potential conditions on the Fokker-Planck equation Risken and Frank [1996], Gardiner [2009]. Recall that these conditions correspond to the having the (pseudo)probability current vanish in the steady state at every point in phase space, where the *pseudoprobability current* $J^{\mu}(\alpha, \beta, t)$ is defined by rewriting the Fokker-Planck equation as a continuity equation:

$$\partial_t P(\alpha, \beta; t) \equiv \partial_{\mu} J^{\mu}(\alpha, \beta; t). \tag{3.92}$$

This constraint allows a direct method for solving for the steady state in terms of a potential function.

Note that in the case where the time-reversal operation $(\alpha, \beta) \to \widetilde{(\alpha, \beta)}$ is *not* the identity, there is no simple potential-condition method for solving Fokker-Planck equations, unless the time-reversal symmetry is known beforehand (see e.g. Ref. Risken and Frank [1996].)

3.8.2 Constructing the classical TRS corresponding to a hidden TRS $\hat{T}$

We briefly outline the correspondence here in the single-mode case, and leave the discussion of the multimode case to Sec. 3.14. For these systems, hidden TRS implies (among other constraints) the constraint

$$\mathcal{J}[\hat{a}] = u\hat{a}, \tag{3.93}$$

where $\mathcal{J}$ is the exchange superoperator as always, and $u = \pm 1$. In Sec. 3.14 we show that, under the assumption that Eq. (3.93) holds, hidden TRS is equivalent to classical detailed balance in the complex-P representation with respect to the following classical time-reversal operation:

$$\widetilde{(\alpha, \beta)} = (u\alpha, u\beta) \tag{3.94}$$

Note that the fact that u squares to one, an intrinsic property of the exchange superoperator, ensures that this is a valid classical time-reversal operation in the effective phase space used for the complex-P representation.

This surprising correspondence is the result of TFD correlation functions of normally-ordered operators coinciding with complex-P correlations. More precisely, if $\mathcal{J}[\hat{a}] = u\hat{a}$ with $u = \pm 1$, then we have (see Sec. 3.14):

$$C^{\mathcal{P}}_{X,\tilde{Y}}(t) = C^{\mathrm{TFD}}_{\hat{X},\hat{Y}}(t) \tag{3.95}$$

where X, Y are the classical representatives of $\hat{X}, \hat{Y}$ in the complex-P representation. Ex-

plicitly, without loss of generality, $\hat{X}, \hat{Y}$ can be written as

$$\hat{X} = \sum_{n,m} \chi_{n,m} (\hat{a}^\dagger)^n \hat{a}^m, \tag{3.96}$$

$$\hat{Y} = \sum_{n,m} \lambda_{n,m} (\hat{a}^\dagger)^n \hat{a}^m. \tag{3.97}$$

In terms of the normally-ordered expressions above, the classical representatives X, Y have the following form:

$$X(\alpha, \beta) \equiv \sum_{n,m} \chi_{n,m} \beta^n \alpha^m, \tag{3.98}$$

$$Y(\alpha, \beta) \equiv \sum_{n,m} \lambda_{n,m} \beta^n \alpha^m. \tag{3.99}$$

Finally, the classical time-reversal operation used to define the reversibility of the Fokker-Planck equation is given in Eq. (3.94). Therefore, in this situation, hidden (quantum) TRS is equivalent to classical TRS in the complex-P representation.

3.8.3 Breakdown of the correspondence principle: going beyond phase-space methods

The simplest situations in which the above correspondence principle breaks down is in systems with higher-order loss dissipators, e.g. a system of the form

$$\frac{d}{dt}\hat{\rho} = -i[\hat{H}, \hat{\rho}] + \kappa \mathcal{D}[\hat{a}^2]\hat{\rho}. \tag{3.100}$$

An example of this is the driven cavity problem considered in Sec. 3.6, in the regime where all single-photon terms are set to zero: $\Lambda_1 = \kappa_1 = 0$. We are left with a model with an interaction, detuning, two-photon drive and two-photon loss. The full master equation in this case conserved photon number parity, and thus does not have a unique steady state.

For this model, we still have hidden-TRS for each of the steady states. The full set of hidden-TRS compatible TFD states, i.e. obtained by solving Eqs. (3.45)-(3.47), has the form:

$$|\psi_T(\gamma,\nu)\rangle \equiv \gamma|\psi_T^+\rangle + \nu|\psi_T^-\rangle. \tag{3.101}$$

where the individual terms $\left|\psi_T^{\pm}\right\rangle$ in the superposition correspond to the two simple thermofield doubled states encountered in Sec. 3.6, and which, upon tracing-out the auxiliary cavity B, correspond to a *single* steady state of the master equation Eq. (3.100):

$$\hat{\rho}_{\rm ss}^{(0)} = {\rm Tr}_B[|\psi_T^+\rangle\langle\psi_T^+|] = {\rm Tr}_B[|\psi_T^-\rangle\langle\psi_T^-|]. \tag{3.102}$$

According to the quantum-classical correspondence outlined in this section, this stationary state corresponds to a stationary complex-P distribution with both a trivial TRS (corresponding to the potential conditions) and an inversion TRS (corresponding to something more complicated):

$$\hat{\rho}_{\rm ss}^{(0)} = \int_{\mathcal{C}} d\alpha \int_{\mathcal{C}'} d\beta \frac{|\alpha\rangle\langle\beta^*|}{\langle\alpha|\beta^*\rangle} P_{ss}(\alpha,\beta) \tag{3.103}$$

$$= \int_{\mathcal{C}} d\alpha \int_{\mathcal{C}'} d\beta \frac{|\alpha\rangle\langle\beta^*|}{\langle\alpha|\beta^*\rangle} P_{ss}(-\alpha,-\beta) \tag{3.104}$$

In light of the above observation, one might interpret the more exotic thermofield doubled state $|\psi(\gamma,\nu)\rangle$ as describing a quantum TRS which corresponds to a "superposition" of both the trivial and inversion TRS, and thus this hidden time-reversal symmetry no longer has a classical analogue.

Indeed, it is well-known that the stationary state obtained via solution of the potential conditions is not the *only* stationary state of the quantum master equation Eq. (3.100) Bartolo et al. [2016], Wang et al. [2016]. Tracing out the auxiliary cavity B for arbitrary

parameters γ, ν reveals a family of quantum steady states:

$$\hat{\rho}_{\rm ss}(\gamma,\nu) \equiv {\rm Tr}_B[|\psi_T(\gamma,\nu)\rangle\langle\psi_T(\gamma,\nu)|]. \tag{3.105}$$

While any $\hat{T}$ and TFD must yield an exchange superoperator $\mathcal{J}$ that acts simply on $\hat{a}^2$ (via Eq. (3.46)), the action on $\hat{a}$ need not be simple. In fact, we only get a simple action when $\nu = 0$ ($\gamma = 0$), in which case $\mathcal{J}[\hat{a}] = \hat{a}$ ($\mathcal{J}[\hat{a}] = -\hat{a}$). For the more general case, the identity Eq. (3.93) is broken. The more complicated nature of the hidden TRS operator and the corresponding $\mathcal{J}$ implies that the steady states corresponding to $|\psi_T(\gamma,\nu)\rangle$ cannot be easily found using the complex-P phase space solution method.

3.9 Doubled-system classical detailed balance

In this section, we prove that classical detailed balance may be equivalently stated as the following symmetry condition:

$$\overline{X_A(t)Y_B(0)} = \overline{Y_A(t)X_B(0)}, \qquad \forall X, Y. \tag{3.106}$$

The reason why the above condition is equivalent to the standard definition of detailed balance is that the doubled-system correlation function $\overline{X_A(t)Y_B(0)}$ is actually a single-system correlation function in disguise:

$$\overline{X_A(t)Y_B(0)} = \sum_{n,m} \bar{p}(n)\delta_{m,\tilde{n}} X(t,n)Y(0,m) \tag{3.107}$$

$$= \sum_{n} \bar{p}(n)X(t,n)Y(0,\tilde{n}) = \overline{X(t)\tilde{Y}(0)}, \tag{3.108}$$

Therefore, the doubled-system correlation function $\overline{X_A(t)Y_B(0)}$ is time-symmetric for all random variables X, Y if and only if

$$\overline{X(t)\tilde{Y}(0)} = \overline{Y(t)\tilde{X}(0)}, \quad \forall X, Y. \tag{3.109}$$

Now, making the replacement $Y \to \tilde{Y}$ in this single-site symmetry condition yields the definition of classical detailed balance used earlier. Therefore, Eq. (3.109) is equivalent to classical detailed balance:

$$\overline{X(t)Y(0)} = \overline{\tilde{Y}(t)\tilde{X}(0)}, \quad \forall X, Y. \tag{3.110}$$

Note that we have implicitly used the fact that $Y \to \tilde{Y}$ is a bijection of the algebra of random variables. In summary, we have shown that the doubled definition Eq. (3.106) of classical detailed balance is completely equivalent to the standard definition Eq. (3.110).

3.10 CQDB rules out stationary coherences between energy eigenstates

We now demonstrate that systems with CQDB have steady state density matrices that are always guaranteed to be diagonal in the energy eigenbasis. There are many references that show this explicitly Kossakowski et al. [1977], Bratteli and Haagerup [1978], Alicki [1976]. However, here we will assume an intermediate result, namely that CQDB implies *modular symmetry* Bratteli and Haagerup [1978], that is, a symmetry of the driven-dissipative dynamics with respect to the unitary dynamics generated by the modular Hamiltonian

$$\hat{H}_\rho \equiv -\log \hat{\rho}_{\rm ss}. \tag{3.111}$$

The reason for taking this symmetry-based perspective is that it informs most of the central results in the theory of quantum detailed balance Fagnola and Umanita [2007], Fagnola and Umanità [2010].

Indeed, once the above symmetry is established, the proof that steady states with CQDB are diagonal in the energy eigenbasis is very easy. We provide here a simple argument that works in the finite-dimensional case. We begin with Lindblad's original expression for the effective Hamiltonian as a classical average Lindblad [1976]:

$$i\hat{H}_{\text{eff}} = \overline{\bar{\mathcal{L}}[U^\dagger] \cdot U} \tag{3.112}$$

where here, U is a Haar-random unitary, and $\bar{\mathcal{L}}$ is the Heisenberg-picture Lindbladian, which generates time-evolution of observables. We now observe how the effective Hamiltonian evolves under the modular (dynamical) group $\hat{O}(t) \equiv \hat{\rho}_{\text{ss}}^{it}\hat{O}\hat{\rho}_{\text{ss}}^{-it}$:

$$i\hat{H}_{\text{eff}}(t) = \overline{\hat{\rho}_{\text{ss}}^{it}\bar{\mathcal{L}}[\hat{U}^\dagger] \cdot \hat{U}\hat{\rho}_{\text{ss}}^{-it}}. \tag{3.113}$$

The above identity holds for any Lindbladian, and thus contains no hidden assumptions about the system in question. Now suppose, however, that $\bar{\mathcal{L}}$ satisfies CQDB, and thus has modular symmetry. Then, in particular, we have

$$\hat{\rho}_{\text{ss}}^{it}\bar{\mathcal{L}}[\hat{U}^\dagger] = \bar{\mathcal{L}}[\hat{\rho}_{\text{ss}}^{it}\hat{U}^\dagger\hat{\rho}_{\text{ss}}^{-it}]\hat{\rho}_{\text{ss}}^{it}. \tag{3.114}$$

Substituting the above identity into the Haar-random average defining the effective non-hermitian Hamiltonian yields a simple result - $\hat{H}_{\text{eff}}$ is time-independent with respect to the unitary dynamics generated by the modular Hamiltonian:

$$i\hat{H}_{\text{eff}}(t) = \overline{\bar{\mathcal{L}}[\hat{U}^\dagger(t)] \cdot \hat{U}(t)} = \overline{\bar{\mathcal{L}}[\hat{U}^\dagger] \cdot \hat{U}} = i\hat{H}_{\text{eff}}(0). \tag{3.115}$$

Therefore, the effective Hamiltonian commutes with the modular Hamiltonian, and thus the effective Hamiltonian commutes with the steady state itself: $[\hat{H}_{\text{eff}}, \hat{\rho}_{\text{ss}}] = 0$. By taking the anti-hermitian part of the commutator, we immediately have that $\hat{H}$ commutes with $\hat{\rho}_{\text{ss}}$.

3.11 Example of broken CQDB: dissipative Rabi-driven qubit

To make the ideas of sections 3.2.4 and 3.2.5 more concrete, we consider simple but ubiquitous system which does not satisfy CQDB, does have hidden TRS.

3.11.1 Violation of CQDB via correlation function asymmetry

Our example is a qubit (with Pauli operators $\hat{\sigma}_{x,y,z}$) subject to a coherent Rabi drive in the presence of loss. Working in the rotating frame set by the drive, and making a rotating wave approximation, the master equation has the form of Eq. (3.8) with $M = 1$ and

$$\hat{H} = \Delta\hat{\sigma}_z + \frac{\Omega}{2}\hat{\sigma}_x, \;\; \hat{c}_1 = \sqrt{\kappa}\hat{\sigma}_-. \tag{3.116}$$

Here Δ is the detuning of the drive from the qubit splitting frequency, Ω is the Rabi frequency, and κ is the decay rate of the qubit excited state. The steady state for this system is easy to find and given in many textbooks, see e.g. Ref. Gardiner and Zoller [2000]:

$$\begin{aligned}\hat{\rho}_{\text{ss}} = \frac{\hat{1}}{2} &- \frac{4\Delta\Omega}{16\Delta^2 + 2\Omega^2 + \kappa^2}\hat{\sigma}_x + \frac{\Omega\kappa}{16\Delta^2 + 2\Omega^2 + \kappa^2}\hat{\sigma}_y \\ &- \frac{16\Delta^2 + \kappa^2}{2(16\Delta^2 + 2\Omega^2 + \kappa^2)}\hat{\sigma}_z\end{aligned} \tag{3.117}$$

Given the external driving, this steady state does not correspond to thermal equilibrium, and hence a priori there is no reason to expect that it will satisfy CQDB. While this may seem obvious, we will now show that CQDB is broken explicitly, by directly uncovering correlation function time-asymmetry in this system. We stress that the CQDB condition in Eq. (3.11)

is contingent on the choice of time-reversal operator $\hat{T}$. We will take a general approach here (and throughout this chapter): we do not pre-select the definition of $\hat{T}$ using on additional knowledge of our system, but rather ask where there is *any* possible anti-unitary $\hat{T}$ which would give rise to a symmetry. Hence to truly rule out CQDB, one must check Eq. (3.11) for all permissible choices of $\hat{T}$. We will thus show that CQDB does not hold no matter what choice is made for $\hat{T}$.

In what follows, for simplicity we assume a resonant drive (i.e. $\Delta = 0$), and introduce the dimensionless Rabi frequency $b \equiv \Omega/\kappa$; CQDB is violated even for non-resonant drives, see Sec. 3.11.2 below. The first step is to parameterize all possible TRS operators. Since CQDB only holds if $\hat{\rho}_{\rm ss}$ is itself invariant under TRS, this constrains the form of TRS. The only permissible TRS operators are then parameterized by a single phase ψ and have the form:

$$\hat{T} = \left[\frac{\sin(\psi/2)}{\sqrt{4b^2+1}}\left(\hat{1} - 2ib\hat{\sigma}_x\right) + i\cos(\psi/2)\hat{\sigma}_z\right]\hat{K}_z \tag{3.118}$$

where $\hat{K}_z$ is the complex conjugation operator acting in the $\hat{\sigma}_z$ basis. The complex conjugation operator $\hat{K}$ is an antilinear operator, $\hat{K}(c_a|a\rangle + c_b|b\rangle) = c_a^*\hat{K}|a\rangle + c_b^*\hat{K}|b\rangle$, whose action is basis dependent Messiah [1962]. In the $\hat{\sigma}_z$ basis (basis state denoted $|\pm\rangle$) the complex conjugation operator $\hat{K}_z$ is defined by $\hat{K}_z(c|\pm\rangle) = c^*\hat{K}_z|\pm\rangle = c^*|\pm\rangle$, i.e. $\hat{K}_z$ leaves the basis states invariant but conjugates complex coefficients.

To show that CQDB cannot hold in this system, it is sufficient to show that at least one correlation function violates Eq. (3.11) for each TRS angle ψ. As our main object of study, we introduce the correlation function defined for positive and negative times:

$$C_{yz}(t) = \begin{cases} \langle\hat{\sigma}_y(t)\hat{\sigma}_z(0)\rangle & t \geq 0 \\ \langle\tilde{\sigma}_z(-t)\tilde{\sigma}_y(0)\rangle & t < 0 \end{cases} \tag{3.119}$$

where $\tilde{\sigma}_j = \hat{T}\hat{\sigma}_j\hat{T}^{-1}$. CQDB holds, then Eq. (3.11) implies time symmetry: $C_{yz}(t) =$

$C_{yz}(-t)$. In what follows we show that the properties of the TRS and the eigenmodes of the Liouvillian do not allow for the time symmetry of $C_{yz}(t)$ and other correlation functions.

The Liouvillian of the driven qubit system is readily diagonalized. Letting λ_j denote its eigenvalues and $\hat{r}_j$ the corresponding right-eigenvectors, we find:

$$\lambda_0 = 0 \qquad \hat{r}_0 = \hat{\rho}_{\rm ss} \tag{3.120}$$

$$\lambda_1 = -\frac{\kappa}{2} \qquad \hat{r}_1 = \hat{\sigma}_x \tag{3.121}$$

$$\lambda_2 = -\frac{\kappa}{4}(3 + i\alpha) \qquad \hat{r}_2 = \hat{\sigma}_y + \frac{(1+i\alpha)}{4b}\hat{\sigma}_z \tag{3.122}$$

$$\lambda_3 = -\frac{\kappa}{4}(3 - i\alpha) \qquad \hat{r}_3 = \frac{(1+i\alpha)}{4b}\hat{\sigma}_y + \hat{\sigma}_z \tag{3.123}$$

where $b \equiv \Omega/\kappa$, $\alpha = \sqrt{16b^2 - 1}$ is the dimensionless damped Rabi frequency. For $b < 1/4$ the qubit is overdamped and the frequency is imaginary: $\alpha \to i\sqrt{1 - 16b^2}$. The essential feature of the eigensystem is that the $\hat{\sigma}_x$ coherence behaves differently from the $\hat{\sigma}_y$ coherence or the classical population ($\hat{\sigma}_z$). The $\hat{\sigma}_x$ coherence decays exponentially with rate $(-\lambda_1) = \kappa/2$. The $\hat{\sigma}_y$ coherence and the classical populations decay with $(-\mathrm{Re}\,\lambda_{2,3}) > \kappa/2$ for any finite b. This implies that $\langle\hat{\sigma}_x(t)\hat{\sigma}_k(0)\rangle$ has a time dependence that is always different from $\langle\hat{\sigma}_y(t)\hat{\sigma}_k(0)\rangle$ or $\langle\hat{\sigma}_z(t)\hat{\sigma}_k(0)\rangle$ for any $\hat{\sigma}_k$.

With this in mind, we turn to the time-reversed operator $\tilde{\sigma}_z$ which, in general is a linear combination of all three Pauli operators. In particular, the $\hat{\sigma}_x$ component is

$$\tilde{\sigma}_z = -(2b/\sqrt{4b^2+1})\sin\psi\hat{\sigma}_x + \cdots \tag{3.124}$$

We can see that for any $\psi \neq 0, \pi$, for which $\sin\psi \neq 0$, the expression $C_{yz}(t < 0)$ will have terms measuring the decay of $\hat{\sigma}_x$ coherence. Thus the time dependence at $t < 0$ *must be* qualitatively different from that at $t > 0$. Even at $\psi = 0, \pi$ the correlation function is generically *not* time symmetric. As an example, we show a generic plot of the time

asymmetry of $C_{yz}(t)$ in Fig. 3.8 for $b = 1$ computed for various ψ. Although the argument breaks down at $\psi = 0, \pi$, we can show definitively that CQDB cannot hold by considering $C_{xz}(t)$, which is defined analogously with $C_{yz}(t)$. Since at $\psi = 0, \pi$ there are no $\hat{\sigma}_x$ terms in $\tilde{\sigma}_z$, the time dependence of $C_{xz}(t < 0)$ must be qualitatively different from the time dependence of $C_{xz}(t > 0)$. Therefore we conclude that the Rabi-driven qubit does not satisfy CQDB.

3.11.2 Violation of CQDB for any detuning

In the preceding section we restricted our analysis to the resonantly driven qubit for which $\Delta = 0$ primarily because the diagonalization of the Liouvillian becomes unwieldy for $\Delta \neq 0$. Here we show by an alternate route that for any detuning, the Rabi driven system violates CQDB.

Recall from Section 3.10 that a system which satisfies CQDB must have a steady state that is diagonal in the energy eigenbasis. The commutator $[\hat{H}, \hat{\rho}_{\text{ss}}]$ is equivalent to taking the cross product between the Hamiltonian "vector" $(\Omega/2, 0, \Delta)$ and the traceless part of $\hat{\rho}_{\text{ss}}$. Imposing the constraint that the commutator is zero requires the form of $\hat{\rho}_{\text{ss}}$ to be

$$\hat{\rho}_{\text{ss}} = \frac{1}{2}\left(\hat{1} + \alpha \hat{H}\right) \tag{3.125}$$

where α is a real constant of proportionality. Crucially, the above expression is linear in Δ and Ω, whereas the true steady state is a quadradic rational function of these parameters *and* the decay rate κ, c.f. Eq. (3.117). Therefore we conclude that for any detuning, the Rabi-driven qubit does not satisfy CQDB. Furthermore, one can numerically diagonalize the Liouvillian at any drive detuning and verify that there does not exist any TRS for which the steady state is invariant and for which all correlation functions are time symmetric.

3.11.3 Permissible TRS

Here we show how the permissible TRS of Eq. (3.118) are determined from the steady state Eq. (3.117). We require only that $\hat{T}$ leaves the steady state invariant as a necessary condition of CQDB. All possible TRS take the form $\hat{T} = \hat{V}\hat{K}_\rho$ for unitary $\hat{V}$ and complex conjugation $\hat{K}_\rho$ in the steady state eigenbasis such that $\hat{T}\hat{\rho}_{\rm ss}\hat{T}^{-1} = \hat{\rho}_{\rm ss}$. This condition implies that the action of $\hat{T}$ on the eigenstates of $\hat{\rho}_{\rm ss}$ (i.e. pointer states) is restricted to be

$$\hat{T}|1\rangle = |1\rangle \tag{3.126}$$

$$\hat{T}|2\rangle = e^{i\psi}|2\rangle \tag{3.127}$$

up to a global phase. Thus in the steady state eigenbasis the permissible TRS take the form $\hat{T} = (|1\rangle\langle 1| + e^{i\psi}|2\rangle\langle 2|)\hat{K}_\rho$ for any ψ, where $\hat{K}_\rho$ is complex conjugation in the steady state eigenbasis and the pointer states are assumed time-reversal invariant: $\hat{K}_\rho|n\rangle = |n\rangle$.

As the final step, we represent $\hat{T}$ *in the familiar* $\hat{\sigma}_z$ *basis.* Recall that in the steady state eigenbasis, $\hat{T} = \hat{V}\hat{K}_\rho$. Given the unitary $\hat{U}$ that diagonalizes the steady state, $\hat{U}\hat{\rho}_{\rm ss}\hat{U}^\dagger = \mathrm{diag}(p_1, p_2)$, the permissible TRS are given in the $\hat{\sigma}_z$ basis as

$$\hat{T} = \hat{U}^\dagger\hat{V}\hat{K}_\rho\hat{U} = \hat{U}^\dagger\hat{V}\hat{U}^*\hat{K}_z. \tag{3.128}$$

Here we use the relation

$$\hat{K}_\rho = \hat{U}^*\hat{K}_z\hat{U}^\dagger \tag{3.129}$$

which defines $\hat{K}_\rho$ in terms of $\hat{K}_z$ Messiah [1962].

For completeness $\hat{U}$ is given in terms of $b \equiv \Omega/\kappa$ and $s \equiv \sqrt{4b^2+1}$ as

$$\hat{U} = \frac{1}{\sqrt{2s}}\begin{pmatrix} i\sqrt{s-1} & \sqrt{s+1} \\ i\sqrt{s+1} & -\sqrt{s-1} \end{pmatrix}. \tag{3.130}$$

Substituting this into the expression for $\hat{T}$ above recovers Eq. (3.118) (which is also Eq. (3.31)).

3.12 Explicit construction of exchange superoperator $\mathcal{J}$

By definition, the exchange superoperator is supposed to act on a single site observable $\hat{O}$ and produce a new single-site observable, $\mathcal{J}[\hat{O}]$, which, upon acting on site B of the thermofield double, produces the same state as one would obtain by acting on site A with the observable $\hat{O}$:

$$\mathcal{J}[\hat{O}]_B|\psi_T\rangle \equiv \hat{O}_A|\psi_T\rangle \tag{3.131}$$

One may interpret the above equation as the vectorization of an operator equation, according to the rules

$$\hat{O}_A|\psi_K\rangle \to \hat{O}\hat{\rho}_{ss}^{1/2}, \tag{3.132}$$

$$\hat{O}_B|\psi_K\rangle \to \hat{\rho}_{ss}^{1/2}\tilde{O}^T, \tag{3.133}$$

where $|\psi_K\rangle$ is the thermofield doubled state where the time-reversal operation $\hat{T} \equiv \hat{K}$ is complex-conjugation in the eigenbasis of the steady state. Explicitly:

$$|\psi_K\rangle = \sum_n \sqrt{p_n}|n\rangle|n\rangle. \tag{3.134}$$

Furthermore, $\hat{O} \to \hat{O}^T$ denotes matrix transposition in the eigenbasis of the steady state.

An arbitrary time-reversal operation can be decomposed as $\hat{T} \equiv \hat{V}\hat{K}$, where $\hat{V}$ commutes with $\hat{\rho}_{\rm ss}$. Explicitly, an arbitrary thermofield doubled state corresponding to a hidden TRS

must always have the expression

$$|\psi_T\rangle = \sum_n \sqrt{p_n}|n\rangle e^{i\theta_n}|n\rangle, \tag{3.135}$$

$$\equiv \sum_n \sqrt{p_n}|n\rangle \hat{V}\hat{K}|n\rangle. \tag{3.136}$$

Under the above rules, the thermofield doubled state with an arbitrary time-reversal operation for a unitary $\hat{V}$ satisfies the following identities:

$$\hat{O}_A|\psi_T\rangle = \hat{O}_A\hat{V}_B|\psi_K\rangle \to \hat{O}\hat{\rho}_{\rm ss}^{1/2}\hat{V}^T \tag{3.137}$$

$$\hat{O}_B|\psi_T\rangle = (\hat{O}\hat{V})_B|\psi_K\rangle \to \hat{\rho}_{\rm ss}^{1/2}(\hat{O}\hat{V})^T \tag{3.138}$$

We now verify the formula $\mathcal{J}[\hat{O}] = \hat{\rho}_{\rm ss}^{1/2}\tilde{O}^\dagger\hat{\rho}_{\rm ss}^{-1/2}$. First of all, any hidden TRS must leave the steady state invariant, and we can rewrite this formula as

$$\mathcal{J}[\hat{O}] \equiv \hat{\rho}_{\rm ss}^{1/2}\hat{O}^T\hat{\rho}_{\rm ss}^{-1/2} \tag{3.139}$$

We can then proceed to verify Eq. (3.131) directly:

$$(\hat{\rho}_{\rm ss}^{1/2}\hat{O}\hat{\rho}_{\rm ss}^{-1/2})_B|\psi_T\rangle \to \hat{\rho}_{ss}^{1/2}\hat{V}^T(\hat{\rho}_{\rm ss}^{1/2}\hat{O}^T\hat{\rho}_{\rm ss}^{-1/2})^T. \tag{3.140}$$

Taking advantage of the fact that $\hat{V}$ commutes with $\hat{\rho}_{\rm ss}$, we have

$$\hat{\rho}_{ss}^{1/2}\hat{V}^T(\hat{\rho}_{\rm ss}^{1/2}\hat{O}^T\hat{\rho}_{\rm ss}^{-1/2})^T = \hat{O}\hat{V}^T\hat{\rho}_{\rm ss}^{1/2} = \hat{O}\hat{\rho}_{\rm ss}^{1/2}\hat{V}^T, \tag{3.141}$$

which is just the operator representation of $\hat{O}_A|\psi_T\rangle$ according to the rules Eqs. (3.137-3.138).

3.13 From CQDB to hidden TRS

In this Section, we will show that, for systems with modular symmetry, CQDB and hidden TRS are equivalent. Since CQDB already implies modular symmetry by itself Kossakowski et al. [1977], Bratteli and Haagerup [1978], this will demonstrate that CQDB necessarily implies hidden TRS. Therefore, CQDB is a strict subphenomenon of hidden TRS.

Indeed, consider an arbitrary driven-dissipative system described by a Lindblad master equation. The definition of the exchange superoperator tells us that

$$C_{X,\mathcal{J}[Y]}(t) = C^{\mathrm{TFD}}_{X,Y}(t), \quad \forall t \geq 0. \tag{3.142}$$

The above correlation function, for negative times, is harder to rephrase as a two-site quantity:

$$C_{X,\mathcal{J}[Y]}(-t) = \langle (\hat{\rho}_{ss}^{-1/2} \hat{Y} \hat{\rho}_{ss}^{1/2})(t) \tilde{X}^\dagger \rangle. \tag{3.143}$$

However, the above expression simplifies considerably in systems with modular symmetry. Indeed, let us now assume that the driven-dissipative system in question is symmetric with respect to the modular Hamiltonian $\hat{H}_\rho$, as is always the case with systems that have CQDB Kossakowski et al. [1977]. Then, we can write $(\hat{\rho}_{ss}^{-1/2} \hat{Y} \hat{\rho}_{ss}^{1/2})(t) = \hat{\rho}_{ss}^{-1/2} \hat{Y}(t) \hat{\rho}_{ss}^{1/2}$. Substituting this identity into Eq. (3.143), we get

$$C_{X,\mathcal{J}[Y]}(-t) = C^{\mathrm{TFD}}_{X,Y}(-t), \quad \forall t \geq 0. \tag{3.144}$$

Therefore, for any driven-dissipative system with modular symmetry,

$$C_{X,\mathcal{J}[Y]}(t) = C^{\mathrm{TFD}}_{X,Y}(t) \quad \forall t \in \mathbb{R}. \tag{3.145}$$

Therefore, since $\mathcal{J}$ is a bijection of the observable algebra, CQDB and hidden TRS are equivalent for this class of systems, as time-symmetry of one set of correlation functions implies time-symmetry of the other.

3.14 Complex-P and hidden TRS correspondence theorem

We now consider a general many-body bosonic Lindblad master equation, with, say, n bosonic modes. Recall that classical detailed balance for this class of master equations can be formulated in the complex-P representation as the time-symmetry of the correlation function

$$C^{\mathcal{P}}_{X,Y}(t) \equiv \begin{cases} \overline{X(t)Y(0)} & t \geq 0 \\ \overline{\tilde{Y}(-t)\tilde{X}(0)} & t < 0 \end{cases} \tag{3.146}$$

where, here, $X(\vec{\alpha}, \vec{\beta}), Y(\vec{\alpha}, \vec{\beta})$ are arbitrary multivariate holomorphic functions, and averages are understood to be taken with respect to the stationary complex-P distribution, e.g.

$$\overline{X} \equiv \int_{\Sigma} d^n\alpha d^n\beta \, P_{ss}(\vec{\alpha}, \vec{\beta}) X(\vec{\alpha}, \vec{\beta}), \tag{3.147}$$

where Σ is a $2n$-dimensional closed integration surface (the many-body analogue of the pair of integration contours $\mathcal{C}, \mathcal{C}'$ mentioned earlier). Furthermore, $X(\vec{\alpha}, \vec{\beta}) \to \tilde{X}(\vec{\alpha}, \vec{\beta})$ is a well-defined classical time-reversal operation, that is, induced by a bijection of the phase-space squaring to one (c.f. Eq. (3.91)).

Recall that hidden TRS for a quantum system is defined as the time-symmetry of the thermofield doubled correlation function, which, e.g. for positive times, is given by a symmetric bilinear form:

$$C^{\mathrm{TFD}}_{\hat{X},\hat{Y}}(t) \equiv \langle\langle \hat{X}(t), \hat{Y} \rangle\rangle_{\mathcal{T}}, \tag{3.148}$$

and for negative times (with a time-reversal invariant steady state), is expressible using the same bilinear form:

$$C^{\mathrm{TFD}}_{\hat{X},\hat{Y}}(-t) \equiv \langle\!\langle \hat{X}, \hat{Y}(t) \rangle\!\rangle_{\mathcal{T}}, \tag{3.149}$$

where the relevant bilinear form (which depends on a particular choice of time-reversal operator $\hat{T}$) is defined as follows:

$$\boxed{\langle\!\langle \hat{X}, \hat{Y} \rangle\!\rangle_{\mathcal{T}} \equiv C^{\mathrm{TFD}}_{\hat{X},\hat{Y}}(t \equiv 0)} \tag{3.150}$$

Clearly, the condition of hidden TRS is equivalent to identifying the left-hand side of Eq. (3.148) with the left-hand side of Eq. (3.149), which, upon examining the right-hand sides of said equations, is equivalent to the symmetry of the Heisenberg-picture time-evolution superoperator $\mathcal{E}_t \equiv e^{-t\bar{\mathcal{L}}}$ with respect to the bilinear form $\langle\!\langle \cdot, \cdot \rangle\!\rangle_{\mathcal{T}}$.

One can form an analogous construction to express classical correlations in the complex-P distribution in terms of a bilinear form. Indeed, for any pair of normally-ordered quantum observables $\hat{X}, \hat{Y}$ and a classical time-reversal operation $X \to \tilde{X}$, one can write

$$C^{\mathcal{P}}_{X,\tilde{Y}}(t) = \langle\!\langle \hat{X}(t), \hat{Y} \rangle\!\rangle_{\mathcal{P}}, \tag{3.151}$$

and for negative times (with a stationary complex-P distribution which is time-reversal invariant), we can also write:

$$C^{\mathcal{P}}_{X,\tilde{Y}}(-t) = \langle\!\langle \hat{X}, \hat{Y}(t) \rangle\!\rangle_{\mathcal{P}}, \tag{3.152}$$

Where we have introduced a new symmetric bilinear form

$$\boxed{\langle\langle \hat{X}, \hat{Y} \rangle\rangle_{\mathcal{P}} \equiv C^{\mathcal{P}}_{X,\tilde{Y}}(t \equiv 0)} \tag{3.153}$$

where X, Y are the normally-ordered symbols of $\hat{X}, \hat{Y}$, i.e. the classical representatives of the observables $\hat{X}, \hat{Y}$ in the complex-P representation. Explicitly, if $\hat{X} = \sum_{IJ} c_{IJ} (\hat{a}_1^\dagger)^{i_1} \cdots (\hat{a}_n^\dagger)^{i_n} \hat{a}_1^{j_1} \cdots \hat{a}_n^{j_n}$, then the normally-ordered symbol X is

$$X = \sum_{IJ} c_{IJ} \beta^{i_1} \cdots \beta^{i_n} \alpha_1^{j_1} \cdots \alpha_n^{j_n}, \quad \text{etc..} \tag{3.154}$$

where $I \equiv \{i_1, \cdots, i_n\}$ and $J \equiv \{j_1, \cdots, j_n\}$ are multi-indices. The condition of classical detailed balance in the complex-P representation, i.e. the time-symmetry of Eq. (3.146), is equivalent to identifying the left-hand side of Eq. (3.151) with the left-hand side of Eq. (3.152), which is equivalent to the symmetry of the Heisenberg-picture time-evolution superoperator $\mathcal{E}_t \equiv e^{-t\bar{\mathcal{L}}}$ with respect to the bilinear form $\langle\langle \cdot, \cdot \rangle\rangle_{\mathcal{P}}$.

With these definitions in hand, we return to the general problem of interest: a Markovian multi-mode bosonic system where each mode is subject to loss. For simplicity, we start by assuming each mode has the same loss rate, implying a master equation of the form

$$\frac{d}{dt}\hat{\rho} = -i[\hat{H}, \hat{\rho}] + \sum_{j=1}^{N} \kappa \mathcal{D}[\hat{a}_j]. \tag{3.155}$$

If this system has hidden TRS with respect to a particular quantum time-reversal operation $\hat{T}$, then as discussed earlier (c.f. Eq. (3.43)) there must exist a $N \times N$ unitary matrix U such that:

$$\mathcal{J}[\hat{a}_j] = \sum_{kj} U_{kj} \hat{a}_k, \quad U^2 \equiv 1. \tag{3.156}$$

Here (as always) $\mathcal{J}$ is the exchange superoperator.

What we will show in this section is a remarkable coincidence between the two families of bilinear forms, under the above jump operator constraint. That is, Eq. (3.156) implies that we can identify both bilinear forms, i.e.

$$\boxed{\langle\!\langle \hat{X}, \hat{Y} \rangle\!\rangle_{\mathcal{P}} \equiv \langle\!\langle \hat{X}, \hat{Y} \rangle\!\rangle_{\mathcal{T}} \quad \forall \hat{X}, \hat{Y}} \tag{3.157}$$

where the classical time-reversal operation on the complex-P side is none other than the change-of-Kraus representation given in Eq. (3.156): $\widetilde{(\vec{\alpha}, \vec{\beta})} \equiv (U\vec{\alpha}, U\vec{\beta})$. In what follows, we first prove this result in the single mode case, then extend to the multi-mode case where each mode has an identical damping rate κ. Finally, we extend the result to the more general case where each mode has a different damping rate κ_j.

Single-mode case

Consider Eq. (3.155) in the single mode limit $N = 1$. If this system has hidden TRS with respect to a particular quantum time-reversal operation $\hat{T}$, then the jump operator constraint reduces to $\mathcal{J}[\hat{a}] = u\hat{a}$, with $u = \pm 1$ a scalar quantity. We show in what follows that this in turn implies the following identity:

$$\langle\!\langle \hat{X}, \hat{Y} \rangle\!\rangle_{\mathcal{P}} \equiv \langle\!\langle \hat{X}, \hat{Y} \rangle\!\rangle_{\mathcal{T}}, \tag{3.158}$$

where the bilinear form on the right-hand side is defined using the classical time-reversal operation $\widetilde{(\alpha, \beta)} = (u\alpha, u\beta)$. To see this, note that both the left- and right-hand sides are bilinear with respect to $\hat{X}, \hat{Y}$, and so it suffices to verify the above identity in a basis of normally-ordered monomials. That is, without loss of generality, we may assume that

$$\hat{X} = (\hat{a}^\dagger)^k \hat{a}^l, \qquad \hat{Y} = (\hat{a}^\dagger)^p \hat{a}^q. \tag{3.159}$$

We begin by computing, e.g.

$$\langle\langle \hat{X}, \hat{Y} \rangle\rangle_{\mathcal{T}} = \langle \psi_T | (\hat{a}^\dagger)^k \hat{a}^l (\hat{b}^\dagger)^p \hat{b}^q | \psi_T \rangle. \tag{3.160}$$

Substituting-in the definition of the exchange superoperator, we get

$$\langle\langle \hat{X}, \hat{Y} \rangle\rangle_{\mathcal{T}} = \langle (\hat{a}^\dagger)^k \hat{a}^l \mathcal{J}[(\hat{a}^\dagger)^p \hat{a}^q] \rangle, \tag{3.161}$$

where, here, $\langle \hat{O} \rangle \equiv \mathrm{Tr}[\hat{\rho}_{\mathrm{ss}} \hat{O}]$ denotes a steady-state expectation value. Now, we utilize the fact that $\mathcal{J}[\hat{O}\hat{O}'] = \mathcal{J}[\hat{O}']\mathcal{J}[\hat{O}]$ for generic $\hat{O}, \hat{O}'$:

$$\langle\langle \hat{X}, \hat{Y} \rangle\rangle_{\mathcal{T}} = \langle (\hat{a}^\dagger)^k \hat{a}^l (u\hat{a})^q \mathcal{J}[(\hat{a}^\dagger)^p] \rangle. \tag{3.162}$$

Finally, by direct computation, we also have that $\mathcal{J}[\hat{O}^\dagger] = \hat{\rho}_{\mathrm{ss}} \mathcal{J}[\hat{O}]^\dagger \hat{\rho}_{\mathrm{ss}}^{-1}$ for generic $\hat{O}$, and so (via the cyclic nature of the trace)

$$\begin{aligned} \langle\langle \hat{X}, \hat{Y} \rangle\rangle_{\mathcal{T}} &= \langle (u\hat{a}^\dagger)^p (\hat{a}^\dagger)^k \hat{a}^l (u\hat{a})^q \rangle \\ &= \int_{\mathcal{C}} d\alpha \int_{\mathcal{C}'} d\beta \, P_{ss}(\alpha, \beta) \tilde{\beta}^p \beta^k \alpha^l \tilde{\alpha}^q \end{aligned} \tag{3.163}$$

Immediately, we recognize here the normally-ordered symbols of $\hat{X}, \hat{Y}$, which are, explicitly:

$$\tilde{Y}(\alpha, \beta) = \tilde{\beta}^p \tilde{\alpha}^q, \quad X(\alpha, \beta) = \beta^k \alpha^l. \tag{3.164}$$

With the above observation, we have thus proved Eq. (3.158), which establishes the equivalence of *generalized* quantum detailed balance, that is, hidden TRS, with classical detailed balance in the complex-P representation. Note that the potential conditions, as well as the original CQA method, as originally formulated in Stannigel et al. [2012b], both correspond in this context to the special case of a trivial TRS, i.e. $U = 1$.

Many-body case

Now, consider the multi-mode master equation Eq. (3.155). If this system has hidden TRS with respect to a particular quantum time-reversal operation $\hat{T}$, then we have the constraint Eq. (3.156) on the jump operators, which we write as

$$\mathcal{J}[\hat{a}_j] = \hat{\alpha}_j, \quad \hat{\alpha}_j \equiv \sum_{jk} U_{jk}\hat{a}_k \tag{3.165}$$

What we will demonstrate in this section is that this jump operator constraint implies the following identity:

$$\langle\langle \hat{X}, \hat{Y} \rangle\rangle_{\mathcal{P}} \equiv \langle\langle \hat{X}, \hat{Y} \rangle\rangle_{\mathcal{T}}, \tag{3.166}$$

where the bilinear form on the right-hand side is defined using the classical time-reversal operation $\widetilde{(\vec{\alpha}, \vec{\beta})} = (U\vec{\alpha}, U\vec{\beta})$. To see this, note that both the left- and right-hand sides are bilinear with respect to $\hat{X}, \hat{Y}$, and so it suffices to verify the above identity in a basis of normally-ordered monomials. That is, without loss of generality, we may assume that

$$\hat{X} = (\hat{a}_1^\dagger)^{k_1} \cdots (\hat{a}_n^\dagger)^{k_n} \hat{a}_1^{l_1} \cdots \hat{a}_n^{l_n}, \tag{3.167}$$

$$\hat{Y} = (\hat{a}_1^\dagger)^{p_1} \cdots (\hat{a}_n^\dagger)^{p_n} \hat{a}_1^{q_1} \cdots \hat{a}_n^{q_n}. \tag{3.168}$$

We begin by computing, e.g.

$$\langle\langle \hat{X}, \hat{Y} \rangle\rangle_{\mathcal{T}} = \langle \psi_T | (\hat{a}_1^\dagger)^{k_1} \cdots (\hat{a}_n^\dagger)^{k_n} \hat{a}_1^{l_1} \cdots \hat{a}_n^{l_n} \tag{3.169}$$

$$\cdot (\hat{b}_1^\dagger)^{p_1} \cdots (\hat{b}_n^\dagger)^{p_n} \hat{b}_1^{q_1} \cdots \hat{b}_n^{q_n} | \psi_T \rangle. \tag{3.170}$$

Substituting-in the definition of the exchange superoperator, we get

$$\langle\langle \hat{X}, \hat{Y} \rangle\rangle_{\mathcal{T}} = \langle (\hat{a}_1^\dagger)^{k_1} \cdots (\hat{a}_n^\dagger)^{k_n} \tag{3.171}$$

$$\cdot \mathcal{J}[(\hat{a}_1^\dagger)^{p_1} \cdots (\hat{a}_n^\dagger)^{p_n} \hat{a}_1^{q_1} \cdots \hat{a}_n^{q_n}] \rangle, \tag{3.172}$$

where, here, $\langle \hat{O} \rangle \equiv \mathrm{Tr}[\hat{\rho}_{\mathrm{ss}} \hat{O}]$ denotes a steady-state expectation value. Again, we now utilize the fact that $\mathcal{J}[\hat{O}\hat{O}'] = \mathcal{J}[\hat{O}']\mathcal{J}[\hat{O}]$ for generic $\hat{O}, \hat{O}'$:

$$\langle\langle \hat{X}, \hat{Y} \rangle\rangle_{\mathcal{T}} = \langle (\hat{a}_1^\dagger)^{k_1} \cdots (\hat{a}_n^\dagger)^{k_n} \tag{3.173}$$

$$\cdot \hat{\alpha}_1^{q_1} \cdots \hat{\alpha}_n^{q_n} \mathcal{J}[(\hat{a}_1^\dagger)^{p_1} \cdots (\hat{a}_n^\dagger)^{p_n}] \rangle. \tag{3.174}$$

Finally, by direct computation, we also have that $\mathcal{J}[\hat{O}^\dagger] = \hat{\rho}_{\mathrm{ss}} \mathcal{J}[\hat{O}]^\dagger \hat{\rho}_{\mathrm{ss}}^{-1}$ for generic $\hat{O}$, and so

$$\langle\langle \hat{X}, \hat{Y} \rangle\rangle_{\mathcal{T}} = \langle (\hat{\alpha}_1^\dagger)^{p_1} \cdots (\hat{\alpha}_n^\dagger)^{p_n} \tag{3.175}$$

$$\cdot (\hat{a}_1^\dagger)^{k_1} \cdots (\hat{a}_n^\dagger)^{k_n} \hat{a}_1^{l_1} \cdots \hat{a}_n^{l_n} \hat{\alpha}_1^{q_1} \cdots \hat{\alpha}_n^{q_n} \rangle$$

$$= \int_\Sigma d^n\alpha d^n\beta \, P_{ss}(\vec{\alpha}, \vec{\beta}) \tilde{\beta}_1^{p_1} \cdots \tilde{\beta}_n^{p_n}$$

$$\cdot \beta_1^{k_1} \cdots \beta_n^{k_n} \alpha_1^{l_1} \cdots \alpha_n^{l_n} \tilde{\alpha}_1^{q_1} \cdots \tilde{\alpha}_n^{q_n} \tag{3.176}$$

Immediately, we recognize here the normally-ordered symbols of $\hat{X}, \hat{Y}$, which are, explicitly:

$$\widetilde{Y}(\vec{\alpha}, \vec{\beta}) = \tilde{\beta}_1^{p_1} \cdots \tilde{\beta}_n^{p_n} \tilde{\alpha}_1^{q_1} \cdots \tilde{\alpha}_n^{q_n} \tag{3.177}$$

$$X(\alpha, \beta) = \beta_1^{k_1} \cdots \beta_n^{k_n} \alpha_1^{l_1} \cdots \alpha_n^{l_n}. \tag{3.178}$$

With the above observation, we have thus proved Eq. (3.166), which establishes the equivalence of *generalized* quantum detailed balance, that is, hidden TRS, with classical detailed balance in the complex-P representation.

Finally, consider the general case where each mode has a different damping rate κ_j. In this case, the corresponding classical TRS is modified to be

$$U_{ij} \to \sqrt{\frac{\kappa_i}{\kappa_j}} U_{ij}, \tag{3.179}$$

which can be proven by trivially repeating the steps above.

3.15 Doubled system correlation function symmetry for TRS

$$\psi = \pi$$

Earlier we showed that the TFD correlation function $C_{yz}^{\mathrm{TFD}}(t)$ is time symmetric for the TRS $\psi = \pi$. We must still explicitly verify that the other two correlation functions, $C_{xy}^{\mathrm{TFD}}(t)$ and $C_{xz}^{\mathrm{TFD}}(t)$, are time symmetric for the same TRS.

The expansion of the TFD correlation functions as in Eq. (3.19) is practically useful for computing correlation functions if the time-dependent operators are easily found because it reduces the problem to computing matrix elements. For the qubit system, the time-dependent operators are readily written in terms of the Liouvillian eigenmodes as

$$\hat{\sigma}_k(t) \equiv \sum_n e^{\lambda_n t} \mathrm{Tr}(\hat{\sigma}_k \hat{r}_n) \hat{l}_n^\dagger. \tag{3.180}$$

This definition ensures that the operators reproduce the correct time averages and single system correlation functions under the hypotheses of the quantum regression theorem. We

can then immediately write the time evolved operators as

$$\hat{\sigma}_x(t) = e^{-\kappa t/2}\hat{\sigma}_x \tag{3.181}$$

$$\hat{\sigma}_y(t) = \langle\hat{\sigma}_y\rangle + \sum_{n=2}^{3} e^{\lambda_n t}\mathrm{Tr}(\hat{\sigma}_y\hat{r}_n)\hat{l}_n^\dagger \tag{3.182}$$

$$\hat{\sigma}_z(t) = \langle\hat{\sigma}_z\rangle + \sum_{n=2}^{3} e^{\lambda_n t}\mathrm{Tr}(\hat{\sigma}_z\hat{r}_n)\hat{l}_n^\dagger \tag{3.183}$$

With these in hand we proceed to compute the matrix elements.

We label the pointer states of the steady state by $|\pm\rangle$ satisfying $\hat{\rho}_{\mathrm{ss}}|\pm\rangle = p_\pm|\pm\rangle$ for eigenvalues $p_\pm = \frac{1}{2}(1 \pm \sqrt{4b^2+1}/\sqrt{2b^2+1})$. The eigenstates lie in the YZ plane of the Bloch sphere, namely

$$|+\rangle = \cos\theta|g\rangle - i\sin\theta|e\rangle \tag{3.184}$$

for some angle θ whose precise value as a function of b does not concern us (except that $0 < \theta < \pi/2$ so that these do not reduce to pure $\hat{\sigma}_y$ or $\hat{\sigma}_z$ eigenstates). The matrix elements of $\hat{\sigma}_x = \hat{\sigma}_x(0)$ and $\hat{\sigma}_x(t)$ follow immediately as

$$\langle\pm|\hat{\sigma}_x(t)|\pm\rangle = 0 \tag{3.185}$$

$$\langle-|\hat{\sigma}_x(t)|+\rangle = \langle+|\hat{\sigma}_x(t)|-\rangle^* = ie^{-\kappa t/2} \tag{3.186}$$

and the matrix elements in the time-reversed pointer state basis are easily found for the TRS $\psi = \pi$ (c.f. Eq. (3.31)):

$$\langle\tilde{\pm}|\hat{\sigma}_x|\tilde{\pm}\rangle = 0 \tag{3.187}$$

$$\langle\tilde{-}|\hat{\sigma}_x|\tilde{+}\rangle = \langle\tilde{+}|\hat{\sigma}_x|\tilde{-}\rangle^* = -i. \tag{3.188}$$

We thus arrive at an interesting result already: the doubled system classically correlated

state has identically zero correlation functions $C^{\mathrm{cl}}_{xy}(t) = 0 = C^{\mathrm{cl}}_{xz}(t)$. We therefore need to compute only the off-diagonal elements of $\hat{\sigma}_y(t)$ and $\hat{\sigma}_z(t)$. Given the TRS $\psi = \pi$ and the form of the pointer states, it is straightforward to compute these in the time-reversed pointer state basis. The relevant result is that they are real and thus

$$\langle \tilde{-}|\hat{\sigma}_y|\tilde{+}\rangle = \langle \tilde{+}|\hat{\sigma}_y|\tilde{-}\rangle, \tag{3.189}$$

$$\langle \tilde{-}|\hat{\sigma}_z|\tilde{+}\rangle = \langle \tilde{+}|\hat{\sigma}_z|\tilde{-}\rangle, \tag{3.190}$$

as required by their hermiticity. To see why this must be true without explicitly computing the matrix elements, note that in the time-reversed pointer state basis, $\hat{\sigma}_x(t)$ is off-diagonal and imaginary and thus plays the role of an effective "$\hat{\sigma}_y$" in this basis. Therefore $\hat{\sigma}_y$ and $\hat{\sigma}_z$ must be linear combinations of the effective "$\hat{\sigma}_x$" and "$\hat{\sigma}_z$" and hence their off-diagonal matrix elements must be real and equal.

Furthermore, we can draw the same conclusion about the matrix elements of the time-dependent $\hat{\sigma}_y(t)$ and $\hat{\sigma}_z(t)$:

$$\langle -|\hat{\sigma}_y(t)|+\rangle = \langle +|\hat{\sigma}_y(t)|-\rangle, \tag{3.191}$$

$$\langle -|\hat{\sigma}_z(t)|+\rangle = \langle +|\hat{\sigma}_z(t)|-\rangle. \tag{3.192}$$

Again $\hat{\sigma}_x$ is off-diagonal and imaginary and because $\hat{l}_2$ and $\hat{l}_3$ have only $\hat{\sigma}_y$ and $\hat{\sigma}_y$ components, the time-dependent operators must remain as linear combinations of the effective "$\hat{\sigma}_x$" and "$\hat{\sigma}_z$" which have real and equal off-diagonal matrix elements.

Finally putting everything together, the TFD correlation functions are

$$C_{xy}^{\mathrm{TFD}}(t) = ie^{-\kappa t/2}\begin{cases}\left[\langle\tilde{-}|\hat{\sigma}_y|\tilde{+}\rangle - \langle\tilde{+}|\hat{\sigma}_y|\tilde{-}\rangle\right] & t \geq 0\\ \left[\langle +|\hat{\sigma}_y(t)|-\rangle - \langle -|\hat{\sigma}_y(t)|+\rangle\right] & t < 0\end{cases}$$
$$= 0 \tag{3.193}$$

and

$$C_{xz}^{\mathrm{TFD}}(t) = ie^{-\kappa t/2}\begin{cases}\left[\langle\tilde{-}|\hat{\sigma}_z|\tilde{+}\rangle - \langle\tilde{+}|\hat{\sigma}_z|\tilde{-}\rangle\right] & t \geq 0\\ \left[\langle +|\hat{\sigma}_z(t)|-\rangle - \langle -|\hat{\sigma}_z(t)|+\rangle\right] & t < 0\end{cases}$$
$$= 0 \tag{3.194}$$

which are obviously time symmetric. Therefore all TFD correlation functions of the Rabi-driven qubit are indeed time symmetric for the TRS $\psi = \pi$, Eq. (3.31).

3.16 Mapping to a cascaded quantum system

In this section, we show that the dual Liouvillian $\overline{\mathcal{L}}^*$, as defined and discussed earlier, can be reinterpreted as a "perfect absorber" of the output radiation of $\overline{\mathcal{L}}$ Stannigel et al. [2012b]. We start with the following identity (which is just a rewriting of the definition of $\mathcal{J}$):

$$\hat{H}_{\mathrm{eff},A}\,|\psi_T\rangle = \mathcal{J}[\hat{H}_{\mathrm{eff}}]_B\,|\psi_T\rangle \tag{3.195}$$
$$\hat{c}_{l,A}\,|\psi_T\rangle = \mathcal{J}[\hat{c}_l]_B\,|\psi_T\rangle \tag{3.196}$$

where $\hat{H}_{\mathrm{eff}}$ is the effective Hamiltonian in our master equation, and $\hat{c}_l$ are the jump operators. We denote the Hermitian (anti-Hermitian) parts of an operator $\hat{A}$ as $\mathrm{Re}\left[\hat{A}\right]$ ($i\mathrm{Im}\left[\hat{A}\right]$). One

can then tautologically rewrite Eq. (3.195) as

$$\Bigg[\hat{H}_A - \mathrm{Re}[\mathcal{J}[\hat{H}_{\mathrm{eff}}]]_B \\ - \left(\frac{i}{2}\sum_{l=1}^{M}\hat{c}_{l,A}^{\dagger}\hat{c}_{l,A} - i\mathrm{Im}[\mathcal{J}[\hat{H}_{\mathrm{eff}}]]_B\right)\Bigg]|\psi_T\rangle = 0. \tag{3.197}$$

A short but nontrivial calculation in Sec. 3.17 then shows that

$$i\mathrm{Im}\left[\mathcal{J}[H_{\mathrm{eff}}]\right] = -\frac{i}{2}\sum_{l=1}^{M}\mathcal{J}[c_l]^{\dagger}\mathcal{J}[c_l], \tag{3.198}$$

so that Eq. (3.197) simplifies to:

$$\Bigg[H_A - \mathrm{Re}[\mathcal{J}[H_{\mathrm{eff}}]]_B \\ - \frac{i}{2}\sum_{l=1}^{M}(c_{l,A}^{\dagger}c_{l,A} - \mathcal{J}[c_l]_B^{\dagger}\mathcal{J}[c_l]_B)\Bigg]|\psi_T\rangle = 0. \tag{3.199}$$

Now, separately note the following algebraic identity (which is independent of Eqs. (3.195-3.196):

$$(c_{l,A}^{\dagger}c_{l,A} - \mathcal{J}[c_l]_B^{\dagger}\mathcal{J}[c_l]_B) \\ = \left(\hat{c}_{l,A} + \mathcal{J}[\hat{c}_l]_B\right)^{\dagger}(\hat{c}_{l,A} - \mathcal{J}[\hat{c}_l]_B) \\ + (\hat{c}_{l,A}^{\dagger}\mathcal{J}[\hat{c}_l]_B - h.c.). \tag{3.200}$$

Using the above equality along with Eq. (3.196) to simplify Eq. (3.199), one obtains:

$$\left[H_A - \mathrm{Re}[\mathcal{J}[H_{\mathrm{eff}}]]_B - \frac{i}{2}\sum_{l=1}^{M}(\hat{c}_{l,A}^{\dagger}\mathcal{J}[\hat{c}_l]_B - h.c.)\right]|\psi_T\rangle = 0,$$

as desired.

3.17 Anti-Hermitian part of the effective Hamiltonian for an electromagnetic absorber

In this Section, we compute the anti-hermitian part of the effective Hamiltonian for the absorber system discussed in Section 3.16:

$$\begin{aligned} i\mathrm{Im}\,\mathcal{J}[\hat{H}_{\mathrm{eff}}] &= \frac{1}{2}(\mathcal{J}[\hat{H}_{\mathrm{eff}}] - \mathcal{J}[\hat{H}_{\mathrm{eff}}]^\dagger) \\ &= \frac{1}{2}(\mathcal{J}[\hat{H}_{\mathrm{eff}}] - \hat{\rho}_{\mathrm{ss}}^{-1}\mathcal{J}[\hat{H}_{\mathrm{eff}}^\dagger]\hat{\rho}_{\mathrm{ss}}) \end{aligned} \tag{3.201}$$

We now apply $\mathcal{J}^2$ to both sides:

$$\begin{aligned} i\mathrm{Im}\,\mathcal{J}[\hat{H}_{\mathrm{eff}}] &= \frac{1}{2}\mathcal{J}[\hat{H}_{\mathrm{eff}} - \hat{\rho}_{\mathrm{ss}}\hat{H}_{\mathrm{eff}}^\dagger\hat{\rho}_{\mathrm{ss}}^{-1}] \\ &= \frac{i}{2}\mathcal{J}[-i(\hat{H}_{\mathrm{eff}}\hat{\rho}_{\mathrm{ss}} - \hat{\rho}_{\mathrm{ss}}\hat{H}_{\mathrm{eff}}^\dagger)\hat{\rho}_{\mathrm{ss}}^{-1}] \end{aligned} \tag{3.202}$$

Now, since $\hat{\rho}_{\mathrm{ss}}$ is a steady state of the Lindbladian $\mathcal{L}$, we have

$$-i(\hat{H}_{\mathrm{eff}}\rho_{ss} - \hat{\rho}_{\mathrm{ss}}H_{\mathrm{eff}}^\dagger) + \sum_l \hat{c}_l\hat{\rho}_{\mathrm{ss}}\hat{c}_l^\dagger \equiv 0. \tag{3.203}$$

Therefore, plugging the above identity into Eq. (3.202), we get

$$\begin{aligned} i\mathrm{Im}\,\mathcal{J}[\hat{H}_{\mathrm{eff}}] &= \frac{i}{2}\mathcal{J}[-\sum_l \hat{c}_l\rho_{ss}\hat{c}_l^\dagger\hat{\rho}_{\mathrm{ss}}^{-1}]. \\ &= -\frac{i}{2}\sum_l \hat{\rho}_{\mathrm{ss}}^{-1}\mathcal{J}[\hat{c}_l^\dagger]\hat{\rho}_{\mathrm{ss}}\mathcal{J}[\hat{c}_l] \\ &= -\frac{i}{2}\sum_l \mathcal{J}[\hat{c}_l]^\dagger\mathcal{J}[\hat{c}_l], \end{aligned} \tag{3.204}$$

which is the expression utilized in Section 3.16.

3.18 The potential conditions: manifestation of trivial TRS in the complex-P representation

The main goal of this Section is to reproduce a well-known result in classical probability theory which is known for Fokker-Planck equations. Specifically, these results apply to Fokker-Planck equations of the form

$$\partial_t P(\vec{x},t) \equiv \partial_\mu [C^\mu(\vec{x}) P(\vec{x},t)] + \partial_\mu \partial_\nu [D^{\mu\nu}(\vec{x}) P(\vec{x},t)], \tag{3.205}$$

where $P(\vec{x},t)$ is the probability distribution of a real-valued random process on $\mathbb{R}^d$, with stationary expectation values of observables $X(\vec{x})$ described in the standard way, e.g.

$$\overline{X} \equiv \int d^d x P_{ss}(\vec{x}) X(\vec{x}). \tag{3.206}$$

The statement about these Fokker-Planck equations that we wish to generalize to the complex-P representation is as follows Pavliotis [2014]: provided that $D^{\mu\nu}(\vec{x})$ is positive definite for all $\vec{x}$, then the potential conditions are equivalent to detailed balance with respect to a trivial time-reversal operation $\tilde{x} \equiv \vec{x}$. By the potential conditions, we mean the statement that the stationary probability current vanishes.

In this Section, we generalize the above result for the pseudo-Fokker-Planck equations encountered in the complex-P representation:

$$\begin{aligned} \partial_t P(\vec{\alpha},\vec{\beta},t) \equiv{}& \partial_\mu [C^\mu(\vec{\alpha},\vec{\beta}) P(\vec{\alpha},\vec{\beta})] \\ &+ \partial_\mu \partial_\nu [D^{\mu\nu}(\vec{\alpha},\vec{\beta}) P(\vec{\alpha},\vec{\beta},t)]. \end{aligned} \tag{3.207}$$

A complex *pseudo*-probability current may then be defined for the complex-P distribution

in the way described in Sec. 3.8:

$$\partial_t P(\vec{\alpha}, \vec{\beta}, t) \equiv \partial_\mu J^\mu(\vec{\alpha}, \vec{\beta}, t) \tag{3.208}$$

However, there are significant departures from standard probability theory: the complex-P distribution is complex-valued, and thus violates the axioms of classical probability. In particular, stationary moments are given by

$$\overline{X} \equiv \int_\Sigma d^n\alpha d^n\beta P_{ss}(\vec{\alpha}, \vec{\beta}, t) X(\vec{\alpha}, \vec{\beta}). \tag{3.209}$$

Here, Σ is a $2n$-dimensional closed integration surface (the many-body analogue of the pair of integration contours $\mathcal{C}, \mathcal{C}'$ mentioned earlier). Furthermore, as the diffusion tensor $D^{\mu\nu}(\vec{\alpha}, \vec{\beta})$ is generically complex, it may fail to be positive-definite.

Despite these differences, in this Section we will nonetheless prove that the standard classical result in Pavliotis [2014] still applies (however, here there will be no assumption on the diffusion tensor $D^{\mu\nu}(\vec{\alpha}, \vec{\beta})$): the potential conditions are equivalent to detailed balance with respect to a trivial time-reversal operation:

$$\widetilde{(\vec{\alpha}, \vec{\beta})} \equiv (\vec{\alpha}, \vec{\beta}). \tag{3.210}$$

This result is critical for bosonic many-body systems with local onsite loss, as, with a non-trivial U parameter, hidden TRS corresponds to a nontrivial classical TRS in the complex-P representation, and thus potentially corresponds to a richer symmetry than that encapsulated by the potential conditions.

We first establish the forward implication: if the stationary pseudoprobability current

Eq. (3.208) vanishes, then a straightforward calculation shows that

$$\mathcal{L}(XP_{\text{ss}}) = P_{\text{ss}}\mathcal{L}^*(X), \tag{3.211}$$

where $\mathcal{L}$ is the Liouvillian for the pseudo Fokker-Planck equation Eq. (3.207), and $\mathcal{L}^*$ is the adjoint Liouvillian, obtained via integration by parts Drummond and Gardiner [1980]. The proof almost exactly follows Pavliotis [2014], except while carrying out the calculation we notice that positive-definiteness of the diffusion tensor $D^{\mu\nu}(\vec{\alpha}, \vec{\beta})$ is not needed in the proof, and thus the assumption of positive-definiteness may be relaxed.

From Eq. (3.211), detailed balance is immediate, as, by integrating by parts on the surface Σ (which is valid, as X, Y are holomorphic), the dual Liouvillian $\mathcal{L}^*$ can then be shown to be symmetric with respect to the bilinear form

$$\langle X, Y\rangle \equiv \int_\Sigma d^n\alpha d^n\beta\, P_{ss} XY. \tag{3.212}$$

From this and the expressions

$$\overline{X(t)Y(0)} = \langle e^{-t\mathcal{L}^*}(X), Y\rangle, \tag{3.213}$$

$$\overline{Y(t)X(0)} = \langle X, e^{-t\mathcal{L}^*}(Y)\rangle, \tag{3.214}$$

we have detailed balance. For the converse direction, the proof follows analogously to the classical case as well: one starts by proving the following (assuming P_{ss} is nonvanishing on Σ):

$$\langle -\mathcal{L}^*(X), Y\rangle = \langle D^{\mu\nu}\partial_\mu X, \partial_\nu Y\rangle + \langle X, P_{ss}^{-1}\partial_\mu Y\, J^\mu_{ss}\rangle \tag{3.215}$$

The above is a generalization of the lemma in Section 4.6 of Pavliotis [2014], to pseudo Fokker-Planck equations, and may be proven by invoking the holomorphicity of X, Y. With

the above, one can compute the asymmetry of the Liouvillian:

$$\begin{aligned}&\langle \mathcal{L}^*(X), Y\rangle - \langle X, \mathcal{L}^*(Y)\rangle \\ &= 2\int_\Sigma d^n\alpha d^n\beta\, Y(\vec{\alpha},\vec{\beta})\partial_\mu X(\vec{\alpha},\vec{\beta}) J^\mu_{ss}(\vec{\alpha},\vec{\beta})\end{aligned} \tag{3.216}$$

Now, if detailed balance holds with respect to a trivial TRS, then the Liouvillian $\mathcal{L}^*$ is symmetric, and thus the right-hand side must vanish for all pairs of holomorphic functions X, Y. The only way that this can happen is if the stationary current vanishes everywhere on the integration surface, i.e.

$$J^\mu_{ss}(\vec{\alpha},\vec{\beta}) \equiv 0 \quad \forall (\vec{\alpha},\vec{\beta}) \in \Sigma. \tag{3.217}$$

However, the above is precisely the statement of the potential conditions.

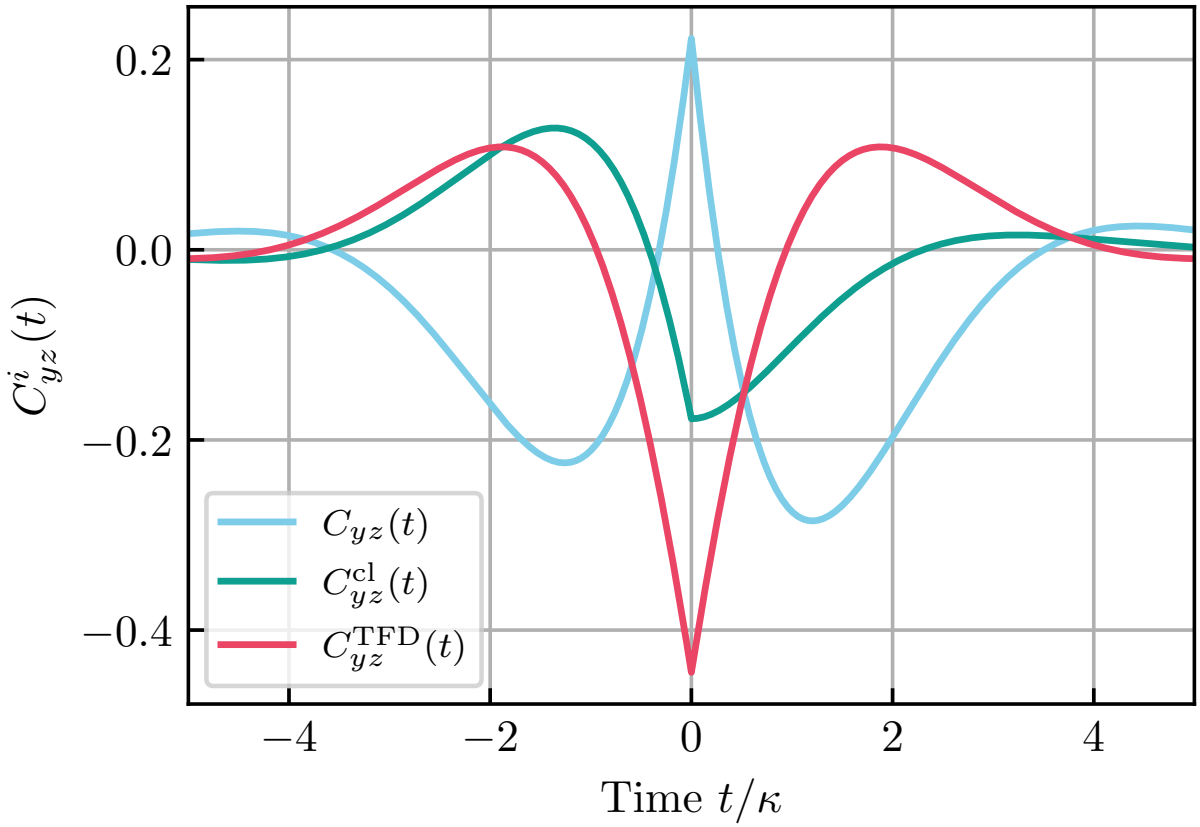

Figure 3.2: Correlation functions and hidden-TRS in a driven qubit. Stationary, connected $\langle\sigma_y(t)\sigma_z(0)\rangle$ correlation functions for the dissipative Rabi-driven qubit system in Eq. (3.30), for a drive Ω equal to the decay rate κ. Blue: the standard single-system correlation function $C_{yz}(t)$ is asymmetric as a function of time, reflecting the fact that this system *does not* satisfy conventional quantum detailed balance. Red: Two-qubit correlator for a system prepared in a TFD state corresponding to the hidden-TRS operator $\hat{T}$ defined in Eq. (3.34). All TFD correlators symmetric in time, reflecting the presence of hidden TRS. Green: "classical" part of the TFD correlator (c.f. Eq. (3.19)), which has no time symmetry. The lack of symmetry shows that the importance of entanglement in the definition of hidden-TRS. Note that the while the correlators $C^{\rm cl}_{yz}(t)$ and $C^{\rm TFD}_{yz}(t)$ are guaranteed to be real by construction, $C_{yz}(t)$; however for our chosen parameters it too is purely real.

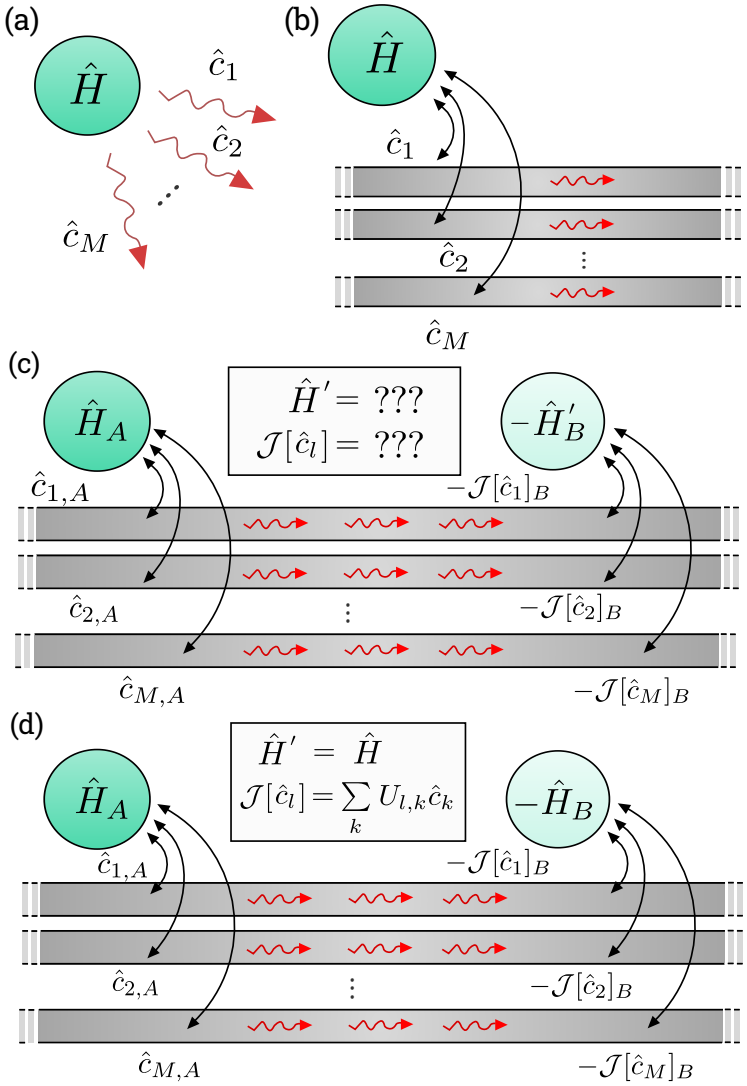

Figure 3.3: Hidden TRS and perfect quantum absorbers. (a) A Markovian quantum system evolves according to a master equation in Lindblad form, with Hamiltonian $\hat{H}$ and jump operators $\hat{c}_l$. (b) A particular realization of the environment as a collection of unidirectional waveguides. (c) The dual Lindbladian $\overline{\mathcal{L}}^*$ always formally solves the "perfect absorber" problem for the Lindbladian $\overline{\mathcal{L}}$ depicted in panel (a): when a system described by $\overline{\mathcal{L}}^*$ placed downstream, it absorbs *all* of the output radiation (red squiggly arrows) emitted by the original A systems. As a result, the two quantum systems A and B relax into a pure entangled state (which has the general form of a thermofield double state). In general, the Hamiltonian $\hat{H}'$ and jump operators $\mathcal{J}[\hat{c}_l]$ of the B system are extremely complex and difficult to find. (d) If the master equation in panel (a) has hidden TRS, then it is extremely easy to construct the Hamiltonian and jump operators of the absorber B system.

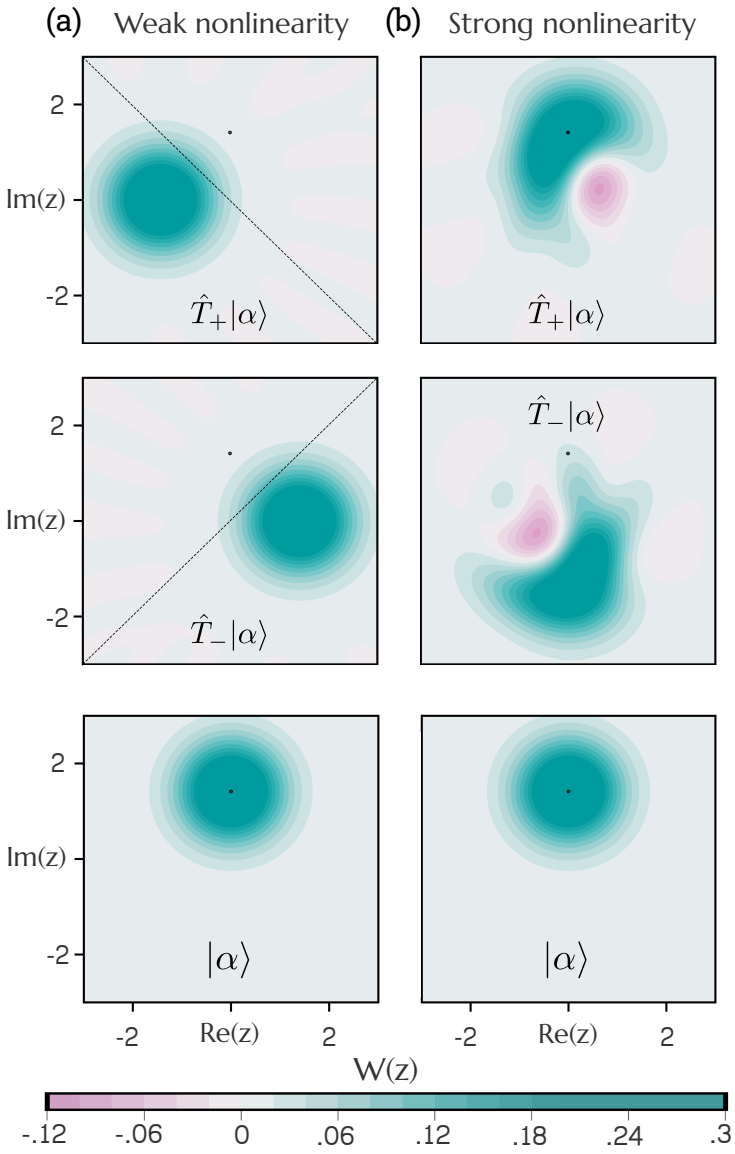

Figure 3.4: Hidden time-reversal symmetry operations in a parametrically-driven Kerr cavity. For vanishing single-photon drive Λ_1, the driven-dissipative cavity model in Eqs. (3.56)-(3.57) has two distinct hidden time-reversal symmetries, corresponding to anti-unitary operators $\hat{T}_\pm$. Here, we plot the Wigner functions of the states $\hat{T}_\sigma |\alpha\rangle$, where $|\alpha\rangle$ is a coherent state (amplitude $\alpha = \sqrt{2}i$, black dots). (a) For weak nonlinearity, $K = 5 \times 10^{-4}\kappa_1$, and two-photon drive $\Lambda_2 = 6.25 \times 10^{-5}\kappa_1$, $\hat{T}_\pm$ are simple phase-space reflections about the axes $\theta = \pm \arg(\Lambda_2/i\kappa)$ (indicated by dashed black lines). (b) For strong nonlinearity, $K = \kappa_1, \Lambda_2 = \kappa/8$, hidden-TRS operations become highly non-Gaussian, as indicated by the presence of significant Wigner negativity in the final states.

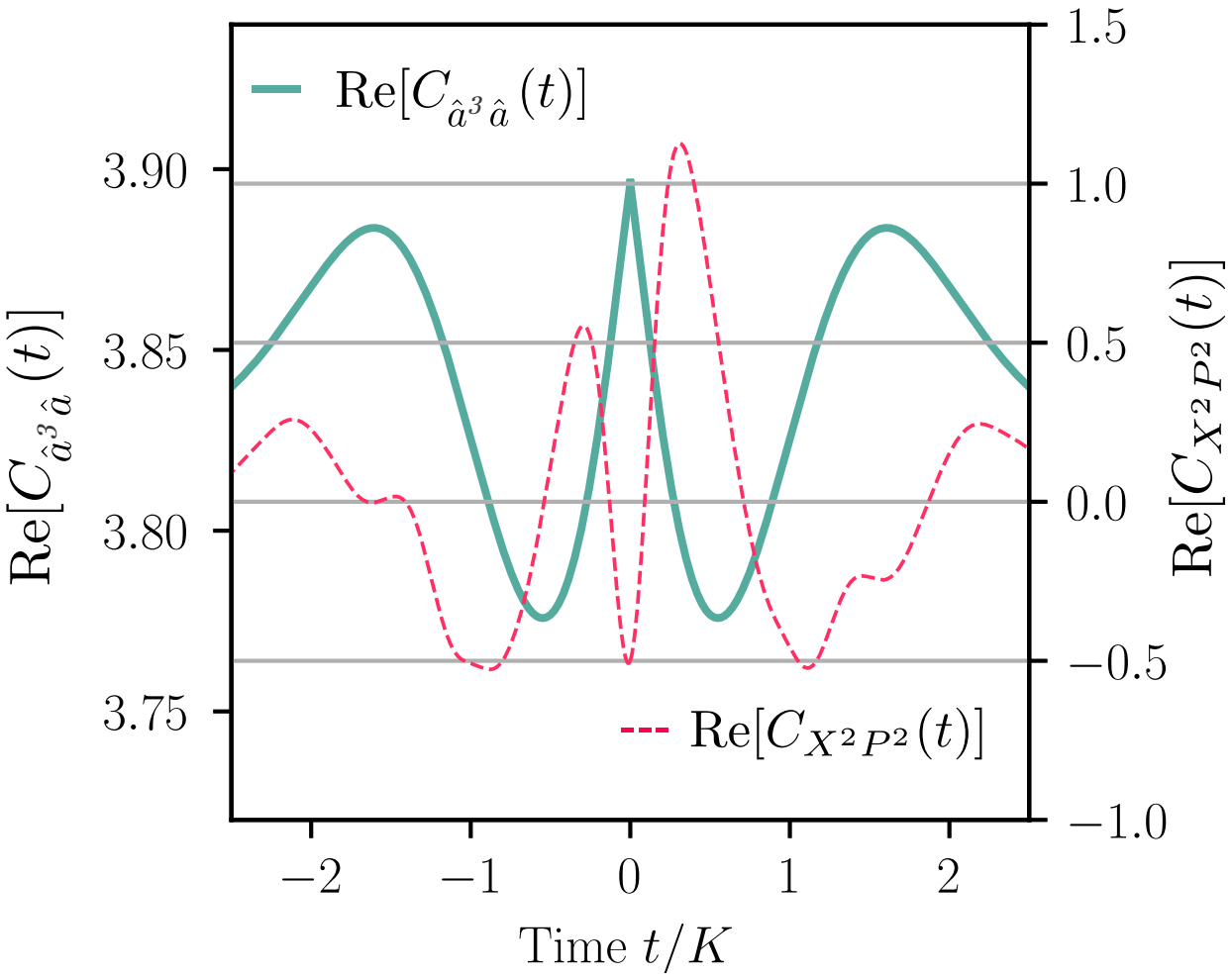

Figure 3.5: Time symmetry of special correlation functions in a driven Kerr resonator. Real part of the connected, steady-state correlation function $C_{a^3,a}(t) \equiv \langle \hat{a}^3(t)\hat{a} \rangle$ (c.f. Eq. (3.63)) for a parametrically driven nonlinear cavity with $\Lambda_2 = K$, $\kappa_1 = 0.4K$ and $\kappa_2 = \Lambda_1 = \Delta = 0$. This correlation function is symmetric in t, something that is guaranteed by the existence of hidden TRS. We also plot another quartic correlation function $C_{X^2P^2}(t)$ (where $\hat{X}$, $\hat{P}$ are canonical quadrature operators). This correlator is clearly asymmetric as a function of time. Hidden-TRS only ensures that a certain restricted class of correlators are time symmetric (in contrast to the more commonly studied CQDB which guarantees all correlators exhibit a form of time-symmetry).

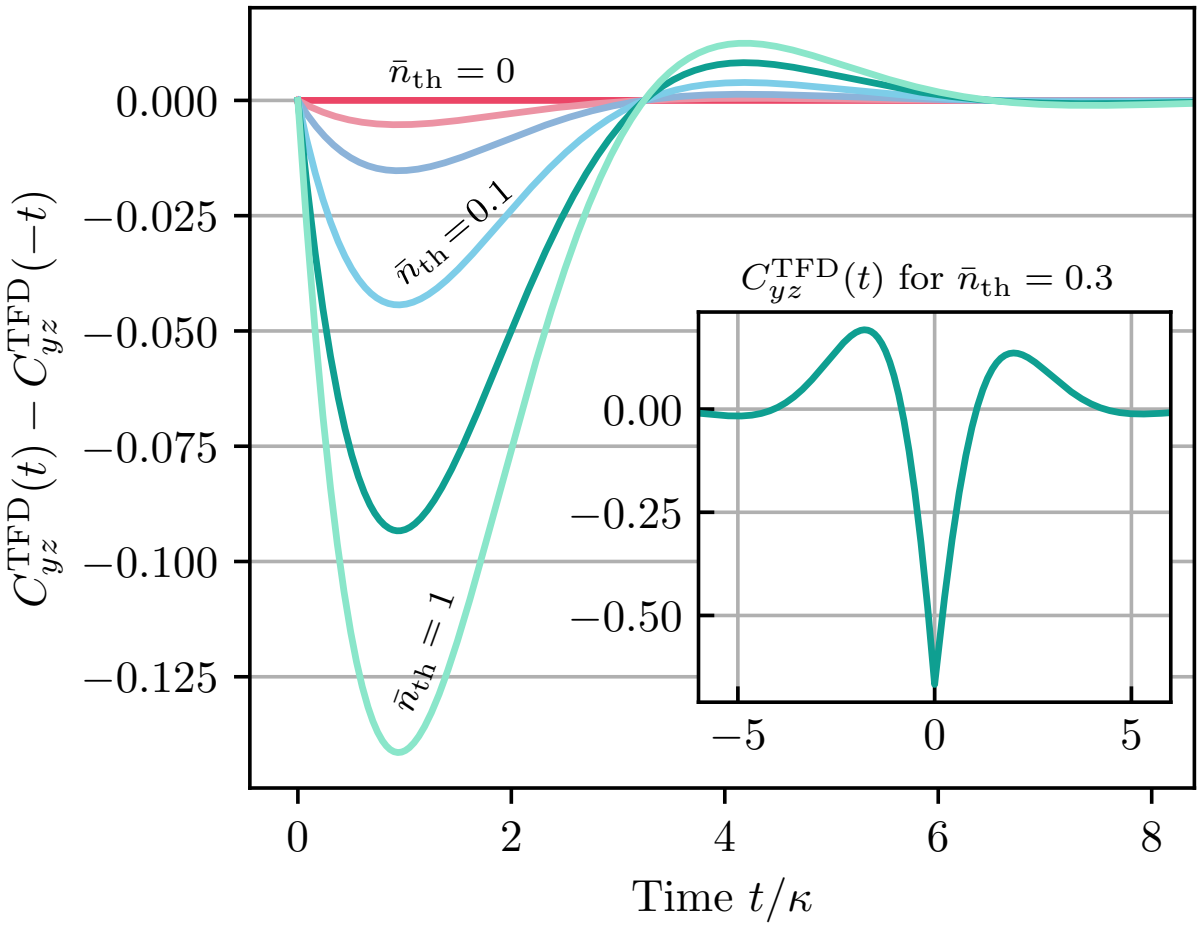

Figure 3.6: Hidden-TRS breaking in a driven qubit. Inset: The doubled-system TFD σ_y-σ_z connected correlation function $C_{yz}^{\rm TFD}(t)$ (c.f. Eq. (3.16)) as a function of time, for a Rabi-driven dissipative qubit for a non-zero temperature corresponding to $\bar{n}_{\rm th} = 0.3$. The TFD state is defined by the hidden-TRS operator $\hat{T}$ (c.f. Eq. (3.34)). Main plot: The time asymmetry of the TFD correlation function $C_{yz}^{\rm th}(t) - C_{yz}^{\rm th}(-t)$ versus time t for various temperatures. The values of $\bar{n}_{\rm th}$ are in order from top to bottom: 0, 0.01, 0.03, 0.1, 0.3, and 1. The $\bar{n}_{\rm th} = 0$ trace is identically zero which reflects the presence hidden TRS at zero temperature. The onset of asymmetry heralds the breaking of hidden-TRS with the introduction of thermal fluctuations. All functions are computed for a resonant Rabi drive with amplitude $\Omega = \kappa(1 + 2\bar{n}_{\rm th})$, where κ is the loss rate.

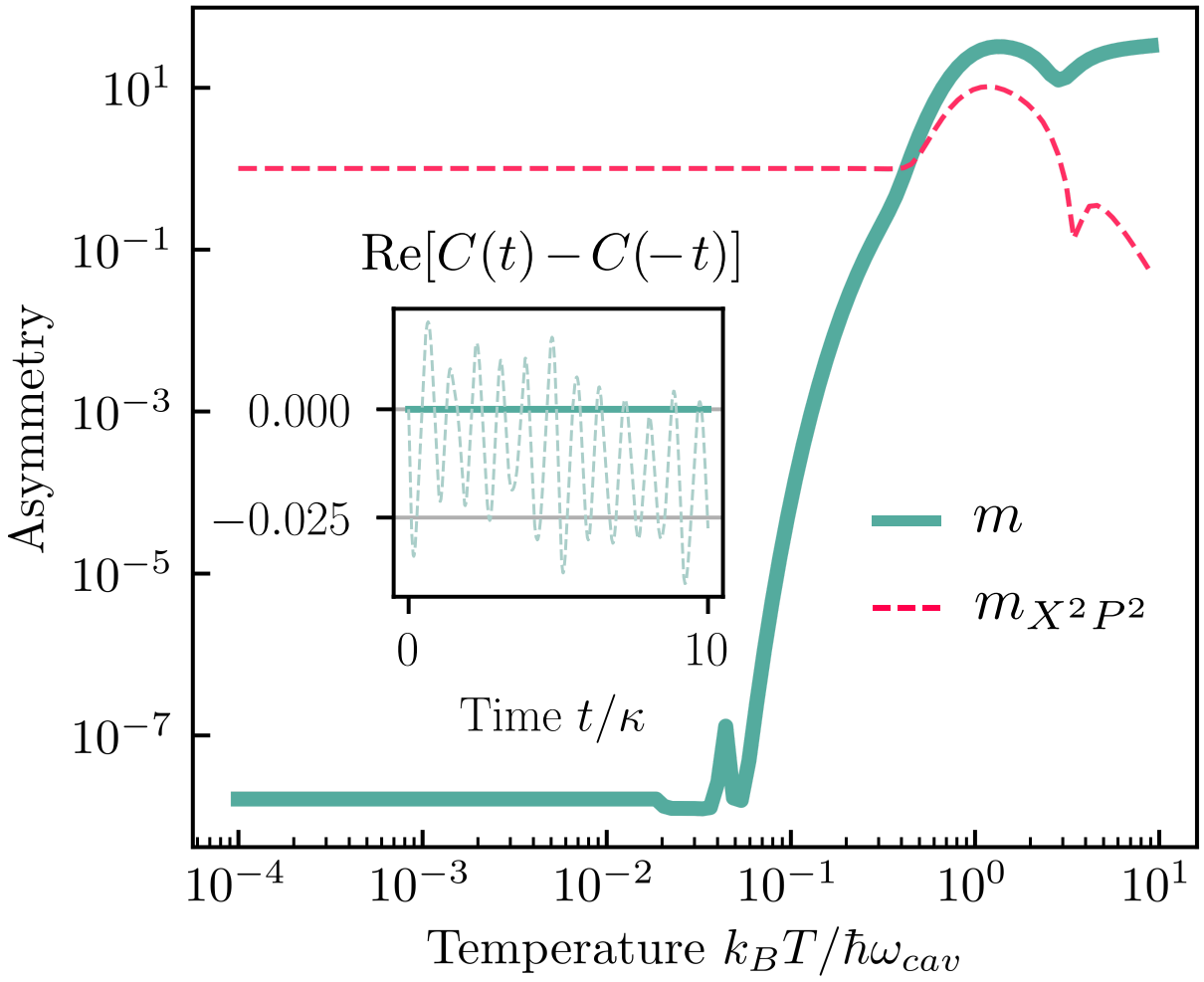

Figure 3.7: Hidden-TRS breaking in a driven nonlinear cavity. Main plot: total correlation function time-asymmetry $m(T)$ vs. temperature for a parametrically-driven Kerr resonator, c.f. Eq. (3.81). Solid green: integrated asymmetry for the special correlation function $C_{a^2,H_{\text{eff}}}(t)$ (c.f. Eq. (3.80)), which is guaranteed to be symmetric if hidden-TRS holds. There is a sudden onset of asymmetry above a threshold temperature, indicating a sharp temperature at which hidden-TRS is broken. In contrast, we also plot the total time asymmetry of a correlation function whose behavior is not constrained by hidden-TRS, function $C_{X^2,P^2}(t)$ (dashed red curve); here $\hat{X}$ and $\hat{P}$ are standard quadrature operators. This correlator is asymmetric already at zero temperature, and shows no strong temperature dependence. Inset: real-part of the correlation function asymmetry of $C(t) \equiv C_{a^2,H_{\text{eff}}}(t)$ for $\bar{n}_{\text{th}} = 0$ (solid green), and $\bar{n}_{\text{th}} = 0.2$ (dashed green). For all plots we take $\Lambda_2 = 3K$, $\kappa_1 = 0.01K$, $\Delta = \Lambda_1 = \kappa_2 = 0$.

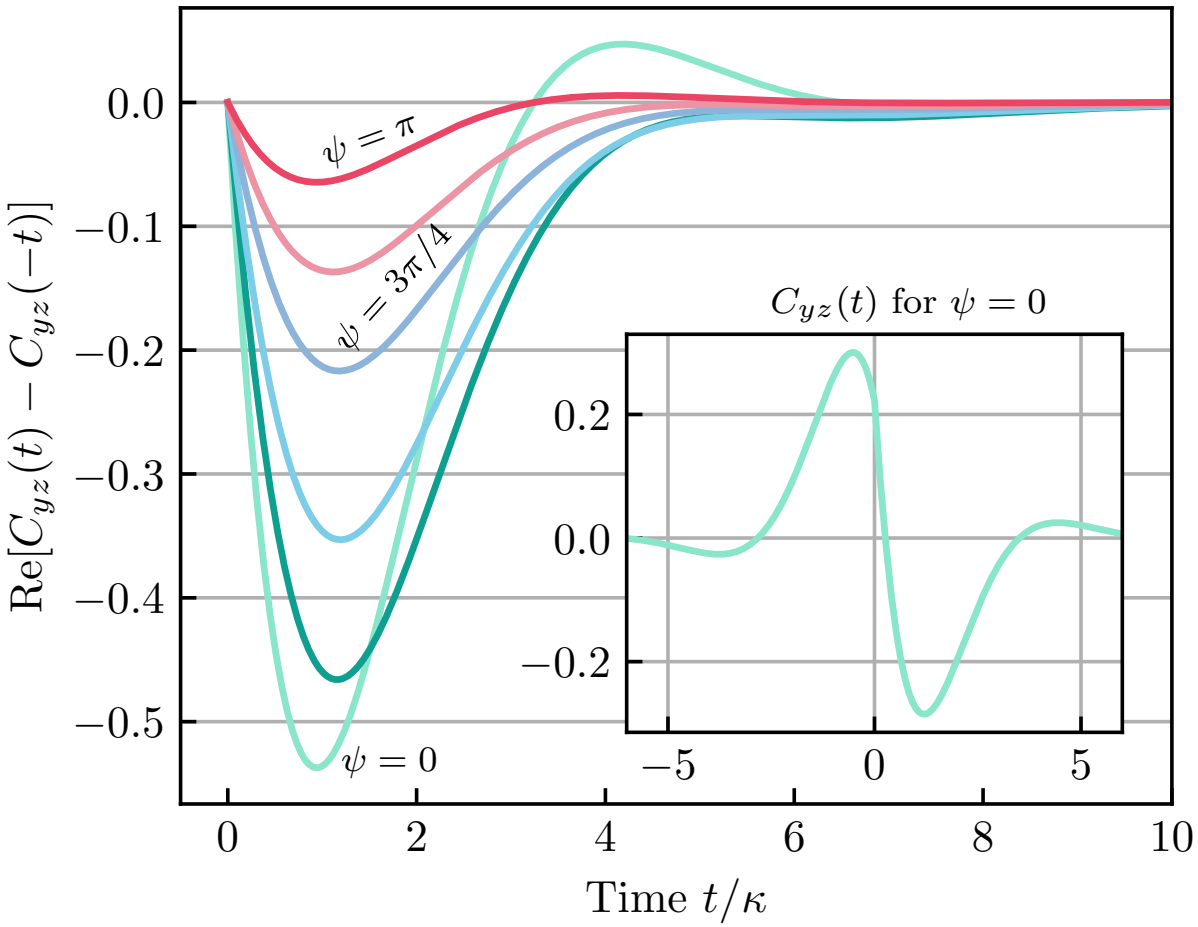

Figure 3.8: The Rabi-driven qubit violates conventional quantum detailed balance. Inset: The correlation function $C_{yz}(t)$ is shown as a function of time for TRS $\psi = 0$. Although time symmetry is not explicitly ruled out for $\psi = 0$, the lack of time symmetry is clear. We show only the connected part which decays to zero for $|t| \gg \kappa$. Main plot: The time asymmetry of the symmetrized correlation function $\mathrm{Re}(C_{yz}(t) - C_{yz}(-t))$ as a function of time t/κ for different permissible TRS. The correlation function is complex in general for $\psi \neq 0, \pi$; however, the time asymmetry is manifest even in the real part alone. The values of ψ in order from top to bottom are: π, $5\pi/6$, $3\pi/4$, $5\pi/8$, $\pi/2$, and 0. All functions are computed for Rabi drive strength $b = 1$.

CHAPTER 4

AN EXACTLY-SOLVABLE MANY-BODY PARAMETRIC OSCILLATOR

4.1 Introduction

Spurred both by applications to quantum information and the advent of controllable dissipative quantum simulators Baumann et al. [2010a], Houck et al. [2012], Fitzpatrick et al. [2017], Fink et al. [2018], Ma et al. [2019] there is a renewed interest in exploring driven-dissipative bosonic quantum systems in the many body limit (see e.g. Diehl et al. [2008], Torre et al. [2013], Sieberer et al. [2013], LeBoite et al. [2013], Hartmann [2016], Biella et al. [2017], Savona [2017], Dykman et al. [2018], Lebreuilly et al. [2019], Rota et al. [2019]). Of particular interest are the possibility of dissipative quantum phase transitions, and the emergence of highly non-thermal steady states. While a variety of numerical approaches have been devised to study such systems, they have limitations. Conventional Gutzwiller mean-field approaches (see e.g. Rokhsar and Kotliar [1991], Krauth et al. [1992a,b], Zwerger [2003]) are unable to account for strong correlations, whereas matrix-product state methods (see e.g. Mascarenhas et al. [2015]) are largely restricted to 1D systems. Alternate numerical approaches for 2D exist Finazzi et al. [2015], Scarlatella et al. [2021a], but these can become numerically infeasible for large systems. Given this, the ability to have exact analytic solutions for higher dimensional models would be extremely valuable.

In this Chapter, we address this outstanding challenge. We introduce a class of strongly-interacting driven-dissipative bosonic models, and show that it is possible to *analytically* describe their dissipative steady states in arbitrary dimensions. The basic system is shown in Fig. 4.1: a set of bosonic modes is subject to arbitrary two-photon driving (both on-site, and between sites), as well as to Markovian single-photon loss and a global Hubbard (Kerr) interaction that depends on total photon number. While there are no conventional hopping

interactions, one still has a lattice structure defined by the intersite two-photon drives. We show that the steady-state density matrix of this model is amenable to exact solution via the hidden time-reversal symmetry method Roberts et al. [2021], Stannigel et al. [2012a]. This method is related to other quantum optical solution methods Drummond and Walls [1980a], Wolinsky and Carmichael [1988b], Kryuchkyan and Kheruntsyan [1996], Kheruntsyan et al. [1997], Kryuchkyan et al. [1999], though attempts to use these in the many-body limit were unsuccessful Cao et al. [2016], Kheruntsyan and Petrosyan [2000].

Our exact solution reveals a wealth of physical phenomena. For weak driving, one sees the emergence of phase transition behaviour as system size is increased, with singularities arising in the thermodynamic limit from the merging of discrete photonic resonances. Unlike well-studied single-site models Minganti et al. [2016a], the phase transition physics here can occur far from the many-photon semiclassical limit, and can show marked deviations from mean-field theory predictions. We also show surprising connections to the representation theory of $SU(1,1)$. Strikingly, we find that with appropriate tuning, the driven-dissipative steady state is directly related to a non-trivial many-body generalization of $SU(1,1)$ pair coherent states Barut and Girardello [1971], Luo [1997], Albert et al. [2019].

We also find surprising behaviour in more strongly-driven regimes: the system can exhibit surprising symmetry breaking phenomena and mode-competition physics, with the exact solution again providing crucial insights. We stress that the class of models we study could be directly realized in e.g. superconducting quantum circuits experiments, and can be viewed as a many-body extension of the driven Kerr parametric oscillator systems that are being studied extensively in the context of bosonic error correction Grimm et al. [2020], Lescanne et al. [2020].

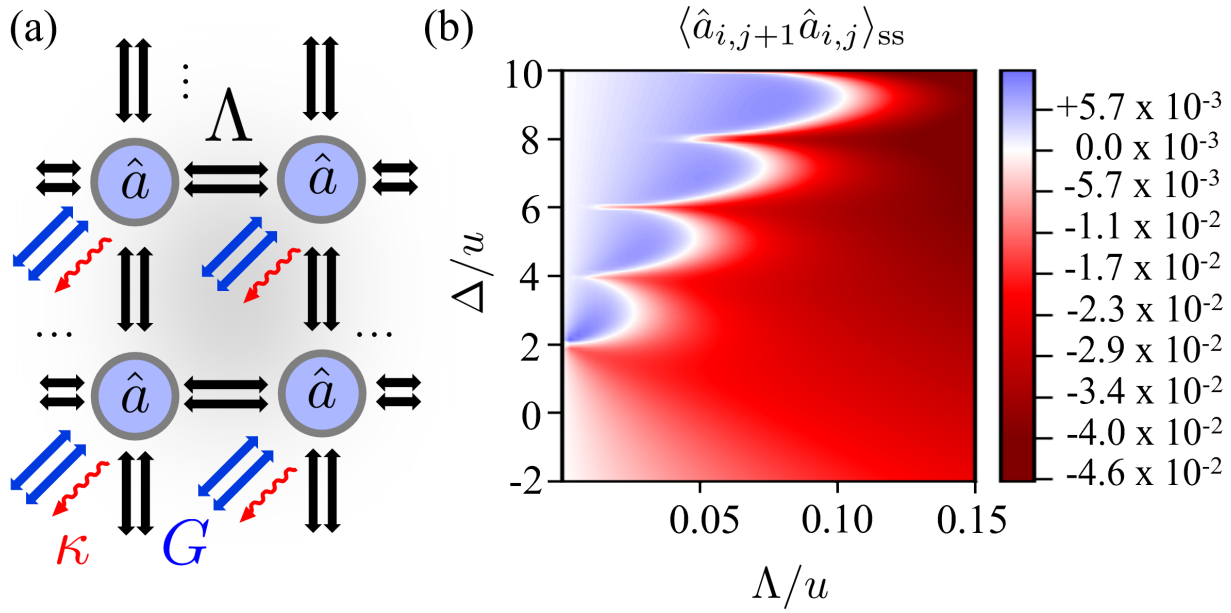

Figure 4.1: (a) Schematic of the model: a lattice of bosonic modes, with two-photon drives on each site (G) and on each nearest-neighbor (nn) bond (Λ). There is also single-photon loss κ on each site, and a global Hubbard (Kerr) interaction U. (b) Our exact solution allows the description of steady-state spatial correlations. Here, nn pairing corelations are plotted as a function of drive detuning Δ and drive amplitude Λ, for a $N = 225$ site 2D lattice with $u \equiv U/N$, $\kappa = 0.01u$. One sees clearly a Mott-lobe like structure associated with multi-photon resonances.

4.2 Two-photon driven global interaction models

We consider a set of N bosonic modes (lowering operators $\hat{a}_j$), subject to arbitrary two-photon (parametric) drives (amplitudes M_{ij}), as well as a global Hubbard interaction (i.e. equal-magnitude self-Kerr and cross-Kerr interactions U/N). Assuming all drives to have an identical detuning Δ from resonance, and working in the common rotating frame, the coherent system dynamics is given by:

$$\hat{H} = \frac{U}{N}\Big(\sum_j \hat{n}_j\Big)^2 - \Delta\sum_j \hat{n}_j + \sum_{i,j}\left(M_{ij}\hat{a}_i^\dagger\hat{a}_j^\dagger + h.c.\right) \tag{4.1}$$

where $\hat{n}_j \equiv \hat{a}_j^\dagger\hat{a}_j$. While our solution technique is more general, we focus here on the case where our modes live on the sites of a D-dimensional hypercubic lattice, and we have translational invariance, with $M_{ii} = G$, and off-diagonals $M_{ij} = \Lambda/2D$ if i, j are nearest neighbour sites, zero otherwise. This represents a modified two-photon driven Bose-Hubbard model, with single-particle hopping replaced with p-wave pairing terms, and the interaction made global. We also include dissipation: independent Markovian single-particle loss on each site. The full dynamics is thus described by the Lindblad master equation

$$\partial_t\hat{\rho} = -i[\hat{H},\hat{\rho}] + \sum_j \kappa\mathcal{D}[\hat{a}_j]\hat{\rho} \equiv \mathcal{L}\hat{\rho}, \tag{4.2}$$

where $\mathcal{D}[\hat{X}]\hat{\rho} \equiv \hat{X}\hat{\rho}\hat{X}^\dagger - (1/2)\{\hat{X}^\dagger\hat{X},\hat{\rho}\}$ denotes the standard dissipative superoperator, constructed from an arbitrary linear operator $\hat{X}$ acting on the Hilbert space of our system. We note that related two-photon driven many-body bosonic models have been recently studied numerically Savona [2017], Lebreuilly et al. [2019], Rota et al. [2019].

Eq. 4.1 exhibits a generic tension common to many driven-dissipative systems. The drives favour populating the system with pairs of photons, creating squeezing correlations. This is opposed by the losses, the energy detuning Δ (which makes pair addition non-resonant), and

most crucially the interaction U (which is like a number-dependent detuning). This yields the possibility of phase transitions, where a high density could self-consistently make the drives resonant. While there is no conventional hopping, the nonlocal pair drives can create spatial correlations (and are like an "Andreev-reflection" hopping process). Note that our model could be realized in a variety of setups including superconducting circuits and more conventional quantum optical platforms. We also note that our solution is even more general than Eq. 4.1. As shown in , for a given set of drive amplitudes M_{ij}, there exist a class of standard hopping terms that can be added to $\hat{H}$ without changing the dissipative steady state. We can thus describe, e.g., bipartite lattices with local hopping and pairing terms.

Our goal in this chapter is to understand the dissipative steady state $\hat{\rho}_{\rm ss}$ of our system, which satisfies $\mathcal{L}\hat{\rho}_{\rm ss} = 0$. Surprisingly, for all parameter values and dimensionalities, this can be done exactly and analytically, using the hidden TRS (hTRS) / coherent quantum absorber approach introduced in Stannigel et al. [2012a], Roberts et al. [2021]. This method postulates the existence of an anti-unitary operator $\hat{T}$, in terms of which the associated purification of $\hat{\rho}_{\rm ss}$ (which lives in a doubled Hilbert space)

$$\hat{\rho}_{\rm ss} \equiv \mathrm{Tr}_R |\Psi_{\hat{T}}\rangle\langle\Psi_{\hat{T}}|, \qquad |\Psi_{\hat{T}}\rangle \equiv \sum_n \sqrt{p_n}|n\rangle_L \hat{T}|n\rangle_R, \tag{4.3}$$

satisfies a generalized symmetry constraint Roberts et al. [2021]. Here $|n\rangle, p_n$ are the eigenvectors and eigenvalues of $\hat{\rho}_{\rm ss}$, L denotes states in the physical Hilbert space, and R denotes states in the auxiliary Hilbert space, which is another copy of the physical Hilbert space. The ansatz that $\hat{T}$ is a hTRS implies a set of conditions on $|\Psi_{\hat{T}}\rangle$ that must be solved. For this system, this can be done analytically .

The resulting solution for the pure state $|\Psi_{\hat{T}}\rangle$ has a striking form. It describes an unusual kind of pair condensate: all particles occupy the same two-body wavefunction whose spatial

structure is determined by the driving amplitudes M_{ij}. We find :

$$|\Psi_{\hat{T}}\rangle = \sum_{m=0}^{\infty} \frac{c_m}{m!} \left(\hat{K}_+\right)^m |\Omega\rangle, \quad \hat{K}_+ := \frac{N}{2U} \sum_{ij} M_{ij} \hat{\alpha}_i^\dagger \hat{\alpha}_j^\dagger, \tag{4.4}$$

where $\hat{K}_+$ is the effective pair creation operator, $\hat{\alpha}_j \equiv (\hat{a}_{j,L} + \hat{a}_{j,R})/\sqrt{2}$, and $|\Omega\rangle \equiv |0\rangle_L |0\rangle_R$ is the vacuum. The coefficients c_m in the expansion take the simple form

$$c_m \propto (-1)^m/(\delta)_m, \tag{4.5}$$

where $(\delta)_m := \delta(\delta+1)\cdots(\delta+m-1)$ denotes the Pochhammer symbol (rising factorial), and where the dimensionless detuning parameter r is

$$\delta := 1 - N\Delta_{\text{eff}}/2U, \;\; \Delta_{\text{eff}} := \Delta + i\kappa/2. \tag{4.6}$$

We stress that when $U \neq 0$, this pure-state pair condensate is highly non-Gaussian and exhibits Wigner-function negativity. The parameter dependence of this state is also remarkable. The global Hubbard interaction U along with the detuning Δ and loss κ determine the effective "fugacity" of our pair gas via the c_m coefficients. In contrast, all spatial structure (encoded in M_{ij}) is encoded completely in the two-body "wavefunction" of each paired boson. Finally, the resulting dissipative steady state is non-thermal, in that it cannot be written as $\exp(-\beta\hat{H})$ for some β .

4.3 Emergence of phase transitions

. The exact solution allows us to study the emergence of dissipative phase transitions as the number of sites N becomes large, i.e. in the thermodynamic limit. This can be done for arbitrary dimensionality D, and while still remaining in low-density regimes where semiclassical approximations would fail. We find a direct connection between first-order phase transitions

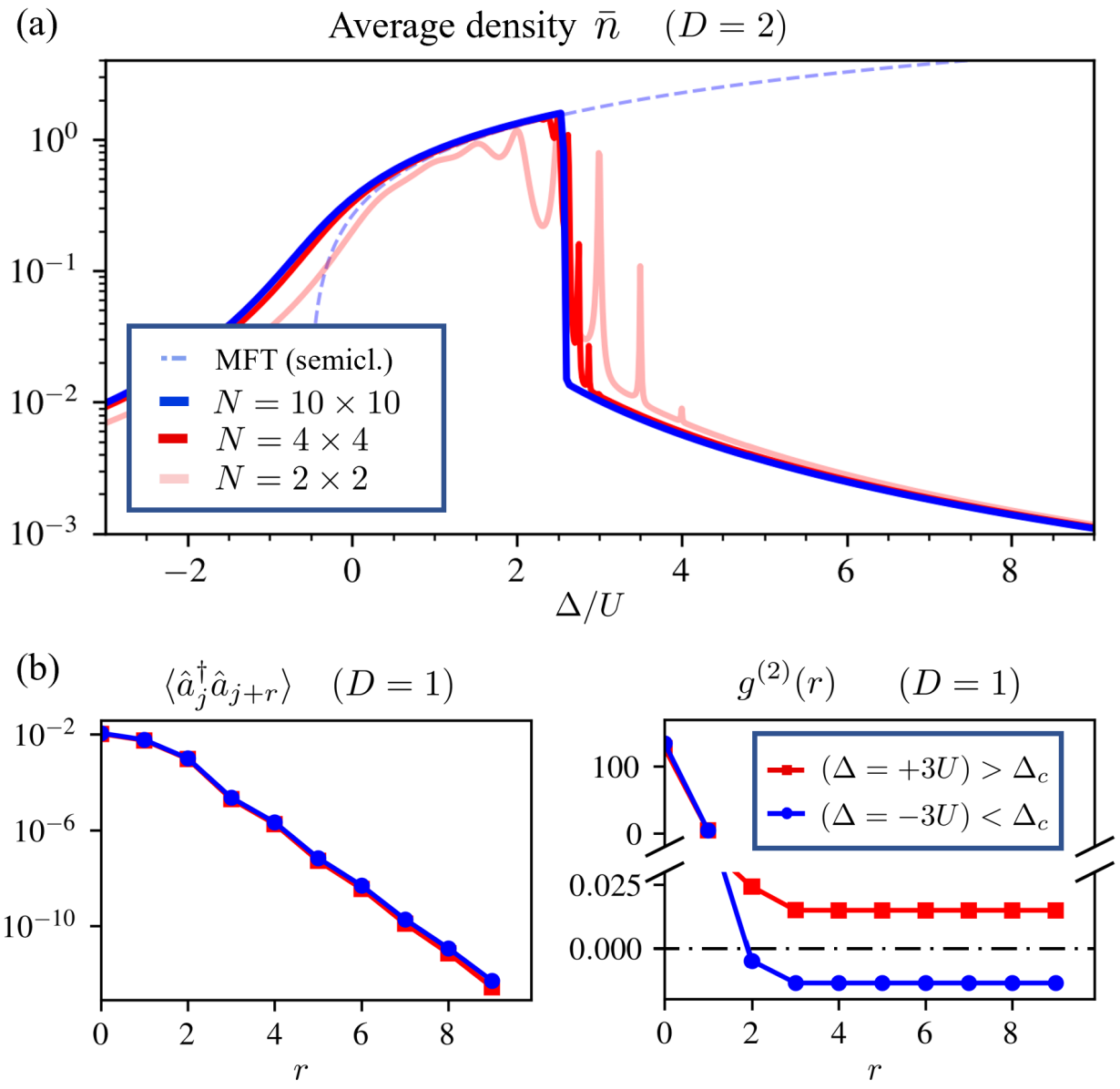

Figure 4.2: Driven-dissipative phase transitions. (a) Average density $\bar{n}$ versus detuning Δ for various sized 2D square lattices (periodic boundary conditions, $\kappa = 0.01U$, $G = U/5, \Lambda = U/4$). As system size increases, discrete resonances merge to yield a jump in the density and a first-order phase transition. We also show the predictions of a basic semiclassical mean-field theory, which predicts a zero-density solution that cannot be shown here due to the log scale on the y-axis. (b) Here, we attempt to distinguish the bunched (red squares) and antibunched (blue circles) phases via their correlations, respectively single-particle (left panel) and density-density (right panel) correlations. We choose $\Delta = +3U$ as representative of the bunched phase and $\Delta = -3U$ as representative of the antibunched phase. Both plots show data for a $N = 100$ site periodic lattice with $D = 1$. All other parameters are the same as in panel (a). All results are computed using the exact solution in Eq. (4.4).

that occur at large N, and discrete multi-photon resonances that can be resolved at smaller N. This is seen clearly in Fig. 4.2(a), which shows the average steady-state photon density versus Δ in a $D = 2$ model, for different system sizes. The discrete resonances at modest N occur when the dimensionless detuning r is close to a negative integer. The exact solution tells us that when $\delta = -n + \epsilon$ with $|\epsilon| \ll 1$, the relative "fugacity" between the $n + 1$ and n pair configurations diverges as $\epsilon \to 0$: $c_{n+1}/c_n = -1/(n + \delta) = O(\epsilon^{-1})$. This divergence (cut-off by κ) leads to an enhanced photon number, and thus sharply-defined resonances occuring at detunings $\Delta_n = 2U(n+1)/N$ (see Fig. 4.2(a)). As $N \to \infty$, the spacing between resonances vanishes, leading to a first-order phase transition where the density exhibits a jump as a function of Δ. Fig. 4.2(a) also shows a comparison against the predictions of a simple semiclassical mean-field theory.

A further virtue of the exact solution is that it gives full access to spatial correlations. We find that these correlations provide a much better way of distinguishing phases compared to purely local observables. In the large-N limit, two-point equal-time correlators in the steady state such as $\langle \hat{a}_{i+r}\hat{a}_i\rangle_{\rm ss}, \langle \hat{a}^\dagger_{i+r}\hat{a}_i\rangle_{\rm ss}$ always decay exponentially with distance (see Fig. 4.2(b)). In stark contrast, the global Hubbard interaction generates long-range (but weak) density-density correlations. To study this quantitatively, we define in $D = 1$ the reduced density-density corelator

$$g^{(2)}(i, r) := \frac{\langle \hat{n}_{i+r}\hat{n}_i\rangle_{\rm ss} - \bar{n}^2}{\bar{n}^2}. \tag{4.7}$$

Here, $\bar{n} \equiv \langle \hat{n}_j\rangle_{\rm ss}$ is the mean onsite occupation in the steady state, and we note that $g^{(2)}(i, r)$ is independent of i away from boundaries. An analogous definition holds for $D > 1$.

We find that the two phases of our model can be cleanly distinguished by the sign of the large-distance density-density correlations, i.e. by $g^{(2)}_\infty \equiv \lim_{|r|\to\infty} g^{(2)}(r)$. We call the phase where $g^{(2)}_\infty > 0$ a "bunched" phase, where density fluctuations are positively-correlated at long distances, and the remaining phase with $g^{(2)}_\infty < 0$ an "antibunched" phase. When κ is

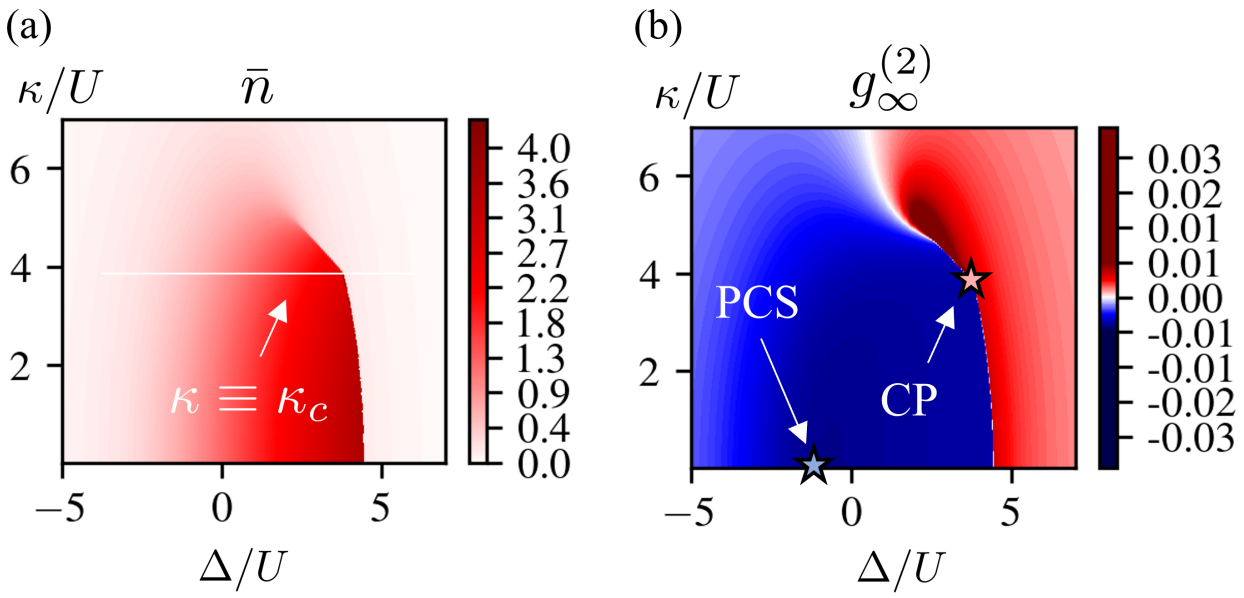

Figure 4.3: Phase diagram for $D = 0$. (a) Average density as a function of detuning Δ and loss κ, with $N = 500$, $\Lambda = 0$, and $G = U$. Phase boundaries can be seen, the critical damping value κ_c is also indicated: for $\kappa > \kappa_c$, the first order PT vanishes. (b) Asymptotic long-distance behavior of the density-density correlation function, as captured by $g_\infty^{(2)}$ (c.f. Eq. (4.7)); the sign of this quantity more clearly distinguishes the two relevant phases in the model. A critical point $\Delta_{\text{eff}}^c := \Delta_c + i\kappa_c/2$ marks the exact location where $g_\infty^{(2)}$ becomes continuous across the phase boundary. Same parameters as in panel (a). The parameter tuning that results in a many-body pair coherent state is indicated with a star.

sufficiently small, these phases are connected by the first-order phase transition mentioned above. The corresponding jump in density is accompanied by a sign change in $g_\infty^{(2)}$, see Fig. 4.2(b), right panel. We also note that for modest values of N, the multiphoton resonance physics described above can also lead to interesting structures resembling Mott lobes LeBoite et al. [2013, 2014], if one looks at intersite correlations. This is shown in Fig. 4.1(b).

4.4 Criticality in the $D = 0$ model

The above physics becomes especially clear in the limit where $\Lambda \equiv 0$, i.e. purely local driving. There is no remaining spatial structure, hence we call this the $D = 0$ limit. As we saw in Fig. 4.2, for $D > 0$, our model has a finite correlation length characterizing the decay of two-point correlators. The $D = 0$ model sets this length to zero, while retaining the more interesting physics associated with density-density correlations. The $D = 0$ limit is also experimentally relevant: it can be realized directly using a relatively simple superconducting circuit .

The $D = 0$ case has another key virtue: it allows a dramatic simplification in the calculation of observables, as now $\hat{K}_+, \hat{K}_+^\dagger$, and $\hat{K}_z \equiv (2NG^2/U)[\hat{K}_+^\dagger, \hat{K}_+]$ form a representation of the Lie algebra of $SU(1,1)$. This makes the problem of evaluating moments with respect to the state $|\Psi_{\hat{T}}\rangle$ given in Eq. (4.4) completely algebraic; one only requires knowledge of the bosonic representation theory of $SU(1,1)$. Further, harmonic analysis in $\mathbb{R}^N$ yields a satisfactory characterization of the requisite representation theory . We are thus able to compute local observables and correlators for systems with tens of thousands of sites and at unit density. For our $D = 0$ model and for large N, we can verify by brute force that $\lim_{\Delta \to \Delta_c^\pm} \mathrm{sign}\{g_\infty^{(2)}\} = \pm 1$, where Δ_c denotes the location of the discontinuity in $\bar{n}$. This confirms that the first-order PT marks the boundary between bunched- and antibunched phases (c.f. Figure 4.2). We also find that this first-order PT only exists when $\kappa < \kappa_c$, where κ_c is a critical damping threshold, akin to a critical pressure in a liquid-gas transition

(c.f. Figure 4.3a). As in a liquid-gas transition, above the critical point the two phases are smoothly connected, as is indicated by the continuity of $g_\infty^{(2)}$ in Figure 4.3b. Here, we use the exact solution to estimate κ_c, by explicitly observing the divergence of the susceptibility $\chi \equiv \partial\bar{n}/\partial\Delta$ as $\kappa \to \kappa_c^+$.

4.5 Many-body pair-coherent states

When $D > 0$, analysis based on the exact solution becomes more challenging. One can still obtain a representation of the Lie algebra $SU(1,1)$ by defining a (generalized) pair-lowering operator $\hat{K}_- := \frac{U}{2N}\sum_{ij}(M^{-1})_{ij}\hat{\alpha}_i\hat{\alpha}_j$, which has the effect of removing a pair of bosons: $\hat{K}_-\hat{K}_+^m|\Omega\rangle \propto \hat{K}_+^{m-1}|\Omega\rangle$. However, $\hat{K}_-$ is not equal or proportional to $\hat{K}_+^\dagger$ unless $D \equiv 0$ or $D \equiv \infty$. The result is that representation-theoretic techniques are of no utility when $D > 0$. Nonetheless, the Lie-theoretic point of view is still useful in helping reveal unusual phenomena.

In particular, at special detuning values, the gas of boson pairs constituting the purification of the steady state (c.f. Eq. (4.4)) forms a many-body pair coherent state (PCS), that is, an eigenstate of the operator $\hat{K}_-$ Barut and Girardello [1971]. From the form of the solution, we see that this happens when $c_{m+1}/c_m = -k/(N/2+m)$, where $k = -1$ is the corresponding eigenvalue of $\hat{K}_-$. From Eq. (4.6), we see that this requires $\delta = N/2$, corresponding to $\kappa \to 0^+$ and

$$\Delta \to \Delta_{PCS} := U(2-N)/N \tag{4.8}$$

Note that for the case of just a single mode $N = 1$, this corresponds to the known physics of a Kerr parametric oscillator Wolinsky and Carmichael [1988b]. In this case, $\Delta = U$ is the same as zero detuning if one normal-orders the Kerr interaction, and $|\Psi_{\hat{T}}\rangle$ reduces to an even-parity cat state.

We stress that there are observable consequences associated with the formation of this many-body PCS. As one approaches the special detuning, there are no fluctuations in the global pairing, as quantified by the operator $\hat{K}_-$. One can explicitly show that:

$$\left\langle \left(\sum_{ij} (M^{-1})_{ij} \hat{a}_i \hat{a}_j \right)^{\dagger n} \left(\sum_{ij} (M^{-1})_{ij} \hat{a}_i \hat{a}_j \right)^{m} \right\rangle_{\text{ss}} \underset{\Delta \to \Delta_{PCS}}{\propto} k^{*n} k^m. \tag{4.9}$$

Similar to their two-mode counterparts Agarwal [1988], Agarwal and Biswas [2005], the many-body PCS we describe here may have utility for bosonic quantum error correction Mirrahimi et al. [2014a], Leghtas et al. [2015a], Puri et al. [2019], Lescanne et al. [2020], Grimm et al. [2020]. We note that the many-body PCS that emerge here are distinct from the multi-mode states discussed in Ref. Albert et al. [2019].

4.6 Symmetry breaking

In the strong-driving regime, our model exhibits a surprising symmetry breaking phenomenon. First, note that the singular values of our matrix of pair-driving amplitudes is

$$\lambda_{\mathbf{k}} = \frac{1}{u} \left| \frac{\Lambda}{D} \sum_{j=1}^{D} \cos k_j + G \right|, \tag{4.10}$$

where the wavevector $\mathbf{k}$ labels standing wave modes. Let λ_* denote the maximum singular value, and s denote the number of distinct modes that it corresponds to (so-called max pairing modes). For large driving, one can analytically show that the steady state Wigner function $W[\{\alpha_{\mathbf{k}}\}]$ corresponds to a uniform distribution over the $(s-1)$-sphere defined by

$$\sum_{\lambda_{\mathbf{k}} = \lambda_*} x_{\mathbf{k}}^2 = \text{const.}, \qquad x_{\mathbf{k}} \equiv e^{-i\theta} \alpha_{\mathbf{k}} \tag{4.11}$$

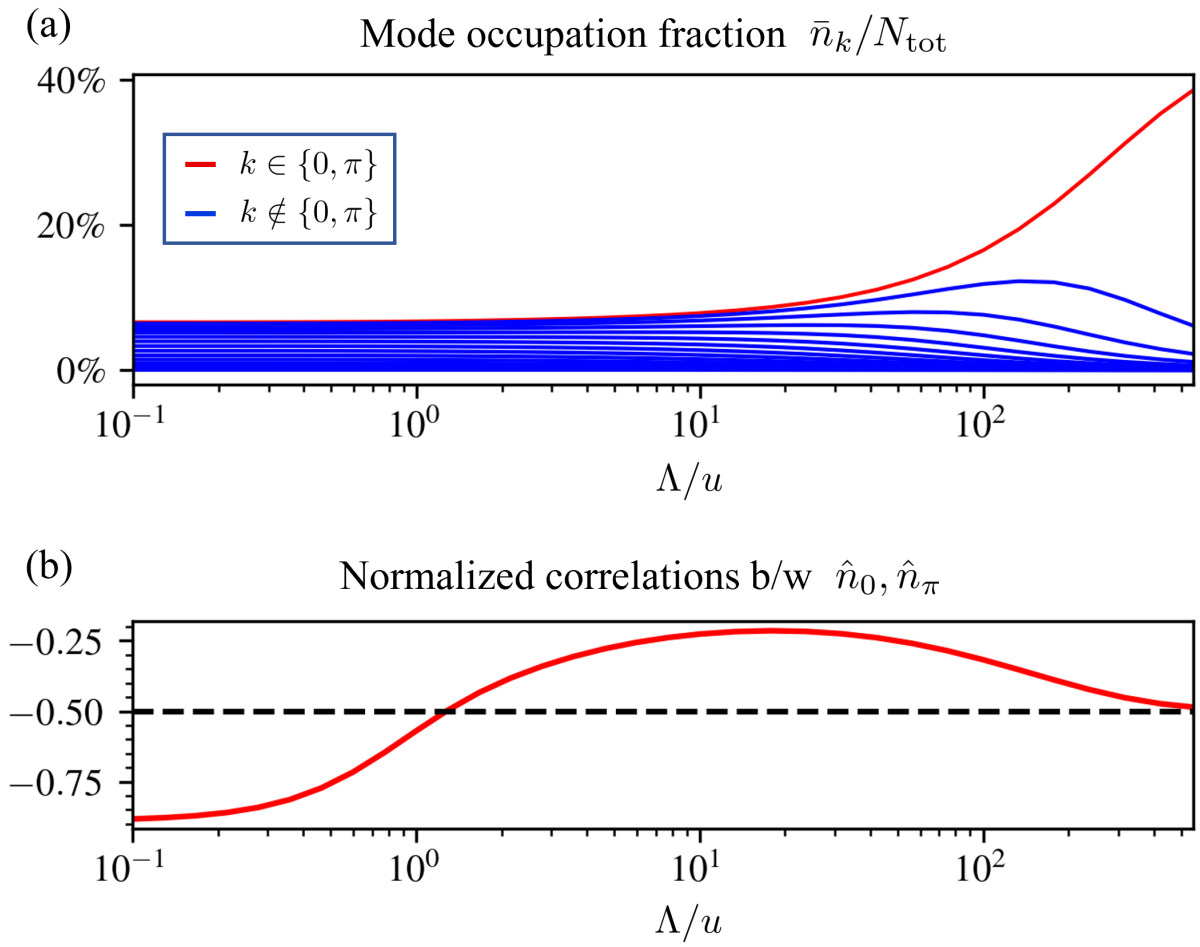

Figure 4.4: Symmetry breaking at strong driving. (a) Occupancy $\bar{n}_k$ of standing wave modes in a odd-length $D = 1$ open chain, as the drive Λ is increased. For large drives, the modes with the largest pairing amplitudes, $k = 0, \pi$, dominate. N_{tot} denotes average total photon number. Parameters are $\Delta = 0, \kappa = u/100$, $u \equiv U/N$, $N = 31$. (b) Normalized density correlations between the modes at $k = 0, \pi$ (red curve), and the horizontal asymptote $y \equiv -1/s$ predicted by a uniform sphere distribution (black dashed line). Here, $s = 2$. Parameters same as in panel (a).

with $x_{\mathbf{k}} \in \mathbb{R}$ and θ an overall phase . Even though there is a near continuum of pairing eigenvalues, for large driving, the max pairing modes completely dominate. This behaviour is shown explicitly in Fig. 4.4(a). The structure of this solution also directly leads to an anti-correlation between mode amplitudes that is purely geometric, see Fig. 4.4(b).

The mode selection in our system can be related to spontaneous symmetry breaking. Real rotations amongst the max-pairing modes form a non-abelian group of weak symmetries isomorphic to $O(s, \mathbb{R})$ which commutes with the Lindbladian $\mathcal{L}$. At high driving strengths we conjecture that this symmetry is spontaneously broken. This is seen clearly at the semiclassical level, where one can show that every point on the max pairing $(s-1)$-sphere is a *stable* stationary state of the dynamics. Each such solution of course breaks the underlying mode-rotation symmetry. In the full quantum theory, fluctuations lead to a slow randomization on this space of symmetry broken solutions, yielding the final unique steady state. The effective mode selection phenomena in our model is reminscient (but not identical) to analogous effects in other systems (see e.g. Narducci et al. [1986], Gong et al. [2007], Stone et al. [2022]). Ref. Wang et al. [2020] also describes (using semiclassical MFT) related phenomena in a many-mode model with uniform pairing, with mode selection being controlled by dispersion as opposed to pairing amplitudes. We stress that in contrast to Wang et al. [2020] our exact solution lets us describe all quantum fluctuation effects, allowing analytical insights into how our mode selection effect emerges as the dimensionless driving rates $G/U, \Lambda/U$ become large, see Fig. 4.4(a).

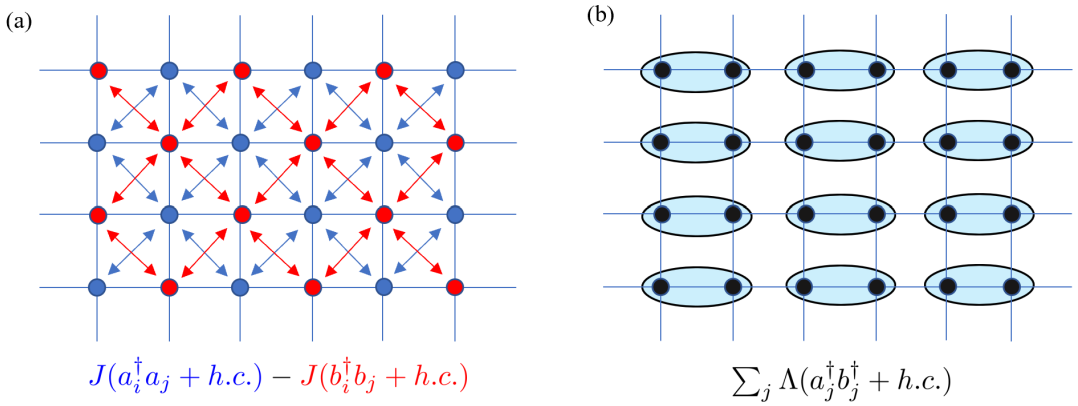

Figure 4.5: Exactly-solvable Bose-Hubbard models with hopping and pair-driving. (a) A bipartite lattice is subjected to chirally-symmetric hopping (depicted using blue and red arrows) as well as pair-driving of the form $\delta\hat{H} = \sum_j (\hat{a}_j^\dagger \hat{b}_j^\dagger + h.c.)$ (not shown in this subpanel), and an infinite-range Bose-Hubbard interaction (not shown in this subpanel). (b) At late times, the steady state becomes stationary with respect to the hopping process depicted in panel (a), and so the steady state can be analyzed by ignoring the hopping processes and considering only the pair-driving process (depicted by blue ovals) and the Hubbard interaction (not shown in this subpanel) in isolation.

4.7 Augmenting the model with hopping terms

The driven-dissipative bosonic lattice model that we solve in this chapter is given by the following Lindblad master equation:

$$\partial_t \hat{\rho} = -i[\hat{H}, \hat{\rho}] + \sum_j \mathcal{D}[\hat{L}_j], \qquad \hat{H} = u\hat{N}^2 - \Delta\hat{N} + \sum_{ij} \left(M_{ij}\hat{a}_i^\dagger \hat{a}_j^\dagger + h.c.\right), \qquad \hat{L}_j = \sqrt{\kappa}\hat{a}_j \tag{4.12}$$

where here, $\hat{N} \equiv \sum_{j=1}^N \hat{a}_j^\dagger \hat{a}_j$ denotes total boson number, and $u \equiv U/N$. In addition, we have an arbitrary complex-valued two-mode squeezing array M_{ij}.

We will now describe how single-photon tunneling terms of the form $J\hat{a}_i^\dagger \hat{a}_j + h.c.$ can be added to the Hamiltonian while preserving its solvability. A proper explanation of this necessitates a discussion of the symmetries of the dissipative evolution generated by the Lindbladian $\mathcal{L}$. We begin by discussing the two-mode squeezing array M. We define the

symmetry group S of the array M to be the group formed by unitary beam-splitter transformations that leave the pairing array invariant. Under such a transformation, represented by a unitary matrix W, the pairing array M transforms as $M \to WMW^T$. Therefore

$$S = \left\{ W \in U(N) : \; WMW^T = M \right\} = V \prod_{\lambda \in \Sigma} O(s_\lambda, \mathbb{R})\, V^\dagger, \tag{4.13}$$

where $M = V\Sigma V^T$ is the Autonne-Takagi factorization of the matrix M with Σ the diagonal matrix of singular values, and where s_λ denotes the degeneracy of the singular value $\lambda \in \Sigma$. In arriving at the result (4.13) we have used the fact that the symmetry group of Σ is the product group $\prod_{\lambda \in \Sigma} O(s_\lambda, \mathbb{R})$. Since S by definition conserves total particle number, any beam-splitter transformation that lies in S is a weak symmetry of the Lindbladian (4.12).

Let us now assume that $\mathcal{L}$ has a unique steady state. Then this steady state must respect the weak symmetries of the Lindbladian $\mathcal{L}$ Buča and Prosen [2012]. In particular, the steady state is invariant under the symmetry group S of the pairing array. In particular, we can add any element in the Lie algebra $\mathfrak{s}$ of S to the Hamiltonian in (4.12) while still preserving the steady state. The Lie algebra of S can be explicitly computed:

$$\mathfrak{s} = \mathcal{V} \left\{ i \sum_{\lambda \in \Sigma} \sum_{i,j \in \underline{s}_\lambda} t_{ij} (\hat{a}_i^\dagger \hat{a}_j - \hat{a}_j^\dagger \hat{a}_i), \quad t_{ij} \in \mathbb{R} \right\} \mathcal{V}^\dagger. \tag{4.14}$$

where $\underline{s}_\lambda$ denotes the subset of mode indices corresponding to the singular value s_λ, and $\mathcal{V}$ is some beam-splitter transformation that implements the unitary transformation V, i.e. $\mathcal{V}^\dagger \hat{a}_i \mathcal{V} \equiv \sum_j V_{ij} \hat{a}_j$.

4.7.1 Imaginary hopping arrangements

When the singular values of the pairing array are fully degenerate, the pairing array is maximally symmetric: in this case, the symmetry group S is, up to the unitary similarity

transform V, just the full rotation group as a subgroup of the unitary group. The simplest example is the case where the pairing array is diagonal and uniform: $M_{ij} = G\delta_{ij}$, which lets us set $V = 1$. Therefore, in this case, the symmetry group of the pairing array is generated by terms of the form

$$\delta\hat{H} \equiv i \sum_{i,j=1}^{N} t_{ij}(\hat{a}_i^\dagger \hat{a}_j - \hat{a}_j^\dagger \hat{a}_i). \tag{4.15}$$

Recall that, since $\delta\hat{H}$ generates a weak symmetry of $\mathcal{L}$, one can add $\delta\hat{H}$ to the Hamiltonian without changing the steady state of $\mathcal{L}$. That is, one can add any set of imaginary hopping terms to the Hamiltonian without changing the steady state of $\mathcal{L}$.

4.7.2 Chirally-symmetric hopping arrangements

Thanks to the similarity transform V appearing in the symmetry group S, there are many situations where our solvable model can be augmented with conventional hopping terms. As a particularly striking example of this, consider a global Bose-Hubbard model defined on a bipartite lattice with $2N$ sites, with corresponding modes $\hat{a}_1, \ldots \hat{a}_N, \hat{b}_1, \ldots, \hat{b}_N$. We can consider a special case of the Lindbladian (4.12) where the pairing array is fully "dimerized", that is, where the Hamiltonian takes the form

$$\hat{H} = u\hat{N}^2 - \Delta\hat{N} + \Lambda \sum_j (\hat{a}_j^\dagger \hat{b}_j^\dagger + h.c.). \tag{4.16}$$

In this case, one can augment the above Hamiltonian with the following hopping terms:

$$\delta\hat{H} \equiv \sum_{ij} J_{ij} \Big((\hat{a}_i^\dagger \hat{a}_j + h.c.) - (\hat{b}_i^\dagger \hat{b}_j + h.c.) \Big). \tag{4.17}$$

Note that such a model describes arbitrary hopping within the A-sublattice, which is mirrored in the B-sublattice. This situation is schematically depicted in Fig. 4.5a. To see explicitly that the hopping terms generate rotational symmetries of $\mathcal{L}$, we have to diagonalize the pairing array. In particular, one can do this by defining modes

$$\hat{c}^\dagger_{j,+} \equiv \frac{\hat{a}^\dagger_j + \hat{b}^\dagger_j}{\sqrt{2}}, \quad \hat{c}^\dagger_{j,-} \equiv \frac{\hat{a}^\dagger_j - \hat{b}^\dagger_j}{i\sqrt{2}}. \tag{4.18}$$

In this mode basis, the Hamiltonian, with the hopping terms included, reads as

$$\hat{H} = u\hat{N}^2 - \Delta\hat{N} + \Lambda\sum_{j,\pm}(\hat{c}^{\dagger 2}_{j,\pm} + h.c.) + i\sum_{i,j=1}^{N} J_{ij}(c^\dagger_{i,-}\hat{c}_{j,+} - h.c.) + i\sum_{i,j=1}^{N} J_{ij}(c^\dagger_{i,+}\hat{c}_{j,-} - h.c.). \tag{4.19}$$

In this diagonal mode basis, it is extremely clear that the hopping terms generate rotations of the modes $\hat{c}_{j,\pm}, \hat{c}^\dagger_{j,\pm}$ that are weak symmetries of the Lindbladian. Therefore, the results of this chapter can be used to analytically describe the steady states of the model (4.16), including the chirally-symmetric hopping arrangement depicted in Fig. 4.5a.

4.8 Hidden TRS conditions

Given a steady-state $\hat{\rho}_{\text{ss}}$ and corresponding time-reversal operation $\hat{T}$, one can construct the *thermofield double state*

$$|\Psi_{\hat{T}}\rangle = \sum_n \sqrt{p_n}|n\rangle_L \hat{T}|n\rangle_R, \tag{4.20}$$

where $|n\rangle$ are the eigenvectors of $\hat{\rho}_{\rm ss}$, and p_n the corresponding eigenvalues. Sufficient conditions for $\hat{T}$ to be a hidden time-reversal symmetry are Fagnola and Umanità [2010]

$$\left[\left(u(\hat{N}_L+\hat{N}_R)-\Delta_{\rm eff}\right)(\hat{N}_L-\hat{N}_R)+2\sum_{ij}M_{ij}\hat{\alpha}^\dagger_{i,+}\hat{\alpha}^\dagger_{j,-}\right]|\Psi_{\hat{T}}\rangle=0,$$

$$\hat{\alpha}_{j,-}|\Psi_{\hat{T}}\rangle=0, \tag{4.21}$$

where $\hat{\alpha}_{j,\pm}\equiv 2^{-1/2}(\hat{a}_{j,L}\pm\hat{a}_{j,R})$. Since the Bogoliubov transformation $\hat{a}_{j,L},\hat{a}_{j,R}\to\hat{\alpha}_{j,+},\hat{\alpha}_{j,-}$ is boson-number preserving, we have $\hat{N}_L+\hat{N}_R=\hat{N}_++\hat{N}_-$, where $\hat{N}_\pm:=\sum_j\hat{\alpha}^\dagger_{j,\pm}\hat{\alpha}_{j,\pm}$. Therefore, we can write the above conditions equivalently as

$$\sum_j\hat{\alpha}^\dagger_{j,-}\left[\left(u(\hat{N}_++\hat{N}_-+1)-\Delta_{\rm eff}\right)\hat{\alpha}_{j,+}+2\sum_i M_{ij}\hat{\alpha}^\dagger_{i,+}\right]|\Psi_{\hat{T}}\rangle=0, \tag{4.22}$$

$$\hat{\alpha}_{j,-}|\Psi_{\hat{T}}\rangle=0. \tag{4.23}$$

Each term in the sum in Eq. (4.22) has exactly one boson in the antisymmetric mode $\hat{\alpha}_{j,-}$ and is thus mutually orthogonal with the remaining terms. Therefore, each term in the sum must separately vanish. Factoring the thermofield double into symmetric and antisymmetric components $|\Psi_{\hat{T}}\rangle=|\Psi_+\rangle|\Psi_-\rangle$, we obtain $|\Psi_-\rangle=|0_-\rangle$, i.e. the antisymmetric component is in vacuum, and

$$\left((u(\hat{N}_++1)-\Delta_{\rm eff})\hat{\alpha}_{j,+}+2\sum_i M_{ij}\hat{\alpha}^\dagger_{i,+}\right)|\Psi_+\rangle=0. \tag{4.24}$$

4.8.1 Exact solution via representation theory

We now proceed to solve the system of equations Eq. (4.24). To begin, we multiply each constraint on the left by $\hat{\alpha}^\dagger_{j,+}$, yielding

$$\left(u(\hat{N}_+ - \Delta_{\text{eff}})\hat{n}_{j,+} + 2\sum_i M_{ij}\hat{\alpha}^\dagger_{i,+}\hat{\alpha}^\dagger_{j,+}\right)|\Psi_+\rangle = 0, \tag{4.25}$$

where $\hat{n}_{j,+} := \hat{\alpha}^\dagger_{j,+}\hat{\alpha}_{j,+}$. We then sum over j:

$$\left(u(\hat{N}_+ - \Delta_{\text{eff}})\hat{N}_+ + 2\sum_{ij} M_{ij}\hat{\alpha}^\dagger_{i,+}\hat{\alpha}^\dagger_{j,+}\right)|\Psi_+\rangle = 0. \tag{4.26}$$

Note how the above operator annihilating $|\Psi_{\hat{T}}\rangle$ is almost like the effective nonhermitian Hamiltonian $\hat{H}_{\text{eff}} := \hat{H} - i\kappa\hat{N}/2$, except that here the lowering operators associated with the drive are not present. We now identify a "hidden" nonunitary representation of $SU(1,1)$ via

$$\hat{K}_+ = \frac{1}{2}\sum_{ij}\frac{M_{ij}}{u}\hat{\alpha}^\dagger_{i,+}\hat{\alpha}^\dagger_{j,+}, \quad \hat{K}_- = \frac{1}{2}\sum_{ij}(uM^{-1})_{ij}\hat{\alpha}_{i,+}\hat{\alpha}_{j,+}, \quad \hat{K}_z = \frac{1}{2}\sum_j\left(\hat{\alpha}^\dagger_{j,+}\hat{\alpha}_{j,+} + \frac{1}{2}\right). \tag{4.27}$$

Note that the representation presented here is unitary if and only if the pairing array is unitary, i.e. $(M/u)^{-1} = (M/u)^\dagger$. In terms of the Lie algebra generators, the hTRS condition simplifies to $\mathcal{H}_{\text{eff},+}|\Psi_+\rangle = 0$, where

$$\mathcal{H}_{\text{eff},+} := \big(\hat{K}_z - N/4 - \Delta_{\text{eff}}/2u\big)\big(\hat{K}_z - N/4\big) + \hat{K}_+. \tag{4.28}$$

To solve this condition, we make the ansatz that the dark state inhabits an irreducible representation of $SU(1,1)$, with the vacuum state constituting the vector of lowest weight (with respect to the subalgebra generated by $\hat{K}_z$). This irreducible representation is spanned

by vectors of the form

$$|\Psi\rangle = \sum_m c_m \hat{K}_+^m |h_0\rangle, \qquad |h_0\rangle := |\Omega\rangle \tag{4.29}$$

The use of the notation h_0 to denote the bosonic vacuum $|\Omega\rangle := |0\rangle_L|0\rangle_R$, as well as the fact that the solution Eq. (4.29) to the constraints Eq. (4.24) is unique will become apparent in later sections when we review the general representation theory of $SU(1,1)$. For now, however, we will treat Eq. (4.29) as an ansatz and proceed to compute the exact coefficients c_m occuring in the expansion:

$$\mathcal{H}_{\text{eff},+}|\Psi_+\rangle = \sum_{m=1}^{\infty} \Big(m(m - \Delta_{\text{eff}}/2u)c_m + c_{m-1} \Big) \hat{K}_+^m |h_0\rangle = 0, \tag{4.30}$$

which yields the solution $c_m \propto (-1)^m/m!(\delta)_m$, where $\delta := 1 - \Delta_{\text{eff}}/2u$, and $(\delta)_m := \delta(\delta+1)\cdots(\delta+m-1)$ denotes the Pochhammer symbol (rising factorial).

4.8.2 Diagonal form of the representation

By treating the raising operators $\hat{\alpha}_{j,+}^\dagger$ as indeterminates, one can interpret the $SU(1,1)$ raising operator $\hat{K}_+$ presented in Eq. (4.27) as a quadratic form over the complex numbers. Its matrix representation M/u is invariant under transposition and thus admits a kind of singular-value decomposition $M/u = V\Sigma V^T$ (called the Autonne-Takagi factorization Autonne [1915]), with V an $N \times N$ unitary matrix and $\Sigma = \text{diag}(\lambda_1, \ldots, \lambda_N)$ the matrix of singular values. Writing $\hat{\beta}_{i,+}^\dagger := \sum_i V_{ij}\hat{\alpha}_{j,+}^\dagger$ for the corresponding basis of singular vectors, we can re-express the $SU(1,1)$ representation (4.27) as follows:

$$\hat{K}_+ = \frac{1}{2}\sum_j \lambda_j \hat{\beta}_{j,+}^{\dagger 2}, \qquad \hat{K}_- = \frac{1}{2}\sum_i \lambda_j^{-1} \hat{\beta}_{j,+}^2, \qquad \hat{K}_z = \frac{1}{2}\sum_j \left(\hat{\beta}_{j,+}^\dagger \hat{\beta}_{j,+} + \frac{1}{2} \right). \tag{4.31}$$

4.9 Exact solution: collective moments

The simplest quantities to compute in our model are collective observables, that is, moments of normally-ordered monomials in the $SU(1,1)$ algebra.

4.9.1 Unitary case

Our job is easiest when the representation Eq. (4.27) satisfies $\hat{K}_+^\dagger \propto \hat{K}_-$. This happens if and only if the singular values of the matrix M/u are all the same. In this case, the $SU(1,1)$ representation can be made unitary by rescaling $\hat{K}_-$, and the diagonal form of the representation is as follows:

$$\hat{K}_+ = \frac{1}{2}\sum_j \lambda \hat{\beta}_{j,+}^{\dagger 2}, \qquad \hat{K}_- = \frac{1}{2}\sum_j \lambda^{-1}\hat{\beta}_{j,+}^{2}, \quad \hat{K}_z = \frac{1}{2}\sum_j \left(\hat{\beta}_{j,+}^\dagger \hat{\beta}_{j,+} + \frac{1}{2}\right), \tag{4.32}$$

with $\lambda > 0$ the unique singular value of the matrix M/u. With this, we now turn to compute moments of monomials of $SU(1,1)$ within the representation:

$$\langle \Psi_{\hat{T}} | \hat{K}_+^n \hat{N}_+^k \hat{K}_-^m | \Psi_{\hat{T}} \rangle = \sum_{p,q} \lambda^{2p} c_p^* c_q \langle h_0 | \hat{K}_-^p \hat{K}_+^n \hat{N}_+^k \hat{K}_-^m \hat{K}_+^q | h_0 \rangle \tag{4.33}$$

We reparametrize the sum by defining an auxiliary non-negative integer $l = p - n = q - m$. In terms of l:

$$\begin{aligned}\langle \Psi_{\hat{T}} | \hat{K}_+^n \hat{N}_+^k \hat{K}_-^m | \Psi_{\hat{T}} \rangle &= \sum_{l=0}^{\infty} \lambda^{2(l+n)} c_{l+n}^* c_{l+m} \langle h_0 | \hat{K}_-^l \hat{K}_-^n \hat{K}_+^n \hat{N}_+^k \hat{K}_-^m \hat{K}_+^m \hat{K}_+^l | h_0 \rangle \\ &= \lambda^{2n} c_n^* c_m \sum_{l=0}^{\infty} (2l)^k |c_l|^2 \lambda^{2l} \frac{c_{n+l}^*}{c_l^* c_n^*} \frac{c_{m+l}}{c_l c_m} f(n,m,l).\end{aligned} \tag{4.34}$$

Using the $SU(1,1)$ commutation relations, we evaluate

$$f(n,m,l) := \langle h_0|\hat{K}_-^l \hat{K}_-^n \hat{K}_+^n \hat{K}_+^m \hat{K}_-^m \hat{K}_+^l|h_0\rangle$$
$$= l!(N/2)_l \frac{(n+l)!}{l!}\frac{(m+l)!}{l!}\frac{(N/2)_{n+l}}{(N/2)_l}\frac{(N/2)_{m+l}}{(N/2)_l} \tag{4.35}$$
$$= \frac{(N/2)_n(N/2)_m}{l!}\frac{(n+l)!(m+l)!(N/2+n)_l(N/2+m)_l}{(N/2)_l}. \tag{4.36}$$

We then compute

$$(2l)^k|c_l|^2\lambda^{2l}\frac{c^*_{n+l}}{c^*_l c^*_n}\frac{c_{m+l}}{c_l c_m} = |c_l|^2\lambda^{2l}\frac{l!n!l!m!}{(n+l)!(m+l)!}\frac{(\delta^*)_l(\delta^*)_n(\delta)_l(\delta)_m}{(\delta^*)_{l+n}(\delta^*)_{l+m}} \tag{4.37}$$
$$= \frac{\lambda^{2l}n!m!}{(n+l)!(m+l)!(\delta^*+n)_l(\delta+m)_l}. \tag{4.38}$$

Putting everything together,

$$\langle\Psi_{\hat{T}}|\hat{K}_+^n\hat{N}_+^k\hat{K}_-^m|\Psi_{\hat{T}}\rangle = \lambda^{2n}c^*_n c_m (N/2)_n(N/2)_m n!m!\sum_{l=0}^{\infty}(2l)^k\frac{\lambda^{2l}}{l!}\frac{(N/2+n)_l(N/2+m)_l}{(N/2)_l(\delta^*+n)_l(\delta+m)_l}$$
$$= \frac{\lambda^{2n}(-1)^{n+m}(N/2)_n(N/2)_m}{(\delta^*)_n(\delta)_m}\left(2z\frac{d}{dz}\right)^k {}_2F_3(N/2+n,N/2+m;N/2,\delta^*+n,\delta+m;z)\Big|_{z=\lambda^2}, \tag{4.39}$$

where here, ${}_pF_q$ denotes the generalized hypergeometric function, defined as the analytic extension of the following infinite series:

$${}_pF_q(a_1,\dots a_p;b_1,\dots b_q;z) = \sum_{l=0}^{\infty}\frac{\prod_{m=1}^p(a_m)_l}{\prod_{m=1}^q(b_m)_l}\frac{z^l}{l!}. \tag{4.40}$$

Up to this point, we have computed $|\Psi_{\hat{T}}\rangle$ up to a normalization prefactor. This normalization can also be computed in closed form: $\langle\Psi_{\hat{T}}|\Psi_{\hat{T}}\rangle = {}_1F_2(N/2;\delta,\delta^*;\lambda^2)$, thus completing the characterization of collective moments in the case that the representation (4.27) is unitary.

4.9.2 Nonunitary case

We now accomplish the same task, but in the more general regime where the singular values λ_j are possibly non-degenerate. In this situation, there is less structure to the calculation, but moments of $SU(1,1)$ monomials may nonetheless be extracted efficiently:

$$\langle \Psi_{\hat{T}} | \hat{K}_+^n \hat{N}_+^k \hat{K}_-^m | \Psi_{\hat{T}} \rangle = \sum_{p,q}^{\infty} c_p^* c_q \langle h_0 | \hat{K}_+^{\dagger p} \hat{K}_+^n \hat{N}_+^k \hat{K}_-^m \hat{K}_+^q | h_0 \rangle \tag{4.41}$$

We reparametrize the sum by defining an auxiliary non-negative integer $l = p - n = q - m$. In terms of l:

$$\begin{aligned} \langle \Psi_{\hat{T}} | \hat{K}_+^n \hat{N}_+^k \hat{K}_-^m | \Psi_{\hat{T}} \rangle &= \sum_{l=0}^{\infty} c_{l+n}^* c_{l+m} (2l)^k \langle h_0 | \hat{K}_+^{\dagger l} \hat{K}_+^{\dagger n} \hat{K}_+^n \hat{K}_-^m \hat{K}_+^m \hat{K}_+^l | h_0 \rangle \\ &= c_n^* c_m \sum_{l=0}^{\infty} |c_l|^2 \frac{c_{l+n}^*}{c_l^* c_n^*} \frac{c_{l+m}}{c_l c_m} (2l)^k g(n,m,l). \end{aligned} \tag{4.42}$$

We evaluate:

$$g(n,m,l) = \frac{(N/2)_{m+l}(m+l)!}{(N/2)_l l!} \langle h_0 | \hat{K}_+^{\dagger (n+l)} \hat{K}_+^{n+l} | h_0 \rangle \tag{4.43}$$

$$:= \frac{(N/2)_{m+l}(m+l)!(n+l)!(n+l)!}{(N/2)_l l!} \Phi_{n+l}(\vec{\lambda}; N), \tag{4.44}$$

where $\Phi_n(\vec{\lambda}; N) := (n!)^2 \langle h_0 | \hat{K}_+^{\dagger n} \hat{K}_+^n | h_0 \rangle$ is a form factor to be evaluated later on. Therefore, in total we have

$$\langle \Psi_{\hat{T}} | \hat{K}_+^n \hat{N}_+^k \hat{K}_-^m | \Psi_{\hat{T}} \rangle = \frac{(-1)^{n+m}(N/2)_m}{(\delta^*)_n (\delta)_m} \sum_{l=0}^{\infty} \frac{(N/2+m)_l (n+l)! (2l)^k}{(\delta^*+n)_l (\delta+m)_l (N/2)_l l!} \Phi_{n+l}(\vec{\lambda}; N). \tag{4.45}$$

All that is left is to compute the normalization, which comes out to

$$\langle \Psi_{\hat{T}} | \Psi_{\hat{T}} \rangle = \sum_{l=0}^{\infty} \Phi_l(\vec{\lambda}; N)/(\delta)_l(\delta^*)_l. \tag{4.46}$$

Up until this point, we have given formulae in terms of the form factors $\Phi_n(\vec{\lambda}; N) := \langle h_0 | \hat{K}_+^{\dagger n} \hat{K}_+^n | h_0 \rangle / (n!)^2$, which, in the nonunitary case, cannot be evaluated purely using the internal relations of the $SU(1,1)$ algebra. Instead, via the multinomial expansion, we are left with a sum over an exponential number of terms:

$$\Phi_n(\vec{\lambda}; N) = \frac{1}{n!^2} \langle h_0 | \left(\frac{1}{2} \sum_j \lambda_j \hat{\beta}_{j,+}^2 \right)^n \left(\frac{1}{2} \sum_j \lambda_j \hat{\beta}_{j,+}^{\dagger 2} \right)^n | h_0 \rangle = \sum_{\sum_j k_j = n} \prod_j (1/2)_{k_j} \lambda_j^{2k_j} \tag{4.47}$$

Our work would not be complete if we did not give an efficient prescription for evaluating these sums. The key to evaluating these sums efficiently is the following observation:

$$\Phi_n(\vec{\lambda}; N) = \sum_{p=0}^{n} (1/2)_p \lambda_N^{2p} \sum_{\sum_{j=1}^{N-1} k_j = n-p} \prod_j (1/2)_{k_j} \lambda_j^{2k_j} = \sum_{p=0}^{n} (1/2)_p \lambda_N^{2p} \Phi_{n-p}(\vec{\lambda}; N-1) \tag{4.48}$$

We note that the above constitutes a recursion relation for $\Phi_n(\vec{\lambda}; N)$ with boundary condition $\Phi_p(\vec{\lambda}; 1) = (1/2)_p \lambda_1^{2p}$. Note that via this recursion relation, and fixing some boson-number cutoff k, the collection $\{\Phi_p(\vec{\lambda}; N)\}_{p \leq k}$ of form factors may be evaluated using only $O(k^2 N)$ floating-point operations.

4.10 Exact solution: local moments

We now turn to a more difficult task: that of computing (equal-time) correlation functions of local observables, that is, observables that are not collective in nature. To accomplish this

efficiently in the unitary case, we must solve the "addition of angular momentum" problem for $SU(1,1)$, i.e. we must understand how to decompose a tensor product of $SU(1,1)$ representations into irreducible components. Luckily, this task is easily solved in terms of the theory of harmonic functions on $\mathbb{R}^N$. In the nonunitary case, however, the $SU(1,1)$ structure is not so useful, and instead some generalization of the combinatorics in (4.48) is needed to compute observables.

To make our task easier, we will compute observables in the basis of modes $\hat{b}_i^\dagger := \sum_j V_{ij}\hat{a}_j^\dagger$ that diagonalizes the pair-driving matrix M/u.

4.10.1 Addition of angular momentum for $SU(1,1)$

We can write our global $SU(1,1)$ representation (4.31) as a tensor product of local representations:

$$\hat{K}_+^{(j)} \equiv \frac{1}{2}\lambda_j \hat{\beta}_{j,+}^{\dagger 2}, \quad \hat{K}_-^{(j)} \equiv \frac{1}{2}\lambda_j^{-1}\hat{\beta}_{j,+}^{2}, \quad \hat{K}_z^{(j)} \equiv \frac{1}{2}\left(\hat{\beta}_{j,+}^\dagger \hat{\beta}_{j,+} + \frac{1}{2}\right) \tag{4.49}$$

It is easy to see that each local representation is reducible, and has the decomposition $V^{(j)} = V_+^{(j)} \oplus V_-^{(j)}$, where $V_\pm^{(j)}$ denotes the subspace consisting of all states with a fixed boson-number parity ± 1. Our global $SU(1,1)$ representation $\hat{K}_+, \hat{K}_-, \hat{K}_z$ is the N-fold tensor product $\otimes_j V^{(j)}$, and has the following decomposition into irreducible subrepresentations:

$$\otimes_j V^{(j)} \simeq \bigoplus_{l=0}^{\infty}\left(\bigoplus_{p=1}^{d_l} V_l^{(p)}\right), \tag{4.50}$$

where each irreducible subrepresentation $V_l^{(p)}$ takes the form

$$|\Psi_l^{(p)}\rangle = \sum_{m=0}^{\infty} c_m \hat{K}_+^m |h_l^{(p)}\rangle, \tag{4.51}$$

and $|h_l^{(1)}\rangle, \ldots, |h_l^{(d_l)}\rangle$ is some orthonormal basis of the subspace of the kernel of $\hat{K}_-$ consisting of those states with fixed total photon number equal to l. Later on we sketch a proof of the decomposition (4.50) using the Segal-Bargmann representation Bargmann [1961, 1967], which represents bosonic states as multivariate analytic functions, and bosonic creation- and annihilation operators as partial differential operators. In the Segal-Bargmann representation, the $SU(1,1)$ vacua $|h_l^{(p)}\rangle$ are represented as homogeneous harmonic polynomials of degree l, hence the notation "h_l".

4.10.2 Unitary case

In the unitary case, the decomposition (4.50) becomes an orthogonal direct-sum decomposition, with the superselection rules $\langle h_l^{(m)}|\hat{K}_+^{\dagger p}\hat{K}_+^q|h_{l'}^{(m')}\rangle = \delta_{l,l'}\delta_{m,m'}\delta_{p,q}p!\lambda^{2p}(N/2+l)_p$. These simple rules allow us to compute any local quantity of interest in our model. For the case of quadratic correlation functions, however, such rules are not necessary. To see this, it suffices to use the weak permutation symmetry $\hat{b}_i \leftrightarrow \hat{b}_j$, as well as the weak parity symmetry $\hat{b}_i \to -\hat{b}_i$ of the Lindbladian $\mathcal{L}$:

$$\langle \hat{b}_i^\dagger \hat{b}_{i+r}\rangle = \delta_{r,0}\frac{1}{N}\sum_j \langle \hat{b}_j^\dagger \hat{b}_j\rangle = \frac{\delta_{r,0}}{N}\langle \Psi_{\hat{T}}|\hat{N}_+|\Psi_{\hat{T}}\rangle, \tag{4.52}$$

$$\langle \hat{b}_i \hat{b}_{i+r}\rangle = \delta_{r,0}\frac{1}{N}\sum_j \langle \hat{b}_j^2\rangle = \frac{\delta_{r,0}}{N}\langle \Psi_{\hat{T}}|\hat{K}_-|\Psi_{\hat{T}}\rangle \tag{4.53}$$

Higher-order correlations, are not expressible in terms of collective moments, and so in general the decomposition (4.50), along with the associated superselection rules, serve as a useful guide. As an example, we compute the pair-correlation function, as well as the density-density correlation function, and leave the general case to the reader. We compute

the pair correlation function first:

$$\langle \hat{b}_i^{\dagger 2} \hat{b}_{i+r}^2 \rangle = \frac{1}{4} \langle \Psi_{\hat{T}} | \hat{\beta}_{i+r,+}^2 \hat{\beta}_{i,+}^{\dagger 2} | \Psi_{\hat{T}} \rangle - \frac{2\delta_{r,0}}{N} \langle \Psi_{\hat{T}} | \hat{K}_z | \Psi_{\hat{T}} \rangle \tag{4.54}$$

$$= \frac{1}{4} \sum_{p,q} c_p^* c_q \langle h_0 | \hat{\beta}_{i,+}^2 \hat{K}_+^{\dagger p} \hat{K}_+^q \hat{\beta}_{i+r,+}^{\dagger 2} | h_0 \rangle - \frac{2\delta_{r,0}}{N} \langle \Psi_{\hat{T}} | \hat{K}_z | \Psi_{\hat{T}} \rangle \tag{4.55}$$

For the calculation to proceed, it is necessary to decompose the states $\hat{\beta}_{i,+}^{\dagger 2} | h_0 \rangle$ into $SU(1,1)$ vacua. Although this can be done by hand in this simple case, in general it is useful to automate this process (especially for higher-order observables). For this purpose, the HFT *Mathematica* package Axler [2020] is especially relevant, in particular the function harmonicDecomposition[], which automatically extracts the decomposition

$$\hat{\beta}_{i,+}^{\dagger 2} | h_0 \rangle = \sqrt{\frac{2N-2}{N}} | h_2^{(i)} \rangle + \frac{2\hat{K}_+}{\lambda N} | h_0 \rangle, \tag{4.56}$$

where $|h_2^{(i)}\rangle := \frac{1}{\lambda} \sqrt{\frac{2N}{N-1}} (\hat{K}_+^{(i)} - \frac{\hat{K}_+}{N}) | h_0 \rangle$ generates an irreducible subrepresentation with weight $N/4 + 1$. We thus obtain:

$$\frac{1}{4} \sum_{p,q} c_p^* c_q \langle h_0 | \hat{\beta}_{i,+}^2 \hat{K}_+^{\dagger p} \hat{K}_+^q \hat{\beta}_{i+r,+}^{\dagger 2} | h_0 \rangle \tag{4.57}$$

$$= \frac{2N-2}{N^3 \lambda^2} \sum_l |c_l|^2 \langle h_0 | \hat{K}_+^{\dagger l+1} \hat{K}_+^{l+1} | h_0 \rangle + \frac{N-1}{2N} \sum_l |c_l|^2 \langle h_2^{(i)} | \hat{K}_+^{\dagger l} \hat{K}_+^l | h_2^{(i+r)} \rangle$$

$$= \left(\frac{2N-2}{N^3} \left[z \frac{\partial}{\partial z} + 1 \right] {}_1F_2(N/2; \delta, \delta^*; z) + \frac{N\delta_{r,0} - 1}{2N} {}_1F_2(N/2+2; \delta, \delta^*; z) \right) \Bigg|_{z=\lambda^2}. \tag{4.58}$$

We now compute the density-density correlation function $\langle \hat{b}_i^\dagger \hat{b}_i \hat{b}_{i+r}^\dagger \hat{b}_{i+r} \rangle$. Since the case $r = 0$ is subsumed by the previous calculation, without loss of generality we can assume $r \neq 0$. Again, we split the calculation into a collective part and a noncollective part (that populates

a higher weight representation):

$$\langle \hat{b}_i^\dagger \hat{b}_i \hat{b}_{i+r}^\dagger \hat{b}_{i+r} \rangle = \frac{1}{4} \sum_{p,q} c_p^* c_q \langle h_0 | \hat{\beta}_i \hat{\beta}_{i+r} \hat{K}_+^{\dagger p} \hat{K}_+^q \hat{\beta}_i^\dagger \hat{\beta}_{i+r}^\dagger | h_0 \rangle - \frac{1}{N} \langle \Psi_{\hat{T}} | \hat{K}_z | \Psi_{\hat{T}} \rangle. \tag{4.59}$$

We evaluate the noncollective part, by noticing that $|h_2^{(i,j)}\rangle := \hat{\beta}_{i,+}^\dagger \hat{\beta}_{j,+}^\dagger |h_0\rangle$ generates an irreducible subrepresentation with weight $N/4+1$:

$$\frac{1}{4} \sum_{p,q} c_p^* c_q \langle h_0 | \hat{\beta}_i \hat{\beta}_{i+r} \hat{K}_+^{\dagger p} \hat{K}_+^q \hat{\beta}_i^\dagger \hat{\beta}_{i+r}^\dagger | h_0 \rangle \tag{4.60}$$

$$= \frac{1}{4} \sum_l |c_l|^2 \langle h_2^{(i,i+r)} | \hat{K}_+^{\dagger l} \hat{K}_+^l | h_2^{(i,i+r)} \rangle = \frac{1}{4} \, {}_1F_2(N/2+2; \delta, \delta^*; \lambda^2). \tag{4.61}$$

Higher-order moments

The general procedure for calculating higher order moments is no different from what we have done in the previous subsection: given a higher-order moment to be evaluated, one writes the expectation value in terms of an antinormally-ordered correlation function involving the mode operators $\hat{\beta}_{j,+}, \hat{\beta}_{j,+}^\dagger$, and then uses standard harmonic analysis software Axler [2020] to decompose the resulting states into components lying in higher-weight subrepresentations. Iterating this process yields formulae in terms of generalized hypergeometric functions and their derivatives.

4.10.3 Nonunitary case

We now turn to the most general task of computing local correlation functions in our global Bose-Hubbard model, in the nonunitary regime. In this case the calculation has the least amount of structure, and so here we just present the most general result. To better organize

the calculation, we will write the purification $|\Psi_{\hat{T}}\rangle$ as a power series

$$|\Psi_{\hat{T}}\rangle = \sum_{\vec{m}\in\mathbb{N}^N} \frac{c_{\vec{m}}}{\vec{m}!} \prod_j \hat{\beta}_{j,+}^{\dagger m_j} |h_0\rangle, \tag{4.62}$$

with $c_{\vec{m}} = \prod_j (4\lambda_j)^{m_j} (1/2)_{m_j} / (\delta)_{\sum_j m_j}$. From the above form of the purification, we can calculate the parametric form of any normally-ordered correlation function:

$$\langle \hat{b}_1^{\dagger n_1} \cdots \hat{b}_N^{\dagger n_N} \hat{b}_1^{m_1} \cdots \hat{b}_N^{m_N} \rangle = \frac{1}{\sqrt{2^{\sum_j n_j + m_j}}} \langle \Psi_{\hat{T}} | \hat{\beta}_{1,+}^{\dagger n_1} \cdots \hat{\beta}_{N,+}^{\dagger n_N} \hat{\beta}_{1,+}^{m_1} \cdots \hat{\beta}_{N,+}^{m_N} | \Psi_{\hat{T}} \rangle \tag{4.63}$$

$$= \frac{1}{\sqrt{2^{\sum_j n_j + m_j}}} \sum_{\vec{k}\in\mathbb{N}^N} \frac{c^*_{\vec{n}+\vec{k}} c_{\vec{m}+\vec{k}}}{\vec{k}!} \tag{4.64}$$

There are a number of issues, however, with the series expression given above: firstly, due to the weak symmetry $\hat{b}_j \to -\hat{b}_j$ of $\mathcal{L}$, only correlation functions with $n_j \equiv m_j$ modulo two are nonzero. Secondly, the series expression naively seems to be useless, as, for a fixed total boson number cutoff, the series contains a number terms that is exponentially growing with N. Therefore, the naive way of evaluating (4.64) scales no better than a direct simulation of the original master equation.

We will resolve both of these issues now: first of all, we can efficiently parametrize all of the nonzero correlators by replacing $\vec{n} \to 2\vec{n} + \vec{b}, \vec{m} \to 2\vec{m} + \vec{b}$, where $\vec{b} \in \mathbb{F}_2^N$ is a fixed vector of booleans. To exponentially reduce the complexity of summing the series (4.64), we define generalized combinatorial form factors

$$\Phi_l(\vec{\lambda}, \vec{n}, \vec{m}, \vec{b}; N) := \sum_{\sum_j k_j = l} \prod_j \frac{(1/2 + n_j + b_j)_{k_j} (1/2 + m_j + b_j)_{k_j}}{(2k_j + b_j)!} (4\lambda_j)^{2k_j}. \tag{4.65}$$

Indeed, in terms of the above form factors, the series expressions for normally-ordered mo-

ments simplify quite considerably:

$$\langle \hat{b}^{\dagger 2\vec{n}+\vec{b}} \hat{b}^{2\vec{m}+\vec{b}} \rangle = \frac{1}{\sqrt{2^{\sum_j n_j+m_j+b_j}}} \sum_{\vec{k}\in\mathbb{N}^N} \frac{c^*_{2\vec{n}+\vec{b}+\vec{k}} c_{2\vec{m}+\vec{b}+\vec{k}}}{\vec{k}!}$$

$$= \frac{1}{\sqrt{2^{\sum_j n_j+m_j+b_j}}} \sum_{\vec{k}\in\mathbb{N}^N} \frac{c^*_{2(\vec{n}+\vec{b}+\vec{k})} c_{2(\vec{m}+\vec{b}+\vec{k})}}{(2\vec{k}+\vec{b})!} \tag{4.66}$$

$$= \frac{c^*_{2(\vec{n}+\vec{b})} c_{2(\vec{m}+\vec{b})}}{\sqrt{2^{\sum_j n_j+m_j+b_j}}} \sum_{l=0}^{\infty} \frac{\Phi_l(\vec{\lambda},\vec{n},\vec{m},\vec{b})}{(\delta^* + \sum_j n_j + \sum_j b_j)_l (\delta + \sum_j m_j + \sum_j b_j)_l}. \tag{4.67}$$

Our job would not be finished if we did not give an efficient prescription for evaluating the form factors Φ_l. Our task is made easier, however, by observing that, when $\vec{n} = \vec{m} = \vec{b} = \vec{0}$, the form factors (4.65) reduce to the form factor $\Phi_n(\vec{\lambda}; N)$ used previously to compute collective moments. In fact, these more general form factors satisfy an analogous recursion relation:

$$\Phi_l(\vec{\lambda},\vec{n},\vec{m},\vec{b};N) = \sum_{p=0}^{n} \frac{(1/2+n_N+b_N)_p (1/2+m_N+b_N)_p}{(2p+b_N)!} (4\lambda_N)^{2p} \Phi_{n-p}(\vec{\lambda},\vec{n},\vec{m},;N-1). \tag{4.68}$$

We note that the above recursion relation has the boundary condition $\Phi_p(\vec{\lambda},\vec{n},\vec{m},\vec{b};1) = (1/2+n_1+b_1)_p (1/2+m_1+b_1)_p (4\lambda_1)^{2p}/(2p+b_1)!$. Therefore, the following kth-order approximant for each normally-ordered moment,

$$\frac{c^*_{2(\vec{n}+\vec{b})} c_{2(\vec{m}+\vec{b})}}{\sqrt{2^{\sum_j n_j+m_j+b_j}}} \sum_{l=0}^{k} \frac{\Phi_l(\vec{\lambda},\vec{n},\vec{m},\vec{b})}{(\delta^* + \sum_j n_j + \sum_j b_j)_l (\delta + \sum_j m_j + \sum_j b_j)_l}, \tag{4.69}$$

may be evaluated using only $O(k^2 N)$ operations. We now factor in considerations as to the scaling of the total-particle-number cutoff k. Assuming the onsite density $\bar{n}$ converges as $N \to \infty$, the total number of particles is $O(N)$, and so the cutoff typically scales with

the system size: $k \sim O(N)$. Therefore, factoring in all considerations, time-complexity of evaluating a single normally-ordered moment is roughly $O(N^3)$.

Quadratic correlation functions

Up until this point, we have given expressions for normally-ordered moments in the basis of singular modes $\hat{b}_i^\dagger := V_{ij}\hat{a}_j^\dagger$. To obtain correlation functions in the spatial mode basis, we must expand each $\hat{a}$-mode in terms of $\hat{b}$-modes:

$$\langle \hat{a}_i^\dagger \hat{a}_{i+r} \rangle = \sum_j V_{i,j} V_{i+r,j}^* \langle \hat{b}_j^\dagger \hat{b}_j \rangle, \qquad \langle \hat{a}_i \hat{a}_{i+r} \rangle = \sum_j V_{i,j}^* V_{i+r,j}^* \langle \hat{b}_j^2 \rangle \tag{4.70}$$

In both cases, one has to evaluate N normally-ordered moments in the $\hat{b}$-basis. By the previous estimates, each normally-ordered moment takes $O(N^3)$ floating-point operations to evaluate, so that in general it takes $O(N^4)$ floating-point operations to evaluate a quadratic correlation function.

Quartic correlation functions

We now turn to evaluate quartic correlators using the same re-expansion technique. We first compute the pair-correlation function:

$$\langle \hat{a}_i^{\dagger 2} \hat{a}_{i+r}^2 \rangle = \sum_{j_1,j_2,j_3,j_4} V_{i,j_1} V_{i,j_2} V_{i+r,j_3}^* V_{i+r,j_4}^* \langle \hat{b}_{j_1}^\dagger \hat{b}_{j_2}^\dagger \hat{b}_{j_3} \hat{b}_{j_4} \rangle \tag{4.71}$$

$$= 2 \sum_{j \neq j'} V_{i,j} V_{i,j'} V_{i+r,j}^* V_{i+r,j'}^* \langle \hat{b}_j^\dagger \hat{b}_{j'}^\dagger \hat{b}_j \hat{b}_{j'} \rangle + \sum_{j,j'} V_{i,j}^2 V_{i+r,j'}^{*2} \langle \hat{b}_j^{\dagger 2} \hat{b}_{j'}^2 \rangle. \tag{4.72}$$

The calculation for the density-density correlation function (assuming $r \neq 0$) is very similar:

$$\begin{aligned}\langle \hat{n}_i \hat{n}_{i+r} \rangle &= \sum_{j_1,j_2,j_3,j_4} V_{i,j_1} V_{i+r,j_2} V^*_{i,j_3} V^*_{i+r,j_4} \langle \hat{b}^\dagger_{j_1} \hat{b}^\dagger_{j_2} \hat{b}_{j_3} \hat{b}_{j_4} \rangle \\ &= \frac{1}{2} \sum_{j \neq j'} |V_{i,j} V_{i+r,j'} + V_{i+r,j} V_{i,j'}|^2 \langle \hat{b}^\dagger_j \hat{b}^\dagger_{j'} \hat{b}_j \hat{b}_{j'} \rangle + \sum_{j,j'} V_{i,j} V_{i+r,j} V^*_{i,j'} V^*_{i+r,j'} \langle \hat{b}^{\dagger 2}_j \hat{b}^2_{j'} \rangle.\end{aligned} \tag{4.73}$$

In both cases, one has to evaluate $O(N^2)$ normally-ordered moments in the $\hat{b}$-basis. By the previous estimates, each normally-ordered moment takes $O(N^3)$ floating-point operations to evaluate, so that in general it takes $O(N^5)$ floating-point operations to evaluate a quartic correlation function.

4.11 Phenomenology of the exact solution

4.11.1 $SU(1,1)$ coherent states

When $\delta = N/2$, the purification $|\Psi_{\hat{T}}\rangle$ is an $SU(1,1)$-coherent state in the sense of Barut and Girardello [1971], that is, an eigenstate of the lowering operator $\hat{K}_-$. This holds regardless of whether the representation is unitary or not:

$$\hat{K}_- |\Psi_{\hat{T}}\rangle = \sum_{m=0}^{\infty} \frac{(-1)^m}{(N/2)_m} \frac{\hat{K}_- \hat{K}_+^m}{m!} |h_0\rangle = \sum_{m=0}^{\infty} \frac{(-1)^{m+1}}{(N/2)_{m+1}} (m+1)(N/2+m) \frac{\hat{K}_+^m}{m!} |h_0\rangle = -|\Psi_{\hat{T}}\rangle. \tag{4.74}$$

The above identity has a dramatic effect on the physical steady state $\hat{\rho}_{\mathrm{ss}}$. In particular, fluctuations in $K := \langle \hat{k}_- \rangle$ exactly vanish when $\delta = N/2$, whereas fluctuations in the onsite pairing $\phi := \langle \hat{a}^2_j \rangle$ remain nonzero and show no special behavior. Here, $\hat{k}_- := \frac{1}{2} \sum_{ij} (uM^{-1})_{ij} \hat{a}_i \hat{a}_j$ is a pair-lowering operator involving only the physical lattice modes $\hat{a}_j$.

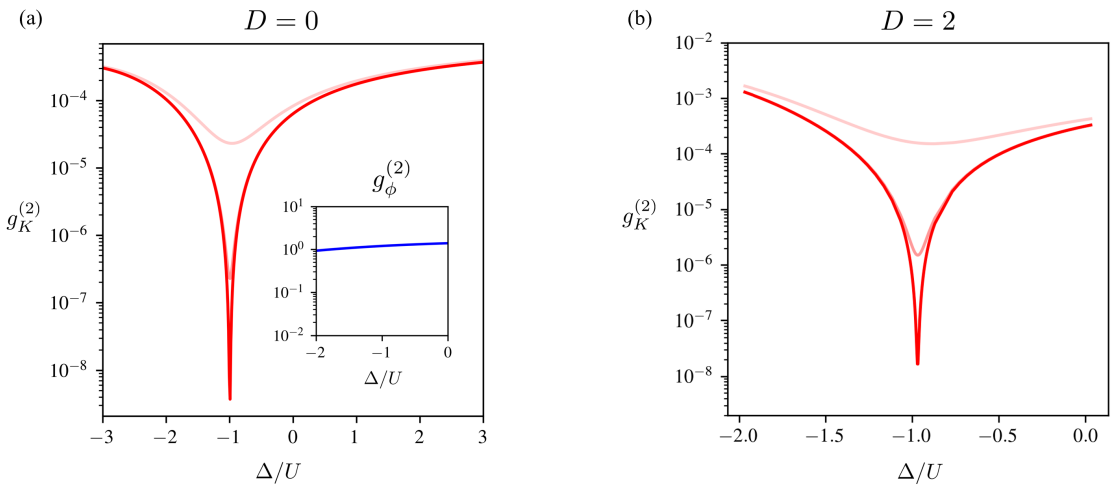

Figure 4.6: Bosonic pairing fluctuations near the PCS regime. (a) Here, we plot the normalized fluctuations $g_K^{(2)} := (\langle \hat{k}_-^\dagger \hat{k}_- \rangle - |K|^2)/|K|^2$ in the nonlocal pairing observable $K := \langle \hat{k}_- \rangle$, for different values of loss $\kappa \in \{0.01U, 0.1U, U\}$ (red curves; transparency increases with increasing loss). Note the sharp dip exactly at $\Delta_{\text{PCS}} = U(2-N)/N$. Here, $G = U, \Lambda = 0, N = 500$. Inset: We plot the normalized fluctuations $g_\phi^{(2)} := (\langle \hat{a}^{\dagger 2} \hat{a}^2 \rangle - |\phi|^2)/|\phi|^2$ in the local onsite pairing $\phi := \langle \hat{a}_j^2 \rangle$. Parameters same as before. (b) Same as panel (a), but for $D = 2$ with $N = 8 \times 8$ and periodic boundary conditions. Here, $\Lambda = 2U = 4G$.

4.11.2 DMFT analysis of the $D = 0$ model

DMFT expansion

We now use dynamical mean field theory (DMFT) to derive a large-N expansion for our $D = 0$ model. To derive this expansion, we first fix a site (labelled $j = 0$) in our lattice model, and attempt to integrate-out the remaining degrees of freedom. Typically this integration procedure is carried out within the Schwinger-Keldysh formalism, which states that the

action for the full $D = 0$ lattice model is

$$S = \int dt \sum_{\sigma=\pm 1} \sigma \Big[\sum_j (\alpha_{j,\sigma} \partial_t \alpha^*_{j,\sigma} - \Delta n_{j,\sigma} + G(\alpha^2_{j,\sigma} + c.c.)) + \frac{U}{N} \Big(\sum_j n_{j,\sigma} \Big)^2 \Big] + i\kappa \int dt \sum_j \Big(\alpha_{j,+} \alpha_{j,-} - \frac{1}{2} \sum_{\sigma=\pm 1} |\alpha_{j,\sigma}|^2 \Big), \tag{4.75}$$

$$n_{j,\sigma} := |\alpha_{j,\sigma}|^2 \tag{4.76}$$

where $\alpha_{j,\pm} = \alpha_{j,\pm}(t)$ are complex fields associated to the bosonic degrees of freedom $\hat{a}_j, \hat{a}^\dagger_j$, as is standard in the Keldysh formalism. Within this formalism, the goal is now to compute the effective action for a fixed site $j = 0$. One can compute a large-N asymptotic expansion for the effective action for the fields $\alpha_{0,+}, \alpha_{0,-}$, which takes the following self-consistent form at leading-order:

$$S_{\text{eff}} = S_{\text{free}} + \int dt \sum_{\sigma=\pm 1} 2\sigma U n_{0,\sigma} \langle n_{0,\sigma} \rangle_{\text{eff}} + O(N^{-1}), \tag{4.77}$$

where S_{free} is the Keldysh action for a single site, without the Bose-Hubbard interaction, and $\langle \cdot \rangle_{\text{eff}}$ denotes an average taken with respect to the effective action. Note that this leading-order theory is Markovian. Therefore, as $N \to \infty$, one can evolve observables for a fixed site using the self-consistent Lindbladian

$$\mathcal{L}_{\text{eff}} \hat{\rho}_0 = -i[\Delta_{\text{eff}}(\hat{\rho}_0) \hat{n}_0 + G \hat{a}_0^{\dagger 2} + h.c., \hat{\rho}_0] + \kappa \mathcal{D}[\hat{a}_0] \hat{\rho}_0, \qquad \Delta_{\text{eff}}(\hat{\rho}_0) = \Delta + 2U \text{Tr}[\hat{\rho}_0 \hat{n}_0]. \tag{4.78}$$

One can then solve for the steady-state density $\bar{n} \equiv \bar{n}^{\text{MF}}$ within this leading-order mean-field description, leading to a cubic equation for $\bar{n}^{\text{MF}}$. This leads to a large-N phase diagram where regions exist with up to three self-consistent solutions for the density. We obtain good

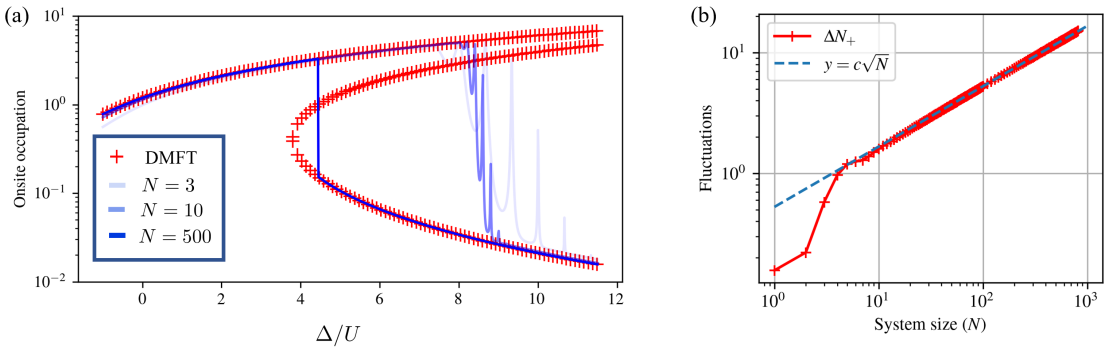

Figure 4.7: Benchmarking DMFT using the exact solution (in $D = 0$). (a) Here, we plot the mean onsite occupation $\bar{n}$ as a function of detuning, for $G = U, \kappa = 0.01U$. Note that we obtain asymptotic agreement with DMFT in the limit that $N \to \infty$. To see work where a similar kind of mean field theory was benchmarked by exact diagonalization results in a permutation-symmetric spin model, see Wang and Fazio [2021]. (b) Here, we plot the rms fluctuations in $\hat{N}_+$ using the exact solution. We observe the empirical scaling $\Delta N_+ := \sqrt{\langle \hat{N}_+^2 \rangle - \langle \hat{N}_+ \rangle^2} = O(N^{1/2})$ so that $\Delta N_+/N$ vanishes as $N \to \infty$, ensuring the asymptotic convergence of the wavefunction $|\Psi_{\hat{T}}\rangle$ of the paired boson gas to the form predicted by DMFT. Here, $G = U/10, \kappa = U/100$, and $\Delta = 0$.

agreement between this leading-order DMFT description and the exact solution, and find that

- The location Δ_c of the 1st-order phase transition obtained from the exact solution approaches the location of the bifurcation in the MFT cubic self-consistency condition as $N \to \infty$. However, this convergence is extremely slow (finite-size effects are still noticeable for $N \sim 10^3$).

- The tristable region of the mean-field phase diagram has a unique point with maximal loss rate κ_*. Let (Δ_*, κ_*) denote this point. We call this point the *mean-field critical-point*. We find that *the mean-field critical point is precisely the same as the critical point* in the phase diagram obtained from the exact solution, that is,

$$\kappa_* = \kappa_c, \qquad \Delta_c(\kappa_c) = \Delta_*.$$

Establishing the validity of DMFT

Normally DMFT expansions are hard to rigorously justify directly, even in the limit of large coordination number $z \to \infty$. We will nonetheless give the standard justification here, and then see how the exact hTRS solution yields a much more direct perspective, at least with respect to the steady state problem. The usual justification for the asymptotic result (4.77) is as follows: note that we can view our Hubbard interaction as a general (extended) Bose-Hubbard interaction for a general graph $\mathcal{G}$ with $\mathcal{G} = K_N$, i.e. a complete graph,

$$\frac{U}{N}\Big(\sum_j \hat{n}_j\Big)^2 = \frac{U}{z}\sum_{\langle i,j\rangle\in\mathcal{G}} \hat{n}_i\hat{n}_j\Big|_{\mathcal{G}=K_N}. \tag{4.79}$$

The large-N asymptotic result (4.77) can be established, by copying exactly the calculation in Scarlatella et al. [2021b], Strand et al. [2015], but by performing the cumulant expansion therein with respect to the density fields $n_{j,\sigma}$ instead of the ordinary complex fields $\alpha_{j,\sigma}$ (the calculation is relatively unilluminating, and for the sake of brevity, we omit it here). This has the effect of establishing the desired result for $\mathcal{G}$ a regular tree graph with coordination number N, instead of a complete graph. After performing such a calculation, one then waves one's hands and claims that the same asymptotics (4.77) holds on a complete graph.

The exact solution yields a more direct way to check the validity of (4.77), at least from the perspective of the steady-state. The steady-state(s) predicted by the leading-order DMFT dynamics $\mathcal{L}_{\text{eff}}$ admit the following purification:

$$|\Psi_{\text{DMFT}}\rangle = \sum_{m=0}^{\infty}\frac{1}{m!}\Big(\frac{2\hat{K}_+}{2U\bar{n}^{\text{MF}}-\Delta_{\text{eff}}}\Big)^m|h_0\rangle, \tag{4.80}$$

where $\bar{n}^{\text{MF}}$ is any solution to the cubic self-consistency condition mentioned in the preceeding subsection. We can directly see that the exact solution indeed converges to this form as $N \to \infty$. We begin by noticing the asymptotics $(N/2U)^m\Gamma(\delta)/\Gamma(m+\delta) \underset{N\to\infty}{\sim} (2Um/N-\Delta_{\text{eff}})^{-m}$

for the Gamma function, which yields the asymptotic estimate

$$|\Psi_{\hat{T}}\rangle \underset{N\to\infty}{\sim} \sum_{m=0}^{\infty} \frac{1}{m!}\left(\frac{2\hat{K}_+}{2Um/N - \Delta_{\text{eff}}}\right)^m |h_0\rangle. \tag{4.81}$$

Notice that the above is identical to (4.80), provided that we replace $m \sim 2\hat{N}_+$ with its average value. Indeed, fluctuations in $\hat{N}_+$ with respect to the exact solution $|\Psi_{\hat{T}}\rangle$ can be evaluated directly via (4.39) and shown to be of order $O(N^{1/2})$, so that m/N becomes a deterministic variable in the large-N limit. The series above thus becomes well-concentrated about $m/N \sim \bar{n}^{\text{MF}}$, leading to the self-consistent form (4.80) predicted by leading-order DMFT.

Establishing the location of the critical point

We will now test the claim made previously, namely that the critical point obtained from the exact solution lies exactly at the mean-field critical point, i.e. we will compute the maximum magnitude of the susceptibility

$$\chi_{\max}(\kappa, N) := \sup_{\Delta} \left|\frac{\partial \bar{n}}{\partial \Delta}\right| \tag{4.82}$$

where all other parameters are held fixed. We confirm that $\chi_{\max}$ diverges as $N \to \infty$ whenever $\kappa < \kappa_*$, and converges otherwise. Repeatedly testing for the convergence of $\chi_{\max}$ in the thermodynamic limit for different values of κ allows us to approximately compute the rate at which $\chi_{\max}$ diverges, thus obtaining the critical exponent γ:

$$\lim_{N\to\infty} \chi_{\max}(\kappa, N) \underset{\kappa\to\kappa_*^+}{\sim} \tau^{-\gamma}, \tag{4.83}$$

with $\tau := (\kappa - \kappa_*)/\kappa_*$. Using a very crude polynomial fitting algorithm, we estimate $\gamma \approx -1$ (see Figure 4.8(b)).

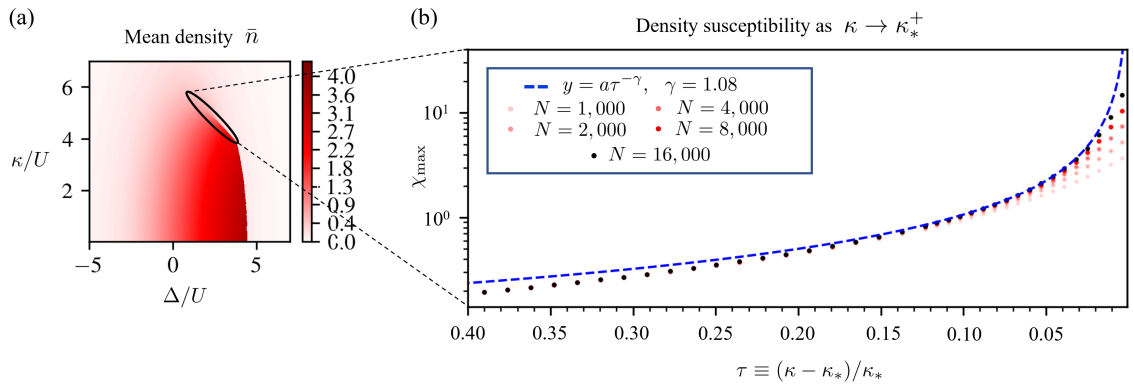

Figure 4.8: Confirming the location of the critical point using the exact solution. (a) Average density as a function of detuning Δ and loss κ, with $N = 500$, $\Lambda = 0$, and $G = U$. Phase boundaries can be seen, provided that $\kappa < \kappa_* \approx 4U$. (b) Maximum absolute value of the susceptibility as a function of κ, for $\kappa \to \kappa_*^+$. Here, $\Lambda = 0$, and $G = U/10$. The polynomial fit used to estimate γ is depicted (dashed blue line).

4.11.3 Semiclassical limit

We now investigate our model without the $D \equiv 0$ restriction, but in the semiclassical limit $\bar{n} \gg 1$. When the onsite photon occupation is large, the dynamics of the field amplitudes $\alpha_j(t) := \mathrm{Tr}[\hat{\rho}(t)\hat{a}_j]$ is well captured by the semiclassical equation of motion

$$iu^{-1}\partial_t \beta_j = 2\lambda_j \beta_j^* + \beta_j \left[\left(2\sum_k |\beta_k|^2 + 1 \right) - \Delta_{\mathrm{eff}}/u \right], \tag{4.84}$$

where

$$\beta_j^* \equiv \sum_{k=1}^{N} V_{j,k} \alpha_k^* \tag{4.85}$$

is the change-of-coordinates on the classical phase space induced by the unitary V in the Autonne-Takagi factorization $M/u = V\Sigma V^T$. We now demonstrate the claim made earlier, namely that the stable stationary states of the above dynamical system are spheres in phase space formed by the max-pairing modes. In particular, the semiclassical fixed-points satisfy

the equations

$$0 = 2\lambda_j \beta_j^* + \beta_j \left[\left(2 \sum_k |\beta_k|^2 + 1 \right) - \Delta_{\text{eff}}/u \right] \tag{4.86}$$

From now on, for clarity, we will use the symbol X to denote the set of fixed points. Note that, trivially, $\vec{0} \in X$. However, we are interested in the *nonzero* fixed points. Therefore, let $\vec{\beta}_{\text{ss}} \in X$ be a nonzero fixed point, i.e. a nonzero solution to (4.86). Whenever $\beta_{j,\text{ss}} \neq 0$, we can divide through by β_j in (4.86), yielding a constraint on the phase $e^{i\theta_j} \equiv \beta_{j,\text{ss}}/|\beta_{j,\text{ss}}|$:

$$e^{-2i\theta_j} = -\frac{2R_{\text{ss}}^2 + 1 - \Delta_{\text{eff}}/u}{2\lambda_j}, \tag{4.87}$$

where $R_{\text{ss}}^2 \equiv \sum_j |\beta_{j,\text{ss}}|^2$. In particular, if $\beta_{i,\text{ss}}, \beta_{j,\text{ss}} \neq 0$ is any pair of nonzero components of $\vec{\beta}_{\text{ss}}$, then, by taking the absolute value of the above equation,

$$\frac{1}{2\lambda_i} |2R_{\text{ss}}^2 + 1 - \Delta_{\text{eff}}/u| = \frac{1}{2\lambda_j} |2R_{\text{ss}}^2 + 1 - \Delta_{\text{eff}}/u|. \tag{4.88}$$

In particular, $\kappa \neq 0$ and so we can divide both sides by $|2R_{\text{ss}}^2 + 1 - \Delta_{\text{eff}}/u|$. Therefore, $\lambda_i = \lambda_j$. We can go even further: (4.87) also means that $e^{2i\theta_i} = e^{2i\theta_j}$. In summary, for each $\vec{\beta}_{\text{ss}} \in X$, there exists a λ, θ such that, for all nonzero components of $\vec{\beta}_{\text{ss}}$,

$$\lambda_j = \lambda, \qquad \beta_{j,\text{ss}} = e^{i\theta} x_j, \qquad x_j \in \mathbb{R}, \tag{4.89}$$

where θ is independent of j and uniquely determined by λ in the following way:

$$e^{-2i\theta} = -\frac{2R_{\text{ss}}^2 + 1 - \Delta_{\text{eff}}/u}{2\lambda}. \tag{4.90}$$

By taking the real and imaginary parts of the above equation, we also have

$$2\lambda \sin 2\theta = -\kappa/2u, \tag{4.91}$$

$$2\lambda \cos 2\theta = -(2R_{\rm ss}^2 + 1 - \Delta/u). \tag{4.92}$$

Instability of solutions with $\lambda < \lambda_*$

Let $\vec{\beta}_{\rm ss} \in X$ be a nonzero fixed point, and λ the corresponding singular value. Also, let $\lambda_* \equiv \sup_j \lambda_j$ denote the maximum singular value. We will now show that if $\lambda \neq \lambda_*$, then $\vec{\beta}_{\rm ss}$ is unstable. For this purpose, it will be useful to rewrite the equations of motion in a coordinate system $(\beta'_1, \ldots, \beta'_N)$ that is adapted to $\vec{\beta}_{\rm ss}$, namely such that

$$(\beta'_{1,\rm ss}, \ldots, \beta'_{N,\rm ss}) = (e^{i\theta}R, 0, \ldots, 0). \tag{4.93}$$

Crucially, by the arguments in the preceeding subsection, we can achieve this via a rotation of the mode amplitudes β_j with $\lambda_j \equiv \lambda$:

$$\beta'_j = \begin{cases} \sum_{\lambda_k=\lambda} A_{j,k}\beta_k & \lambda_j = \lambda \\ \beta_j & \lambda_j \neq \lambda \end{cases}, \qquad A \in O(s_\lambda, \mathbb{R}), \tag{4.94}$$

where s_λ denotes the multiplicity of the singular value λ. Since the above transformation is a symmetry of the equations of motion (4.84), the equations of motion are covariant with respect to this transformation:

$$iu^{-1}\partial_t \beta'_j = 2\lambda_j(\beta'_j)^* + \beta'_j\left(2\sum_k |\beta'_k|^2 + 1 - \Delta_{\rm eff}/u\right). \tag{4.95}$$

Now let $\delta\beta'_j \equiv \beta'_j - \beta'_{j,\mathrm{ss}}$ denote the fluctuations about $\vec{\beta}_{\mathrm{ss}}$. Assuming these fluctuations are small, we can obtain linearized equations of motion for these fluctuations:

$$iu^{-1}\partial_t \delta\beta'_j = 2\lambda_j\left((\delta\beta'_j)^* - \frac{\lambda}{\lambda_j}e^{-2i\theta}\delta\beta'_j\right) + 2\beta'_{j,\mathrm{ss}}\sum_k((\beta'_{k,\mathrm{ss}})^*\delta\beta'_k + c.c.) + O(\delta\beta'^2) \quad (4.96)$$

where we have implicitly used (4.87). We now wish to argue that, if $\lambda \neq \lambda_*$, then the Hurwitz criterion fails, that is, the associated dynamical matrix contains an eigenvalue with positive real part. It suffices to examine the stability of the fluctuations $\delta\beta'_j$ for $j \neq 1$, which evolve within this linear approximation as follows:

$$iu^{-1}\partial_t \delta\beta'_j = 2\lambda_j\left((\delta\beta'_j)^* - \frac{\lambda}{\lambda_j}e^{-2i\theta}\delta\beta'_j\right) \quad (4.97)$$

$$= 2\lambda_j(\delta\beta'_j)^* - \frac{\kappa}{2}\delta\beta'_j - i\left(\Delta - u(2R_{\mathrm{ss}}^2 + 1)\right)\delta\beta'_j, \quad (4.98)$$

where we have shown explicitly that this is the equation of motion for a detuned parametric amplifier, with detuning modified by the presence of the Hubbard interaction u. Proceeding with the calculation, we then split the fluctuations into real and imaginary parts via $e^{-i\theta}\delta\beta'_j = \delta x_j + i\delta y_j$, and obtain the equations of motion

$$u^{-1}\partial_t(\delta x_j + i\delta y_j) = -2\lambda_j e^{-2i\theta}\left((1+\lambda/\lambda_j)\delta y_j + i(1-\lambda/\lambda_j)\delta x_j\right). \quad (4.99)$$

The corresponding eigenvalues of the dynamical matrix, using (4.91), are

$$\gamma_j^{\pm} = -\kappa/2 \pm \sqrt{(\kappa/2)^2 - 4u^2(\lambda^2 - \lambda_j^2)}, \quad (4.100)$$

Therefore, if $\lambda_j > \lambda$, then the eigenvalue γ_j^+ has positive real part. Therefore, if $\lambda \neq \lambda_*$, then $\vec{\beta}_{\mathrm{ss}}$ is unstable. We also have a partial converse statement: if $\lambda_j < \lambda$, then the fluctuations $\delta\beta'_j$ are stable.

Stability of solutions with $\lambda = \lambda_*$

Let $\vec{\beta}_{\rm ss} \in X$ be a nonzero fixed point with corresponding singular value λ_*. We will now investigate the conditions under which $\vec{\beta}_{\rm ss}$ is stable. By (4.100), the fluctuations $\delta\beta'_j$ for $j = 2, 3, \ldots N$ are all appropriately damped. We thus must investigate the stability of the remaining fluctuations $\delta\beta'_1$, which have the following linearized equations of motion:

$$u^{-1}\partial_t(e^{-i\theta}\delta\beta'_1) = -4\lambda_* e^{-2i\theta}\delta y_1 - 4iR_{\rm ss}^2\delta x_1. \tag{4.101}$$

The corresponding eigenvalues of the dynamical matrix, using (4.91-4.92), are

$$\gamma_j^{\pm} = -(\kappa/2) \pm \sqrt{(\kappa/2)^2 - 8u^2R_{\rm ss}^2(2R_{\rm ss}^2+1) + 8u\Delta R_{\rm ss}^2}. \tag{4.102}$$

Therefore, $\vec{\beta}_{\rm ss}$ is stable if and only if

$$8u^2R_{\rm ss}^2(2R_{\rm ss}^2+1) + 8u\Delta R_{\rm ss}^2 > 0, \tag{4.103}$$

which happens if and only if $u^2(2R_{\rm ss}^2+1) - u\Delta > 0$. To see whether this criterion is satisfied, we must use the fact that $\vec{\beta}_{\rm ss}$ is a fixed point in order to obtain an additional constraint on $R_{\rm ss}$. In particular, taking the absolute value squared of (4.87) yields a quadratic equation for $R_{\rm ss}^2 + 1$, with two possible solutions:

$$2R_{\rm ss}^2 + 1 = \Delta/u \pm \sqrt{(2\lambda_*)^2 - (\kappa/2)^2}. \tag{4.104}$$

Therefore, criterion (4.103) is satisfied if and only if

$$R_{\rm ss} = \sqrt{\frac{\Delta/u - 1 + \sqrt{(2\lambda_*)^2 - (\kappa/2)^2}}{2}} > 0. \tag{4.105}$$

Finally, let β_j for $j = 1, 2, \ldots, s$ denote the eigenmodes corresponding to the maximum singular value λ_*, i.e. the so-called "max-pairing modes". Since rotations $A \in O(s, \mathbb{R})$ of the max-pairing modes are symmetries of the equations of motion, any such rotation A must send a stable fixed point to another stable fixed point. Therefore, when the inequality (4.105) is satisfied, the space $X^{\text{stab.}} \subset X$ of nonzero stable fixed points is a sphere:

$$X^{\text{stab.}} = e^{i\theta}\left\{ x_j \in \mathbb{R}^s : \quad \sum_{\lambda_j = \lambda_*} x_j^2 = R_{\text{ss}}^2 \right\} \tag{4.106}$$

In particular, when $s > 1$, the fluctuations tangent to $X^{\text{stab.}}$ are Goldstone modes, i.e. zero-modes for the linearized dynamics. We can verify this explicitly by fixing a point $\vec{\beta}_{\text{ss}} \in X^{\text{stab.}}$, and expanding the linearized equations of motion for the resulting fluctuations $e^{-i\theta}\delta\beta_j' = \delta x_j + i\delta y_j$, in the coordinate frame adapted to $\vec{\beta}_{\text{ss}}$:

$$iu^{-1}\partial_t(\delta x_j + i\delta y_j) = -4i\lambda_* e^{-2i\theta}\delta y_j, \qquad j = 2, \ldots, s \tag{4.107}$$

In particular, the real-components $\delta x_j \in T_{\vec{\beta}_{\text{ss}}} X^{\text{stab.}}$ of the fluctuations are zero modes of the dynamical matrix, as was expected.

4.12 Mathematical background

4.12.1 Proof of the $SU(1,1)$ decomposition theorem

We now establish the decomposition (4.50). To make our task easier, we establish the desired decomposition for a dense subspace of the Hilbert space. The corresponding decomposition for the full Hilbert space can then be proven using standard functional-analytic techniques.

In particular, let $V^{(j)}$ be the local nonunitary $SU(1,1)$ representations defined in (4.49). We define $W^{(j)} \subset V^{(j)}$ to be the *algebraic* part of each representation, that is, the part of the representation consisting of finite linear superpositions of Fock staes:

$$W^{(j)} := \left\{ \sum_n a_n \hat{\beta}_{j,+}^{\dagger n} |h_0\rangle \in V^{(j)}, \qquad \text{finitely many } a_n \text{ nonzero} \right\} \tag{4.108}$$

The above subspaces allow us to conveniently establish the following theorem:

Theorem. *The global nonunitary $SU(1,1)$ representation $\otimes_j W^{(j)}$ decomposes into irreducible subrepresentations as follows*:

$$\otimes_j W^{(j)} \simeq \bigoplus_{l=0}^{\infty} \left(\bigoplus_{p=1}^{d_l} W_l^{(p)} \right), \tag{4.109}$$

where the spaces $W_l^{(p)} \subset V_l^{(p)}$ are defined analogously:

$$W_l^{(p)} := \left\{ \sum_n a_n \hat{K}_+^n |h_l^{(p)}\rangle, \qquad \text{finitely many } a_n \text{ nonzero} \right\}. \tag{4.110}$$

Proof. This can be proved by going to the Segal-Bargmann representation. Within this

representation, a finite-boson number state is represented as a polynomial:

$$\sum_n a_n \hat{\beta}_{j,+}^{\dagger n} |h_0\rangle \in W^{(j)} \to \sum_n a_n x_j^n \in \mathbb{C}[x_j], \tag{4.111}$$

with $\mathbb{C}[x_j]$ the univariate polynomial ring generated by x_j. It then follows that the tensor product $\otimes_j W^{(j)}$ is the multivariate polynomial ring $\mathbb{C}[x_1, \ldots, x_N]$ generated by the indeterminates $x_1, \ldots x_N$. Finally, creation and annihilation operators are represented by partial differential operators:

$$\hat{\beta}_{j,+} \to \frac{\partial}{\partial x_j}, \qquad \hat{\beta}_{j,+}^{\dagger} \to x_j. \tag{4.112}$$

We first establish our decomposition under the assumption that the singular values $\lambda_j \equiv \lambda$ are all completely degenerate, and then generalize the argument to the generic non-degenerate case $\lambda_i \neq \lambda_j$. In the degenerate case, the global $SU(1,1)$ representation takes the simple form

$$\hat{K}_+ = \frac{\lambda}{2} \sum_j x_j^2, \quad \hat{K}_- = \frac{1}{2\lambda} \sum_j \frac{\partial^2}{\partial x_j^2} \tag{4.113}$$

Therefore, within the Segal-Bargmann representation, our decomposition theorem is equivalent to the following decomposition of the polynomial ring $\otimes_j W^{(j)}$:

$$\mathbb{C}[x_1, ..., x_N] \simeq \bigoplus_{l=0}^{\infty} \left(\bigoplus_{p=1}^{d_l} \mathbb{C}[R^2] h_l^{(p)} \right), \tag{4.114}$$

where $R^2 = \sum_j x_j^2$, and $h_l^{(1)}, ..., h_l^{(d_l)}$ is some orthonormal basis of the space of harmonic homogeneous polynomials of degree l. When interpreted pointwise, the above isomorphism

reads as a harmonic expansion of a fixed polynomial:

$$p(x_1, ..., x_N) = \sum_{l=0}^{\infty} \sum_{p=1}^{d_l} q_l^{(p)}(R^2) h_l^{(p)}(\vec{x}) \tag{4.115}$$

where the $q_l^{(p)}$ are univariate polynomials. The decomposition (4.114) is then equivalent to the statement that the above mapping, interpreted as a mapping from the RHS to the LHS, is an isomorphism of $SU(1,1)$-representations. The representation (4.113) acts the same on both sides, so it suffices to establish the isomorphism at the vector space level, i.e. prove that the above mapping is both injective and surjective. For injectivity, it suffices to show that the subspaces $\mathbb{C}[R^2]h_l^{(p)}$ are all mutually nonintersecting (except at $\{0\}$), which can be verified by direct calculation:

$$\langle R^{2n} h_l^{(p)} | R^{2m} h_{l'}^{(q)} \rangle = \left(\frac{2}{\lambda}\right)^{4n} \delta_{p,q} \delta_{l,l'} \delta_{n,m} n! (N/2 + l)_n \tag{4.116}$$

To demonstrate surjectivity, we must demonstrate that, for *any* polynomial p on the LHS of (4.115), a decomposition of the form given on the RHS exists. This seems considerably more challenging to establish. However, here we are helped by a basic fact from harmonic analysis:

Lemma. *let p denote a homogeneous polynomial of degree l. Then*

$$p(x_1, ..., x_N) = h(\vec{x}) + R^2 q(x_1, ..., x_N), \tag{4.117}$$

where q is a homogeneous polynomial of degree $l-2$, and h is a homogeneous harmonic polynomial of degree l.

A proof is usually given in standard textbooks on harmonic function theory (see, e.g. Axler et al. [2001]). In any case, iterating the above lemma, we obtain, for any homogeneous

polynomial p a decomposition

$$p(x_1, ..., x_N) = \sum_{m=0,1,...} R^{2m} h_{\deg p - 2m}(\vec{x}), \tag{4.118}$$

where h_l denotes a homogeneous harmonic polynomial of degree l, so that the expansion (4.115) can be established simply by writing out the polynomial on the LHS of (4.115) as a sum of homogeneous components, and then expanding the harmonic polynomials appearing on the RHS of (4.118) into a basis.

The preceeding arguments constitute a proof of the theorem for the degenerate case $\lambda \equiv \lambda_j$. Therefore, all that is left is to reproduce the above proof in the non-degenerate case $\lambda_i \neq \lambda_j$. Luckily, the proof for the non-degenerate case follows immediately from the degenerate case. In particular, we can write the $SU(1,1)$ representation as

$$\hat{K}_+ = \frac{1}{2} \sum_j y_j^2, \qquad \hat{K}_- = \frac{1}{2} \sum_j \frac{\partial^2}{\partial y_j^2} \tag{4.119}$$

where we have made the change of variables $x_j \to y_j := \lambda_j^{1/2} x_j$. In particular, just by making the replacements $x_j \to y_j$ in (4.114), we obtain the desired result:

$$\mathbb{C}[y_1, ..., y_N] \simeq \bigoplus_{l=0}^{\infty} \left(\bigoplus_{p=1}^{d_l} \mathbb{C}[R^2] h_l^{(p)} \right), \tag{4.120}$$

with R^2 and $h_l^{(p)}$ defined just as in (4.114), but with the replacements $x_j \to y_j$. This completes the proof of our theorem in the non-degenerate case.

4.12.2 Exact solution for the steady-state Wigner function

We now compute a closed form for the Wigner function $W_{\rm ss}$ of the steady-state density matrix $\hat{\rho}_{\rm ss}$. The arguments in Roberts and Clerk [2020] generalize in a straightforward manner to the N-mode case. In particular, the steady-state Wigner function for our system satisfies the identity

$$W_{\rm ss}(\vec{\alpha}) = 2^N Q_{|\Psi_+\rangle}\Big(\sqrt{2}\vec{\alpha}\Big), \tag{4.121}$$

where $Q_{|\Psi_+\rangle}$ is the Husimi-Q representation of the N-mode pure state $|\Psi_+\rangle$. Therefore, to express the Wigner function $W_{\rm ss}$ of the steady state in closed form it suffices to express the Husimi-Q representation of $|\Psi_+\rangle$ in closed form. This task is solved easily via the Segal-Bargmann representation Bargmann [1961, 1967] of $|\Psi_+\rangle$, which can be calculated in a straightforward manner from (4.29):

$$\Psi_{\rm SB}(\vec{\alpha}) = \frac{{}_0F_1\big(\delta; -\frac{1}{2}\sum_{ij}\frac{M_{ij}}{u}\alpha_i\alpha_j\big)}{\sqrt{\mathcal{N}}}, \qquad \mathcal{N} = \sum_{l=0}^{\infty}\frac{\Phi_l(\vec{\lambda};N)}{(\delta)_l(\delta^*)_l}. \tag{4.122}$$

Now, the Q-function of a pure state $|\Psi\rangle$ is given by $Q_{|\Psi\rangle}(\vec{\alpha}) = \pi^{-N}|\Psi_{\rm SB}(\vec{\alpha}^*)|^2 e^{-|\vec{\alpha}|^2}$, where $\Psi_{\rm SB}$ is the Segal-Bargmann representation of $|\Psi\rangle$. Therefore, (4.121) yields

$$W_{\rm ss}(\vec{\alpha}) = \frac{1}{\mathcal{N}}\left(\frac{2}{\pi}\right)^N \left|{}_0F_1\left(\delta; -\sum_{ij}\frac{M_{ij}}{u}\alpha_i^*\alpha_j^*\right)\right|^2 e^{-2|\vec{\alpha}|^2}, \tag{4.123}$$

Scaling limit for the Wigner function

We now investigate the expression for the Wigner function in the high-density limit $M_{ij}/u \to \infty$. Note that the expression (4.123) for the Wigner function is non-negative, and thus can be interpreted as a bona-fide probability measure. In the limit $M_{ij}/u \to \infty$, this probability

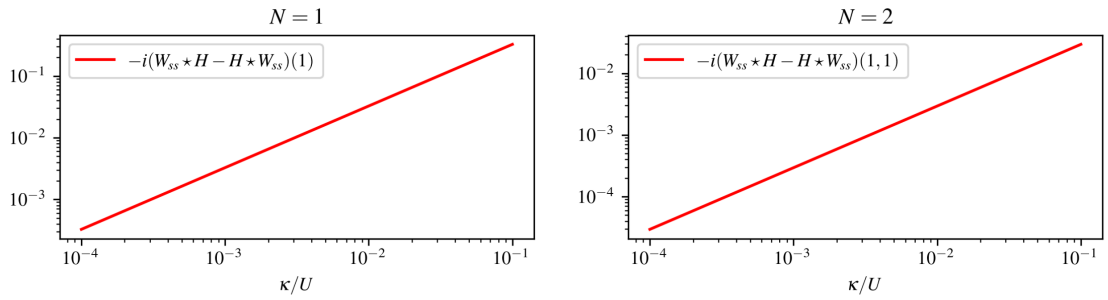

Figure 4.9: Nonthermal nature of the steady state. The exact solution (4.126) for the Wigner function can be used to symbolically check that the Hamiltonian and steady state do not commute. Here, we evaluate the phase-space commutator $H \star W_{\text{ss}} - W_{\text{ss}} \star H$ in the case $G = \kappa = U$, and $\Lambda = 0$, for the cases (a) $N = 1$, in which case we choose to evaluate the result at the phase space point $\alpha = 1$ and (b) $N = 2$, in which case we choose to evaluate the result at the phase space point $\alpha_1 = \alpha_2 = 1$. Note that, since H, W_{ss} are both purely real, the result is always purely imaginary. As expected, the result always vanishes in the limit $\kappa \to 0^+$.

measure will become supported on larger and larger regions of phase space, and so it is useful to re-scale the phase space in such a way that the resulting rescaled distribution converges to a limit.

The correct scaling turns out to be $\beta_j := \sqrt{-\lambda_*}\tilde{\beta}_j$, where $\lambda_* \equiv \sup_j \lambda_j$ is the maximum singular value appearing in the Autonne-Takagi factorization $M/u = V\Sigma V^T$, and

$$\beta_j^* \equiv \sum_{k=1}^{N} V_{j,k}\alpha_k^* \tag{4.124}$$

is the change-of-coordinates on the classical phase space of our system, induced by the unitary V appearing in the factorization. The explicit form of V can be recovered from the spectral decomposition of the Laplacian of our underlying connectivity graph. One can show that, at least when $\Delta = 0$, $\kappa = 0^+$, in which case the Bessel function sitting inside the absolute value in (4.123) becomes a hyperbolic cosine, the steady-state Wigner function $W_{\text{ss}}(\tilde{\beta})$ limits to a

uniform distribution on the sphere

$$S \equiv \left\{ (\tilde{\beta}_1, \ldots, \tilde{\beta}_s, 0, \ldots, 0) \in \mathbb{R}^N : \quad \sum_{j=1}^{s} \tilde{\beta}_j^2 = 1 \right\}, \tag{4.125}$$

where $\beta_1, \ldots, \beta_s$ are the max-pairing modes. This can be established by expanding the Wigner function (4.123) into a sum of four exponentials, and then solving the associated saddle-point equations.

4.12.3 Using the Wigner function to verify the nonthermal character of the steady state

The exact solution for the Wigner function can be used to explicitly showcase the nonequilibrium character of the steady state. One non-thermal feature of the steady state is that it does not commute with the Hamiltonian, that is, $[H, \rho_{\rm ss}] \neq 0$. Therefore, the steady state cannot be written as $\exp(-\beta \hat{H})$ for some β. This can be verified efficiently when $\Lambda = 0$, in which case we can write down the closed-form solution

$$W_{\rm ss}(\vec{\alpha}) = \left(\frac{2}{\pi}\right)^N \frac{\left| {}_0F_1\left(\delta; -2\lambda \sum_j \alpha_j^{*2}\right) \right|^2}{{}_1F_2(N/2; \delta, \delta^*; \lambda^2)} e^{-2|\vec{\alpha}|^2}, \tag{4.126}$$

with $\lambda = NG/U$ in this case corresponding to the unique singular value of the pairing matrix. To show that the steady state and the Hamiltonian do not commute, we pass to the phase-space formulation of quantum mechanics. In the phase space formulation of quantum mechanics, the noncommutativity of the steady state and the Hamiltonian is equivalent to the statement that

$$W_{\rm ss} \star H - H \star W_{\rm ss} \neq 0, \tag{4.127}$$

where $\star$ is the Moyal product Moyal [1949], and H denotes the symmetrically-ordered (i.e. Weyl) symbol of the Hamiltonian. Because H is a polynomial, the following derivative expansion terminates at a finite order and hence can be calculated symbolically in closed form using a simple computer algebra program:

$$(f \star g)(\vec{\alpha}) = \exp\left(-\frac{1}{2} \sum_{j=1}^{N} \left(\frac{\partial}{\partial x_j^*} \frac{\partial}{\partial y_j} - \frac{\partial}{\partial x_j} \frac{\partial}{\partial y_j^*} \right) \right) f(\vec{x}) g(\vec{y}) \Big|_{\vec{x}=\vec{y}=\vec{\alpha}} \tag{4.128}$$

Since both the Wigner function and Hamiltonian are generically smooth functions of $\vec{\alpha}$, the phase-space function 4.127 is generically a smooth function of $\vec{\alpha}$. In Fig. 4.9 we exhibit a single point where this phase-space function is non-vanishing.

4.13 Experimental realization using superconducting circuits

$(D = 0)$

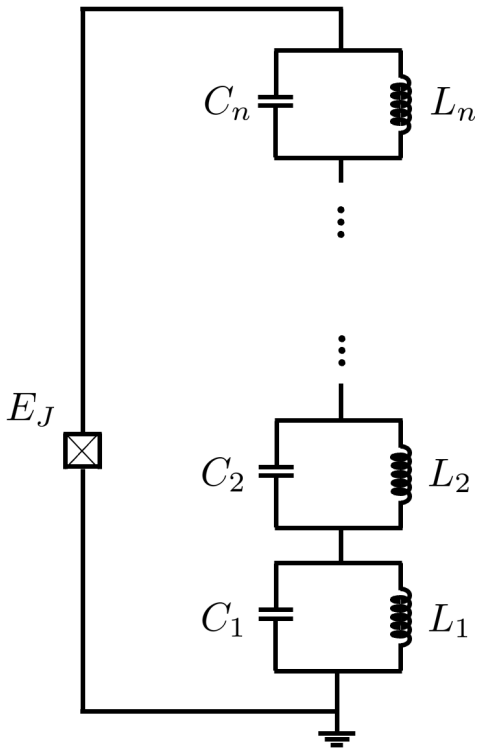

Figure 4.10: First iteration of the circuit (no driving). A Josephson tunnel junction is placed in parallel with a chain of LC oscillators to provide a global Hubbard interaction.

Our $D = 0$ model is relatively easily realizable using a simple superconducting circuit with only three nonlinear elements. To see this, we first attempt to realize the $D = 0$ Hamiltonian without the driving. We begin by placing a chain of N uncoupled LC oscillators in series. Via examination of Kirchoff's current laws, the Hamiltonian that describes the equations of motion for the chain is the following:

$$H = \sum_j \left(\frac{Q_j^2}{2C_j} + \frac{\Phi_j^2}{2L_j} \right), \tag{4.129}$$

where here, Q_j denotes the charge stored on the jth capacitor, and Φ_j denotes the time-

integrated voltage across each inductor. One may diagonalize this Hamiltonian by defining dimensionless creation- and annihilation operators

$$\hat{\Phi}_j := \Phi_j^{\text{zpf}}(\hat{a}_j + \hat{a}_j^\dagger), \qquad \hat{Q}_j := -iQ_j^{\text{zpf}}(\hat{a}_j - \hat{a}_j^\dagger), \tag{4.130}$$

where here, $Q_j^{\text{zpf}}, \Phi_j^{\text{zpf}}$ are the zero-point vacuum fluctuations of the charge and phase across the inductive and capacitive branches of each LC oscillator.

To add an infinite-range Bose-Hubbard interaction, we place a Josephson junction in parallel with the chain of oscillators (c.f. Figure 4.10). The Josephson junction, in the limit of extremely weak junction capacitance $C_J \ll C_j$, can be modelled accurately to leading order via the following interaction Hamiltonian:

$$\hat{H}_{\text{int}} = E_J \cos\bigg(\sum_j \varphi_j(\hat{a}_j + \hat{a}_j^\dagger)\bigg), \tag{4.131}$$

where $\varphi_j := \Phi_j^{\text{zpf}}/2\pi\Phi_0$. We now tune the dimensionless phase fluctuations φ_j to be parametrically small and uniform across all modes, that is $\varphi_j \equiv \varphi \ll 1$. Note that this can be done without constraining the resonant frequencies of each oscillator. Taylor's theorem then says that

$$\hat{H}_{\text{int}} = -\frac{E_J\varphi^2}{\hbar 2!}\bigg(\sum_j \hat{a}_j + h.c.\bigg)^2 + \frac{E_J\varphi^4}{\hbar 4!}\bigg(\sum_j \hat{a}_j + h.c.\bigg)^4 + O(\varphi^6). \tag{4.132}$$

We then go into a rotating frame with respect to the free Hamiltonian $H_{\text{free}} := \hbar\sum_j \omega_j \hat{n}_j$, where ω_j is the bare resonance frequency of each LC resonator in the chain. Now we choose the resonant frequencies of each mode so that the fundamental frequency Ω of the rotating-frame Hamiltonian is much larger than the rate $\hbar^{-1}E_J\varphi^2$. In this regime, the rotating-wave

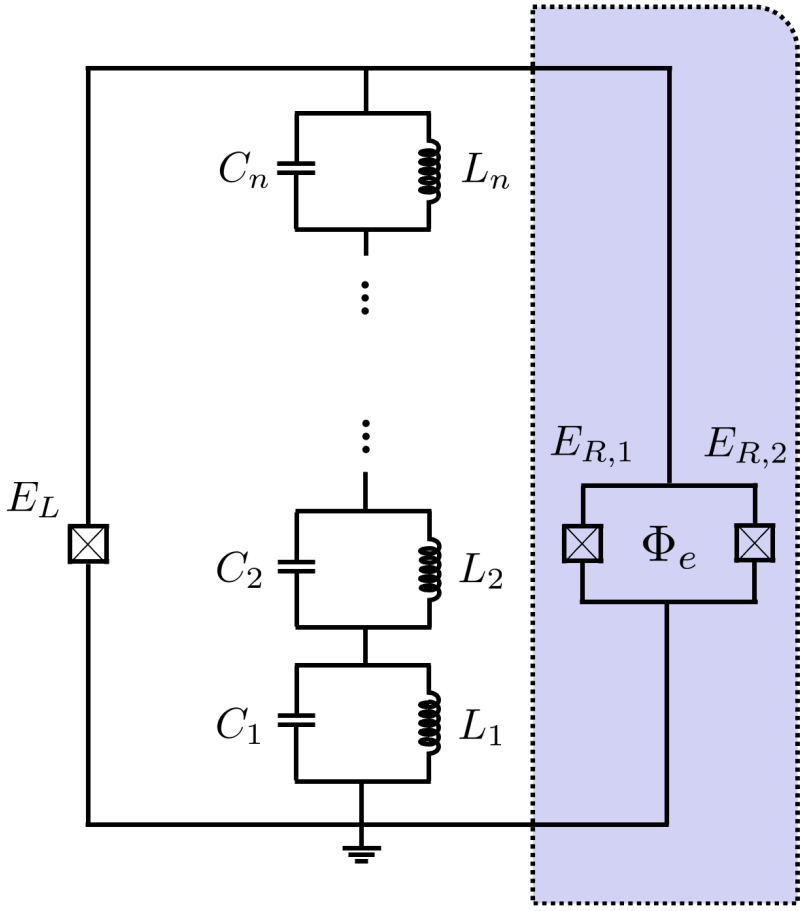

Figure 4.11: Circuit incorporating coherent two-photon driving. The global parametric drive is supplied by a flux-tunable transmon (blue shaded region).

approximation is valid and yields

$$\hat{H}_{\mathrm{RWA}} = -E_J\varphi^2 \sum_j \hat{n}_j + \frac{E_J\varphi^4}{2}\Big(\sum_j \hat{n}_j\Big)^2. \tag{4.133}$$

4.13.1 Adding a two-photon drive

To obtain the $D = 0$ Hamiltonian for our model, we just have to add two-photon driving to the above scheme. To do this, we play the same trick as above: this time we add a symmetric SQUID in parallel with the oscillator chain. Assuming that the junction capacitances in the SQUID are also much smaller than the capacitances present in the oscillator chain, the new

interaction Hamiltonian is simply

$$\hat{H}_{\text{int}} = E_L \cos\left(\varphi \sum_j \hat{a}_j + h.c.\right) + 2E_R \cos\left(\frac{\Phi_e}{2\pi\Phi_0}\right) \cos\left(\varphi \sum_j \hat{a}_j + h.c.\right), \tag{4.134}$$

where $E_R = E_{R,1}, E_{R,2}$ is the Josephson energy of each junction in the symmetric SQUID. We then choose to drive the SQUID in such a way that

$$\frac{\Phi_e}{2\pi\Phi_0} = \frac{\pi}{2} - \epsilon_p(t). \tag{4.135}$$

We also assume that $E_R \ll E_L$. As a result, we can truncate the expansion of the SQUID potential at quadratic order, while continuing to truncate the expansion of the left junction at quartic order:

$$\hat{H}_{\text{int}} = -E_R\varphi^2\epsilon_p(t)\left(\sum_j \hat{a}_j + h.c.\right)^2 - \frac{E_L\varphi^2}{2!}\left(\sum_j \hat{a}_j + h.c.\right)^2 \tag{4.136}$$

$$+ \frac{E_L\varphi^4}{4!}\left(\sum_j \hat{a}_j + h.c.\right)^4 + O(E_L\varphi^6) + O(E_R\varphi^4). \tag{4.137}$$

By modulating the pump amplitude appropriately via

$$\epsilon_p(t) := \epsilon_0 \sum_j \cos(2\omega_j - 2\omega_p)t, \tag{4.138}$$

and going into a rotating frame with respect to the free Hamiltonian $\hat{H}_{\text{free}} = \hbar\sum_j(\omega_j - \omega_p)\hat{n}_j$, and again assuming that the mode frequencies are all appropriately detuned from each other, we obtain the following rotating-wave Hamiltonian:

$$\hat{H}_{\text{RWA}} = \frac{E_L\varphi^4}{2}\left(\sum_j \hat{n}_j\right)^2 + \sum_j(\hbar\omega_p - E_L\varphi^2)\hat{n}_j - E_R\varphi^2\epsilon_0\sum_j(\hat{a}_j^2 + h.c.) \tag{4.139}$$

We thus obtain the exact parameters of our solvable model in the regime $D = 0$ (in SI units!):

$$U = \frac{NE_L\varphi^4}{2\hbar}, \quad G = -\frac{E_R\varphi^2\epsilon_0}{\hbar}, \quad \Delta = \omega_p - \frac{E_L\varphi^2}{\hbar}, \quad \varphi = \sqrt{\frac{\hbar}{2}}\frac{(L_j/C_j)^{1/4}}{2\pi\Phi_0} \equiv \text{const.} \tag{4.140}$$

4.13.2 Effect of junction capacitances

We now compute the corrections to the Hamiltonian due to junction capacitances, and demonstrate that these capacitances can be neglected when they are much smaller than the capacitances in the oscillator chain. To simplify the analysis we assume the junction capacitances in the symmetric SQUID are the same, and define a new parameter $C_\Sigma := C_L + 2C_R$ corresponding to the sum of the three junction capacitances. The Maxwell capacitance relation of the circuit, assuming the junction capacitances are all zero, is

$$\vec{q} = C_0\dot{\vec{\phi}}, \qquad C_0 := \begin{pmatrix} C_1 & -C_2 & 0 & \cdots & 0 \\ -C_2 & C_2+C_3 & -C_3 & & \vdots \\ 0 & -C_3 & C_3+C_4 & -C_4 & \\ \vdots & & -C_4 & \ddots & \\ & & & & -C_{N-1} \\ 0 & \cdots & & -C_{N-1} & C_N \end{pmatrix}, \tag{4.141}$$

where the nodal charges q_j can be expressed in terms of the charges Q_j in the capacitance chain via

$$Q_{N-j} = \sum_{k=0}^{j} q_{N-k}, \tag{4.142}$$

With the junction capacitances included, the new capacitance matrix is obtained in a very simple manner from C_0:

$$C = C_0 + \begin{pmatrix} 0 & \cdots & 0 \\ \vdots & & \vdots \\ 0 & \cdots & C_\Sigma \end{pmatrix}. \tag{4.143}$$

To obtain the corrections to the Hamiltonian that were neglected in the previous analysis, we use the Sherman-Morrison formula, which is *exact*:

$$C^{-1}_{k,k} = (C_0^{-1})_{k,k'} + \frac{C_\Sigma (C_0^{-1})_{k,N} (C_0^{-1})_{N,k'}}{1 + C_\Sigma (C_0^{-1})_{N,N}}, \tag{4.144}$$

so that the correction to the Hamiltonian is rigorously

$$\delta\hat{H} = \frac{C_\Sigma}{2} \sum_{k,k'} \frac{(C_0^{-1})_{k,N} (C_0^{-1})_{N,k'}}{1 + C_\Sigma (C_0^{-1})_{N,N}} q_k q_{k'}, \tag{4.145}$$

which goes to zero as $C_\Sigma (C_0^{-1})_{i,j} \to 0$, as expected.

CHAPTER 5

THE INFINITE-RANGE DISSIPATIVE TRANSVERSE-FIELD ISING MODEL

5.1 Introduction

Dissipative transverse-field Ising (DTI) models are a paradigmatic class of open quantum systems in atomic physics, quantum information and quantum simulation. In these systems, a collection of spins interact on a lattice via Ising interactions, while subject to local magnetic fields that are transverse to the interaction axis; these fields can represent local Rabi drives in a rotating frame. Markovian dissipation is most commonly introduced via Lindblad dynamics with jump operators that induce either local dephasing Marcuzzi et al. [2014], Borish et al. [2020] or local T_1 relaxation along chosen axes Jin et al. [2018], Lee et al. [2012], Kazemi and Weimer [2023], Singh and Weimer [2022], Weimer [2015], Overbeck et al. [2017]. Interest in this model stems from its direct relevance in understanding diverse experimental platforms ranging across atomic physics. In dilute Rydberg gases, the mean-field equations of the DTI have been used to qualitatively capture bistability and hysteresis in the magnetization density when sweeping laser detunings Carr et al. [2013], Malossi et al. [2014], Paris-Mandoki et al. [2017]. In quantum simulation platforms such as trapped ions, the DTI model has been realized with tunable power-law decaying interactions $J_{ij} = J_0/|i-j|^\alpha$ that approach the infinite-range limit with $0 < \alpha < 3$ Britton et al. [2012]. More recently, arrays of Rydberg atoms, with much shorter-range and stronger Ising interactions, have emerged as a versatile platform for simulating many-body quantum systems, and have realized the DTI on, e.g. triangular and hypercubic lattices Ebadi et al. [2021], Scholl et al. [2021].

Solutions for the DTI nonequilibrium steady state have been lacking, mainly due to the difficulty in understanding the competition between the transverse field and the dissipation. Without a transverse field, the Lindblad dynamics is integrable due to the existence of a

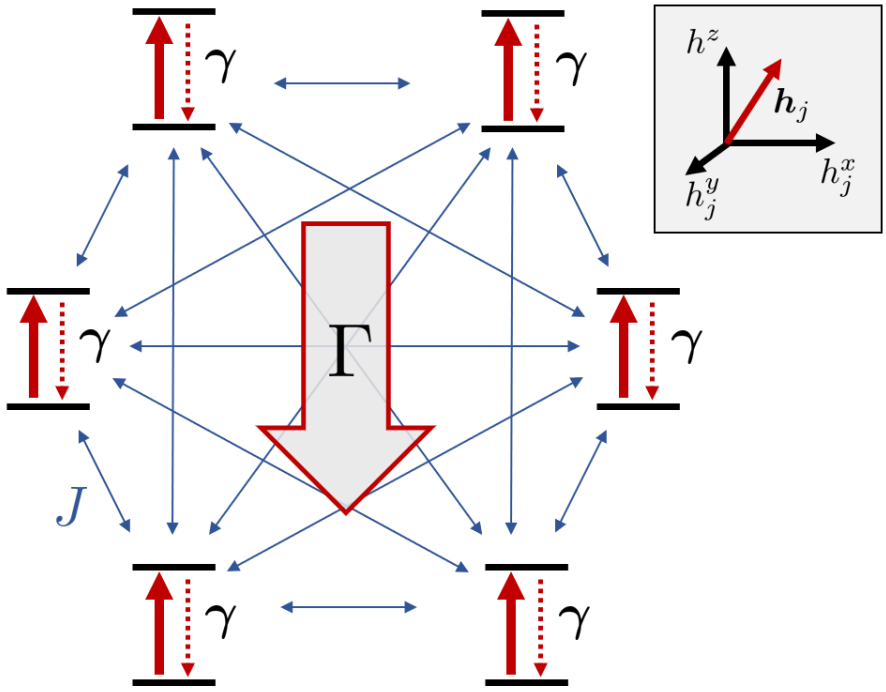

Figure 5.1: Schematic of our solvable dissipative transverse-field Ising model. A collection of N spin-1/2 particles, represented here as a collection of driven-dissipative two-level systems, is subject to local T_1 decay at a rate γ, as well as collective decay at a rate Γ. The two-level systems interact via an all-to-all Ising interaction with strength J. Inset: each spin is subject to a separate external magnetic field with both axial and transverse components. The axial component of the external field is the same for each spin, whereas the transverse part can vary.

complete set of commuting weak symmetries Foss-Feig et al. [2013], McDonald and Clerk [2022], and the steady-state problem is essentially a classical one. However, when the transverse field is present, even in the simplest case $\alpha = 0$, an analytical solution that is valid in all parameter regimes is still lacking. In this Letter, we address this issue by finding a "hidden" symmetry Roberts et al. [2021], Fagnola and Umanità [2010] in the dynamics of the DTI model, leading to an exact solution for its dissipative steady state in the infinite-range limit. Our analytical solution remains valid for systems with inhomogeneous transverse fields, where the dynamics is not simplified by permutation symmetry.

Equipped with the exact solution, we are able to derive closed-form expressions for correlation functions of any order, offering valuable insights into the system's behavior. We also investigate a novel spin blockade effect characterized by unconventional correlation properties, and uncover an effective "thermodynamic potential" which allows us to fully understand the large-N limit, and which incorporates non-mean-field information, including the location of first-order phase transitions in regimes far from the critical point Marcuzzi et al. [2014], Paz and Maghrebi [2021].

5.2 Dissipative transverse-field Ising model

We consider a dissipative system consisting of spin-1/2 particles described by the local spin observables $\hat{S}_j^\mu = \hat{\sigma}_j^\mu/2$, with $\mu = x, y, z$ denoting the spin direction and $j = 1, 2, \ldots, N$ indexing the lattice sites. Here, $\hat{\sigma}_j^\mu$ denote the Pauli matrices. The spins are coupled via an all-to-all Ising interaction, and we allow for each lattice site to experience a different magnetic field h_j^μ, which can have both transverse and axial components:

$$\hat{H}_{\mathrm{TFIM}} = J \sum_{i \neq j} \hat{S}_i^z \hat{S}_j^z + \sum_{j,\mu} h_j^\mu \hat{S}_j^\mu \tag{5.1}$$

This Hamiltonian can be viewed as representing a collection of Rabi-driven two-level systems in the rotating frame, with the transverse- and axial fields corresponding to the drive amplitude and detuning of each local two-level system.

The full dynamics of our solvable model Singh and Weimer [2022], Huybrechts et al. [2020b] also includes both collective and local T_1 decay for each two-level system and is described by the Lindblad master equation

$$\dot{\hat{\rho}} = -i[\hat{H}_{\mathrm{TFIM}}, \hat{\rho}] + \gamma \sum_j \mathcal{D}[\hat{\sigma}_j^-]\hat{\rho} + \Gamma \mathcal{D}[\hat{S}_-]\hat{\rho} \equiv \mathcal{L}\hat{\rho}, \tag{5.2}$$

where $\mathcal{D}[\hat{X}]\hat{\rho} \equiv \hat{X}\hat{\rho}\hat{X}^\dagger - (1/2)\{\hat{X}^\dagger\hat{X}, \hat{\rho}\}$ is the usual Lindblad dissipative superoperator, $\gamma \equiv 1/T_1$ is the local longitudinal relaxation rate, and Γ is a rate for collective relaxation that is relevant in many platforms, capturing effects such as superradiant decay Carr et al. [2013]. Finally, $\hat{S}_- := \hat{S}^x - i\hat{S}^y$ is the lowering operator for the collective $SU(2)$ representation $\hat{S}^\mu := \sum_j \hat{S}_j^\mu$. Throughout the rest of this Letter, we will fix the axial component of the magnetic field to be spatially uniform ($h_j^z \equiv h^z$), and will (without loss of any generality) set $h_j^y = 0$.

We focus exclusively on finding the steady states of this system, i.e. density matrices $\hat{\rho}_{\mathrm{SS}}$ satisfying

$$\mathcal{L}\hat{\rho}_{\mathrm{SS}} = 0. \tag{5.3}$$

We briefly summarize prior work on this model. In the case that the external field h_j^μ is uniform, the model is known as the dissipative LMG model Schneider and Milburn [2002], Morrison and Parkins [2008], Kessler et al. [2012], which has no known exact solution for its steady state, although there has been much work studying asymptotic expansions for the transverse-field Ising steady state in the semiclassical limit $N \to \infty$ Lee et al. [2012], Lee and Chan [2013], Ates et al. [2012], Weimer [2015], Paz and Maghrebi [2021]. Mean-field

approximations for the steady states satisfying Eq. (5.3) have been used to qualitatively model dissipative phase transitions in dilute Rydberg gases trapped in, e.g. vapor cells Carr et al. [2013], Malossi et al. [2014], Marcuzzi et al. [2014], and have been proven to be exact in the limit $N \to \infty$ Carollo and Lesanovsky [2021], Fiorelli et al. [2023]. For N finite, the dissipative steady state has been studied using numerical methods that take advantage of the permutation symmetry of the problem Huybrechts et al. [2020a], Jo et al. [2022], although these break down when the external fields are allowed to vary nontrivially.

5.3 Exact steady-state solution

Suppose that $\mathcal{L}$ were the Liouvillian for a classical master equation. In this case, a common method for solving Eq. (5.3) would be to impose detailed balance conditions on the steady-state probability density Kelley [1979]. In our case, we factor the steady state into two pieces, $\hat{\rho}_{\rm SS} = \hat{\Psi}\hat{\Psi}^\dagger$, with $\hat{\Psi}$ antilinear, and impose the *quantum* detailed balance conditions Fagnola and Umanita [2007], Fagnola and Umanità [2010]

$$\hat{H}_{\rm eff}\hat{\Psi} = \hat{\Psi}\hat{H}_{\rm eff}^\dagger, \qquad \hat{L}_k\hat{\Psi} = \hat{\Psi}\hat{L}_k^\dagger, \tag{5.4}$$

where $\hat{L}_k \in \{\hat{\sigma}_1^-, \ldots, \hat{\sigma}_N^-, \hat{S}_-\}$ ranges over the set of Lindblad operators in (2), and $\hat{H}_{\rm eff} \equiv \hat{H} - (i/2)\sum_k \hat{L}_k^\dagger \hat{L}_k$ is an effective non-Hermitian Hamiltonian which allows us to write the Lindbladian in the form

$$\mathcal{L}\hat{\rho} = -i(\hat{H}_{\rm eff}\hat{\rho} - \hat{\rho}\hat{H}_{\rm eff}^\dagger) + \sum_k \hat{L}_k\hat{\rho}\hat{L}_k^\dagger. \tag{5.5}$$

Using (5.5), we confirm that if $\hat{\Psi}$ is a solution to the detailed balance conditions (5.4), then $\hat{\rho} := \hat{\Psi}\hat{\Psi}^\dagger$ is a valid steady state of the master equation.

To solve Eqs. (5.4), we write $\hat{\Psi} = \hat{\Phi}\hat{K}$, with $\hat{K} = \hat{K}_z\hat{U}_x$, where $\hat{K}_z$ denotes complex

conjugation in the eigenbasis of the commuting operators $\hat{\sigma}_1^z, \ldots, \hat{\sigma}_N^z$, and $\hat{U}_x := \prod_j \hat{\sigma}_j^x$ is the global x-parity operator. Remarkably, whenever $\Gamma \equiv 0$ or the transverse fields are uniform, i.e. $h_j^x \equiv h^x$, we can explicitly solve for $\hat{\Phi}$, and hence obtain $\hat{\rho}_{\rm SS}$. In both situations, we obtain

$$\hat{\rho}_{\rm SS} = \hat{\Phi}\hat{\Phi}^\dagger/\mathcal{N}, \qquad \hat{\Phi} = (1 - \hat{\mathbb{S}}_-)^{h^z_{\rm eff}/J_{\rm eff}}, \tag{5.6}$$

where we have defined an effective complex Ising coupling $J_{\rm eff} := J + i\Gamma/2$, and an effective complex longitudinal field $h^z_{\rm eff} := h^z - i(\gamma + \Gamma)/2$. Finally, $\mathcal{N} \equiv \mathrm{tr}(\hat{\Phi}\hat{\Phi}^\dagger)$ is a normalization constant. We have also defined a non-unitary representation of $SU(2)$,

$$\hat{\mathbb{S}}_- := \sum_j \frac{2J_{\rm eff}\hat{\sigma}_j^-}{h_j^x}, \quad \hat{\mathbb{S}}_+ := \sum_j \frac{h_j^x \hat{\sigma}_j^+}{2J_{\rm eff}}. \tag{5.7}$$

Explicitly, $\hat{\mathbb{S}}^x := (\hat{\mathbb{S}}_+ + \hat{\mathbb{S}}_-)/2$, $\hat{\mathbb{S}}^y := (\hat{\mathbb{S}}_+ - \hat{\mathbb{S}}_-)/2i$, along with $\hat{\mathbb{S}}^z := \hat{S}^z$ satisfy the commutation relations of the $SU(2)$ algebra. However, since $\hat{\mathbb{S}}_-^\dagger \neq \hat{\mathbb{S}}_+$, $\hat{\rho}_{\rm SS}$ does not in general preserve the decomposition of the Hilbert space into irreducible representations for the $\hat{\mathbb{S}}^\mu$ operators, reflecting the non-collective nature of the dissipative dynamics. In the fully collective limit $\gamma \equiv 0$ with no Ising interaction or inhomogeneity, we recover the solution of the driven Dicke model Puri and Lawande [1979], Drummond [1980], Lawande et al. [1981], Schneider and Milburn [2002], Nagy et al. [2010a], Hannukainen and Larson [2018]. In what follows, we investigate the physics that emerges from our solution (5.6, 5.7).

5.4 Spin blockade

Setting $h^z_{\rm eff}/J_{\rm eff} = 0, 1, 2, \cdots$ yields an interesting class of states:

$$\hat{\Phi} = (1 - \hat{\mathbb{S}}_-)^n, \qquad n = 0, 1, 2, \ldots \tag{5.8}$$

This condition can be realized by setting $h^z = nJ$, where n is a non-negative integer, and letting $\gamma, \Gamma \to 0^+$. The condition on the longitudinal field can be understood as a resonance between all spins down and a configuration where all but n spins are excited. In this situation, even for drive amplitudes $h^x \lesssim J$, which would seem to preclude being able to excite many spins starting from an all-down state, one obtains a steady state with an extremely high excitation density, see Figure 5.2. The truncated form of the steady state at a blockade value of h^z leads to extremely subtle correlation properties. In particular, the rescaled coherence

$$h^x_{i_1} \cdots h^x_{i_n} \langle \hat{\sigma}^+_{i_1} \cdots \hat{\sigma}^+_{i_n} \rangle_{\rm SS} \tag{5.9}$$

is independent of $i_1, \cdots, i_n$. Furthermore, the kth-order coherence for $k > n$ vanishes. In the simplest case $n = 0$, the steady state is a completely depolarized state, and *all* coherences vanish. The case $n = 1$ is nontrivial. In this situation, the rescaled transverse magnetization $h^x_j \langle \hat{\sigma}^+_j \rangle_{\rm SS}$ is independent of j. Since

$$\mathrm{Re}\, \langle \hat{\sigma}^+_i \hat{\sigma}^+_j \rangle_{\rm SS} = \langle \hat{\sigma}^x_i \hat{\sigma}^x_j \rangle_{\rm SS} - \langle \hat{\sigma}^y_i \hat{\sigma}^y_j \rangle_{\rm SS}, \tag{5.10}$$

the transverse correlation functions coincide in this limit, c.f. the inset in Figure 5.2a.

If we also set $|J_{\rm eff}/h^x_j| \gg 1$, then we can further approximate $\hat{\Phi} \approx \hat{\mathbb{S}}^n_-$. In this limit, there is a vanishing probability to observe a spin configuration with fewer than n spins down in the steady state. In particular, the limiting distribution is a binomial distribution :

$$\mathrm{Prob}(M^z = N - k) \sim \binom{N}{k} \binom{k}{n}, \tag{5.11}$$

where here, $\hat{M}^\mu = 2\hat{S}^\mu$ is the total magnetization.

The exact solution allows us to obtain a precise bound on the modulus of $\epsilon \equiv h^z_{\rm eff}/J_{\rm eff} - n$

within which the above effects are observable. To do this, we consider the corrections to (5.8) by retaining the remaining terms in the binomial series. Assuming the transverse fields are uniform, a simple estimate comparing the Hilbert-Schmidt norms of the nth and Nth terms in the series yields the bound $|\epsilon| < w_n$, with

$$w_n = \frac{1}{(N-n-1)!}\sqrt{\lambda^{n-N}\binom{N}{n}}, \tag{5.12}$$

where we have defined $\lambda := 2|J_{\text{eff}}/h^x|^2$. The above bound yields extremely accurate estimates for the full-width at half maximum (FWHM) of each blockade feature, c.f. Figure 5.2b.

5.5 Other special cases

Another interesting situation is the case $h^z_{\text{eff}}/J_{\text{eff}} = -1, -2, -3, \cdots$, in which case $\hat{\Phi}$ is an integer power of a geometric series:

$$\hat{\Phi} = \left(\frac{1}{1-\hat{\mathbb{S}}}\right)^k = (1 + \hat{\mathbb{S}} + \hat{\mathbb{S}}^2 + \cdots)^k \tag{5.13}$$

This class of parameter regimes is nice because it allows us to discuss the case $h^z_{\text{eff}}/J_{\text{eff}} = -1$, where one can recover the exact solution via more elementary methods. Note that, in this situation, $\hat{\Phi}$ is a pure geometric series in $\hat{S}$. In this situation, if $\gamma = h^z = 0$ and the transverse fields $h_j \equiv h$ are uniform, then $\mathcal{L} \propto \mathcal{D}[1-\hat{\mathbb{S}}]$, and in a two-line calculation it may be verified that Drummond [1980], Puri and Lawande [1979]

$$\mathcal{D}[1-\hat{\mathbb{S}}]((1-\hat{\mathbb{S}})^{-1}(1-\hat{\mathbb{S}}^\dagger)^{-1}) = 0 \tag{5.14}$$

However, if $\gamma \neq 0$, then the Lindbladian can no longer be expressed as a single dissipator, and the above argument breaks down. More generally, setting the imaginary part of $h^z_{\text{eff}}/J_{\text{eff}}$ equal to zero yields the constraint $\text{Re}[h^z_{\text{eff}}/J_{\text{eff}}] = -\Gamma|h^z_{\text{eff}}|^2/(\Gamma+\gamma) < 0$. Therefore, while

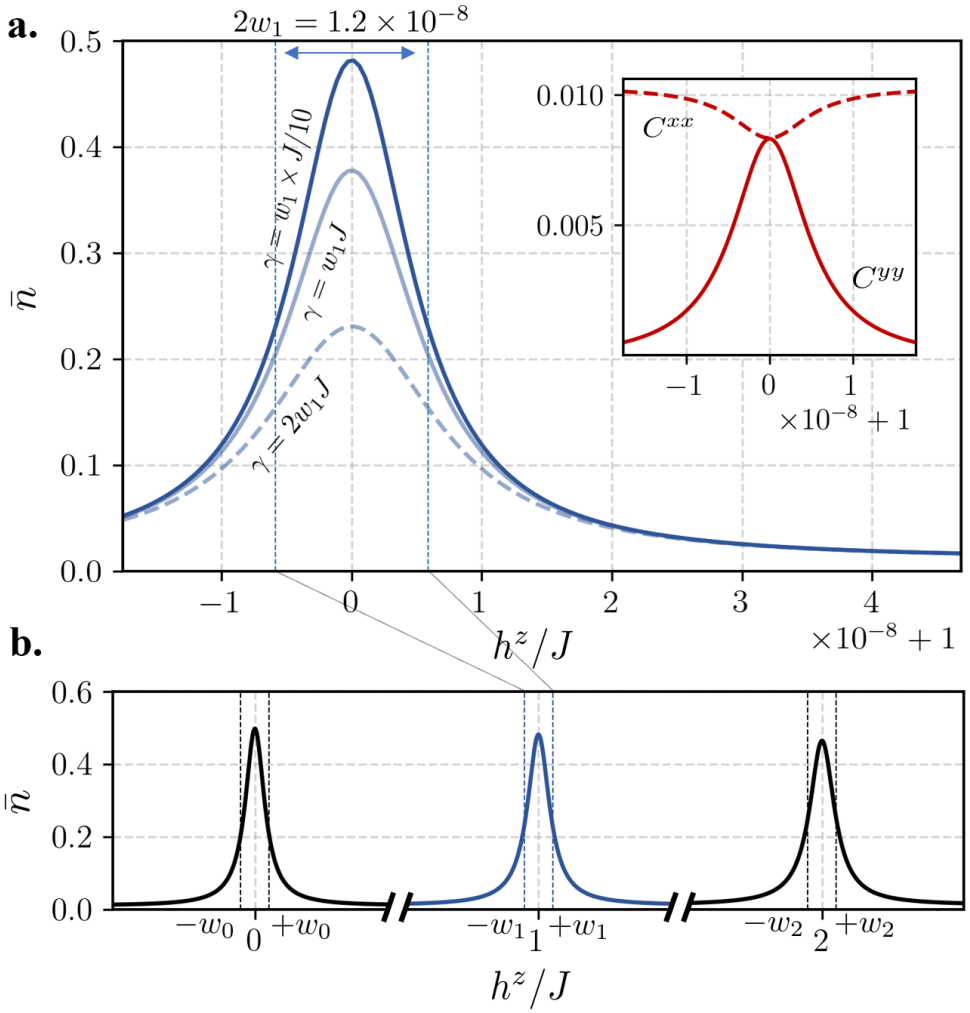

Figure 5.2: Blockade effect in the dissipative transverse-field Ising model. Top panel (a): plot of the density of up-spins, $\bar{n} = \sum_j \langle \hat{\sigma}_j^+ \hat{\sigma}_j^- \rangle_{\rm SS}/N$, near a first-order blockade, for $h^x = 4J$, $\Gamma = 0$, and $N = 22$. Inset: Plot of the correlation functions C^{xx} (dashed red line) and C^{yy} (solid red line) for the same parameters, where $C^{\mu\mu} := \langle \hat{\sigma}_1^\mu \hat{\sigma}_2^\mu \rangle_{\rm SS}$. Bottom panel (c): Close-ups of the first three blockades, $n = 0, 1, 2$. Parameters are the same as in panel (b). The exact solution yields extremely precise estimates for the widths of these features, see (5.12) for more details.

positive real values are unatainable, by appropriately tuning parameters, all negative real values of $h^z_{\text{eff}}/J_{\text{eff}}$ are achievable with nonzero loss rates. Therefore, in contrast to the spin blockades, this new class of regimes is well within the achievable parameter space, although their physical significance is less clear.

5.6 Phase transitions and the large-N limit

At the mean-field level, as one sweeps the longitudinal field h^z (corresponding to sweeping the drive-detuning in the driven qubit realization), a spin-configuration with $O(N)$ spins pointing up can become self-consistently resonant, leading to features of a first-order phase transition, such as bistability and hysteresis in the magnetization density Marcuzzi et al. [2014], Carr et al. [2013]. Our exact solution yields several new insights into this transition, including the fact that this transition is fundamentally a transition between a polarized and a depolarized state, with the magnetization density serving as a *proxy* for the amount of polarization in the steady state. The exact solution also allows us to transparently see such a phase transition emerge in the large-N limit, and reveals insights that go beyond mean-field theory, including the location of first-order phase transitions, as well as the behavior of multispin correlations across the transition.

Our starting point is the binomial expansion of $\hat{\Phi}$. Defining $r = h^z_{\text{eff}}/J_{\text{eff}}$, this is

$$\hat{\Phi} = 1 - r\sum_{k=1}^{N}(1-r)\cdots(k-1-r)\frac{\hat{\mathbb{S}}_-^k}{k!}. \tag{5.15}$$

The relative weight of each monomial $\hat{\mathbb{S}}_-^m$ in this expansion determines an important piece of physics: if the lowest powers of $\hat{\mathbb{S}}_-$ dominate, $\hat{\rho}_{\text{SS}}$ is close to a maximally mixed (depolarized) state, and the magnetization density $m^\mu = \langle \hat{M}^\mu \rangle / N$ approaches zero. On the other hand, if the highest powers of $\hat{\mathbb{S}}_-$ dominate, the steady state is close to a completely polarized state and the (longitudinal) magnetization approaches its minimum value $m^z \equiv -1$.

We can make this intuition more precise. We start with the identity $\mathrm{tr}(\hat{\mathbb{S}}_-^{\dagger M}\hat{M}^z\hat{\mathbb{S}}_-^{M'}) = -M\mathrm{tr}(\hat{\mathbb{S}}_-^{\dagger M}\hat{\mathbb{S}}_-^{M'})$ involving the (longitudinal) magnetization. As a result, we have the somewhat suggestive formula

$$\langle \hat{M}^z \rangle_{\mathrm{SS}} = -\frac{\sum_M M p_M}{\sum_M p_M} \tag{5.16}$$

where $p_M = \|\binom{r}{M}\hat{\mathbb{S}}_-^M\|_{\mathrm{HS}}^2$ is the size of the term proportional to $\hat{\mathbb{S}}_-^M$ in the expansion of $\hat{\Phi}$ with respect to the Hilbert-Schmidt norm. Eq. (5.16) makes precise the intuition described above: if the distribution p_M is biased towards terms with $M \ll N$, then the magnetization density vanishes in the thermodynamic limit, and the steady state is close to a depolarized state. The opposite occurs when the distribution is skewed towards terms with $M \to N$, in which case the steady state approaches a completely polarized state.

To understand the large-N behavior, we write the magnetization density in the suggestive form

$$m^z = -\frac{\sum_m m\, e^{-Nf(m)}}{\sum_m e^{-Nf(m)}}, \tag{5.17}$$

with $m = M/N$ now a variable ranging between zero and one, representing how polarized the steady state is. Here, $f(m) \equiv -N^{-1}\log p_{Nm}$ is a dimensionless "free energy" that controls the relative weight of the terms in the expansion of $\hat{\Phi}$. To approach the thermodynamic limit, we must hold $\bar{J}_{\mathrm{eff}} := NJ_{\mathrm{eff}}$ fixed, which fixes the renormalized parameters $\bar{r} := h^z_{\mathrm{eff}}/\bar{J}_{\mathrm{eff}}$, and $\bar{\lambda}_j := 2|\bar{J}_{\mathrm{eff}}/h^x_j|^2$.

To make it easier to calculate the free energy, we assume that the transverse fields are uniform, $h^x_j \equiv h^x$. In this case, we have an asymptotic series for $f(m)$ in the large-N limit, with a leading-order contribution

$$f(m) = \log\frac{m^m(1-m)^{1-m}}{(m-\bar{r})^{m-\bar{r}}(m-\bar{r}^*)^{m-\bar{r}^*}} - (\log\bar{\lambda} - 2)m, \tag{5.18}$$

with $O(N^{-1})$ corrections to f given later on. Since r (and hence $\bar{r}$) cannot be a non-negative real number, f must be an analytic function of m. As such, the analytic function $f(m)$ plays an analogous role to an equlibrium free energy in Landau theory Landau [1937], and lets us rigorously describe the phase transition physics in our model.

In particular, the global minima m^* of the potential f correspond to the thermodynamic limit $\lim_{N\to\infty} m^z$ of the magnetization density. Whenever f has *two* degenerate global minima, the magnetization density is the average of the two minima, and we have a first-order phase transition from a polarized to a depolarized state, c.f. Fig. 5.3c. More details can be seen in Fig. 5.3a, where we also show that the location of the first-order transition line in our model is not accurately predicted by a simple Maxwell construction (indicating the non-equilibrium nature of the model). Whenever the first three derivatives of f vanish at a global minimum, we have a quantum critical point and a second-order phase transition, c.f. Fig. 5.3b. Note that the formula (5.17) is still valid for the case of an inhomogeneous magnetic field. Later on, we study these phase transitions in the presence of transverse-field disorder, and also connect them to a sign-change in a particular connected correlation function.

5.7 Correlation functions

Finally, the exact solution allows one to analytically solve for equal-time correlation functions of arbitrary order in our spin model. For the purpose of succinctly stating the main results, it is useful to define $\hat{\sigma}^{\pm}_C \equiv \prod_{j\in C} \hat{\sigma}^{\pm}_j$, for $C \subset \{1, 2, 3, \ldots, N\}$ an arbitrary cluster of spins. Given such a cluster, it is convenient to use the notation $C^c \equiv \{1, 2, 3, \ldots, N\} \setminus C$ to denote its complement, and $|C|$ to denote its size. Given a pair of clusters C_1, C_2, our exact solution yields the expectation value of the normally-ordered product $\hat{\sigma}^{+}_{C_1} \hat{\sigma}^{-}_{C_2}$. To express the answer in a compact form, we define auxiliary regions $R_{12} = C_1 \cup C_2$, and $R_j \equiv (C_1 \cup C_2) \setminus C_j$. In the situation where the external fields h^μ are uniform, one can express the solution for the

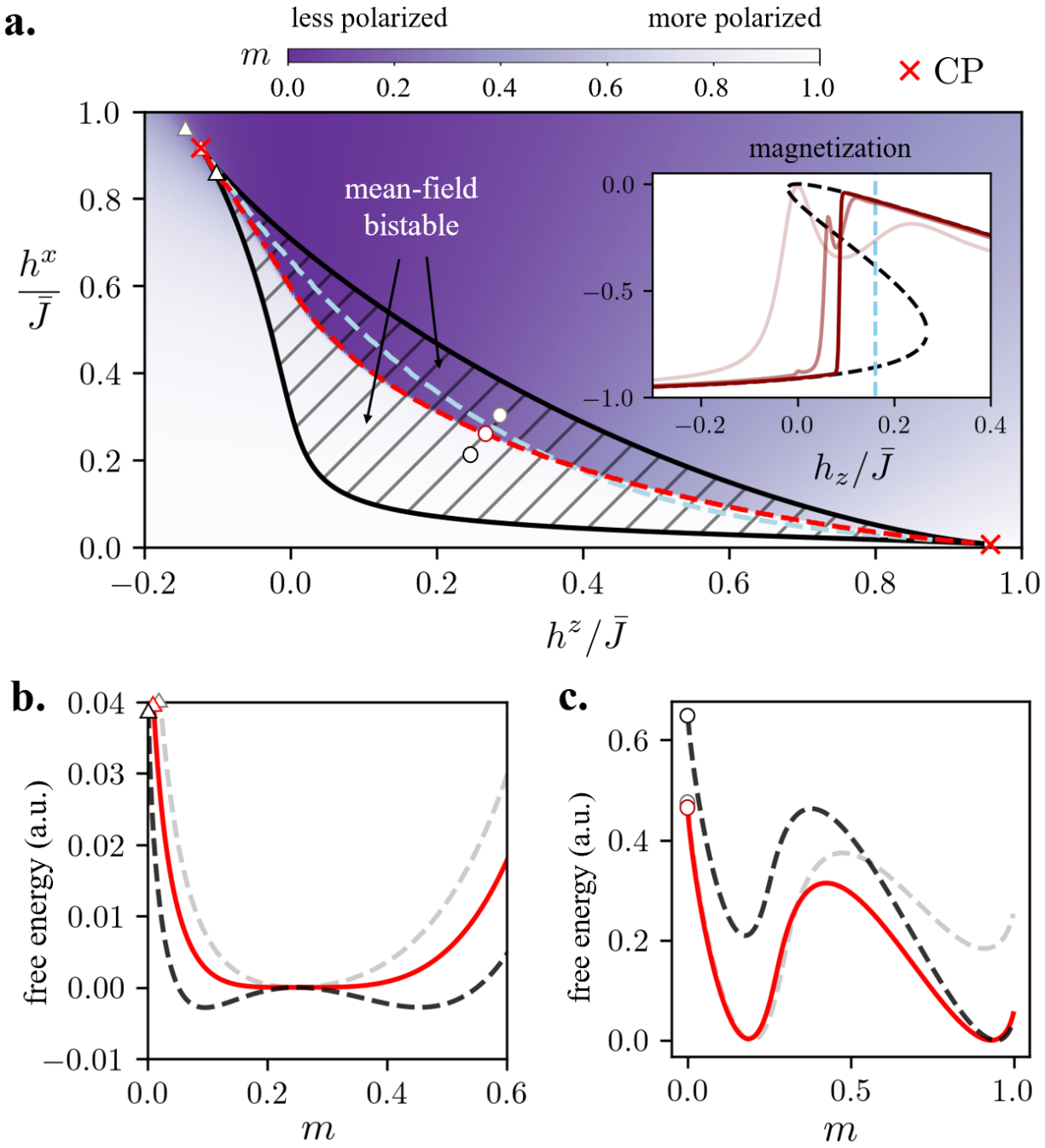

Figure 5.3: First- and second-order phase transitions in the dissipative transverse-field Ising model. Top panel (a): Steady-state polarization density $m = -\sum_j \langle \hat{\sigma}_j^z \rangle_{\rm SS}/N$, for $\gamma = \bar{J}/10$, $N = 128$, and $\Gamma = 0$. The shaded region enclosed by solid black lines denotes parameters where mean field theory predicts bistability. The first-order phase transition occurs when the local minima in f become degenerate, and is traced by a red dashed curve. The location of this transition predicted by the Maxwell construction is given by the blue dashed curve. Critical points where the first three derivatives of f vanish are marked by red crosses. Inset: Steady-state magnetization for $h^x = 0.4\bar{J}$, and $\gamma = \bar{J}/100$, for $N = 4, 16, 128$. Increasing values of N correspond to increasing opacity. Black dashed curves are used to denote the mean-field solutions. Bottom panel: free energy landscape $f(m)$ determining the amount of polarization m in the steady state $\hat{\rho}_{\rm SS}$, for three parameter choices near (b) a second-order phase transition, and (c) a first-order phase transition.

expectation value in terms of generalized hypergeometric polynomials:

$$\langle \hat{\sigma}^+_{C_1} \hat{\sigma}^-_{C_2} \rangle_{\rm SS} = \frac{2^{|R^c_{12}|} \mathcal{K}^*(R_1)\mathcal{K}(R_2)}{\mathcal{N}} \times {}_3F_0(|R_1| - r^*, |R_2| - r, |R_{12}| - N; -2|J_{\rm eff}/h^x|^2), \tag{5.19}$$

where $\mathcal{N} = 2^N \, {}_3F_0(-r^*, -r, -N; -2|J_{\rm eff}/h^x|^2)$. We have also defined form factors $\mathcal{K}(X) = (-r)_{|X|} \prod_{j\in X}(2J_{\rm eff}/h^x_j)$, where $(z)_m \equiv z(z+1)\cdots(z+m-1)$ is the Pochhammer symbol, or rising factorial [1].

More generally, in the case of an inhomogeneous field, we obtain the expression

$$\langle \hat{\sigma}^+_{C_1} \hat{\sigma}^-_{C_2} \rangle_{\rm SS} = \frac{2^{|R^c_{12}|} \mathcal{K}^*(R_1)\mathcal{K}(R_2)}{\mathcal{N}} \times \sum_m (|R_1| - r^*)_m (|R_2| - r)_m \mathcal{I}_m(R^c_{12}), \tag{5.20}$$

where we have defined the form factors $\mathcal{I}_m(X) \equiv \sum_{Y\subseteq X, |Y|=m} \prod_{j\in Y}(2|J_{\rm eff}/h^x_j|^2)$. These form factors satisfy the recursion relation $\mathcal{I}_m(X) = \mathcal{I}_m(X \setminus \{j\}) + 2\frac{|J_{\rm eff}|^2}{|h^x_j|^2}\mathcal{I}_{m-1}(X \setminus \{j\})$, which is useful when evaluating the expectation value in the thermodynamic limit.

5.8 Exact solution for the steady state

The mixed-field Ising model, in the infinite-range limit, has the following Hamiltonian:

$$\hat{H} = J \sum_{i\neq j} \hat{S}^z_i \hat{S}^z_j + \sum_{j,\mu} h^\mu_j \hat{S}^\mu_j \tag{5.21}$$

Here, $\mu = x, y, z$, and $\hat{S}^\mu_j \equiv \hat{\sigma}^\mu_j/2$ are the local $SU(2)$ operators used earlier. We consider a Lindblad master equation with both collective and local loss, $\partial_t \hat{\rho} = -i[\hat{H}, \hat{\rho}] + \mathcal{L}_1[\hat{\rho}] + \mathcal{L}_2[\hat{\rho}]$,

1. In this case, the external fields are uniform, and so we can use the simpler formula $\mathcal{K}(X) = (-r)_{|X|}(2J_{\rm eff}/h^x)^{|X|}$.

that is, with

$$\mathcal{L}_1[\hat{\rho}] = \frac{\gamma}{2}\sum_j \left(2\hat{\sigma}_j^- \hat{\rho}\hat{\sigma}_j^+ - \{\hat{\sigma}_j^+\hat{\sigma}_j^-, \hat{\rho}\}\right), \tag{5.22}$$

$$\mathcal{L}_2[\hat{\rho}] = \frac{\Gamma}{2}\sum_j \left(2\hat{S}_- \hat{\rho}\hat{S}_+ - \{\hat{S}_+\hat{S}_-, \hat{\rho}\}\right). \tag{5.23}$$

The loss operators above, together with their adjoints, generate the entire algebra of observables for our spin system. Therefore, thanks to the centralizer condition in Evans [1977], we know that the above Lindblad master equation must have a unique steady state. We now make the ansatz that this steady state satisfies a quantum detailed balance condition, namely s-QDB with $s = 1/2$ Goldstein and Lindsay [1995], Fagnola and Umanità [2010], Ramezani et al. [2018]. A sufficient condition for 1/2-QDB is that the steady state admits an antilinear square root $\hat{\Psi}$ with unit Hilbert-Schmidt norm, satisfying Fagnola and Umanita [2007]

$$\hat{O}\hat{\Psi} = \hat{\Psi}\hat{O}^\dagger, \tag{5.24}$$

for all linear operators $\hat{O} \in \mathrm{span}\{H_{\mathrm{eff}}, \hat{L}_1, \cdots, \hat{L}_l\}$, where $l = N + 1$ is the number of jump operators. Letting $\hat{\Phi} := \hat{\Psi}\hat{K}$ with $\hat{K}$ an antiunitary operator, we can gauge transform these conditions into

$$\hat{O}\hat{\Phi} = \hat{\Phi}(\hat{K}^\dagger \hat{O}\hat{K})^\dagger, \qquad \forall \hat{O} \in \mathrm{span}\{\hat{H}_{\mathrm{eff}}, \hat{L}_1, \cdots, \hat{L}_l\} \tag{5.25}$$

5.8.1 Solution in permutation-symmetric case

We now assume the external magnetic field is homogeneous, $h_j^\mu \equiv h^\mu$. Then the constraint Eq. (5.24) is permutation symmetric, and furthermore has at most one solution (otherwise the master equation would have multiple steady states, which is impossible, as was discussed

in the previous section). Therefore, any solution $\hat{\Psi}$, if it exists, must be permutation symmetric. Now suppose in Eq. (5.25) that we choose a $\hat{K}$ which is permutation symmetric. Then $\hat{\Phi} = \hat{\Psi}\hat{K}$ is also permutation symmetric. If we further choose $\hat{K}$ so that the quadratic casimir for the collective $\mathfrak{su}(2)$ representation $\hat{S}^x, \hat{S}^y, \hat{S}^z$, i.e.

$$\hat{\mathfrak{C}} = (\hat{S}^x)^2 + (\hat{S}^y)^2 + (\hat{S}^z)^2 \tag{5.26}$$

commutes with $\hat{K}$, then any monomial $\hat{\mathfrak{C}}^m$ also commutes with $\hat{K}$, and therefore we can add any polynomial in the Casimir element with complex coefficients to any of the operators $\hat{O}$ in (5.25), without changing the space of solutions. In particular, this is useful for the case $\hat{O} = \hat{H}_{\text{eff}}$, which we can then deform into a non-Hermitian Ising model:

$$\hat{G}_{\text{eff}} := \hat{H}_{\text{eff}} + \frac{i\gamma N}{4} + \frac{i\Gamma\hat{\mathfrak{C}}}{2} = J_{\text{eff}}\hat{S}_z^2 + h_{\text{eff}}^z\hat{S}_z + \frac{1}{2}(h\hat{S}_+ + h.c.), \tag{5.27}$$

where $J_{\text{eff}} = J + i\Gamma/2$, and we have introduced two effective complex magnetic fields: $h_{\text{eff}}^z = h^z - i(\gamma+\Gamma)/2$, and $h = h_x - ih_y$. Choosing the antiunitary $\hat{K} = \hat{K}_z\hat{U}_x$ referenced earlier, we obtain:

$$(\hat{K}^\dagger\hat{G}_{\text{eff}}\hat{K})^\dagger = J_{\text{eff}}\hat{S}_z^2 - h_{\text{eff}}^z\hat{S}_z + \frac{1}{2}(h\hat{S}_+ + h.c.), \tag{5.28}$$

Furthermore, the jump operators are $\hat{K}$-invariant: $(\hat{K}^\dagger\hat{\sigma}_j^-\hat{K})^\dagger = \hat{\sigma}_j^-$. Therefore our condition Eq. (5.25) reduces to $[\hat{\sigma}_j^-, \hat{\Phi}] = 0$, and

$$\hat{G}_{\text{eff}}\hat{\Phi} - \hat{\Phi}(\hat{K}^\dagger\hat{G}_{\text{eff}}\hat{K})^\dagger = J_{\text{eff}}[\hat{S}_z, \{\hat{S}_z, \hat{\Phi}\}] + h_{\text{eff}}^z\{\hat{S}_z, \hat{\Phi}\} + \frac{1}{2}[(h\hat{S}_+ + h.c.), \hat{\Phi}] = 0. \tag{5.29}$$

Substituting $[\hat{S}_-, \hat{\Phi}] = 0$ yields

$$\frac{\hat{G}_{\text{eff}}\hat{\Phi} - \hat{\Phi}(\hat{K}^\dagger \hat{G}_{\text{eff}} \hat{K})^\dagger}{J_{\text{eff}}} = [\hat{S}_z, \{\hat{S}_z, \hat{\Phi}\}] + r\{\hat{S}_z, \hat{\Phi}\} + \frac{h}{2J_{\text{eff}}}[\hat{S}_+, \hat{\Phi}] = 0, \tag{5.30}$$

where we have used the definition $r \equiv h^z_{\text{eff}}/J_{\text{eff}}$ used earlier. The only solution to the set of constraints $[\hat{\sigma}_j^-, \hat{\Phi}] = 0$ is a polynomial in the lowering operators with complex coefficients, that is, $\hat{\Phi} \in \mathbb{C}[\hat{\sigma}_1^-, \ldots, \hat{\sigma}_N^-]$. Because $\hat{\Phi}$ is permutation symmetric, this is a symmetric polynomial. By the fundamental theorem of symmetric polynomials, $\hat{\Phi}$ can further be expanded as a polynomial in the elementary symmetric polynomials. Because $\hat{\sigma}_j^-$ squares to zero, the elementary symmetric polynomials are each proportional to some power of $\hat{S}_-$. Therefore we can write

$$\hat{\Phi} = \sum_k c_k \hat{S}_-^k. \tag{5.31}$$

To solve for the coefficients $\{c_k\}_k$, we substitute the above polynomial into Eq. (5.30). Defining $\hat{B}_k := (2\hat{S}_z + k)\hat{S}_-^k$, and using standard spin commutation relations, we get

$$\{\hat{S}_z, \hat{S}_-^k\} = \hat{B}_k, \quad [\hat{S}_+, \hat{S}_-^k] = k\hat{B}_{k-1}, \quad [\hat{S}_z, \hat{B}_k] = -k\hat{B}_k, \tag{5.32}$$

so that, noting that $\hat{B}_N = 0$, we get

$$\frac{\hat{G}_{\text{eff}}\hat{\Phi} - \hat{\Phi}(\hat{K}^\dagger \hat{G}_{\text{eff}} \hat{K})^\dagger}{J_{\text{eff}}} = \sum_{k=0}^{N-1} \left(\frac{h}{2J_{\text{eff}}}(k+1)c_{k+1} - (k-r)c_k \right) \Phi_k = 0. \tag{5.33}$$

Since the operators $\hat{B}_k$ are linearly independent, each coefficient must vanish, yielding a first-order recursion relation for $\{c_k\}_k$, which yields the binomial series solution

$$\hat{\Phi} = \sum_{k=0}^{\infty} \binom{r}{k} (-\hat{\mathbb{S}}_-)^k, \tag{5.34}$$

where $\hat{\mathbb{S}}_-$ is the non-unitary $SU(2)$ lowering operator defined earlier, and $\binom{z}{k} = z(z-1)\cdots(z-k+1)/k!$ is the generalized binomial coefficient. Explicitly,

$$\hat{\mathbb{S}}_- = \frac{2J_{\text{eff}}}{h}\hat{S}_-. \tag{5.35}$$

In the following section, we will show how one can generalize this solution to the case where the transverse-plane magnetic fields $h_j := h_j^x - ih_j^y$ have arbitrary spatial dependence, but at the cost of removing the collective loss term (5.23) from the Lindbladian.

5.8.2 Solution without permutation symmetry, $\Gamma = 0$

We now consider the following conditions but possibly allowing for a spatially-inhomogeneous magnetic field:

$$\hat{O}\hat{\Phi} = \hat{\Phi}(\hat{K}^\dagger \hat{O}\hat{K})^\dagger \qquad \forall \hat{O} \in \text{span}\{\hat{H}_{\text{eff}}, \hat{L}_1, \cdots, \hat{L}_l\} \tag{5.36}$$

In this case it seems that the lack of permutation symmetry would invalidate all of the arguments we used previously to calculate the solution $\hat{\Phi}$. Indeed, we cannot add a polynomial in the Casimir element to $\hat{H}_{\text{eff}}$ to obtain $\hat{G}_{\text{eff}}$, and are instead stuck with an inhomogeneous mixed-field XXZ model:

$$\hat{H}_{\text{eff}} = J\hat{S}_z^2 - \frac{i\Gamma}{2}(\hat{S}_x^2 + \hat{S}_y^2) + h_{\text{eff}}^z \hat{S}_z + \frac{1}{2}\sum_j (h_j \hat{\sigma}_j^+ + h_j^* \hat{\sigma}_j^-) \tag{5.37}$$

However, we can still solve the detailed balance condition if $\Gamma = 0$. In this case the imaginary XY term vanishes. Using the same choice of $\hat{K}$ as before, the condition Eq. (5.25) with

$\hat{O} = \hat{H}_{\text{eff}}$ reduces to

$$\frac{\hat{H}_{\text{eff}}\hat{\Phi} - \hat{\Phi}(\hat{K}^\dagger \hat{H}_{\text{eff}} \hat{K})^\dagger}{J} = [\hat{S}_z, \{\hat{S}_z, \hat{\Phi}\}] + r\{\hat{S}_z, \hat{\Phi}\} + \sum_j \frac{h_j}{2J}[\hat{\sigma}_j^+, \hat{\Phi}] = 0. \tag{5.38}$$

The inhomogeneity in the transverse-plane magnetic field can now be removed via a similarity transformation $\hat{\mathcal{G}} := \prod_j e^{\hat{S}_j^z \log(2J_{\text{eff}}/h_j)}$, which reduces the above condition to a special case of Eq. (5.30):

$$\hat{\mathcal{G}}\frac{\hat{H}_{\text{eff}}\hat{\Phi} - \hat{\Phi}(\hat{K}^\dagger \hat{H}_{\text{eff}} \hat{K})^\dagger}{J}\hat{\mathcal{G}}^{-1} = [\hat{S}_z, \{\hat{S}_z, \hat{\Phi}_{\mathcal{G}}\}] + r\{S_z, \hat{\Phi}_{\mathcal{G}}\} + [\hat{S}_+, \hat{\Phi}_{\mathcal{G}}] = 0, \tag{5.39}$$

where $\hat{\Phi}_{\mathcal{G}} \equiv \hat{\mathcal{G}}^{-1}\hat{\Phi}\hat{\mathcal{G}}$ is the transformed solution. Comparing Eq. (5.39) with Eq. (5.30) immediately yields

$$\hat{\Phi}_{\mathcal{G}} = (1 - \hat{S}_-)^r. \tag{5.40}$$

The general solution cited earlier then follows from the fact that our two $SU(2)$ representations are precisely related by this similarity transformation: $\hat{\mathbb{S}}^\mu = \hat{\mathcal{G}}\hat{S}^\mu\hat{\mathcal{G}}^{-1}$.

5.9 Spin blockade

We now derive the bounds used earlier to determine the threshold where blockade effects become observable. A good estimate for this threshold is obtained as the point where $p_n = p_N$, where $\{p_m\}_m$ is the probability distribution defined earlier. We now calculate this threshold:

$$p_n = \left\| \binom{r}{n} \hat{\mathbb{S}}_-^n \right\|_{\text{HS}}^2, \qquad p_N = \left\| \binom{r}{N} \hat{\mathbb{S}}_-^N \right\|_{\text{HS}}^2 \tag{5.41}$$

We calculate

$$\frac{p_N}{p_n} = \frac{n!^2}{N!^2}|(-\epsilon)(-\epsilon-1)\cdots(-\epsilon-N+n+1)|^2 \frac{\|\hat{\mathbb{S}}_-^N\|_{\rm HS}^2}{\|\hat{\mathbb{S}}_-^n\|_{\rm HS}^2}. \tag{5.42}$$

We calculate the L^2 norm of $\hat{\mathbb{S}}_-^n$ by brute force using the multinomial expansion:

$$\|\hat{\mathbb{S}}_-^n\|_{\rm HS}^2 = n!^2 \sum_{X\subset\{1,2,\cdots,N\},\ |X|=n} \Big\| \prod_{j\in X} \frac{2J_{\rm eff}}{h_j^x}\hat{\sigma}_j^- \Big\|_{\rm HS}^2 = n!^2 2^N \mathcal{I}_n, \tag{5.43}$$

where $\mathcal{I}_n \equiv \mathcal{I}_n(\{1,2,\ldots,N\})$ is the form factor defined earlier. We thus obtain the asymptotic estimate

$$\frac{p_N}{p_n} \sim |\epsilon|^2 \times (N-n-1)!^2 \frac{\mathcal{I}_n}{\mathcal{I}_N} \qquad (\epsilon \to 0) \tag{5.44}$$

Setting the ratio equal to one yields the result $|\epsilon| < (N-n-1)!^{-1}\sqrt{\mathcal{I}_n/\mathcal{I}_N}$. In the uniform driving limit, $\mathcal{I}_n = \lambda^n \binom{N}{n}$, where $\lambda = 2|J_{\rm eff}/h^x|^2$ is the dimensionless driving parameter defined earlier. This yields the bound

$$|\epsilon| < \frac{1}{(N-n-1)!}\sqrt{\lambda^{n-N}\binom{N}{n}}. \tag{5.45}$$

Blockade effect with $\gamma \approx J$

Despite what the previous discussion might suggest, the condition $\gamma \ll J$ is not strictly necessary for observing the blockade effect. For this purpose, let us assume that the Hilbert-Schmidt norm $\|\hat{\mathbb{S}}_-\|_{\rm HS}$ is less than one half. This effectively sets $h_j/J_{\rm eff} \sim O(N)$, or equivalently $h_j/\bar{J}_{\rm eff} \sim O(1)$. In this case,

$$\|\log(1-\hat{\mathbb{S}}_-)\|_{\rm HS} \le \log(1-\|\hat{\mathbb{S}}_-\|_{\rm HS}) < 1. \tag{5.46}$$

As a result, the following series uniformly converges when $|\epsilon| < 1$:

$$\hat{\Phi} = (1 - \hat{\mathbb{S}}_-)^n \bigg(1 + \epsilon \log(1 - \hat{\mathbb{S}}_-) + \cdots \bigg). \tag{5.47}$$

In this case, the threshold to observe an effective blockade is $|\epsilon| < 1$, and thus the effect remains observable well into the thermodynamic limit. However, the constraint $\|\mathbb{S}_-\|_{\mathrm{HS}} < 1/2$ means that the steady state is close to an infinite-temperature state. Representative results are shown in Figure 5.4.

5.9.1 Distribution for the magnetization

We now calculate the distribution for the total magnetization at a blockade. We attempt to calculate the quantity,

$$p(q_1, \cdots, q_N) = \langle q_1, \cdots, q_N | \hat{\Phi}\hat{\Phi}^\dagger | q_1, \cdots, q_N \rangle = \| \hat{\Phi}^\dagger | q_1, \cdots, q_N \rangle \|^2 \tag{5.48}$$

where q_j is a Boolean variable that is zero if the jth spin is pointing up, and one otherwise. In the limit $h_j^x / J_{\mathrm{eff}} \ll 1$ we can approximate $\hat{\Phi} \approx \hat{\mathbb{S}}_-^n$, and we obtain

$$p(q_1, \cdots, q_N) = \langle q_1, \cdots, q_N | \hat{\Phi}\hat{\Phi}^\dagger | q_1, \cdots, q_N \rangle \tag{5.49}$$

$$= \| \hat{\Phi}^\dagger | q_1, \cdots, q_N \rangle \|^2 \sim \sum_{A \subset \{1,2,\ldots,N\},\ |A|=n} \prod_{j \in A} \lambda_j q_j, \tag{5.50}$$

where $\lambda_j = 2|J_{\rm eff}/h^x_j|^2$. To obtain the distribution for the total magnetization, it suffices to coarse-grain the above distribution over $k = \sum_j q_j$. We obtain

$$p_k = \sum_{\sum_j q_j = k} p(q_1, \cdots, q_N) = \sum_{B \subset \{1,2,\ldots,N\},\ |B|=k} \sum_{A \subset B,\ |A|=n} \prod_{j \in A} \lambda_j \tag{5.51}$$

$$= \sum_{A \subset \{1,2,\cdots,N\},\ |A|=n} \left(\prod_{j \in A} \lambda_j \sum_{B \supset A,\ |B|=k} 1 \right) \tag{5.52}$$

$$= \sum_{A \subset \{1,2,\cdots,N\},\ |A|=n} \left(\prod_{j \in A} \lambda_j \binom{N-n}{k-n} \right) \tag{5.53}$$

$$= \binom{N-n}{k-n} \mathcal{I}_n \propto \binom{N}{k}\binom{k}{n}, \tag{5.54}$$

which yields the binomial distribution given earlier.

5.10 Thermodynamic limit $N \to \infty$

We now calculate the distribution $\{p_M\}_M$ in the limit that $N \to \infty$. To make this task easy, we assume that the external magnetic fields are uniform, $h^\mu_j \equiv h^\mu$. The exact expression is

$$p_M = |2J_{\rm eff}/h|^{2M} \left| \binom{r}{M} \right|^2 \|\hat{\mathbb{S}}^M_-\|^2_{\rm HS} = 2^{N-M} M!^2 |2J_{\rm eff}/h|^{2M} \binom{N}{M} \left| \binom{r}{M} \right|^2 \tag{5.55}$$

$$= |(-r)_M|^2 \frac{N!}{(N-M)!} \frac{\lambda^M}{M!}$$

$$= |(-N\bar{r})_M|^2 \frac{N!}{(N-M)!} \frac{\bar{\lambda}^M}{N^{2M} M!}, \tag{5.56}$$

where we have dropped all M-independent constants, and have recalled the definitions given earlier:

$$\bar{r} \equiv \frac{h^z_{\rm eff}}{\bar{J}_{\rm eff}}, \qquad \bar{\lambda} = 2|\bar{J}_{\rm eff}/h^x|^2, \tag{5.57}$$

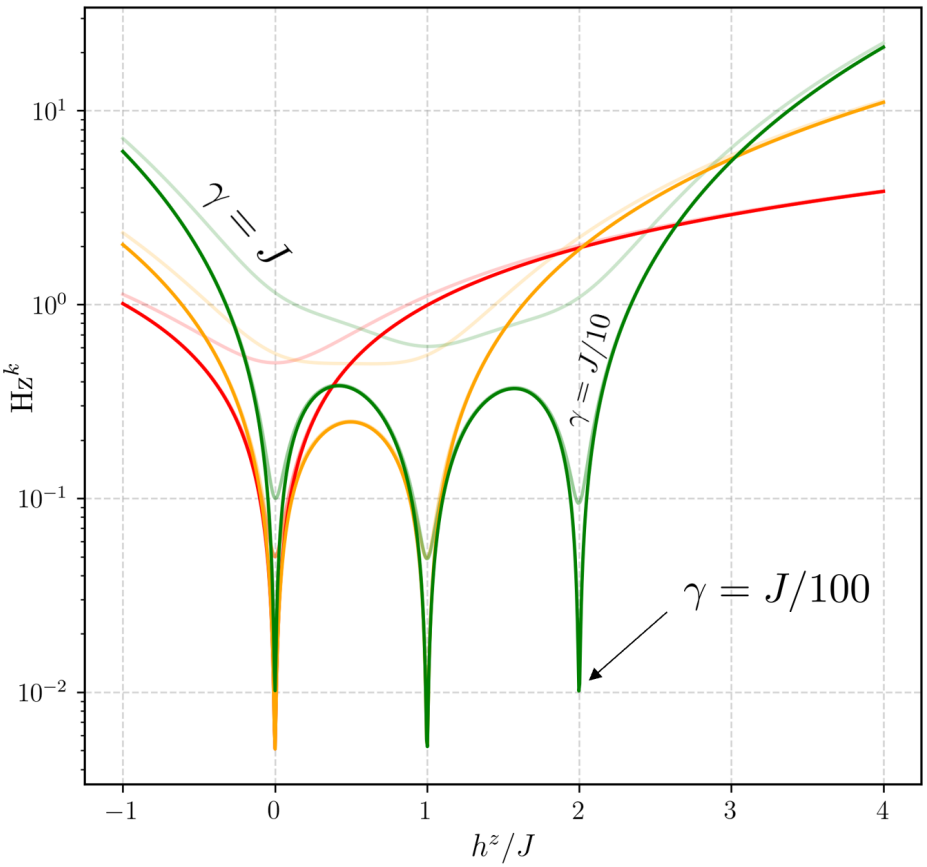

Figure 5.4: Spin blockade effect with $\|\hat{\mathbb{S}}_-\|_{\mathrm{HS}} = 2/3$. Rescaled coherence tensor $h_{i_1} \cdots h_{i_k} C_{i_1,\cdots,i_k}$, for $k = 1$ (red), $k = 2$ (orange) and $k = 3$ (green). Here, $N = 22, h^x = 3NJ, h^y = 0$, and $\Gamma = 0$. $\gamma \in \{J, J/10, J/100\}$, with greater transparency indicating greater loss rates. Note how the dips in the rescaled coherence are noticeable even with loss rates γ comparable to the interaction strength J. Furthermore, these dips have a sizeable width $\sim O(1)$.

where $\bar{J}_{\text{eff}} \equiv N J_{\text{eff}}$. We now expand

$$(-N\bar{r})_M = N^M(-\bar{r}) \cdot \left(\frac{1}{N} - \bar{r}\right) \cdots \left(\frac{M-1}{N} - \bar{r}\right), \tag{5.58}$$

$$\frac{N!}{(N-M)!} = N^M 1 \cdot \left(1 - \frac{1}{N}\right) \cdots \left(1 - \frac{M-1}{N}\right). \tag{5.59}$$

Substituting $m \equiv M/N$ allows us to write the logarithm of (5.56) as a Riemann sum:

$$N^{-1} \log p_M = m \log N\bar{\lambda} - N^{-1} \log M! + \sum_{m' \in \{k/N\}_{k=0}^{M-1}} \log(1-m')|\bar{r} - m'|^2 \Delta m' \tag{5.60}$$

with $\Delta m' \equiv 1/N$. We can simplify the terms excluding the Riemann sum by using Stirling's approximation $\log M! = M \log M - M + O(\log M)$:

$$m \log N\bar{\lambda} - N^{-1} \log M! = m\left(1 + \log \frac{\bar{\lambda}}{m}\right) + O(N^{-1}), \tag{5.61}$$

where again we have neglected M-independent constants. We therefore arrive at the asymptotic estimate

$$f(m) = -\int_0^m dm' \log(1-m')|\bar{r} - m'|^2 - m\left(1 + \log \frac{\bar{\lambda}}{m}\right) + O(N^{-1}). \tag{5.62}$$

Carrying out the integral analytically yields the closed-form expression utilized earlier.

5.10.1 $1/N$ corrections to the potential

The leading-order corrections to the potential come from both (1) including the $O(N^{-1})$ terms in Stirling's approximation, and (2) writing the Riemann sum as an asymptotic series

(whose terms are each Riemman integrals). For (1), note the improved estimate

$$m \log N\bar{\lambda} - N^{-1} \log M! = m\left(1 + \log \frac{\bar{\lambda}}{m}\right) + \frac{1}{2N} \log m + O(N^{-2}), \tag{5.63}$$

where again, we have dropped M-independent constants. Finally, for the Riemann sum, we note that the integrand $g(m) \equiv \log(1-m)|\bar{r} - m|^2$ is a real-analytic function on the domain $m \in (0, 1)$. This is because r, as was discussed earlier, cannot be a non-negative real number. Therefore, we have the asymptotic series expansion

$$\begin{aligned} \int_0^m dm'\, g(m') &= \sum_{m' \in \{k/N\}_{k=0}^{M-1}} g(m')\Delta m' + \sum_{k=1}^{\infty} \frac{(\Delta m')^m}{(k+1)!} \sum_{m' \in \{k/N\}_{k=0}^{M-1}} g^{(k)}(m')\Delta m', \\ &= \sum_{m' \in \{k/N\}_{k=0}^{M-1}} g(m')\Delta m' + \frac{\Delta m'}{2} \int_0^m dm'\, g'(m') + O(N^{-2}). \end{aligned} \tag{5.64}$$

This leads to the following improved estimate for the Riemann sum:

$$\begin{aligned} \sum_{m' \in \{k/N\}_{k=0}^{M-1}} \log(1-m')|\bar{r} - m'|^2 \Delta m' &= \int_0^m dm'\, \log(1-m')|\bar{r} - m'|^2 \\ &\quad - \frac{1}{2N} \log(1-m)|\bar{r} - m|^2 + O(N^{-2}) \end{aligned} \tag{5.65}$$

Putting both $O(N^{-1})$ corrections together yields the following shift in the free energy:

$$\delta f(m) = \frac{1}{2N} \log \frac{|m - \bar{r}|^2(1-m)}{m} + O(N^{-2}). \tag{5.66}$$

5.10.2 Critical points of the potential

To understand the large-N behavior of our infinite-range DTI model, it is useful to calculate the derivative of the potential:

$$f'(m) = \log \frac{m}{\bar{\lambda}(1-m)|m-\bar{r}|^2}. \tag{5.67}$$

The critical equation $f'(m) = 0$ is thus equivalent to the cubic equation $m = \bar{\lambda}(1-m)|m-\bar{r}|^2$. On the other hand, the mean-field equations for $S_\mu := \langle \hat{\sigma}^\mu \rangle_{\mathrm{SS}}$ are

$$0 = -2\bar{J}S_yS_z - \frac{\tilde{\gamma}}{2}S_x + \bar{\Gamma}S_xS_z + i(h^zS_y - h^yS_z), \tag{5.68}$$

$$0 = -2\bar{J}S_xS_z - \frac{\tilde{\gamma}}{2}S_y + \bar{\Gamma}S_yS_z + ih^x + i(h^xS_z - h^zS_x), \tag{5.69}$$

$$0 = -\frac{\tilde{\gamma}}{2}(2S_z+1) - \bar{\Gamma}(S_x^2+S_y^2) + i(h^yS_x - h^xS_y), \tag{5.70}$$

where $\tilde{\gamma} = \gamma + \bar{\Gamma}/N$, with $\bar{\Gamma} := N\Gamma$ Huybrechts et al. [2020a]. Writing $S_\mu = 2m_\mu$, and substituting Eqs. (5.68), (5.69) into Eq. (5.70), while letting $N \to \infty$, we obtain

$$m_z^3 + (1+2\mathrm{Re}\,\bar{r})m_z^2 + |\bar{r}|^2 + (|\bar{r}+1|^2 - 1 + \bar{\lambda}^{-1})m_z = 0, \tag{5.71}$$

which is precisely the critical equation $f'(m) = 0$, once we substitute the identity $m = -m^z$. This demonstrates that the critical points of $f(m)$ are in one-to-one correspondence with the mean-field solutions for m_z, for *all* possible values of $\gamma, \Gamma, J, h^x, h^y, h^z$ (forming a 6-dimensional parameter space).

5.11 Correlation functions

We now proceed to calculate the expectation values of normally-ordered strings of Pauli operators. This process largely adheres to the formalism described in the supplementary

information (SI) of Roberts and Clerk [2023]. It's worth noting that the particular methodology of Roberts and Clerk [2023] was in fact initially devised during the investigation of the current model (both exactly-solvable models were discovered at around the same time, in mid 2021), for which the calculation is much simpler:

$$\hat{\sigma}^+_{C_1}\hat{\sigma}^-_{C_2} \equiv \prod_{i\in C_1}\hat{\sigma}^+_i \prod_{j\in C_2}\hat{\sigma}^-_j\,, \tag{5.72}$$

where $C_1, C_2 \subset \{1,2,3,\ldots,N\}$ are the clusters of spins mentioned earlier. We use the multinomial expansion $\hat{\mathbb{S}}^k_- = k!\sum_{|A|=k}\alpha^A\hat{\sigma}^-_A$ to write

$$\begin{aligned}\langle\hat{\sigma}^+_{C_1}\hat{\sigma}^-_{C_2}\rangle_{\rm SS} &= \frac{1}{\mathcal{N}}\sum_{k,l}(-1)^{k+l}\binom{r^*}{k}\binom{r}{l}\mathrm{tr}(\hat{\mathbb{S}}^{\dagger k}_-\hat{\sigma}^+_{C_1}\hat{\sigma}^-_{C_2}\hat{\mathbb{S}}^l_-)\\ &= \frac{1}{\mathcal{N}}\sum_{A_1,A_2\subset\{1,2,3,\ldots,N\}}(-r^*)_{|A_1|}(-r)_{|A_2|}\alpha^{*A_1}\alpha^{A_2}\mathrm{tr}(\hat{\sigma}^+_{A_1}\hat{\sigma}^+_{C_1}\hat{\sigma}^-_{C_2}\hat{\sigma}^-_{A_2}).\end{aligned} \tag{5.73}$$

where $\alpha_j \equiv 2J_{\rm eff}/h_j$, and we have used the shorthand notation $\alpha^A \equiv \prod_{j\in A}\alpha_j$. The fundamental trace $\mathrm{tr}(\hat{\sigma}^+_{A_1}\hat{\sigma}^+_{C_1}\hat{\sigma}^-_{C_2}\hat{\sigma}^-_{A_2})$ inside the sum vanishes unless $A_j \subseteq C_j^c$, and $A_1 \amalg C_1 = A_2 \amalg C_2$. Because of the former constraint, we can write

$$A_j = A_j \cap R_{12}^c \amalg A_j \cap R_j \tag{5.74}$$

where $\amalg$ denotes the disjoint union, and R_{12}, R_j are the regions defined earlier. The constraint $A_1 \amalg C_1 = A_2 \amalg C_2$, yields

$$A_j \cap R_j = R_j, \qquad A_1 \cap R_{12}^c = A_2 \cap R_{12}^c \equiv X. \tag{5.75}$$

Furthermore, we can write $A_j = X \amalg R_j$ and $A \amalg C_j = X \amalg R_{12}$, and hence $(A_1, A_2) \to X \equiv A_j \setminus R_j$ is a bijection from the support of the sum in Eq. (5.73), to the power set (the set of all subsets) of R_{12}^c. Therefore,

$$\langle \hat{\sigma}^+_{C_1} \hat{\sigma}^-_{C_2} \rangle_{\mathrm{SS}} = \frac{\alpha^{*R_1} \alpha^{R_2} (-r^*)_{|R_1|} (-r)_{|R_2|}}{\mathcal{N}} \times \sum_{X \subset R_{12}^c} (|R_1| - r^*)_{|X|} (|R_2| - r)_{|X|} 2^{N-|X|-|R_{12}|} \prod_{j \in X} |\alpha_j|^2, \tag{5.76}$$

Eq. (5.76) immediately leads to the formula given earlier.

5.11.1 Permutation-symmetric limit

With permutation symmetry, the recursion relation for $\mathcal{I}_m(X)$ presented earlier admits the closed-form solution

$$\mathcal{I}_m(X) = \binom{|X|}{m} (2|J_{\mathrm{eff}}/h|^2)^m. \tag{5.77}$$

Substituting this solution for $\mathcal{I}_m$ into the general formula given earlier yields

$$\langle \hat{\sigma}^+_{C_1} \hat{\sigma}^-_{C_2} \rangle_{\mathrm{SS}} = \frac{2^{|R_{12}^c|} \mathcal{K}^*(R_1) \mathcal{K}(R_2)}{\mathcal{N}} \sum_m (|R_1| - r^*)_m (|R_2| - r)_m \frac{(-|R_{12}^c|)_m}{m!} \left(- \frac{2|J_{\mathrm{eff}}|^2}{|h_j|^2} \right)^m$$

which leads to the solution used earlier, once we recall the definition of the generalized hypergeometric function:

$${}_pF_q(a_1, \ldots a_p; b_1, \ldots b_q; z) = \sum_{l=0}^{\infty} \frac{\prod_{m=1}^p (a_m)_l}{\prod_{m=1}^q (b_m)_l} \frac{z^l}{l!}. \tag{5.78}$$

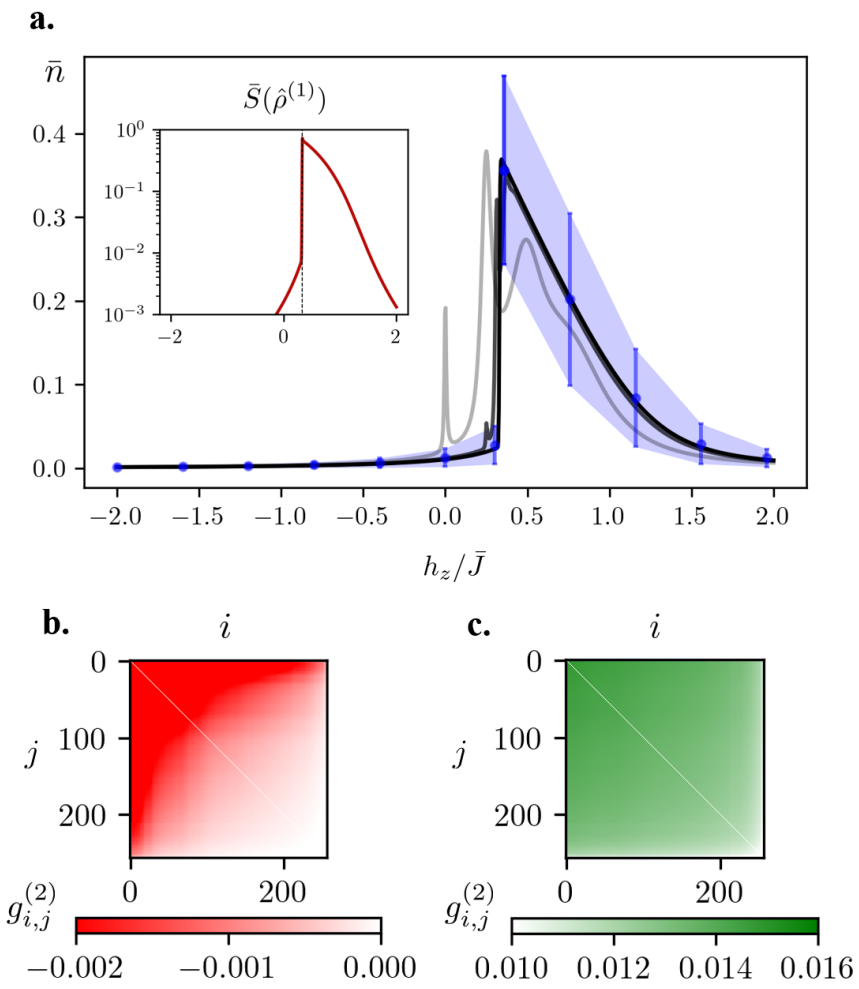

Figure 5.5: **Dissipative phase transitions in a random transverse-field Ising model**. (a) Solid curves: density of up spins $\bar{n} = \sum_j \langle \hat{\sigma}_j^+ \hat{\sigma}_j^- \rangle_{\rm SS}/N$, for $N \in 4$ (lightest gray), $N = 16$ (light gray), and $N = 128$ (black). Parameters are $\gamma = \bar{J}/100$, $\Gamma = 0$, and $h^x = \bar{J}/5, h^y = 0$. Blue dots and error bars denote $\bar{n}$ and $\Delta\bar{n} \equiv \sqrt{\sum_j (\langle \hat{\sigma}_j^+ \hat{\sigma}_j^- \rangle_{\rm SS} - \bar{n})^2}$ respectively, for a $N = 128$ random transverse-field Ising model with the same parameters, but with h_j^x sampled from a normal distribution with mean h^x and variance $\sigma = h^x/2$. Results are all for a single disorder realization. Inset: von-Neumann entropy of the 1-spin reduced density matrix for the non-random transverse-field Ising model with $N = 128$ (black curve). Bottom panel: connected density-density correlation function $g^{(2)}_{i,j}$ for a $N = 256$ random transverse-field Ising model with the same parameters (i.e. $h_j^{x,y}, \gamma, \Gamma, J$) as in panel (a), but with $h^z = 0.30\bar{J}$ (b) and $h^z = 0.36\bar{J}$ (c).

5.11.2 Phase transitions in the disordered model

We use the above solutions for correlation functions to investigate phase transitions in the disordered version of our model. We plot these correlation functions for single disorder realizations in Figure 5.5, where we obtain the following preliminary findings:

- The phase transition remains sharp, even with strong disorder. The location of the transition also doesn't seem to shift at all, even with transverse-field disorder $\Delta h^x/h^x \sim O(1)$.
- As in Roberts and Clerk [2022], the sign of the connected density-density correlation function

$$g^{(2)}_{i,j} \equiv \frac{\langle \hat{n}_i \hat{n}_j \rangle - \bar{n}_i \bar{n}_j}{\bar{n}_i \bar{n}_j} \tag{5.79}$$

  flips at the transition point. Note: in panels (b) and (c) of Figure 5.5, the spins are reordered so that h^x_j is an increasing function of j.

5.12 Conclusion

In this chapter, we have solved exactly for the steady state of the dissipative variant of the transverse-field Ising model, in the situation where the Ising interaction is infinitely-long ranged. We used the exact solution to reveal a novel spin blockade effect where low-order coherences diminish in the steady state. We uncovered a "thermodynamic potential" that governs the magnetization density in the thermodynamic limit, enabling an analytical determination of the phase diagram, including the location of first-order phase transitions. Finally, we used the solution to investigate the robustness of these phase transitions to transverse-field disorder, as well as their connection to a sign-change in a particular connected correlation function . While our study focused on the fully-connected transverse-field Ising

model, future work could be directed towards the study of this model on a cubic lattice where the dimension $d < \infty$, where an analytical understanding is also lacking. More broadly, future research could also delve into driven-dissipative spin systems defined on more general graphs.

REFERENCES

G. S. Agarwal. Open quantum Markovian systems and the microreversibility. *Z. Phys.*, 258(5):409–422, October 1973. ISSN 0939-7922. doi:10.1007/BF01391504. URL https://doi.org/10.1007/BF01391504.

G. S. Agarwal. Nonclassical statistics of fields in pair coherent states. *J. Opt. Soc. Am. B*, 5(9):1940–1947, Sep 1988. doi:10.1364/JOSAB.5.001940. URL http://opg.optica.org/josab/abstract.cfm?URI=josab-5-9-1940.

G S Agarwal and Asoka Biswas. Quantitative measures of entanglement in pair-coherent states. *Journal of Optics B: Quantum and Semiclassical Optics*, 7(11):350–354, oct 2005. doi:10.1088/1464-4266/7/11/006. URL https://doi.org/10.1088/1464-4266/7/11/006.

V. V. Albert and L. Jiang. Symmetries and conserved quantities in Lindblad master equations. *Phys. Rev. A*, 89(2):022118, February 2014.

Victor V. Albert, Shantanu O. Mundhada, Alexander Grimm, Steven Touzard, Michel H. Devoret, and Liang Jiang. Pair-cat codes: autonomous error-correction with low-order nonlinearity. *Quantum Science and Technology*, 4(3):035007, June 2019. ISSN 2058-9565. doi:10.1088/2058-9565/ab1e69. URL https://doi.org/10.1088/2058-9565/ab1e69.

Robert Alicki. On the detailed balance condition for non-hamiltonian systems. *Rep. Math. Phys.*, 10(2):249 – 258, 1976. ISSN 0034-4877. doi:https://doi.org/10.1016/0034-4877(76)90046-X. URL http://www.sciencedirect.com/science/article/pii/0034487776900 46X.

Cenap Ates, Beatriz Olmos, Juan P. Garrahan, and Igor Lesanovsky. Dynamical phases and intermittency of the dissipative quantum Ising model. *Physical Review A*, 85(4):043620, April 2012. doi:10.1103/PhysRevA.85.043620.

Leon Autonne. *Sur les matrices hypohermitiennes et sur les matrices unitaires,*. A. Rey, Lyon, 1915. OCLC: 3213505.

Sheldon Axler. HFT.m, December 2020. URL https://www.axler.net/HFT_Math.html.

Sheldon Axler, Paul Bourdon, and Wade Ramey. *Harmonic Function Theory*, volume 137 of *Graduate Texts in Mathematics*. Springer, second edition, 2001. URL https://link.springer.com/book/10.1007/b97238.

M. Bamba, A. Imamoglu, I. Carusotto, and C. Ciuti. Origin of strong photon antibunching in weakly nonlinear photonic molecules. *Phys. Rev. A*, 83:021802(R), Feb 2011. doi:10.1103/PhysRevA.83.021802. URL https://link.aps.org/doi/10.1103/PhysRevA.83.021802.

V. Bargmann. On a Hilbert space of analytic functions and an associated integral transform part I. *Communications on Pure and Applied Mathematics*, 14(3):187–214, 1961. ISSN 1097-0312. doi:10.1002/cpa.3160140303. URL http://onlinelibrary.wiley.com/doi/abs/10.1002/cpa.3160140303.

V. Bargmann. On a Hilbert Space of Analytie Functions and an Associated Integral Transform. Part II. A Family of Related Function Spaces Application to Distribution Theory. *Communications on Pure and Applied Mathematics*, 20(1):1–101, 1967. ISSN 1097-0312. doi:10.1002/cpa.3160200102. URL http://onlinelibrary.wiley.com/doi/abs/10.1002/cpa.3160200102.

N. Bartolo, F. Minganti, W. Casteels, and C. Ciuti. Exact steady state of a Kerr resonator with one- and two-photon driving and dissipation: Controllable Wigner-function multimodality and dissipative phase transitions. *Physical Review A*, 94(3):033841, September 2016. doi:10.1103/PhysRevA.94.033841. URL https://link.aps.org/doi/10.1103/PhysRevA.94.033841.

A. O. Barut and L. Girardello. New "coherent" states associated with non-compact groups. *Communications in Mathematical Physics*, 21(1):41–55, January 1971. ISSN 0010-3616, 1432-0916. URL https://projecteuclid.org/journals/communications-in-mathematical-physics/volume-21/issue-1/New-coherent-states-associated-with-non-compact-groups/cmp/1103857258.full.

Kristian Baumann, Christine Guerlin, Ferdinand Brennecke, and Tilman Esslinger. Dicke quantum phase transition with a superfluid gas in an optical cavity. *Nature*, 464(7293):1301–1306, 2010a. doi:10.1038/nature09009. URL https://doi.org/10.1038/nature09009.

Kristian Baumann, Christine Guerlin, Ferdinand Brennecke, and Tilman Esslinger. Dicke quantum phase transition with a superfluid gas in an optical cavity. *Nature*, 464(7293):1301–1306, April 2010b. ISSN 1476-4687. doi:10.1038/nature09009. URL https://www.nature.com/articles/nature09009. Number: 7293 Publisher: Nature Publishing Group.

Alberto Biella, Florent Storme, José Lebreuilly, Davide Rossini, Rosario Fazio, Iacopo Carusotto, and Cristiano Ciuti. Phase diagram of incoherently driven strongly correlated photonic lattices. *Phys. Rev. A*, 96:023839, Aug 2017. doi:10.1103/PhysRevA.96.023839. URL https://link.aps.org/doi/10.1103/PhysRevA.96.023839.

Ralf Blattmann, Peter Hanggi, and Sigmund Kohler. Qubit interference at avoided crossings: The role of driving shape and bath coupling. *Physical Review A*, 91(4):042109, April 2015. doi:10.1103/PhysRevA.91.042109. URL https://link.aps.org/doi/10.1103/PhysRevA.91.042109. Publisher: American Physical Society.

V. Borish, O. Marković, J. A. Hines, S. V. Rajagopal, and M. Schleier-Smith. Transverse-Field Ising Dynamics in a Rydberg-Dressed Atomic Gas. *Physical Review Letters*, 124(6):063601, February 2020. doi:10.1103/PhysRevLett.124.063601.

William F. Braasch, Oscar D. Friedman, Alexander J. Rimberg, and Miles P. Blencowe. Wigner current for open quantum systems. *Phys. Rev. A*, 100:012124, Jul 2019. doi:10.1103/PhysRevA.100.012124. URL https://link.aps.org/doi/10.1103/PhysRevA.100.012124.

Ola Bratteli and Uffe Haagerup. Unbounded derivations and invariant states. *Commun. Math. Phys.*, 59(1):79–95, February 1978. ISSN 1432-0916. doi:10.1007/BF01614156. URL https://doi.org/10.1007/BF01614156.

Ola Bratteli and Derek W. Robinson. *Operator Algebras and Quantum Statistical Mechanics*. Springer Berlin Heidelberg, 1997. doi:10.1007/978-3-662-03444-6. URL https://doi.org/10.1007%2F978-3-662-03444-6.

Heinz-Peter Breuer and Francesco Petruccione. *The Theory of Open Quantum Systems*. Oxford University Press, 2002.

Joseph W. Britton, Brian C. Sawyer, Adam C. Keith, C.-C. Joseph Wang, James K. Freericks, Hermann Uys, Michael J. Biercuk, and John J. Bollinger. Engineered two-dimensional Ising interactions in a trapped-ion quantum simulator with hundreds of spins. *Nature*, 484(7395):489–492, April 2012. ISSN 1476-4687. doi:10.1038/nature10981. URL https://www.nature.com/articles/nature10981.

Yury A. Brychkov. *Handbook of Special Functions: Derivatives, Integrals, Series and Other Formulas*. URL https://www.crcpress.com/Handbook-of-Special-Functions-Derivatives-Integrals-Series-and-Other/Brychkov/p/book/9781584889564.

Berislav Buca and Dieter Jaksch. Dissipation Induced Nonstationarity in a Quantum Gas. *Physical Review Letters*, 123(26):260401, December 2019. doi:10.1103/PhysRevLett.123.260401. URL https://link.aps.org/doi/10.1103/PhysRevLett.123.260401. Publisher: American Physical Society.

Berislav Buča and Tomaž Prosen. A note on symmetry reductions of the lindblad equation: transport in constrained open spin chains. *New Journal of Physics*, 14(7):073007, July 2012. doi:10.1088/1367-2630/14/7/073007. URL https://doi.org/10.1088/1367-2630/14/7/073007.

Santiago F. Caballero-Benitez and Igor B. Mekhov. Quantum Optical Lattices for Emergent Many-Body Phases of Ultracold Atoms. *Physical Review Letters*, 115(24):243604, December 2015. doi:10.1103/PhysRevLett.115.243604. URL https://link.aps.org/doi/10.1103/PhysRevLett.115.243604. Publisher: American Physical Society.

K. E. Cahill and R. J. Glauber. Density Operators and Quasiprobability Distributions. *Phys. Rev.*, 177(5):1882–1902, January 1969. doi:10.1103/PhysRev.177.1882. URL https://link.aps.org/doi/10.1103/PhysRev.177.1882.

Bin Cao, Khan W. Mahmud, and Mohammad Hafezi. Two coupled nonlinear cavities in a driven-dissipative environment. *Physical Review A*, 94(6):063805, December 2016.

doi:10.1103/PhysRevA.94.063805. URL https://link.aps.org/doi/10.1103/PhysRevA.94.063805.

Eric A. Carlen and Jan Maas. Gradient flow and entropy inequalities for quantum markov semigroups with detailed balance. *J. Func. Anal.*, 273(5):1810 – 1869, 2017. ISSN 0022-1236. doi:https://doi.org/10.1016/j.jfa.2017.05.003. URL http://www.sciencedirect.com/science/article/pii/S0022123617301878.

H. J. Carmichael. Quantum trajectory theory for cascaded open systems. *Phys. Rev. Lett.*, 70(15):2273–2276, April 1993. doi:10.1103/PhysRevLett.70.2273. URL https://link.aps.org/doi/10.1103/PhysRevLett.70.2273.

H. J. Carmichael and D. F. Walls. Detailed balance in open quantum Markoffian systems. *Z. Phys. B*, 23(3):299–306, September 1976. ISSN 1431-584X. doi:10.1007/BF01318974. URL https://doi.org/10.1007/BF01318974.

Federico Carollo and Igor Lesanovsky. Exactness of mean-field equations for open dicke models with an application to pattern retrieval dynamics. *Phys. Rev. Lett.*, 126:230601, Jun 2021. doi:10.1103/PhysRevLett.126.230601. URL https://link.aps.org/doi/10.1103/PhysRevLett.126.230601.

C. Carr, R. Ritter, C. G. Wade, C. S. Adams, and K. J. Weatherill. Nonequilibrium Phase Transition in a Dilute Rydberg Ensemble. *Physical Review Letters*, 111(11):113901, September 2013. doi:10.1103/PhysRevLett.111.113901.

Fabio Cipriani. Dirichlet Forms and Markovian Semigroups on Standard Forms of von Neumann Algebras. *J. Funct. Anal.*, 147(2):259–300, July 1997. ISSN 0022-1236. doi:10.1006/jfan.1996.3063. URL http://www.sciencedirect.com/science/article/pii/S0022123696930633.

A. Denisov, H. M. Castro-Beltran, and H. J. Carmichael. Time-asymmetric fluctuations of light and the breakdown of detailed balance. *Phys. Rev. Lett.*, 88:243601, May 2002. doi:10.1103/PhysRevLett.88.243601. URL https://link.aps.org/doi/10.1103/PhysRevLett.88.243601.

S. Diehl, A. Micheli, A. Kantian, B. Kraus, H. P. Büchler, and P. Zoller. Quantum states and phases in driven open quantum systems with cold atoms. *Nature Phys.*, 4(11):878–883, 2008. doi:10.1038/nphys1073. URL https://doi.org/10.1038/nphys1073.

Nishant Dogra, Manuele Landini, Katrin Kroeger, Lorenz Hruby, Tobias Donner, and Tilman Esslinger. Dissipation-induced structural instability and chiral dynamics in a quantum gas. *Science*, 366(6472):1496–1499, 2019. ISSN 0036-8075. doi:10.1126/science.aaw4465. URL https://science.sciencemag.org/content/366/6472/1496. Publisher: American Association for the Advancement of Science _eprint: https://science.sciencemag.org/content/366/6472/1496.full.pdf.

P. D. Drummond. Observables and moments of cooperative resonance fluorescence. *Physical Review A*, 22(3):1179–1184, September 1980. doi:10.1103/PhysRevA.22.1179.

P D Drummond and C W Gardiner. Generalised p-representations in quantum optics. *J. Phys. A*, 13(7):2353–2368, jul 1980. doi:10.1088/0305-4470/13/7/018. URL https://doi.org/10.1088%2F0305-4470%2F13%2F7%2F018.

P. D. Drummond and D. F. Walls. Quantum theory of optical bistability. I. Nonlinear polarisability model. *J. Phys. A*, 13(2):725–741, February 1980a. ISSN 0305-4470. doi:10.1088/0305-4470/13/2/034. URL https://doi.org/10.1088%2F0305-4470%2F13%2F2%2F034.

P. D. Drummond and D. F. Walls. Quantum theory of optical bistability. I. Nonlinear polarisability model. *J. Phys. A*, 13(2):725–741, February 1980b. ISSN 0305-4470. doi:10.1088/0305-4470/13/2/034. URL https://doi.org/10.1088%2F0305-4470%2F13%2F2%2F034.

P. D. Drummond, K. J. McNeil, and D. F. Walls. Non-equilibrium Transitions in Sub/second Harmonic Generation. *Optica Acta: International Journal of Optics*, 28(2):211–225, 1981. doi:10.1080/713820531. URL https://doi.org/10.1080/713820531.

Rocco Duvenhage and Machiel Snyman. Balance between quantum markov semigroups. In *Ann. Henri Poincaré*, volume 19, pages 1747–1786. Springer, 2018.

M. Dykman. Periodically modulated quantum nonlinear oscillators. In M. Dykman, editor, *Fluctuating Nonlinear Oscillators*. Oxford, 2012.

M. I. Dykman and M. A. Krivoglaz. Theory of fluctuational transitions between the stable states of a non-linear oscillator. *Zh. Eksp. Teor. Fiz.*, 77:60, 1979. [Sov. Phys. - JETP 50, 30 (1979).

M. I. Dykman and V. N. Smelyanskii. Quantum-theory of transitions between stable states of a nonlinear oscillator interacting with the medium in a resonant field. *Zh. Eksp. Teor. Fiz.*, 94:61, 1988. [Sov. Phys. - JETP 67, 1769 (1988)].

M. I. Dykman, Christoph Bruder, Niels Lörch, and Yaxing Zhang. Interaction-induced time-symmetry breaking in driven quantum oscillators. *Phys. Rev. B*, 98:195444, Nov 2018. doi:10.1103/PhysRevB.98.195444. URL https://link.aps.org/doi/10.1103/PhysRevB.98.195444.

Sepehr Ebadi, Tout T. Wang, Harry Levine, Alexander Keesling, Giulia Semeghini, Ahmed Omran, Dolev Bluvstein, Rhine Samajdar, Hannes Pichler, Wen Wei Ho, Soonwon Choi, Subir Sachdev, Markus Greiner, Vladan Vuletić, and Mikhail D. Lukin. Quantum phases of matter on a 256-atom programmable quantum simulator. *Nature*, 595(7866):227–232, July 2021. ISSN 1476-4687. doi:10.1038/s41586-021-03582-4.

Artur K. Ekert, Carolina Moura Alves, Daniel K. L. Oi, Michał Horodecki, Paweł Horodecki, and L. C. Kwek. Direct estimations of linear and nonlinear functionals of a quantum state. *Phys. Rev. Lett.*, 88:217901, May 2002. doi:10.1103/PhysRevLett.88.217901. URL `https://link.aps.org/doi/10.1103/PhysRevLett.88.217901`.

Matthew Elliott and Eran Ginossar. Applications of the Fokker-Planck equation in circuit quantum electrodynamics. *Phys. Rev. A*, 94(4):043840, October 2016. doi:10.1103/PhysRevA.94.043840. URL `https://link.aps.org/doi/10.1103/PhysRevA.94.043840`.

David E. Evans. Irreducible quantum dynamical semigroups. *Communications in Mathematical Physics*, 54(3):293 – 297, 1977.

Franco Fagnola and Veronica Umanita. Generators of Detailed Balance Quantum Markov Semigroups. *Infinite Dimensional Analysis, Quantum Probability and Related Topics*, 10(03):335–363, September 2007. ISSN 0219-0257, 1793-6306. doi:10.1142/S0219025707002762.

Franco Fagnola and Veronica Umanità. Generators of KMS Symmetric Markov Semigroups on $${\mathcal{B}({\rm h})}$$ Symmetry and Quantum Detailed Balance. *Communications in Mathematical Physics*, 298(2):523–547, September 2010. ISSN 0010-3616, 1432-0916. doi:10.1007/s00220-010-1011-1.

Franco Fagnola and Veronica Umanità. Generators of KMS Symmetric Markov Semigroups on $${\mathcal{B}({\rm h})}$$ Symmetry and Quantum Detailed Balance. *Commun. Math. Phys.*, 298(2):523–547, September 2010. ISSN 0010-3616, 1432-0916. doi:10.1007/s00220-010-1011-1. URL `http://link.springer.com/10.1007/s00220-010-1011-1`.

Alejandro Ferron, Daniel Dominguez, and María Jose Sanchez. Tailoring Population Inversion in Landau-Zener-St\"uckelberg Interferometry of Flux Qubits. *Physical Review Letters*, 109(23):237005, December 2012. doi:10.1103/PhysRevLett.109.237005. URL `https://link.aps.org/doi/10.1103/PhysRevLett.109.237005`. Publisher: American Physical Society.

S. Finazzi, A. Le Boité, F. Storme, A. Baksic, and C. Ciuti. Corner-Space Renormalization Method for Driven-Dissipative Two-Dimensional Correlated Systems. *Physical Review Letters*, 115(8):080604, August 2015. doi:10.1103/PhysRevLett.115.080604.

Thomas Fink, Anne Schade, Sven Höfling, Christian Schneider, and Ataç Imamoglu. Signatures of a dissipative phase transition in photon correlation measurements. *Nature Phys.*, 14(4):365–369, 2018. doi:10.1038/s41567-017-0020-9. URL `https://doi.org/10.1038/s41567-017-0020-9`.

Eliana Fiorelli, Markus Müller, Igor Lesanovsky, and Federico Carollo. Mean-field dynamics of open quantum systems with collective operator-valued rates: Validity and application, February 2023.

Mattias Fitzpatrick, Neereja M. Sundaresan, Andy C. Y. Li, Jens Koch, and Andrew A. Houck. Observation of a dissipative phase transition in a one-dimensional circuit qed lattice. *Phys. Rev. X*, 7:011016, Feb 2017. doi:10.1103/PhysRevX.7.011016. URL https://link.aps.org/doi/10.1103/PhysRevX.7.011016.

Michael Foss-Feig, Kaden R. A. Hazzard, John J. Bollinger, and Ana Maria Rey. Nonequilibrium dynamics of arbitrary-range Ising models with decoherence: An exact analytic solution. *Physical Review A*, 87(4):042101, April 2013. doi:10.1103/PhysRevA.87.042101.

C. W. Gardiner. Driving a quantum system with the output field from another driven quantum system. *Phys. Rev. Lett.*, 70(15):2269–2272, April 1993. doi:10.1103/PhysRevLett.70.2269. URL https://link.aps.org/doi/10.1103/PhysRevLett.70.2269.

C. W. Gardiner and M. J. Collett. Input and output in damped quantum systems: Quantum stochastic differential equations and the master equation. *Phys. Rev. A*, 31:3761–3774, Jun 1985. doi:10.1103/PhysRevA.31.3761. URL https://link.aps.org/doi/10.1103/PhysRevA.31.3761.

C. W. Gardiner and P. Zoller. *Quantum Noise*. Springer, Berlin, 2000.

Crispin Gardiner. *Stochastic Methods: A Handbook for the Natural and Social Sciences*. Springer Series in Synergetics. Springer-Verlag, Berlin Heidelberg, 4 edition, 2009. ISBN 978-3-540-70712-7. URL https://www.springer.com/gp/book/9783540707127.

L. Gilles, B. M. Garraway, and P. L. Knight. Generation of nonclassical light by dissipative two-photon processes. *Phys. Rev. A*, 49(4):2785–2799, April 1994. doi:10.1103/PhysRevA.49.2785. URL https://link.aps.org/doi/10.1103/PhysRevA.49.2785.

Stanislaw Goldstein and J. Martin Lindsay. KMS-symmetric Markov semigroups. *Mathematische Zeitschrift*, 219(1):591–608, May 1995. ISSN 0025-5874, 1432-1823. doi:10.1007/BF02572383.

Mali Gong, Yanyang Yuan, Chen Li, Ping Yan, Haitao Zhang, and Suying Liao. Numerical modeling of transverse mode competition in strongly pumped multimode fiber lasers and amplifiers. *Optics Express*, 15(6):3236–3246, March 2007. ISSN 1094-4087. doi:10.1364/OE.15.003236.

H. Goto. Bifurcation-based adiabatic quantum computation with a nonlinear oscillator network. *Sci. Rep.*, 6(1):21686, February 2016.

A. Grimm, N. E. Frattini, S. Puri, S. O. Mundhada, S. Touzard, M. Mirrahimi, S. M. Girvin, S. Shankar, and M. H. Devoret. The kerr-cat qubit: Stabilization, readout and gates. *arXiv:1907.1213v1*, 2019.

A Grimm, N E Frattini, S Puri, S O Mundhada, S Touzard, M Mirrahimi, S M Girvin, S Shankar, and Michel Devoret. Stabilization and operation of a Kerr-cat qubit. *Nature*, 584(7820):1–7, August 2020.

Lingzhen Guo. *Quantum Effects in Driven Nonlinear Systems*. PhD thesis, Karlsruher Institut fur Technologie, 2013.

Lingzhen Guo, Vittorio Peano, M. Marthaler, and M. I. Dykman. Quantum critical temperature of a modulated oscillator. *Phys. Rev. A*, 87:062117, Jun 2013. doi:10.1103/PhysRevA.87.062117. URL `https://link.aps.org/doi/10.1103/PhysRevA.87.062117`.

E. E. Hach III and C. C. Gerry. Generation of mixtures of schrodinger-cat states from a competitive two-photon process. *Physical Review A*, 49(1):490–498, January 1994. doi:10.1103/PhysRevA.49.490. URL `https://link.aps.org/doi/10.1103/PhysRevA.49.490`.

Julia Hannukainen and Jonas Larson. Dissipation-driven quantum phase transitions and symmetry breaking. *Phys. Rev. A*, 98:042113, Oct 2018. doi:10.1103/PhysRevA.98.042113. URL `https://link.aps.org/doi/10.1103/PhysRevA.98.042113`.

Michael J Hartmann. Quantum simulation with interacting photons. *Journal of Optics*, 18 (10):104005, sep 2016. doi:10.1088/2040-8978/18/10/104005. URL `https://doi.org/10.1088/2040-8978/18/10/104005`.

Andrew A. Houck, Hakan E. Türeci, and Jens Koch. On-chip quantum simulation with superconducting circuits. *Nature Phys.*, 8(4):292–299, 2012. doi:10.1038/nphys2251. URL `https://doi.org/10.1038/nphys2251`.

Dolf Huybrechts, Fabrizio Minganti, Franco Nori, Michiel Wouters, and Nathan Shammah. Mean-field validity in a dissipative critical system: Liouvillian gap, $\mathbb{PT}$-symmetric antigap, and permutational symmetry in the XYZ model. *Physical Review B*, 101(21):214302, June 2020a. ISSN 2469-9950, 2469-9969. doi:10.1103/PhysRevB.101.214302.

Dolf Huybrechts, Fabrizio Minganti, Franco Nori, Michiel Wouters, and Nathan Shammah. Validity of mean-field theory in a dissipative critical system: Liouvillian gap, $\mathbb{PT}$-symmetric antigap, and permutational symmetry in the XYZ model. *Physical Review B*, 101(21):214302, June 2020b. doi:10.1103/PhysRevB.101.214302.

A. Imamoglu, H. Schmidt, G. Woods, and M. Deutsch. Strongly Interacting Photons in a Nonlinear Cavity. *Phys. Rev. Lett.*, 79(8):1467–1470, August 1997. doi:10.1103/PhysRevLett.79.1467. URL `https://link.aps.org/doi/10.1103/PhysRevLett.79.1467`.

E. L. Ince. *Ordinary Differential Equations*. Courier Corporation, 1956.

Rajibul Islam, Ruichao Ma, Philipp M Preiss, M Eric Tai, Alexander Lukin, Matthew Rispoli, and Markus Greiner. Measuring entanglement entropy in a quantum many-body system. *Nature*, 528(7580):77–83, December 2015.

D. A. Ivanov, T. Y. Ivanova, S. F. Caballero-Benitez, and I. B. Mekhov. Feedback-Induced Quantum Phase Transitions Using Weak Measurements. *Physical Review Letters*, 124(1): 010603, January 2020. doi:10.1103/PhysRevLett.124.010603. URL `https://link.aps.org/doi/10.1103/PhysRevLett.124.010603`. Publisher: American Physical Society.

Simon B. Jager, John Cooper, Murray J. Holland, and Giovanna Morigi. Dynamical Phase Transitions to Optomechanical Superradiance. *Physical Review Letters*, 123(5):053601, August 2019. doi:10.1103/PhysRevLett.123.053601. URL `https://link.aps.org/doi/10.1103/PhysRevLett.123.053601`. Publisher: American Physical Society.

Jiasen Jin, Alberto Biella, Oscar Viyuela, Cristiano Ciuti, Rosario Fazio, and Davide Rossini. Phase diagram of the dissipative quantum Ising model on a square lattice. *Physical Review B*, 98(24):241108, December 2018. doi:10.1103/PhysRevB.98.241108.

Minjae Jo, Bukyoung Jhun, and B. Kahng. Resolving mean-field solutions of dissipative phase transitions using permutational symmetry, March 2022.

Alex Kamenev. *Field Theory of Non-Equilibrium Systems*. Cambridge University Press, 2011. doi:10.1017/CBO9781139003667.

I. Kamleitner and A. Shnirman. Time-dependent Markovian master equation for adiabatic systems and its application to Cooper-pair pumping. *Physical Review B*, 84(23):235140, December 2011. doi:10.1103/PhysRevB.84.235140. URL `https://link.aps.org/doi/10.1103/PhysRevB.84.235140`. Publisher: American Physical Society.

Adam M. Kaufman, M. Eric Tai, Alexander Lukin, Matthew Rispoli, Robert Schittko, Philipp M. Preiss, and Markus Greiner. Quantum thermalization through entanglement in an isolated many-body system. *Science*, 353(6301):794–800, 2016.

Javad Kazemi and Hendrik Weimer. Driven-dissipative rydberg blockade in optical lattices. *Phys. Rev. Lett.*, 130:163601, Apr 2023. doi:10.1103/PhysRevLett.130.163601. URL `https://link.aps.org/doi/10.1103/PhysRevLett.130.163601`.

F.P. Kelley. *Reversibility and Stochastic Networks*. Cambridge University Press, 1979.

E. M. Kessler, G. Giedke, A. Imamoglu, S. F. Yelin, M. D. Lukin, and J. I. Cirac. Dissipative phase transition in a central spin system. *Physical Review A*, 86(1):012116, July 2012. doi:10.1103/PhysRevA.86.012116.

K. V. Kheruntsyan. Wigner function for a driven anharmonic oscillator. *Journal of Optics B: Quantum and Semiclassical Optics*, 1(2):225–233, January 1999. ISSN 1464-4266. doi:10.1088/1464-4266/1/2/005. URL `https://doi.org/10.1088%2F1464-4266%2F1%2F2%2F005`.

K. V. Kheruntsyan and K. G. Petrosyan. Exact steady-state wigner function for a nondegenerate parametric oscillator. *Phys. Rev. A*, 62:015801, Jun 2000. doi:10.1103/PhysRevA.62.015801. URL https://link.aps.org/doi/10.1103/PhysRevA.62.015801.

K. V. Kheruntsyan, D. S. Krähmer, G. Yu Kryuchkyan, and K. G. Petrossian. Wigner function for a generalized model of a parametric oscillator: phase-space tristability, competition and nonclassical effects. *Optics Communications*, 139(1):157–164, 1997. ISSN 0030-4018. doi:https://doi.org/10.1016/S0030-4018(96)00753-5. URL https://www.sciencedirect.com/science/article/pii/S0030401896007535.

G. Kirchmair, B. Vlastakis, Z. Leghtas, S. E Nigg, H. Paik, E. Ginossar, M. Mirrahimi, L. Frunzio, S. M. Girvin, and R. J. Schoelkopf. Observation of quantum state collapse and revival due to the single-photon Kerr effect. *Nature*, 495(7440):205–209, March 2013.

Andrzej Kossakowski, Alberto Frigerio, Vittorio Gorini, and Maurizio Verri. Quantum detailed balance and KMS condition. *Commun. Math. Phys.*, 57(2):97–110, June 1977. ISSN 1432-0916. doi:10.1007/BF01625769. URL https://doi.org/10.1007/BF01625769.

Werner Krauth, Michel Caffarel, and Jean-Philippe Bouchaud. Gutzwiller wave function for a model of strongly interacting bosons. *Phys. Rev. B*, 45:3137–3140, Feb 1992a. doi:10.1103/PhysRevB.45.3137. URL https://link.aps.org/doi/10.1103/PhysRevB.45.3137.

Werner Krauth, Michel Caffarel, and Jean-Philippe Bouchaud. Gutzwiller wave function for a model of strongly interacting bosons. *Phys. Rev. B*, 45:3137–3140, Feb 1992b. doi:10.1103/PhysRevB.45.3137. URL https://link.aps.org/doi/10.1103/PhysRevB.45.3137.

L. Krippner, W. J. Munro, and M. D. Reid. Transient macroscopic quantum superposition states in degenerate parametric oscillation: Calculations in the large-quantum-noise limit using the positive P representation. *Phys. Rev. A*, 50(5):4330–4338, November 1994. doi:10.1103/PhysRevA.50.4330. URL https://link.aps.org/doi/10.1103/PhysRevA.50.4330.

G Kryuchkyan, Karen Kheruntsyan, Val Papanyan, and K Petrossian. Exact quantum treatment of the parametric chi (3)-interaction. *Quantum and Semiclassical Optics: Journal of the European Optical Society Part B*, 7:965, 01 1999. doi:10.1088/1355-5111/7/6/005.

G. Yu Kryuchkyan and K. V. Kheruntsyan. Exact quantum theory of a parametrically driven dissipative anharmonic oscillator. *Optics Communications*, 127(4):230–236, 1996. ISSN 0030-4018. doi:https://doi.org/10.1016/0030-4018(96)00021-1. URL https://www.sciencedirect.com/science/article/pii/0030401896000211.

Lev Davidovich Landau. On the theory of phase transitions. I. *Phys. Z. Sowjet.*, 11:26, 1937.

Renate Landig, Lorenz Hruby, Nishant Dogra, Manuele Landini, Rafael Mottl, Tobias Donner, and Tilman Esslinger. Quantum phases from competing short- and long-range interactions in an optical lattice. *Nature*, 532(7600):476–479, April 2016. ISSN 1476-4687. doi:10.1038/nature17409. URL https://www.nature.com/articles/nature17409. Number: 7600 Publisher: Nature Publishing Group.

S. V. Lawande, R. R. Puri, and S. S. Hassan. Non-resonant effects in the fluorescent Dicke model. I. Exact steady state analysis. *Journal of Physics B: Atomic and Molecular Physics*, 14(21):4171, November 1981. ISSN 0022-3700. doi:10.1088/0022-3700/14/21/028.

A. LeBoite, G. Orso, and C. Ciuti. Steady-State Phases and Tunneling-Induced Instabilities in the Driven Dissipative Bose-Hubbard Model. *Physical Review Letters*, 110(23):233601, June 2013. doi:10.1103/PhysRevLett.110.233601. URL https://link.aps.org/doi/10.1103/PhysRevLett.110.233601.

A. LeBoite, G. Orso, and C. Ciuti. Bose-Hubbard model: Relation between driven-dissipative steady states and equilibrium quantum phases. *Physical Review A*, 90(6):063821, December 2014. doi:10.1103/PhysRevA.90.063821. URL https://link.aps.org/doi/10.1103/PhysRevA.90.063821.

José Lebreuilly, Camille Aron, and Christophe Mora. Stabilizing arrays of photonic cat states via spontaneous symmetry breaking. *Phys. Rev. Lett.*, 122:120402, Mar 2019. doi:10.1103/PhysRevLett.122.120402. URL https://link.aps.org/doi/10.1103/PhysRevLett.122.120402.

Tony E. Lee and Ching-Kit Chan. Dissipative transverse-field Ising model: Steady-state correlations and spin squeezing. *Physical Review A*, 88(6):063811, December 2013. doi:10.1103/PhysRevA.88.063811.

Tony E. Lee, H. Häffner, and M. C. Cross. Collective Quantum Jumps of Rydberg Atoms. *Physical Review Letters*, 108(2):023602, January 2012. doi:10.1103/PhysRevLett.108.023602.

Z. Leghtas, S. Touzard, I. M. Pop, A. Kou, B. Vlastakis, A. Petrenko, K. M. Sliwa, A. Narla, S. Shankar, M. J. Hatridge, M. Reagor, L. Frunzio, R. J. Schoelkopf, M. Mirrahimi, and M. H. Devoret. Confining the state of light to a quantum manifold by engineered two-photon loss. *Science*, 347(6224):853–857, February 2015a. doi:10.1126/science.aaa2085. URL https://www.science.org/doi/10.1126/science.aaa2085.

Z. Leghtas, S. Touzard, I. M. Pop, A. Kou, B. Vlastakis, A. Petrenko, K. M. Sliwa, A. Narla, S. Shankar, M. J. Hatridge, M. Reagor, L. Frunzio, R. J. Schoelkopf, M. Mirrahimi, and M. H. Devoret. Confining the state of light to a quantum manifold by engineered two-photon loss. *Science*, 347(6224):853–857, February 2015b. ISSN 0036-8075, 1095-9203. doi:10.1126/science.aaa2085. URL http://science.sciencemag.org/content/347/6224/853.

Marc-Antoine Lemonde, Nicolas Didier, and Aashish A. Clerk. Antibunching and unconventional photon blockade with Gaussian squeezed states. *Phys. Rev. A*, 90(6):063824, December 2014. doi:10.1103/PhysRevA.90.063824. URL https://link.aps.org/doi/10.1103/PhysRevA.90.063824.

R. Lescanne, M. Villiers, T. Peronnin, A. Sarlette, M. Delbecq, B. Huard, T. Kontos, M. Mirrahimi, and Z. Leghtas. Exponential suppression of bit-flips in a qubit encoded in an oscillator. *arXiv:1907.11729v1*, 2019.

Raphaël Lescanne, Marius Villiers, Théau Peronnin, Alain Sarlette, Matthieu Delbecq, Benjamin Huard, Takis Kontos, Mazyar Mirrahimi, and Zaki Leghtas. Exponential suppression of bit-flips in a qubit encoded in an oscillator. *Nature Physics*, 16(5): 509–513, May 2020. ISSN 1745-2481. doi:10.1038/s41567-020-0824-x. URL https://www.nature.com/articles/s41567-020-0824-x.

T. C. H. Liew and V. Savona. Single Photons from Coupled Quantum Modes. *Phys. Rev. Lett.*, 104(18):183601, May 2010. doi:10.1103/PhysRevLett.104.183601. URL https://link.aps.org/doi/10.1103/PhysRevLett.104.183601.

G. Lindblad. On the generators of quantum dynamical semigroups. *Comm. Math. Phys.*, 48 (2):119–130, 1976. URL https://projecteuclid.org:443/euclid.cmp/1103899849.

Shunlong Luo. SU(1,1) coherent states and associated Wick symbol calculus. *Journal of Mathematical Physics*, 38(7):3478–3488, July 1997. ISSN 0022-2488. doi:10.1063/1.531863.

Ruichao Ma, Brendan Saxberg, Clai Owens, Nelson Leung, Yao Lu, Jonathan Simon, and David I. Schuster. A dissipatively stabilized Mott insulator of photons. *Nature*, 566(7742): 51–57, February 2019. ISSN 1476-4687. doi:10.1038/s41586-019-0897-9. URL https://www.nature.com/articles/s41586-019-0897-9.

W. A. Majewski. The detailed balance condition in quantum statistical mechanics. *J. Math. Phys.*, 25(3):614–616, 1984. doi:10.1063/1.526164. URL https://doi.org/10.1063/1.526164.

W. A. Majewski and R. F. Streater. Detailed balance and quantum dynamical maps. *J. Phys. A. Math Gen*, 31(39):7981–7995, January 1999.

N. Malossi, M. M. Valado, S. Scotto, P. Huillery, P. Pillet, D. Ciampini, E. Arimondo, and O. Morsch. Full Counting Statistics and Phase Diagram of a Dissipative Rydberg Gas. *Physical Review Letters*, 113(2):023006, July 2014. doi:10.1103/PhysRevLett.113.023006.

M. Mamaev. *Entangled Cavity State Generation through Engineered Dissipation*. McGill University Libraries, 2018.

M. Mamaev, L. C. G. Govia, and A. A. Clerk. Dissipative stabilization of entangled cat states using a driven bose-hubbard dimer. *Quantum*, 2:58, 2018. doi:10.22331/q-2018-03-27-58.

Matteo Marcuzzi, Emanuele Levi, Sebastian Diehl, Juan P. Garrahan, and Igor Lesanovsky. Universal Nonequilibrium Properties of Dissipative Rydberg Gases. *Physical Review Letters*, 113(21):210401, November 2014. doi:10.1103/PhysRevLett.113.210401.

M. Marthaler and M. I. Dykman. Switching via quantum activation: A parametrically modulated oscillator. *Phys. Rev. A*, 73(4):042108, April 2006.

Eduardo Mascarenhas, Hugo Flayac, and Vincenzo Savona. Matrix-product-operator approach to the nonequilibrium steady state of driven-dissipative quantum arrays. *Phys. Rev. A*, 92:022116, Aug 2015. doi:10.1103/PhysRevA.92.022116. URL https://link.aps.org/doi/10.1103/PhysRevA.92.022116.

A. McDonald and A.A. Clerk. Exact Solutions of Interacting Dissipative Systems via Weak Symmetries. *Physical Review Letters*, 128(3):033602, January 2022. doi:10.1103/PhysRevLett.128.033602. URL https://link.aps.org/doi/10.1103/PhysRevLett.128.033602.

Albert Messiah. *Quantum Mechanics*, volume 2. North-Holland Publishing Company, Amsterdam, 1962.

Fabrizio Minganti, Nicola Bartolo, Jared Lolli, Wim Casteels, and Cristiano Ciuti. Exact results for Schrödinger cats in driven-dissipative systems and their feedback control. *Scientific Reports*, 6:26987, May 2016a. doi:10.1038/srep26987. URL https://www.nature.com/articles/srep26987.

Fabrizio Minganti, Nicola Bartolo, Jared Lolli, Wim Casteels, and Cristiano Ciuti. Exact results for Schrödinger cats in driven-dissipative systems and their feedback control. *Scientific Reports*, 6:26987, May 2016b. doi:10.1038/srep26987. URL https://www.nature.com/articles/srep26987.

Mazyar Mirrahimi, Zaki Leghtas, Victor V. Albert, Steven Touzard, Robert J. Schoelkopf, Liang Jiang, and Michel H. Devoret. Dynamically protected cat-qubits: a new paradigm for universal quantum computation. *New Journal of Physics*, 16(4):045014, April 2014a. ISSN 1367-2630. doi:10.1088/1367-2630/16/4/045014. URL https://doi.org/10.1088/1367-2630/16/4/045014.

Mazyar Mirrahimi, Zaki Leghtas, Victor V. Albert, Steven Touzard, Robert J. Schoelkopf, Liang Jiang, and Michel H. Devoret. Dynamically protected cat-qubits: a new paradigm for universal quantum computation. *New J. Phys.*, 16(4):045014, April 2014b. ISSN 1367-2630. doi:10.1088/1367-2630/16/4/045014. URL https://doi.org/10.1088%2F1367-2630%2F16%2F4%2F045014.

Farokh Mivehvar, Helmut Ritsch, and Francesco Piazza. Cavity-Quantum-Electrodynamical Toolbox for Quantum Magnetism. *Physical Review Letters*, 122(11):113603, March 2019. doi:10.1103/PhysRevLett.122.113603. URL https://link.aps.org/doi/10.1103/PhysRevLett.122.113603. Publisher: American Physical Society.

S. Morrison and A. S. Parkins. Dynamical Quantum Phase Transitions in the Dissipative Lipkin-Meshkov-Glick Model with Proposed Realization in Optical Cavity QED. *Physical Review Letters*, 100(4):040403, January 2008. doi:10.1103/PhysRevLett.100.040403.

J. E. Moyal. Quantum mechanics as a statistical theory. *Mathematical Proceedings of the Cambridge Philosophical Society*, 45(1):99–124, 1949. doi:10.1017/S0305004100000487.

Juan A. Muniz, Diego Barberena, Robert J. Lewis-Swan, Dylan J. Young, Julia R. K. Cline, Ana Maria Rey, and James K. Thompson. Exploring dynamical phase transitions with cold atoms in an optical cavity. *Nature*, 580(7805):602–607, April 2020. ISSN 1476-4687. doi:10.1038/s41586-020-2224-x. URL `https://www.nature.com/articles/s41586-020-2224-x`. Number: 7805 Publisher: Nature Publishing Group.

D. Nagy, G. Kónya, G. Szirmai, and P. Domokos. Dicke-Model Phase Transition in the Quantum Motion of a Bose-Einstein Condensate in an Optical Cavity. *Physical Review Letters*, 104(13):130401, April 2010a. doi:10.1103/PhysRevLett.104.130401.

D. Nagy, G. Konya, G. Szirmai, and P. Domokos. Dicke-Model Phase Transition in the Quantum Motion of a Bose-Einstein Condensate in an Optical Cavity. *Physical Review Letters*, 104(13):130401, April 2010b. doi:10.1103/PhysRevLett.104.130401. URL `https://link.aps.org/doi/10.1103/PhysRevLett.104.130401`. Publisher: American Physical Society.

L. M. Narducci, J. R. Tredicce, L. A. Lugiato, N. B. Abraham, and D. K. Bandy. Mode-mode competition and unstable behavior in a homogeneously broadened ring laser. *Physical Review A*, 33(3):1842–1854, March 1986. doi:10.1103/PhysRevA.33.1842.

Vincent R. Overbeck, Mohammad F. Maghrebi, Alexey V. Gorshkov, and Hendrik Weimer. Multicritical behavior in dissipative Ising models. *Physical Review A*, 95(4):042133, April 2017. ISSN 2469-9926, 2469-9934. doi:10.1103/PhysRevA.95.042133.

Asaf Paris-Mandoki, Christoph Braun, Jan Kumlin, Christoph Tresp, Ivan Mirgorodskiy, Florian Christaller, Hans Peter Büchler, and Sebastian Hofferberth. Free-Space Quantum Electrodynamics with a Single Rydberg Superatom. *Physical Review X*, 7(4):041010, October 2017. ISSN 2160-3308. doi:10.1103/PhysRevX.7.041010.

K. R. Parthasarathy. *An Introduction to Quantum Stochastic Calculus*. Modern Birkhäuser Classics. Birkhäuser Basel, 1992. ISBN 978-3-0348-0565-0. doi:10.1007/978-3-0348-0566-7. URL `https://www.springer.com/gp/book/9783034805650`.

Grigorios A. Pavliotis. *Stochastic Processes and Applications: Diffusion Processes, the Fokker-Planck and Langevin Equations*. Texts in Applied Mathematics. Springer-Verlag, New York, 2014. ISBN 978-1-4939-1322-0. doi:10.1007/978-1-4939-1323-7. URL `https://www.springer.com/gp/book/9781493913220`.

Daniel A. Paz and Mohammad F. Maghrebi. Driven-dissipative Ising model: An exact field-theoretical analysis. *Physical Review A*, 104(2):023713, August 2021. doi:10.1103/PhysRevA.104.023713.

R. R. Puri and S. V. Lawande. Exact steady-state density operator for a collective atomic system in an external field. *Physics Letters A*, 72(3):200–202, July 1979. ISSN 0375-9601. doi:10.1016/0375-9601(79)90003-3.

S. Puri, S. Boutin, and A. Blais. Engineering the quantum states of light in a Kerr-nonlinear resonator by two-photon driving. *npj Quant. Inf.*, 3(1), December 2017.

Shruti Puri, Alexander Grimm, Philippe Campagne-Ibarcq, Alec Eickbusch, Kyungjoo Noh, Gabrielle Roberts, Liang Jiang, Mazyar Mirrahimi, Michel H. Devoret, and S. M. Girvin. Stabilized Cat in a Driven Nonlinear Cavity: A Fault-Tolerant Error Syndrome Detector. *Physical Review X*, 9(4):041009, October 2019. doi:10.1103/PhysRevX.9.041009.

M. Ramezani, F. Benatti, R. Floreanini, S. Marcantoni, M. Golshani, and A. T. Rezakhani. Quantum detailed balance conditions and fluctuation relations for thermalizing quantum dynamics. *Phys. Rev. E*, 98(5):052104, November 2018. doi:10.1103/PhysRevE.98.052104. URL `https://link.aps.org/doi/10.1103/PhysRevE.98.052104`.

Viktor Reimer, Kim G. L. Pedersen, Niklas Tanger, Mikhail Pletyukhov, and Vladimir Gritsev. Nonadiabatic effects in periodically driven dissipative open quantum systems. *Physical Review A*, 97(4):043851, April 2018. doi:10.1103/PhysRevA.97.043851. URL `https://link.aps.org/doi/10.1103/PhysRevA.97.043851`. Publisher: American Physical Society.

Hannes Risken and Till Frank. *The Fokker-Planck Equation: Methods of Solution and Applications*. Springer Series in Synergetics. Springer-Verlag, Berlin Heidelberg, 2 edition, 1996. ISBN 978-3-540-61530-9. doi:10.1007/978-3-642-61544-3. URL `https://www.springer.com/gp/book/9783540615309`.

David Roberts and A. A. Clerk. Competition between two-photon driving, dissipation, and interactions in bosonic lattice models: An exact solution. *Phys. Rev. Lett.*, 130:063601, Feb 2023. doi:10.1103/PhysRevLett.130.063601. URL `https://link.aps.org/doi/10.1103/PhysRevLett.130.063601`.

David Roberts and Aashish Clerk. Competition between two-photon driving, dissipation and interactions in bosonic lattice models: An exact solution, August 2022.

David Roberts and Aashish A. Clerk. Driven-dissipative quantum kerr resonators: New exact solutions, photon blockade and quantum bistability. *Phys. Rev. X*, 10:021022, Apr 2020. doi:10.1103/PhysRevX.10.021022. URL `https://link.aps.org/doi/10.1103/PhysRevX.10.021022`.

David Roberts, Andrew Lingenfelter, and A. A. Clerk. Hidden Time-Reversal Symmetry, Quantum Detailed Balance and Exact Solutions of Driven-Dissipative Quantum Systems. *PRX Quantum*, 2(2):020336, June 2021. doi:10.1103/PRXQuantum.2.020336. URL `https://link.aps.org/doi/10.1103/PRXQuantum.2.020336`.

Daniel S. Rokhsar and B. G. Kotliar. Gutzwiller projection for bosons. *Phys. Rev. B*, 44: 10328–10332, Nov 1991. doi:10.1103/PhysRevB.44.10328. URL https://link.aps.org/doi/10.1103/PhysRevB.44.10328.

Riccardo Rota, Fabrizio Minganti, Cristiano Ciuti, and Vincenzo Savona. Quantum Critical Regime in a Quadratically Driven Nonlinear Photonic Lattice. *Physical Review Letters*, 122(11):110405, March 2019. doi:10.1103/PhysRevLett.122.110405. URL https://link.aps.org/doi/10.1103/PhysRevLett.122.110405.

J. J. Sakurai and J. Napolitano. *Modern Quantum Mechanics by J. J. Sakurai*. Cambridge University Press, second edition, September 2017. doi:10.1017/9781108499996. URL /core/books/modern-quantum-mechanics/AAE1925F1A0963C6124421B03D7801AE.

Vincenzo Savona. Spontaneous symmetry breaking in a quadratically driven nonlinear photonic lattice. *Phys. Rev. A*, 96:033826, Sep 2017. doi:10.1103/PhysRevA.96.033826. URL https://link.aps.org/doi/10.1103/PhysRevA.96.033826.

Orazio Scarlatella, Aashish A. Clerk, Rosario Fazio, and Marco Schiró. Dynamical mean-field theory for markovian open quantum many-body systems. *Phys. Rev. X*, 11:031018, Jul 2021a. doi:10.1103/PhysRevX.11.031018. URL https://link.aps.org/doi/10.1103/PhysRevX.11.031018.

Orazio Scarlatella, Aashish A. Clerk, Rosario Fazio, and Marco Schiró. Dynamical Mean-Field Theory for Markovian Open Quantum Many-Body Systems. *Physical Review X*, 11 (3):031018, July 2021b. doi:10.1103/PhysRevX.11.031018. URL https://link.aps.org/doi/10.1103/PhysRevX.11.031018. Publisher: American Physical Society.

S. Schneider and G. J. Milburn. Entanglement in the steady state of a collective-angular-momentum (Dicke) model. *Physical Review A*, 65(4):042107, March 2002. doi:10.1103/PhysRevA.65.042107.

Pascal Scholl, Michael Schuler, Hannah J. Williams, Alexander A. Eberharter, Daniel Barredo, Kai-Niklas Schymik, Vincent Lienhard, Louis-Paul Henry, Thomas C. Lang, Thierry Lahaye, Andreas M. Läuchli, and Antoine Browaeys. Quantum simulation of 2D antiferromagnets with hundreds of Rydberg atoms. *Nature*, 595(7866):233–238, July 2021. ISSN 0028-0836, 1476-4687. doi:10.1038/s41586-021-03585-1.

I. E. Segal. Mathematical characterization of the physical vacuum for a linear bose-einstein field. *Illinois J. Math*, 6:500, 1962.

I. E. Segal. Mathematical problems of relativistic physics. In M. Kac, editor, *Proceedings of the Summer Seminar, Boulder, Colorado, 1960*, volume 2 of *Lectures in applied mahematics*, Providence, R.I., 1963. Am. Math. Soc.

L. M. Sieberer, S. D. Huber, E. Altman, and S. Diehl. Dynamical Critical Phenomena in Driven-Dissipative Systems. *Physical Review Letters*, 110(19):195301, May 2013. doi:10.1103/PhysRevLett.110.195301.

L. M. Sieberer, A. Chiocchetta, A. Gambassi, U. C. Täuber, and S. Diehl. Thermodynamic equilibrium as a symmetry of the schwinger-keldysh action. *Phys. Rev. B*, 92:134307, Oct 2015. doi:10.1103/PhysRevB.92.134307. URL https://link.aps.org/doi/10.1103/PhysRevB.92.134307.

L M Sieberer, M Buchhold, and S Diehl. Keldysh field theory for driven open quantum systems. *Rep. Prog. Phys.*, 79(9):096001–69, August 2016.

Vijay Pal Singh and Hendrik Weimer. Driven-Dissipative Criticality within the Discrete Truncated Wigner Approximation. *Physical Review Letters*, 128(20):200602, May 2022. doi:10.1103/PhysRevLett.128.200602.

V.V. Sivak, N.E. Frattini, V.R. Joshi, A. Lingenfelter, S. Shankar, and M.H. Devoret. Kerr-free three-wave mixing in superconducting quantum circuits. *Phys. Rev. Applied*, 11: 054060, May 2019. doi:10.1103/PhysRevApplied.11.054060. URL https://link.aps.org/doi/10.1103/PhysRevApplied.11.054060.

K. Stannigel, P. Rabl, and P. Zoller. Driven-dissipative preparation of entangled states in cascaded quantum-optical networks. *New Journal of Physics*, 14(6):063014, June 2012a. ISSN 1367-2630. doi:10.1088/1367-2630/14/6/063014. URL https://doi.org/10.1088/1367-2630/14/6/063014.

K. Stannigel, P. Rabl, and P. Zoller. Driven-dissipative preparation of entangled states in cascaded quantum-optical networks. *New Journal of Physics*, 14(6):063014, June 2012b. ISSN 1367-2630. doi:10.1088/1367-2630/14/6/063014. URL https://doi.org/10.1088%2F1367-2630%2F14%2F6%2F063014.

Jordan R. Stone, Gregory Moille, Xiyuan Lu, and Kartik Srinivasan. Conversion Efficiency in Kerr-Microresonator Optical Parametric Oscillators: From Three Modes to Many Modes. *Physical Review Applied*, 17(2):024038, February 2022. doi:10.1103/PhysRevApplied.17.024038.

Hugo U.R. Strand, Martin Eckstein, and Philip Werner. Nonequilibrium Dynamical Mean-Field Theory for Bosonic Lattice Models. *Physical Review X*, 5(1):011038, March 2015. doi:10.1103/PhysRevX.5.011038. URL https://link.aps.org/doi/10.1103/PhysRevX.5.011038. Publisher: American Physical Society.

Yasushi Takahashi and Hiroomi Umezawa. Thermo Field Dynamics. *Int. J. Mod. Phys. B*, 10(13):1755, January 1996.

Emanuele G. Dalla Torre, Sebastian Diehl, Mikhail D. Lukin, Subir Sachdev, and Philipp Strack. Keldysh approach for nonequilibrium phase transitions in quantum optics: Beyond the dicke model in optical cavities. *Phys. Rev. A*, 87:023831, Feb 2013. doi:10.1103/PhysRevA.87.023831. URL https://link.aps.org/doi/10.1103/PhysRevA.87.023831.

S Touzard, A Grimm, Z Leghtas, S O Mundhada, P Reinhold, C Axline, M Reagor, K Chou, J Blumoff, K M Sliwa, S Shankar, L Frunzio, R J Schoelkopf, M Mirrahimi, and Michel Devoret. Coherent Oscillations inside a Quantum Manifold Stabilized by Dissipation. *Phys. Rev. X*, 8(2):021005, April 2018.

D. F. Walls and Gerard J. Milburn. *Quantum Optics*. Springer-Verlag, Berlin, 2008.

Chen Wang, Yvonne Y Gao, Philip Reinhold, R W Heeres, Nissim Ofek, Kevin Chou, Christopher Axline, Matthew Reagor, Jacob Blumoff, K M Sliwa, L Frunzio, S M Girvin, Liang Jiang, M Mirrahimi, Michel Devoret, and R J Schoelkopf. A Schrödinger cat living in two boxes. *Science*, 352(6289):1087–1091, May 2016.

Pei Wang and Rosario Fazio. Dissipative phase transitions in the fully connected ising model with p-spin interaction. *Phys. Rev. A*, 103:013306, Jan 2021. doi:10.1103/PhysRevA.103.013306. URL `https://link.aps.org/doi/10.1103/PhysRevA.103.013306`.

Zijian Wang, Carlos Navarrete-Benlloch, and Zi Cai. Pattern formation and exotic order in driven-dissipative bose-hubbard systems. *Phys. Rev. Lett.*, 125:115301, Sep 2020. doi:10.1103/PhysRevLett.125.115301. URL `https://link.aps.org/doi/10.1103/PhysRevLett.125.115301`.

Hendrik Weimer. Variational analysis of driven-dissipative Rydberg gases. *Physical Review A*, 91(6):063401, June 2015. doi:10.1103/PhysRevA.91.063401.

M. Wolinsky and H. J. Carmichael. Quantum noise in the parametric oscillator: From squeezed states to coherent-state superpositions. *Phys. Rev. Lett.*, 60(18):1836–1839, May 1988a. doi:10.1103/PhysRevLett.60.1836. URL `https://link.aps.org/doi/10.1103/PhysRevLett.60.1836`.

M. Wolinsky and H. J. Carmichael. Quantum noise in the parametric oscillator: From squeezed states to coherent-state superpositions. *Phys. Rev. Lett.*, 60:1836–1839, May 1988b. doi:10.1103/PhysRevLett.60.1836. URL `https://link.aps.org/doi/10.1103/PhysRevLett.60.1836`.

Yaxing Zhang and M. I. Dykman. Nonlocal random walk over floquet states of a dissipative nonlinear oscillator. *Phys. Rev. E*, 100:052148, Nov 2019. doi:10.1103/PhysRevE.100.052148. URL `https://link.aps.org/doi/10.1103/PhysRevE.100.052148`.

D. Zhu and C. Monroe. Generation of thermofield double states and critical ground states with a quantum computer. *Proc. Nat. Acad. Sci.*, September 2020.

Wilhelm Zwerger. Mott Hubbard transition of cold atoms in optical lattices. *Journal of Optics B: Quantum and Semiclassical Optics*, 5(2):S9–S16, April 2003. ISSN 1464-4266. doi:10.1088/1464-4266/5/2/352. URL `https://doi.org/10.1088/1464-4266/5/2/352`. Publisher: IOP Publishing.